Swansea University
Prifysgol Abertawe

Towards state-of-the-art vacuum locks for a novel continuous PVD galvanising process

Samuel James Benjamin Minshell

Submitted to the Swansea University in fulfilment of the requirements for the Degree of Doctor of Engineering

Swansea University 2019

Abstract

Physical Vapour Deposition (PVD) is used in various industries to create thin coatings ranging from aluminizing crisp packaging through to thin ZnO films on solar cells and glass windows providing thermochromic control [1]. Vacuum locks are used during manufacturing to transport material into and out of the coating chamber, sometimes as a continuous process.

In 2012, POSCO installed a wide PVD pilot plant [2] and in 2017 Arcelor Mittal opened a €63 million commercial air to air coating line, therefore demonstrating the technology is commercially viable [3]. The advantage of PVD coating over more traditional methods such as a galvanising bath is a greater control on the coating thickness, excellent corrosion resistant properties and uniform coating across the substrate. A review of patents and publications on the state-of-the-art in vacuum lock design for the PVD steel coating technology showed that air bearings had the potential for an improved design with a greater flexibility in dealing with variable strip width and thickness.

A new vacuum lock for a continuous steel strip process has been designed and prototyped by using a combination of computational modelling, continuum fluid dynamics and discrete molecular models, validated against benchmarks and experimentation. Using a set pump speed (198 m^3/hr) at the outlet, the lock was designed to maintain a pressure drop of -79.3kPa and would form the first of a sequence of vacuum locks ultimately reducing the vacuum level to the pressure of 0.01 Pa required within the PVD chamber.

Whilst no single computational model was able to capture the entire flow regime, the continuum models were able to suggest possible pressure drops from changing outlet mass flow rates, which was used to develop the design. By using an air bearing system at the lock entrance with thin slider blocks to adjust the gap, the lock can accommodate a steel strip with a reduced or increased thickness and width.

Declarations

Declaration: This work has not previously been accepted in substance for any degree and is not being concurrently submitted in candidature for any degree.

Signed:  Date: 24/03/2021

Statement 1: This thesis is the result of my own investigations, except where otherwise stated. Other sources are acknowledged by footnotes giving explicit references. A bibliography is appended.

Signed:  Date: 24/03/2021

Statement 2: I hereby give consent for my thesis, if accepted, to be made available online in the University's Open Access Repository and for inter-library loan **after expiry of a bar on access approved by Swansea University**.

Signed:  Date: 24/03/2021

Acknowledgments

I would like to give a huge thank you, to my academic supervisors Professor Nicholas Lavery and Professor David Penney. I am greatly indebted to Nick for his guidance and mentoring throughout my project. Dave has kept my spirits up through the long and hard process of undertaking a doctorate and is one of the reasons the scheme exists in the first place. Another big thank you to the M2A team, that have greatly supported me throughout the entire process.

This work would not exist without financial support. Therefore, I would like to say thank you to all the industrial sponsors, Tata Steel, ESF, ESPRC and WEFO. A big part of sponsorship is the industrial input, which was provided to me by my supervisors from Tata Steel, thank you to Edzo Zoestbergen and Colin Commandeur for taking time to support my doctorate. Also thank you to Swansea University for the opportunity to study for an Engineering Doctorate.

A massive thank you to my parents Patricia and Leonard Minshell for always believing in me and supporting me, they have always been there when I needed them. Also thank you to the rest of my family, uncle George, uncle Terry, my elder brothers Richard, Graham and Cliff and my cousins Christine, Nicola, Mark, Emma and Jasmine, you have all supported me too and helped me keep my sanity. One last big thank you to my friends who have joined me in this challenge and supported me along the way; to name a few, James, Michael, Ben, Catherine, Callum, Luis and Alex.

I dedicate my work in loving memory to my Grandmother Mimie Simmonds and Grandfather James Simmonds, they always supported me with love and kindness and are dearly missed. Also, my Uncle William, Auntie Marie, Auntie Diana and Uncle Neville.

List of Figures

Glossary

CAD – Computer Aided Design

CFD – Computational Fluid Dynamics

CGL – Continuous Galvanising Lines

CVD – Chemical Vapour Deposition

DSMC – Direct Simulation Monte Carlo

EB – Electron Beam

EGL – Electrolytic Galvanising Lines

EMELI – Electro Magnetic Evaporation Line IJMuiden

EML – Electromagnetic Levitation

FEA – Finite Element Analysis

FEM – Finite Element Method

FVM – Finite Volume Method

OpenFOAM – Open Field Operation And Manipulation

JVD – Jet Vapour Deposition

LPM – Normal Litre Per Minute

MD – Molecular Dynamics

MPM – metres per minute

PDE – Partial Differential Equation

PVD – Physical Vapour Deposition

REACH – Registration Evaluation Authorisation and Restriction of Chemicals

SEM – Scanning Electron Microscope

SLPM – Standard Litre Per Minute

XRD – X-Ray Diffraction

Contents

1. Introduction

Steel is one of the most common materials in the world. In 2014 the global production of Zn and Zn Alloy steel was 120 million metric tonnes [4]. From the industrial revolution steel has become very prevalent in modern society in the structural reinforcement of buildings, the panels on cars, cutlery, packaging and many more applications [5]. Steel is a very versatile material, with excellent material properties, however a very undesirable attribute is that it suffers badly from corrosion. The corrosion weakens the steel and reduces the strength which can lead to structural failure; rust also ruins the appearance. Varying steel production compositions and methods are used to reduce corrosion in steel and coating steel with other metals is an established method to reduce corrosion from occurring [5].

Galvanising is a process used to prevent corrosion in steel by dipping steel in a hot molten bath of zinc. The global zinc consumption in 2012 was 13 million tonnes and there are only 250 million tonnes of extractable reserves. Most zinc consumption is attributed to alloying with other materials including 50% associated with steel plating [6]. Physical vapour deposition (PVD) is an emerging film coating technology, carried out under vacuum conditions that uses less zinc. PVD offers a better quality, thinner coating over traditional galvanised coated steel. PVD is currently being used to generate a variety of high quality products such as semiconductors, glass, displays, crisp packets, solar cells, etc [7]. Tata Steel has two PVD test equipment rigs. An Electro Magnetic Evaporation Line IJMuiden (EMELY) which is a to roll batch chamber and Betsy, a plate batch chamber. Galvanised steel is required to be coated at high speed, running 24 hours per day, 7 days per week. If the PVD line is implemented, the coating line must be able to run continuously at high speed to be a viable replacement to hot dip galvanising.

One of the fundamental requirements for a PVD process is operation in vacuum conditions. These conditions must remain constant and stable for the coating process to work [2]. To allow the steel strip to be transported into and out of the coating chamber, state of the art vacuum locks are required to maintain the pressure difference between atmospheric pressure outside the chamber and the low-pressure vacuum

condition inside. The vacuum locks must also accommodate the variation in strip width and thickness, without interruption to the process. The development of vacuum locks has tried to deal with leakages entering the system, these are mainly the clearances between the rollers and the chamber walls and the clearance between the edge of the band material and the rollers. This is very complex as the vacuum is required to be maintained constantly with the strip passing in and out of the coating chamber. The design of a state-of-the-art vacuum locks is crucial in the process being successful.

In the steel PVD galvanising process there is flow of metallic particles in the coating chamber and pressure changes in the vacuum locks. The analysis of metallic vapour in the coating chamber and vacuum locks next to the coating chamber requires a particle-based analysis due to the rarefied conditions caused by low pressure. Existing research highlights the Direct Simulation Monte Carlo (DSMC) method as a powerful tool for simulating metallic vapour behaviour in a vacuum. This is due to DSMC being a probabilistic method saving massive computational expense [8].

There is a variety of engineering software that can be used for the continuum method analysis, but not as many for the particle-based analysis. A benchmarking exercise looks at the software, ANSYS, COMSOL and OpenFOAM to investigate the performance of the software and using the most appropriate set up to perform the vacuum lock simulation. ANSYS Fluent is CFD software that is well established in analysing flow using a Navier-Stokes based continuum method [9]. COMSOL has a variety of Multiphysics and CFD programs including a free molecular flow module and is also well established [10]. OpenFOAM is a newer open source software that has a DSMC solver which can be used to track particle movement as well as a wall interaction model and additional absorbing wall function that can record the number of particles colliding with surfaces [11], [12].

Research into the existing patented vacuum lock and air bearing lock technology was conducted to identify the current advancements with the technology and the advantages and disadvantages between traditional and air bearing locks. The information provided an understanding of the operation of vacuum locks and how this could be applied to design a vacuum lock for the continuous PVD coating process. A

prototype of an air bearing vacuum lock was designed through constant revision and investigation so that the design could be applied in a steel line configuration with varying steel strip width and gauges. Simulations were run to determine the pressure reduction within the entry lock at certain pumping capacities. The prototype was built and tested for verification of the modelling work.

1.1 Objectives

I. It is essential that steel strip is transported in a continuous way into and out of the vacuum coating chamber.
II. Vacuum locks are required to maintain a specified pressure difference between the vacuum chamber and the outside atmosphere.
III. Vacuum locks also need to be able to deal with varying strip width and thicknesses.

1.2 Deliverables

I. To model an air bearing lock and to determine the required pumping capacity to achieve a certain pressure.
II. Make a comparison of the air bearing technology with alternative conventional vacuum lock technologies available and to identify the advantages and disadvantages of the different technologies.
III. Identify how the air bearing technology can be applied in a steel line configuration with varying steel strip width and gauges.
IV. Verification of the modelling work.
V. Vacuum lock Patent complete with CAD design, drawings, simulation and experimental results.
VI. Optimisation of air bar pressure and pumping to provide the most efficient operation and optimised energy consumption.
VII. Simulation of consecutive locks (daisy chained) showing pumping down to adequate coating chamber pressure.

1.3 Presentations and Publications

I. Simulating Physical Vapour Deposition on Steel Substrate Using the Direct Simulation Monte Carlo (DSMC) Method: Paper presented at Galvatech Tokyo 2017, November 12th-16th

II. Simulating Physical Vapour Deposition on Steel Substrate Using the Direct Simulation Monte Carlo (DSMC) Method: Presented at Armouers & Brasiers Postgraduate Research Symposium on Ferrous Metallurgy at Armourers' Hall, London 2018, 27th February.

2. Galvanised Steel Processes

In 2008 approximately 140 million metric tonnes of galvanised steel was produced worth 130 billion dollars. This steel is used to produce a range of products such as automotive panels and parts, construction sections, home appliances and bodies and closures of cans [2]. Galvanising is the process used to apply a protective zinc coating to steel or iron. The instability of zinc supply predicted by the steady increase in price and consumption will consequence in instabilities of supply. Reducing production costs of coated steels is a major challenge for the steel industry. There is demand for low price, high performance steel that is also environmentally friendly. Customers have requested smart coated products with thinner coatings using environmentally friendly processes and higher productivity rates [2].

This chapter will review the established methods of hot dip and electro galvanising used to coat steel strip and the problems associated with them. A new coating process called electromagnetic levitation (EML) PVD is currently being developed by Tata Steel to provide more suitable products for customer requirements and overcome problems associated with traditional methods. It is important to acknowledge that zinc is a predominant metal used for coating steel strip and the reason why. It is also crucial to understand the required operating conditions of the EML-PVD process to develop the equipment required for the line coating process.

2.1 Steel Strip Coating Materials

Steel requires to be coated for protection against corrosion. The corrosion of steel is an electrochemical process that happens when steel is exposed to air and moisture. Steel reacts with oxygen and water in the air to form hydrated iron oxide, this results in corrosion of the steel known as rust. A zinc coating is applied to steel to form a protective layer as zinc corrodes more rapidly [13]. The corrosion products from the zinc precipitate onto the steel forming a non-porous layer on the surface protecting the steel against further oxidation from being exposed to air and moisture. The zinc acts as an anode sacrificing metal to protect the steel which acts as a cathode. This is known

as cathodic protection. Depending on what metals are used for the formation of the oxide layer, protection can be applied with varying results.

The Pilling-Bedworth ratio determines the volume of the oxide layer formed on the metal surface [14]. Represented by the following equation:

$$P - B\ ratio = \frac{M_o \times \rho_m}{nM_m \times \rho_o} = \frac{M_o \times V_o}{nM_m \times V_m} \quad (2.1)$$

ρ_m – Metal Density

ρ_o – Oxide Density

V_m – Metal Volume

V_o – Oxide Volume

M_m – Atomic Mass Number Metal

M_o – Atomic Mass Number Oxide

n – Number of metal atoms in the oxide molecule.

The ratio is used to determine how suitable the metal oxide layer will be, given below:

- P-B ratio < 1 – The oxide film is porous because the oxide layer is less volume than the metal from which it was formed.
- 1 < P-B ratio < 2 – The oxide film is nonporous and protective as the volumes are approximately equal.
- P-B ratio > 2 – The oxide film is initially protective but due to the thickness, compressive stresses cause cracking and flaking [15].

The zinc oxide film that forms on galvanised steel falls within the P-B ratio between 1 and 2. This is the desired range for oxide film coatings. Nonporous and protective in nature is perfect for coating steel. Zinc coatings are traditionally regarded as a very effective protective coating for steel corrosion [16]. However, zinc coating is insufficient for extreme atmospheric or saltwater conditions, welding is also likely to

melt the zinc due to the low melting temperature of 420 °C. Adding magnesium to zinc to produce an Zn-Mg alloy can improve the corrosion resistance compared with zinc alone. Even small amounts of added magnesium can increase corrosion protection performance [4] [17].

2.2 Hot Dip Galvanising

Hot dip galvanising is the traditional coating process for steel. The galvanisation process applies a protective zinc coating to steel to prevent corrosion. First the steel strip is chemically pre-treated by degreasing and pickling. The pickling process removes scale, oxides and corrosion impurities from the surface [5]. The cold rolled steel is then annealed before being passed through a molten zinc bath. The thickness of the coating is controlled by air knives and is usually 14 to 49 μm [18]. To produce a uniform thickness, x-ray fluorescent measurement is used continuously over above the zinc bath in the centre of the strip, giving direct control of the air knives and transversely over the width of the strip [18]. Figure 1 shows a simple diagram of a steel strip galvanising line taken from Hot-Dip Galvanising of Steel Structures [5].

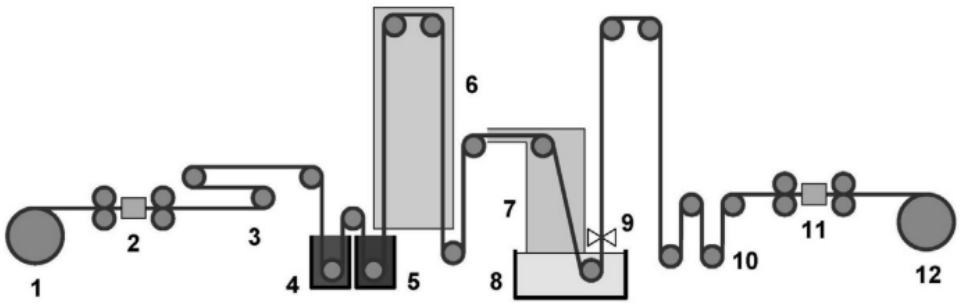

Figure 2.1 Diagram of a line for continuous sheet metal galvanizing. 1. strip unwinding, 2. welding, 3. leveling loop, 4. degreasing, 5. pickling, 6. full annealing, 7. surface activation in a reduction atmosphere, 8. zinc bath, 9. air wiping knives, 10. leveling, 11. shearing, 12. winding the galvanized strip into a coil.

Figure 1: Diagram of a hot dip galvanising line from Kuklík (2016) [5].

2.3 Electro-Galvanising

Electro-galvanising uses electrolysis to coat steel with another metal such as nickel, tin or zinc or an alloy such as zinc-nickel. An electric current is passed through an

electrolyte solution by two electrodes connected to a power supply. The positive zinc electrode (anode) is connected to the positive pole of the power source. The negative steel electrode (cathode) is connected to the negative pole of the power source. The zinc ions move through the electrolyte solution to the steel cathode and are deposited on the surface forming a protective zinc layer. Figure 2 is a diagram of this process. The thickness of the deposited zinc layer is approximately 10 to 20 μm and the process allows great control of thickness [5].

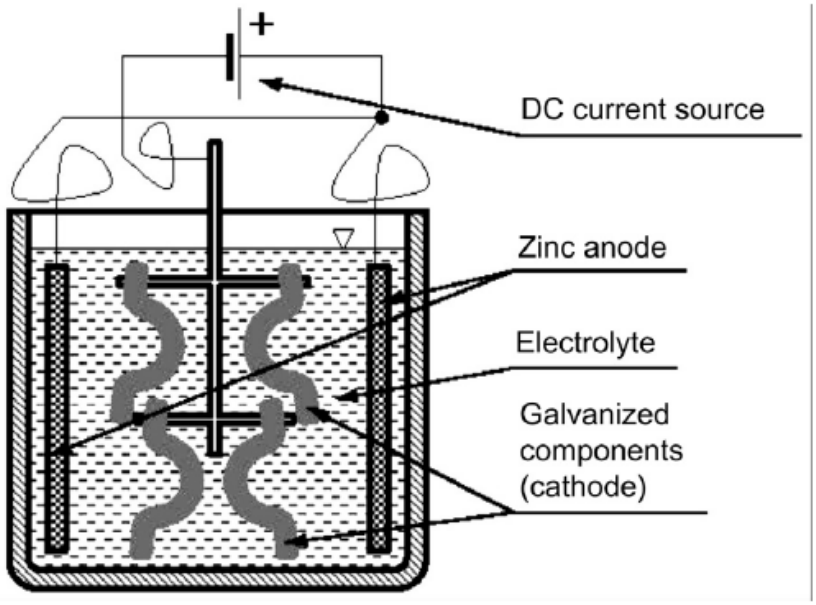

Figure 2: Electro-galvanising zinc plating diagram from Kuklík (2016) [5].

2.4 Problems Associated with Existing Galvanising Methods

Due to their simple production galvanised steels produced from a hot dip galvanising process are cost affective and have high productivity. However, the high coating weight in hot dip galvanising increases cost due to using more zinc [2]. The temperature for hot dip galvanising is normally 460 ^{o}C. The temperature can have a negative effect on the microstructure and mechanical properties of the steel, for example adverse effects from hydrogen diffusion [19]. Conventional galvanisation techniques produce steel that is inconsistently or inadequately coated resulting in bare spots prone to rusting [20]. Modern techniques have been added to hot dip galvanising

to overcome poorly coated Steel. For example the automotive industry increasingly requires high strength and formability steels which enable manufacturers to produce more fuel efficient and lighter weight vehicles [21]. The type of steel used to make vehicles lightweight are called advanced high strength steel (AHSS).

These steels are alloyed with manganese, silicon, and aluminium. A good technique for galvanising AHSS is using pre-oxidation [20]. To produce AHSS Tata developed a pre-oxidation technique on the Zodiac line to wet the surface with zinc. A jet of gas is applied directly onto the steel strip surface at a specific oxygen concentration within the annealing furnace [20]. The gas mixture is applied across the strip surface using newly developed equipment providing an accurate and consistent supply of oxygen, which provides a cost effective and improved coating quality and consistency [16].

Electro-galvanising has the advantage of being performed at lower temperatures, therefore reducing thermal effects seen in hot dip galvanising [19]. Electroplated steel has superior surface quality and thin coating layer but is less competitive due to high energy consumption, low productivity and waste water treatment cost [2]. Electro-galvanising finishes can include the use of toxic metals such as chromium and cadmium, which are a recognised source of global environmental pollution [22]. Cadmium and Chromium VI have been restricted under the Registration Evaluation Authorisation and Restriction of Chemicals (REACH) regulation, which could increase demand on other coating metals. These have been replaced with chromate free coatings in recent years.

2.5 Physical Vapour Deposition (PVD)

Expectations of better quality coatings compared with traditional galvanising processes has led to increased interest in PVD technology. This has resulted in escalated development of ‘high rate’ evaporation processes with better uniform thickness coating [23]. The increasing interest in PVD technology means there is a requirement for commercial PVD lines to be developed. The process is required to be continuous for the PVD coated steel to be competitive against the traditional galvanising methods.

PVD is a thin film coating process where solid metal is vaporised and transported through vacuum conditions and deposited onto a surface. Deposition can be divided into two main processes:

- Droplet transfer (plasma/arc/wire-explosion spraying and detonation gun coating)
- Atom by atom transfer (PVD evaporation ion plating and sputtering, CVD and electrodeposition)

Droplet transfer is disadvantaged by the porosity in the final deposit which effect material properties [24]. Multiple types of PVD technologies are shown in figure 3. Continuous coating has been applied to aluminium, copper and stainless-steel strip using mainly electron beam and sputtering techniques. These processes are not suitable for corrosion resistant coatings on steel strip because of physical limitations of vapour pressure difference and dynamic deposition rate [2] [25]. Magnetron sputtering deposition rates are too low, commercial production of steel strip requires thicker layer and higher production rates. Technologies that are more suitable are electron beam (EB) PVD, jet vapour deposition (JVD) and Electromagnetic Levitation PVD (EML-PVD) [23].

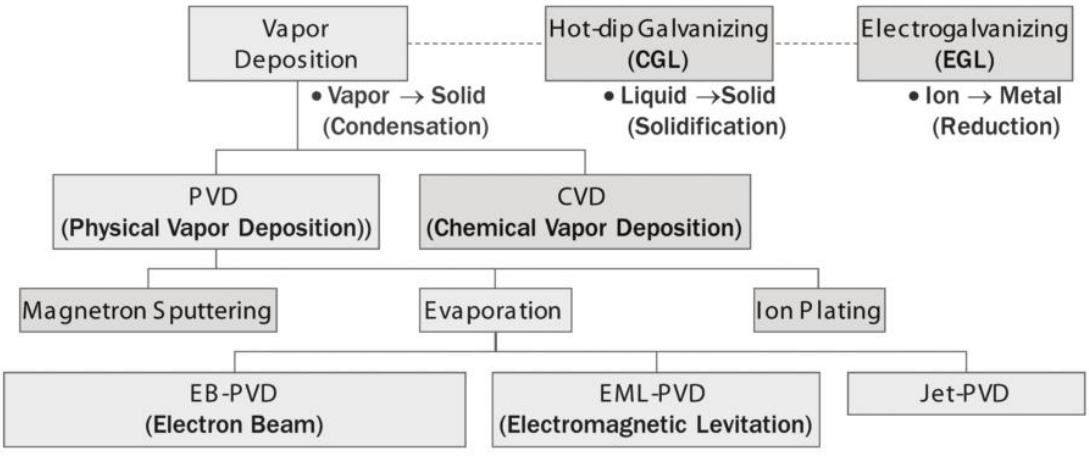

Figure 3: Classification of coating technologies available for steel strip coatings from Kim et al (2013) [2].

2.5.1 JVD Technology

The jet vapour deposition (JVD) process heats metal in a crucible. The vapour generated is transported by a supersonic flow of Argon carrier gas to the strip through a nozzle. The strip is inside a rapidly pumped vacuum chamber [26]. Figure 4 shows an example of a wire fed hot filament jet JVD process. A gold tin alloy wire is heated up by a heated filament coil or rod and is vaporised. The separate gold and tin atoms travel downstream by a jet to the substrate. In addition, a second hot filament produces a high current argon plasma carried by the jet to the substrate, to enable the high rate deposition and also precleans the growing coating film [27]. The coating speed of JVD is relatively high at 100 metres per minute (mpm), the coating control is precise, and the equipment is simple [2].

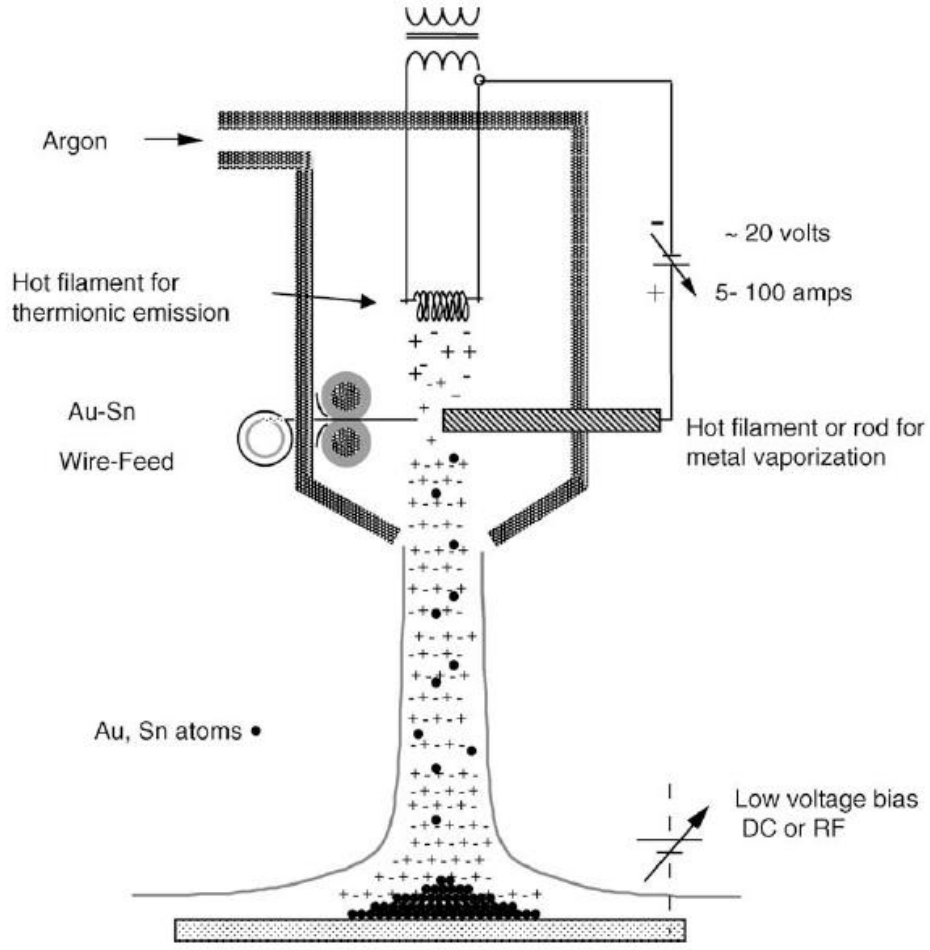

Figure 4: Wire fed hot filament Jet JVD process from Martin (2010) [27]**.**

JVD uses a high vapour distribution system and is therefore deemed a good choice for high vapour yields (over 98%). A drawback is JVD is limited to high vapour pressure and low melting point metals with lower chemical reactivity to container material [23]. Zinc and magnesium have very high vapour pressure and can be applied to jet evaporation for high speed deposition. To produce a Zn-Mg alloy coating jet evaporation requires technical preparation such as vapour mixing preceding to the deposition to use alloy vapour simultaneously from a single evaporation source. Therefore it is difficult to alloy the coating [2].

2.5.2 EB-PVD technology

In the EB PVD process metal is exposed to radiation in a crucible, vapour is generated and then transported to the strip. The process can be used to coat metals and ceramics but has low coating speed of 10 mpm. Figure 5 is an example of double source EB PVD for large area strip coating. The aluminium in the crucibles is bombarded with an electron beam gun on each side causing evaporation of the metal. Two guns are used to generate an evenly distributed layer thickness on the substrate under the conditions of a high vacuum [27] [28].

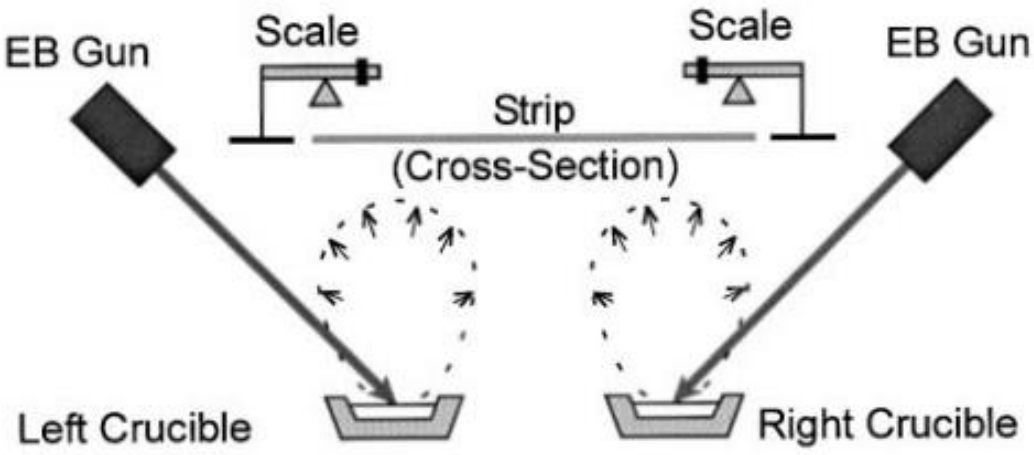

Figure 5: Double source EB PVD for large area strip coating from Reinhold et al (2000) [28]**.**

EB PVD is the preferred method for low vapour pressure and/or high melting point metals because it has precise coating control. EB PVD is an open crucible technology. There is a considerable distance between the evaporating surface and target substrate resulting in low vapour yields (typically max 60 – 80%), which is undesirable when good uniformity of coating thickness is required. The distance is necessary to allow the electron beam to have free access to the evaporating surface [23]. The dynamic deposition of PVD processed corrosion resistant steel should be higher than 450µm/min assuming a thin coating layer with higher corrosion resistance is applied. Hot dip galvanising is above 1000 µm/min and electro-galvanising is around 400µm/min. Converting the dynamic deposition rate to evaporation rate can result in approximately 3-4 kg/min, which is not attainable by electron beam evaporation or sputtering processes [2].

2.5.3 EML-PVD Technology

It has been a difficult challenge for Ijmuiden Technology Centre of Corus Research (now Tata) to develop a vapour source with an equal or higher power density than JVD or EB that can also be combined with a vapour distribution system [23]. A heating technology was required that could efficiently transfer the required energy for heating up and evaporating through the walls of a closed vapour distribution system. The system requires a material that can withstand the high temperatures involved desirably without cooling [23].

The solution found at Ijmuiden was based upon the principle of magnetic levitation. High frequency induction is the most efficient method to pass energy through the ceramic walls of the vapour distribution system, achieving a high power density in the evaporated material [23]. The high frequency magnetic induction field is designed so the evaporated metal is levitated without any direct contact with the walls, heat is only lost to radiation. The vapour produced can only leave the system through the nozzles of the vapour distribution box. The nozzles are placed near to the strip substrate resulting in good vapour application and minimal vapour escaping [23]. EML-PVD combines the advantages of both EB and JVD whilst removing some of the disadvantages that limited their development for industrial steel coating applications.

EML-PVD is has a high coating speed of approximately 200 mpm, high vapour yield and high energy efficiency, making it possible to alloy coatings [2].

Figure 6 shows the EML PVD Evaporation technology. The design utilises an induction coil combined with a high frequency power supply providing an induced current, which heats up the metal droplet inside the coil and levitates it [25]. The vapour distribution box guides the droplet generated surface vapour evenly distributing it onto the steel strip above. The evaporated metal can be replenished by a liquid metal feed from the bottom of the induction coil [25].

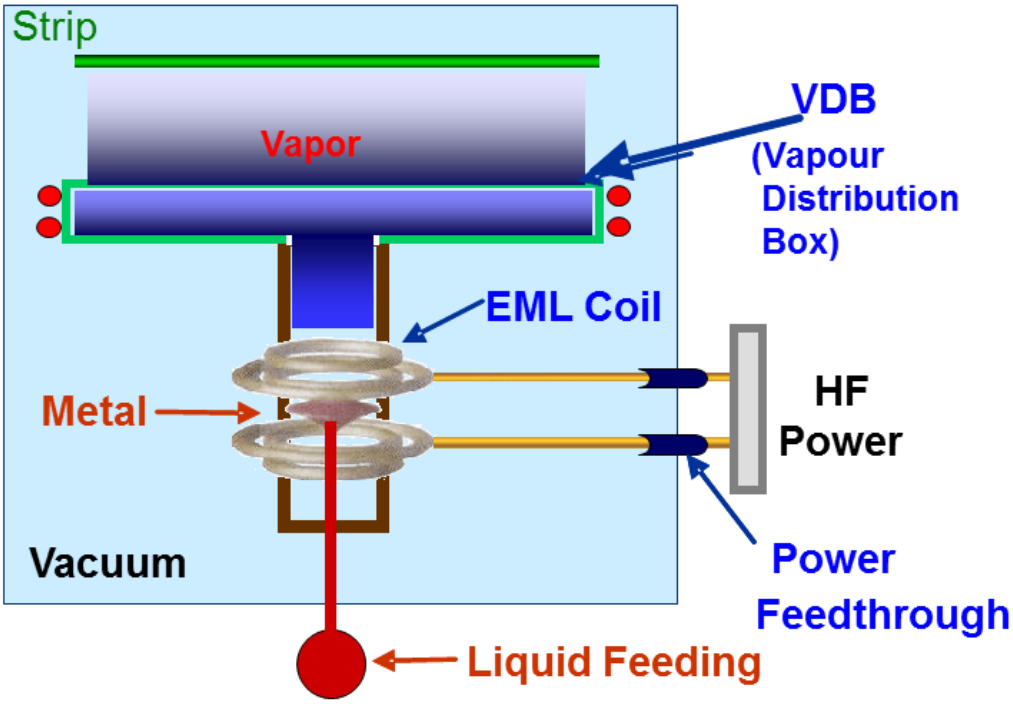

Figure 6: Schematic drawing of the structure of the EML-PVD evaporation from Kim (2011) [25].

The induced current has a third function to uniformly mix the zinc and magnesium in a liquid state to yield a simultaneous co-deposition of the strip by keeping the surface composition the same all the time. The composition of the liquid metal fed from outside the vacuum chamber to the vapour inside can be maintained [25]. The coating applied to the steel strip is an Zn-Mg alloy and Zn layer or a Zn-Mg layer between the substrate and coating layer [29]. The layers provide good corrosion resistance and

adhesion for paint [29]. The good adhesion of the coating to the substrate is desirable in the automotive industry for sheet operations such as drawing and stamping it prevents the coating detaching from the substrate, which results in visible defects or reduces structural integrity [29].

2.6 EML-PVD ZnMg Coating

A Zn-Mg steel alloy has been recognised to produce a layer that is very effective in protecting the steel strip against corrosion. There is a desire to produce PVD with a thin, higher Mg content in the Zn-Mg layer deposited from one evaporation source simultaneously to reduce complexity and cost [25].

Two ways the high corrosion resistant PVD coatings can be produced are:

1. A two-step process, first zinc is deposited onto the steel strip and then pure magnesium. The strip must then be annealed to produce the ZnMg coating with the desired corrosion properties [30].
2. A one step ZnMg deposition process from a single ZnMg source, this can be applied directly onto the steel strip or onto a zinc base coat [30].

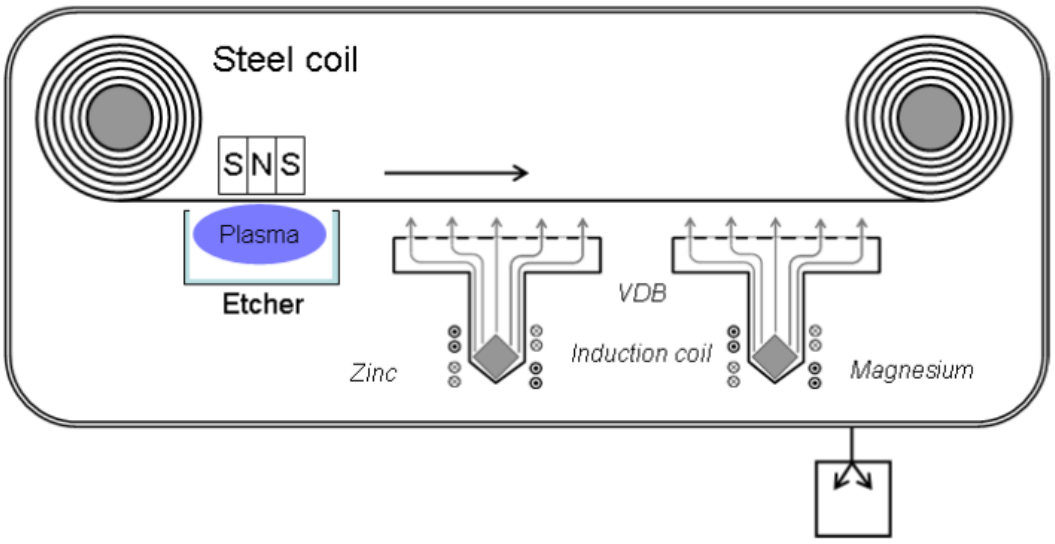

Figure 7: VDB deposition line set up from Zoestbergen et al (2015) [30].

Figure 7 shows the way the VDB is set up in a deposition line. The VDB is heated to 850 ^{o}C prior to deposition to ensure no condensation occurs. The strip is cleaned using a reverse magnetron unit prior to deposition and after being zinc deposited is left to cool down before the magnesium film is deposited [30]. Combined SEM (scanning electron microscope) and XRD (X-Ray Diffraction) results showed that $MgZn_2$ was formed in all samples and a reliable growth constant for $MgZn_2$ phase at 175 ^{o}C was achieved. PVD has potential with good coating characteristics using the batch testing equipment.

2.7 Deposition Coating Temperature

It is important to heat the steel substrate to a suitable temperature when coating steel with zinc vapour and zinc-magnesium vapour. The temperature of 175 ^{o}C above agrees with the investigation into the correct substrate temperature for PVD coating, conducted by Nisshin Steel Company and Mitsubishi Heavy Industries in 1985 [31]. The findings revealed excellent adhesion characteristics for temperatures above 150 ^{o}C and at 250 ^{o}C. Excellent condition occurred when the substrate had become a silvery white colour [31]. The paper on *Diffusion of Zinc and Magnesium in Physical Vapour Deposited Thin Films at 175°C* also studies the behaviour of Zn and Mg within the same temperature range [30]. The paper investigates the ZnMg phases at 175 ^{o}C as PVD is usually carried out at this temperature and paint bake cycles are in the automotive industry are performed between 170 ^{o}C and 200 ^{o}C [30].

In the paper, *Effect of deposition temperature on microstructure, corrosion behavior and adhesion strength of Zn-Mg coatings on mild steel,* La states “as the deposition temperature of coating increased above 100 ^{o}C, the fracture and detachment phenomena of the Zn-Mg coatings during deformation decreased” [16]. Indicating that the adhesion of the Zn-Mg coating depends on the temperature. It has been observed that poor adhesion occurs between Zn-Mg coating and advanced high strength steels. Adding a layer of Zn between the steel and Zn-Mg layer provides a solution to this [17].

2.8 Outcome of the Tata Steel EML-PVD Coating Process

The EML-PVD coating process developed by Tata provides a proof of concept that can be developed into a commercial solution to the problems associated with existing galvanising methods. A thinner coating has been achieved, that has good adhesion and corrosion resistance. The combined coating thickness in the coated samples range between 2.9 and 8.2 μm [30]. This is very thin compared to hot-dip galvanising which is typically 35 to 250 μm and similar to electro-galvanising which is up to 20 μm [5]. The temperature for coating steel using the EML-PVD process is hundreds of degrees lower than hot dip galvanising, 175 ^{o}C compared to 460 ^{o}C, therefore not causing unwanted changes to the microstructure or mechanical properties of the steel.

The process has the potential to overcome the low productivity and wastewater treatment cost associated with electro-galvanising. EML-PVD has high coating speed, high vapour yield and high energy efficiency. This is similar to JVD but with the advantage of being able to alloy the coating and has a coating speed of approximately 200 mpm in comparison to 100 mpm for JVD [2]. EB-PVD has precise coating control and uniformity of coating thickness but with the disadvantage of low coating speed, yield and efficiency. EML-PVD is more suitable to compete with traditional methods of coated steel strip as its yield is close to the capacity of hot dip galvanising. Energy consumption is still a consideration as well at the challenge to upscale the process into continuous coating lines.

3. Vacuum Coating Technology

The EML-PVD process operates under vacuum conditions therefore vacuum technology is required to form a production line. A vacuum is a volume that contains less gas particles, atoms and molecules than in the external atmosphere, therefore a vacuum has lower particle density and gas pressure. Particles in a vacuum are in constant motion, when they hit the walls of a vacuum chamber they exert a force on its surface area, this is known as pressure [32]. The lower the number of gas particles in the system, the lower the pressure and the higher the vacuum. The number of gas particles in a sealed system are removed using vacuum pumps. A break in the seal of a vacuum system results in a leak. A leak is highly undesirable as it increases the pressure and reduces the vacuum.

A continuous PVD coating line requires clearance for steel strip to travel from the outside atmosphere into the vacuum coating chamber and back out the other side. It is critical that the clearances are as tight as possible to minimise the leak and maintain a low pressure in the vacuum coating chamber. This chapter reviews vacuum coating technology currently used to produce a continuous line. Evaluating what has been achieved so far to restrict airflow and what can be improved upon in the existing continuous PVD coating lines and vacuum lock patents. Determining the approach required to develop a new state of the art vacuum lock for the Tata Steels EML-PVD coating process.

An important note to make is that even if suitable vacuum technology exists that could be used for the EML-PVD process it is not necessarily obtainable or cost effective for Tata Steel to procure.

3.1 Creating a Vacuum

To produce a vacuum, the various gases are removed from the contained volume. This is done by using a variety of vacuum pumps [32]. Vacuum pumps can be considered as two classes:

- Vacuum pumps that remove particles from the volume by real pumping into the atmosphere known as compression pumps [32] [33]. The gas particles are pumped by positive displacement using rotary pistons, rotary vanes and trochoid pumps or partial displacement/momentum transfer using fast moving fan/turbine blades or a high velocity jet stream of fluid [34].
- Vacuum pumps that trap particles by binding them through physical or chemical forces are known as condensation and getter pumps [32] [18]. Vapours are pumped away by condensation at very low temperatures using cryopumps or particles are bonded to a surface by adsorption or absorption using sorption pumps [33] [34].

The choice of pump depends on the gas characteristics within the chamber. When gas becomes rarefied and there are much fewer particles it is difficult to extract those particles using compression pumps. At that stage condensation or getter pumps are required. In PVD there is not an abundance of dangerous or reactive gasses, the normal gasses present are argon, nitrogen and oxygen. PVD requires a clean duty primary pump [35].

For experimental or batch type PVD coating the vacuum chamber ranges from a simple bell jar or rectangular box to test rigs and batch line processes. These are sealed systems where the coating is contained within a vacuum system. Vacuums are normally produced in a sealed system. The vacuum system for a continuous production line will not be completely sealed as it requires a clearance for the steel strip to pass continuously in and out of the vacuum chamber. More complex equipment is required for continuous production applications. The equipment for large scale applications consist of a deposition chamber with loading and unloading chambers (vacuum locks) attached to the deposition chambers by manifolds with isolating high vacuum valves [24]. These are referred to as continuous or air to air PVD coating lines.

3.2 Nisshin Mitsubishi Zinc Vapour PVD Line

The first zinc vapour deposition line for steel strip was developed by Nisshin Steel Company and Mitsubishi Heavy Industries in 1985. Steel strip can be coated to a

desired thickness on both sides using this process [31]. Good galvanising was produced even under high pressure to enable reduced processing time. Zinc adhesion is similar when compared with traditional hot dip galvanising. Operational experiments obtained desired results at the pilot plant built at Hanshin Works of Nisshin Steel Company Ltd [31]. In a vacuum sealing system where each vacuum chamber seal each other, the gap should be small as physically possible in order for the flow resistance to increase. To produce a small gap Nisshin and Mitsubishi adopted a pinch-roller type apparatus shown in figure 8.

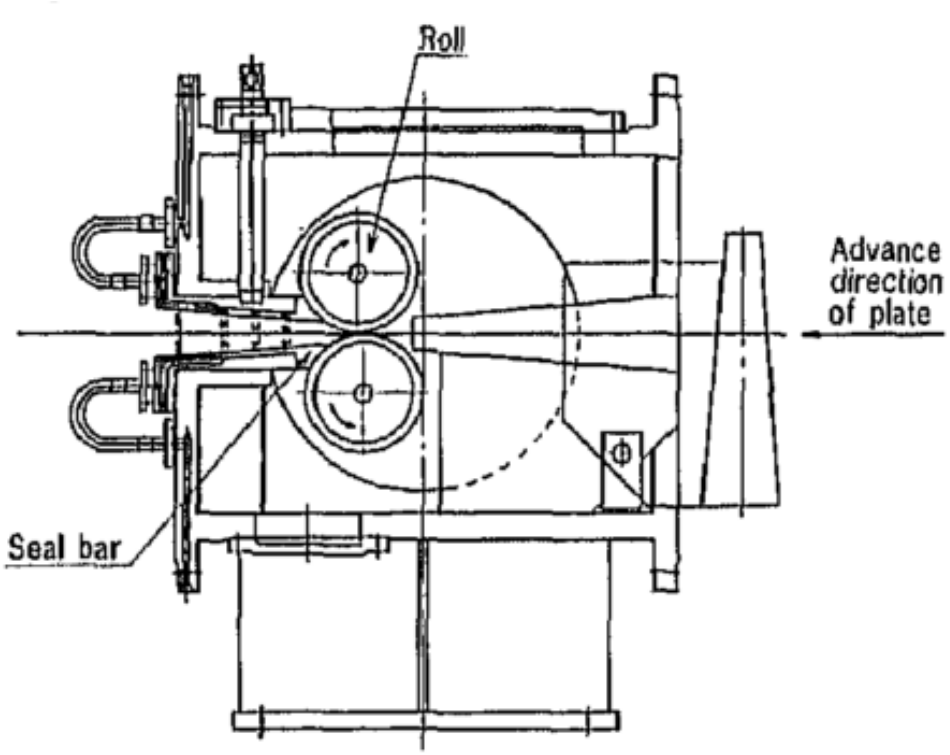

Figure 8: Structural drawing of sealing apparatus from Maeda et al (1985) [31]**.**

Maeda et al (1985), [31], explains the apparatus design works as following:

- The strip is tightly fitted in the two rollers minimising the gap between the strip and the casing.
- Gas is sealed from leakage by a seal bar with narrow and long passages from the upstream side, therefore rolls or strip can be free from flaws.
- The upper roll is designed to be vertically movable to allow for changes in thickness and tracking of the strip.

When transferring an object into the vacuum chamber, Maeda et al (1985), [31], states the vacuum lock operation is as follows.

- The entry lock is opened to the external atmosphere remaining sealed to the vacuum chamber.
- The substrate is introduced into the entry lock.
- The external side of the lock is closed, and the vacuum lock chamber is evacuated by a pump.
- The internal lock side is opened, and the object is transferred from the lock into the vacuum chamber
- The exit lock, the vacuum chamber is opened, and the object is transported inside, with the lock closing afterwards
- The object is withdrawn to the atmosphere from the exit vacuum lock

The steel strip is transported into the continuous vacuum deposition coating process from the external ambient atmospheric pressure (101,325 pascals) to the coating chamber. As the system is not completely closed and has an inlet, external gas always enters the coating chamber, therefore vacuum pumps are mandatory [31]. The vacuum pump compresses low pressure gas and releases it in a high-pressure state. To sustain the vacuum conditions the coating chamber space is subdivided into a number of vacuum chambers [31].

A sealing system uses gas flow resistance to produce a pressure gradient between atmospheric pressure and the coating chamber. A differential evacuation system connects the evacuation system to each of the vacuum chambers [31]. The differential evacuation system is used in order to subsequently reduce pressure and a significant pumping power reduction can be achieved when compared with a single-stage evacuation system; shown in figure 9 [31]. Figure 9 shows the pressure drop in the first lock from atmospheric pressure down to 26,700 Pa (pascals). There are a total of 6 stages (vacuum locks) and the power difference between stage drops and one drop is the difference between 170 kW and 1.7×10^{-5} Pa. This is a significant energy saving.

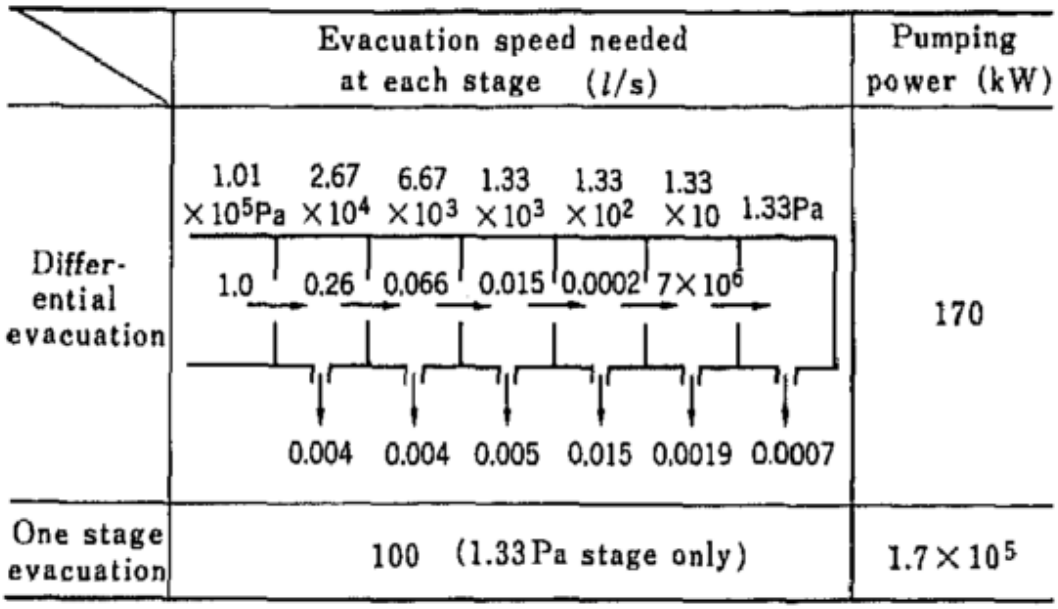

Figure 9: Comparison of throughout characteristics between one stage evacuation and multi-stage evacuation from Maeda et al (1985), [31]**.**

Deposition was performed at varying pressure within the coating chamber. Vacuum vapour deposition was generally performed at pressures of 1.33×10^{-1} to 1.33×10^{-3} Pa. At these pressures, the deposition distance became shorter than the mean path of the vaporised atoms. For a continuous coating line, it is desirable to have higher pressure for the compact design of the system. It was found that excellent zinc deposition can be achieved, even at higher pressures where there is a short mean free path of the vaporised atoms and they tend to have a continuous flow [31].

In a high pressure vacuum chamber, the gas flow through becomes viscous flow and intermediate or molecular flow occurs in low pressure vacuum chambers [31]. Maeda et al (1985), [31], shows that with viscous flow, when upstream pressure P_0 is constant and downstream pressure P_1 is decreased, the passing mass flow rate becomes:

$P_1/P_0 > 0.53$ Flow rate increases with decreasing P_1 (specific heat ratio of gases)

$P_1/P_0 \leq 0.53$ Constant flow rate, in the gap, flow velocity becomes sonic (critical)

When the condition is critical, the flow rate is determined by the upstream pressure P_0 and the area gap [31]. In low pressure vacuum chambers, the mean free path of the gas is equal to or larger than the length of gap in each one of the seals [31]. The Nisshin Mitsubishi Zinc Vapour PVD Line shows some positive achievements in steel strip PVD coating however some important attributes were not mentioned such as line speed, the thickness and widths of the strip and how long the operation can be continuously run. Another important characteristic is although it says continuous, closing and opening of locks are mentioned which means this is a batch process not a constant continuous line.

3.3 POSCO Air to Air PVD Line

An air to air PVD production line or plant allows sheet metal substrate to pass continuously in and out of a vacuum chamber without breaking the vacuum, application for this type of technology has already been established with Aluminium [25]. This time the process is a constant continuous process where the locks are not closed or opened. The locks are continuously open in operation although no time is given so it is not known whether this is for hours, days or months. Kim et al (2013), [2], explains how POSCO have developed an Air to Air production line with the following features:

- The strip enters the line through six lock chambers.
- Upon vacuum entry the steel strip is cleaned and activated by a plasma pre-treatment consisting of Argon (Ar) plasma from six inverse magnetron sputter etchers.
- After pre-treatment there are two separate coating chambers, one electron beam (EB) PVD chamber and one EML-PVD chamber.
- The EB-PVD chamber has two 200kW EB guns each with dual functions of evaporation and steel strip pre-heating.
- In the EML-PVD chamber contains an EML evaporation source of 300 kW with an installation of 1.6 kg of droplet inside.
- The strip exits the process through seven lock chambers out of the vacuum to the exit side of the strip handling and a shear and tension reel.

The production line is capable of a maximum speed of 200 metres per minute (mpm) with a gauge of 300mm wide steel strip and 2mm thick. This has allowed the development of a high output process that can compete with existing coating lines such as continuous galvanising lines (CGL) and electrolytic galvanising lines (EGL) [25]. POSCO has achieved further commercial scale development by installing an air to air PVD pilot plant with a maximum width of 1550mm and maximum line speed of 140 mpm. It allows samples of production for quality evaluation and certification fitting more than 80% of total applications in the automotive, appliances and construction industries [2].

A feature of the pilot plant is that it saves on construction cost of entry and exit sections by being connected to the existing production line. The vacuum zone is connected to an existing production line in order to minimise risk of investment [2]. The vacuum zones consist of three main sections, which are vacuum locks, plasma treatment and EML-PVD coating [2]. The basic principle of the vacuum lock system developed by POSCO is subsequent pressure drops using vacuum locks comprising of two rolls and four seal blocks together with vacuum pumps [2]. Pumping stations use rotary and mechanical booster pumps.

The performance of the vacuum lock system is shown in figure 10, At entry and exit ends of the vacuum lock chamber there is similar pressure regardless of line speed [2]. The vacuum pumping system consists of four types of vacuum pumps, which are rotary, mechanical booster, oil diffusion and turbo-molecular pumps [2]. The vacuum lock section uses rotary and mechanical booster pumps to evacuate the lock. The plasma section contains rotary, mechanical booster and turbo-molecular pumps. The coating section has rotary, mechanical booster and oil diffusion pumps [2]. Each sections pumping system can evacuate the process chamber below 5×10^{-3} Pa and there is minimal deviation detected with the strip running [2].

The full width pilot plant has been installed and successfully commissioned allowing a full range of PVD research facilities in POSCO. Fundamental outputs from the narrow width PVD pilot plant validated their application to strip coating and the commercial production is to be proven with the wide width pilot plant [2]. With the

strip running the pressure of the vacuum zone in the wide width plant remained very stable, indicating that the designed pressure decoupling works correctly [2].

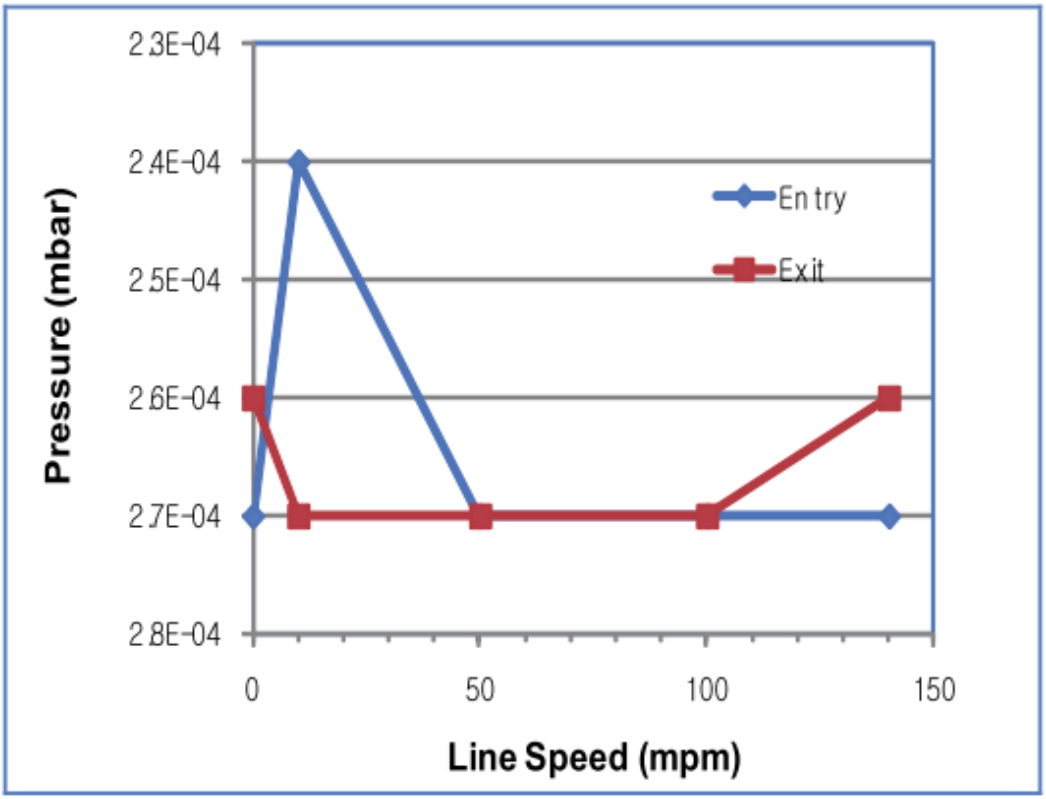

Figure 10: Dependence of pressure decoupling performance of vacuum-lock system with variation of line speed from Kim et al (2013) [2].

3.4 Vacuum Locks

Vacuum locks are mentioned as a main section of the air to air PVD line. Unlike a batch system where the coating line is completely sealed air to air or continuous PVD lines are open to the atmosphere. Vacuum locks are required to maintain the required pressure difference between the vacuum chamber and the outside atmosphere. A traditional vacuum lock consists of an adjacent chamber to the vacuum system, which can be opened to the external atmosphere or to the vacuum system. Vapour deposition has been in operation for decades and over time different types of vacuum lock technologies have been produced. Air bearing technology is being introduced claiming to reduce the required pumping capacity although this is currently with foil or glass products.

The requirements for the vacuum lock for the EML-PVD process requested by Tata Steel are:

- Provide continuous transport of steel strip continuously into and out of the coating chamber.
- Maintain an operating pressure of 0.01 Pa inside the coating chamber.
- Able to accommodate varying widths and thicknesses.

Traditional and air bearing patents will be reviewed in this section and then the technology will be discussed to determine the development of a state of the art design.

3.5 Review of Traditional Vacuum Locks

For the purpose of this investigation traditional vacuum locks are associated with locks that do not include air bearings. A review of traditional vacuum locks was conducted analysing the claims to gain information on the operation of locks. The mechanisms, clearances, operating pressures and geometry of substrate are of specific interest to aid the development of the design requirements for the state of the art lock. Problems with vacuum lock designs have been flagged in the patent literature. Coolen (2011), [36] and Hein (2013), [37] review of previous designs concluded that:

- Most existing designs have not resulted in industrial implementation.
- Most batch processes avoid locks and are contained within a sealed unit
- There is an inability to maintain equipment.
- Vacuum lock housing is limited in height and access is difficult.
- Difficult insertion of the strip into the vacuum lock
- Some inventions require the vacuum lock to be completely dismantled to check the state of the rollers.
- Leakage causes vacuum losses resulting in high consumption of electricity and more pumping power required.
- The thermal expansion of the rollers in length due to the heated steel strip may result in seizing due to the contact with the lateral walls of the chamber.

- Pneumatically inflatable tube pressed against the substrate, do not maintain good contact with the substrate, which can spoil the finish and may rupture under stress.
- Inflatable belts between the rollers to fill lateral gaps when inflated can increase on one side applying pressure on the substrate.
- If conveyor belts are used in contact with the substrate the passage gap is reduced but are now in constant contact of substrate, which then requires maintenance to regularly replace the belt
- If the substrate is transported between only one cylinder and a sealing block, a complete sealing might not be obtained

It is important to acknowledge the previous design flaws and avoid them. In the patents vacuum locks are sometimes referred to as air locks. Next in this chapter is a review of traditional vacuum lock patents that claim to be for continuous processes or have overcome problems associated with older designs.

3.5.1 Patent DE 4240488 C1

Title: Apparatus for reducing pressure in feeding channels leading to treatment chamber – using vacuum pumps connected in series to gradually reduce the pressure from atmospheric to the pressure required [38].

The objective of the invention in figure 11 is to provide a cost-effective solution to evacuate steel strip locks with multiple pressure stages and valves to maintain the vacuum of the treating chamber and strip sealing gates [38]. The band valves (rollers) are inserted in pairs at entry and exit of the treatment chamber, located in the space between the belt valves (rollers) through a valve coupled to the pump system of the treatment chamber and or through a further valve that serves to evacuate one of the higher-pressure stage vacuum pumps [38]. The vacuum treatment chamber is also vented. Adjacent pressure levels can be maintained under vacuum by the inventive arrangement of the belt locks. The intermediate space through a valve to the treatment chamber roots pump is connected so that the pressure stages can be left when the system is under vacuum [38].

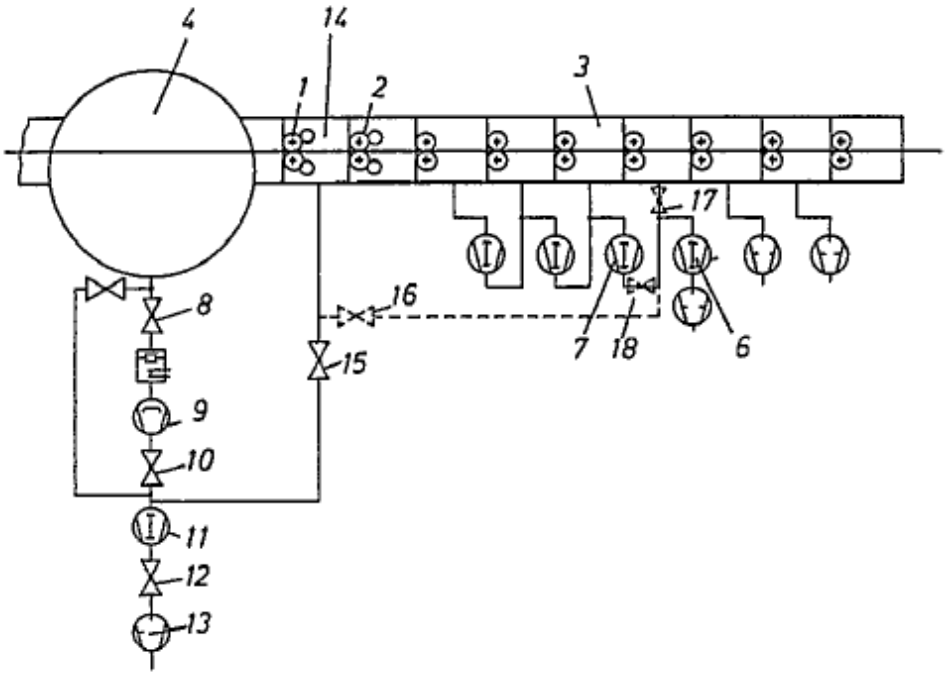

Figure 11: Band valve arrangement with an upstream band lock and downstream processing chamber from Erbkamm et al (1992) [38]**.**

Erbkamm et al (1992) patent claims are limited, important points are:

- Valve arrangement is important for maintaining a vacuum and reducing pumping requirement.
- The arrangement of separated band valves and pumps aid evacuation of the chamber by having several pressure stages gradually reducing from atmospheric pressure in the first stage to target pressure in the coating chamber.
- A root pump is connected in the intermediate space (empty space in the chamber) by a valve at the higher pressure stage (initial stage entry lock).
- A root pump is connected in the intermediate space by a valve at the treatment chamber (initial stage entry lock).
- A root pump is connected in the intermediate space by a Ven valve at the third pressure stage (third lock).
- The rollers are arranged in pairs immediately before and after the treatment chamber allowing band widths of 800mm wide and 0.5 mm thick. Previously

0.5mm thickness would cause to much air leaking into the system for diffusion pumps to operate.

- The treatment chamber has a diffusion pump connected to lower the pressure further.
- Multiple pressure stages provide a cost saving solution.

Erbkamm states that “It has also been shown that with increasing strip thickness there is a progressive increase in the leak”. This is because as the strip thickness increases the gaps between the rollers increase and without additional features to block the air path the air ingress into the lock increases. The arrangement of the paired band valves (rollers) allows an implied thickness of 0.5mm. The lock arrangement uses separate chambers to provide subsequent pressure stages. Separate connected locks have been utilised in the existing PVD lines and stated in patents including this one. The exact information of how the band valve pairs help with increased steel thickness is not clearly defined. There is also no mention of the invention handling varying widths and thicknesses.

3.5.2 Patent DE 4240489 C1

Title: System for feeding strip into treatment chamber - has rollers operating valve system between different pressure stages [39].

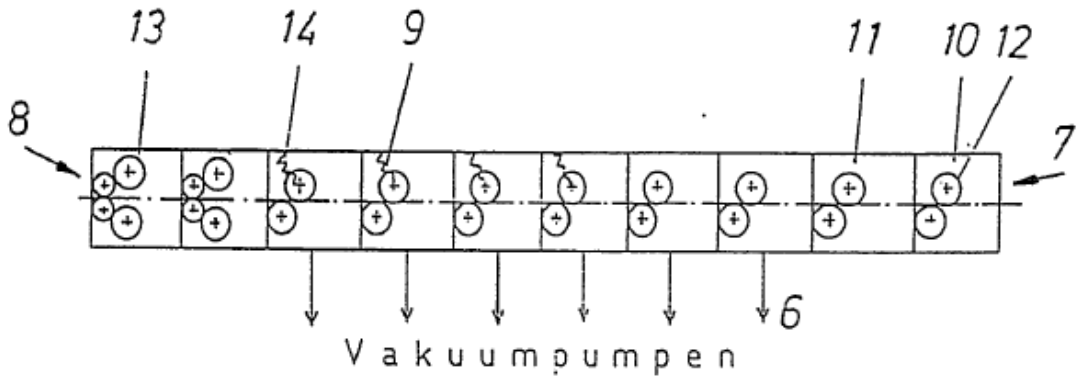

Figure 12: Band valve assembly from Erbkamm et al (1994) [39]**.**

The invention in figure 12 relates to a multiple roller belt lock assembly of step-down pressure stages with the entry lock starting at atmospheric pressure. The rollers are

sealed radially and laterally relative to the housing, the upper roller has vertical movement and the lower roller is rigid [39]. Each pressure stage is connected to a vacuum pump to gradually decrease the pressure to gain the target pressure of the processing chamber. This is well-known arrangement used for feeding strip material into and out of coating chambers. The roll seals must provide pressure onto the steel strip to generate sufficient flow resistance and extremely slight leakage, but not at consequence to damage the surface to the strip material or applied coating [39]. To ensure adequate sealing contact, the upper rollers use a tension or compression spring to provide enough force acting on the strip. Uneven loading can cause surface damage. The object of this invention is to provide a reliable strip lock arrangement under all operating conditions including all pressure differentials, strip gauges and widths [39].

This invention is an improvement on the previous design DE4240489 and the claims from Erbkamm et al (1994) [39] are:

- For the entry lock arrangement. An additional strip sealing gate is used in which the upper roller is provided with an additional force generating element. the additional pressure gate is filled with inert gas.
- Upper rollers at all printing stages, press on the strip with torque greater than the sum of the acceleration and friction of the roller.
- Force equalisation is controlled by a springs of adjustable spring force. A constant pressing can be provided by selecting the appropriate characteristics for the spring and can also be provided for varying thickness.
- The bearing force does not deviate or exceed a maximum of 10% on the individual upper rollers, resulting in a near constant pressing force.
- In the outer band locks next to the open orifice to atmospheric pressure (first and last) provide a pressure compensation.
- Solution to damaging the surface is the weight or pressure compensation are equal or only slightly different than each other.
- The roller size of the inner band locks can be reduced as lower weight is required to provide pressure as less force is required to seal the strip and choke to flow.

- Over the first two locks there is a difference of 13000 Pa from atmospheric pressure giving an approximate pressure of 88,325 Pa in the second lock.
- The vacuum lock preceding the coating chamber is 5 Pa (compression stage)
- The solution provides a high reliability even with varying thickness of strip and damage to the surface is safely excluded.

The patent does claim to provide a reliable solution for coating varying widths and thicknesses of steel strip. The invention mentions a sealing gate used in the entry lock filled with inert gas to restrict leaks into the lock, this could prove useful in the state of the art design. The coating chamber pressure is not revealed however the second lock pressure is given as 88,325 Pa and the lock preceding the chamber is stated as 5 Pa. The arrangement of the roller is now offset rather than vertically above and with this arrangement enough pressure is applied to the strip with pressing force being adjusted including the use of springs to ensure no damage occurs as a result. The dimensions for the varying width and thicknesses are not disclosed.

3.5.3 Patent US 6334751 B1

Title: Air Lock

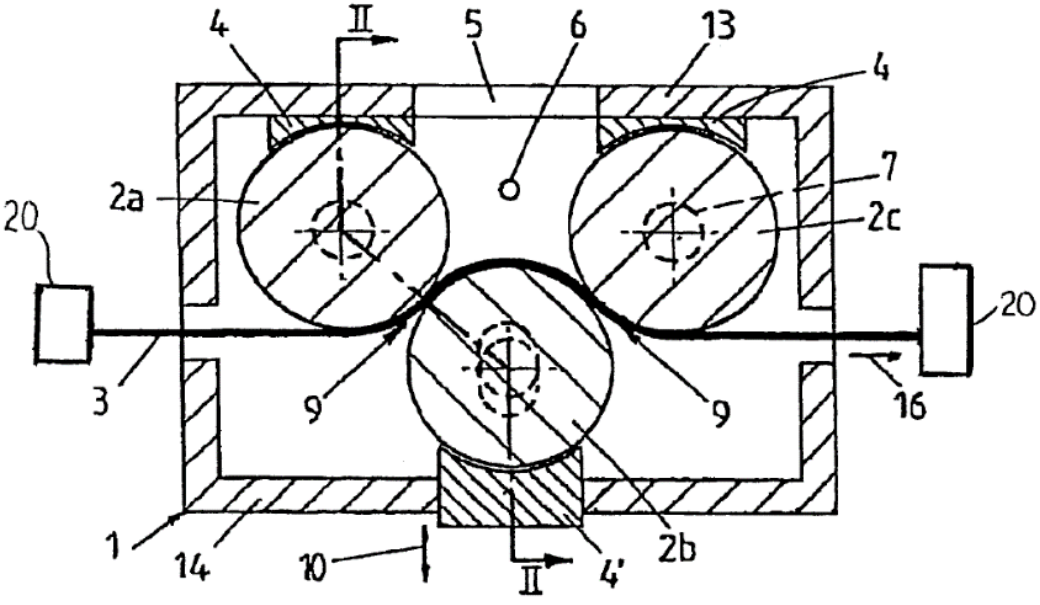

Figure 13: Longitudinal section of a first embodiment of the air lock from Donckel (2002), [39]

The purpose of this invention is to provide a minimum sized air lock that achieves maximum air tightness. Rollers are mounted and rotate around parallel axes. The enclosure contains at least three successive rollers in the direction of transport of the strip. The first and third roller are placed on one side of the passage and the second roller on the opposite side shown in figure 13. Air tightness is ensured by minimal clearance between the side of the rollers and the wall of the chamber and a minimal clearance between the rollers and sealing members (shoes) [40]. The main restriction to airflow is provided by the set pressure contact between the strip and the rollers.

The only significant leakage occurs in the area at the side of the strip (slots) between the cylindrical part of the rollers, and at the side walls of the chamber between the flat ends of the rollers. Leaks are inevitable and a vacuum pump is used to compensate for them. Roller bearings for the second roller are mounted to allow slight vertical movement, also the corresponding sealing member (shoe) to this roller is also free to slide vertically. To ensure air tightness in the region between roller one and three where the pump is attached, there should be balance between the pressure difference in this region and the surrounding regions [40].

The performance of the air lock depends on the strip thickness. For a pressure difference of 50,000 Pa, a roller of with a diameter of 600 mm and strip thickness of 1 mm, the tension to be exerted on the strip should be 3000 kg in the direction of travel. This works out as 3 kg/mm^3. If the strip is 0.5 mm thick then the tension should be double to 6 kg/mm^3 and if restricted to 6 kg/mm^3 as the maximum tension, a strip of 0.25 mm thick would only provide air tightness to maximum pressure difference of 25,000 Pa [40]. In the second embodiment of the air lock (figure 14) more successive rollers provide more regions to overcome the maximum pressure difference of the first arrangement. This further steps down the pressure providing additional air tightness.

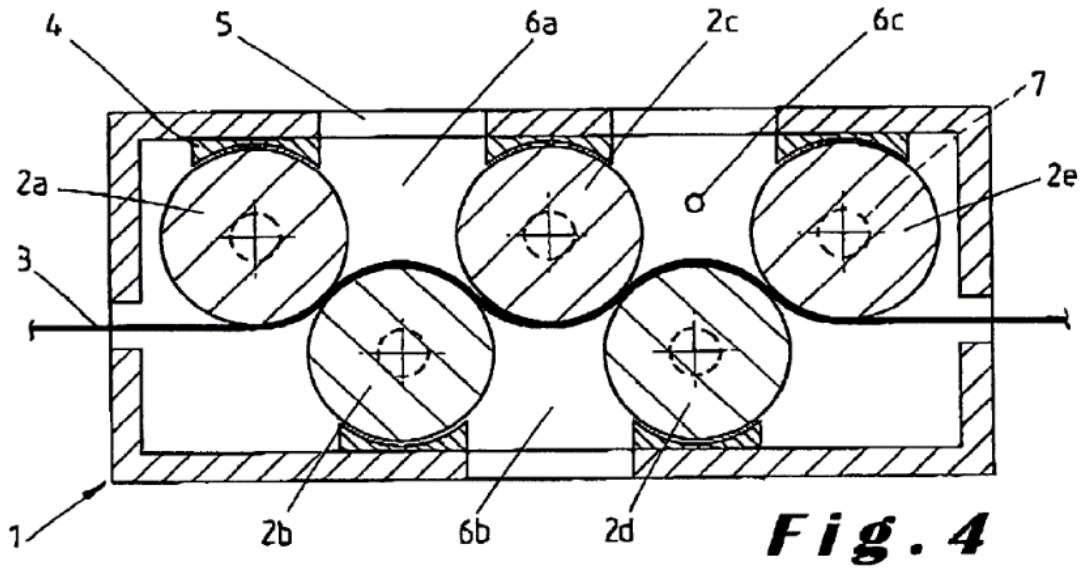

Figure 14: Second embodiment longitudinal section of air lock with more rollers Donckel (2002), [39]

Donckel (2002), [40], claims of the invention as follows:

- The air lock permits steel strip to continuously pass both in and out of the vacuum chamber.
- An airtight seal is created between the first and third roller, with a vacuum pump connected.
- The diameter of the metal rollers is generally identical for all three, which is high enough not to cause any plastic deformation. For a metal strip of 1mm thickness, the diameter is 600 mm
- The vertical movement in the bearing mounted roller allows adjustment for varying strip thicknesses.
- An adjustable component is provided to apply pressure to the strip resting on the rollers.
- The sealing members are made of Teflon but could also be manufactured from metal.
- A clearance of 0.2 mm is achieved between the rollers and sealing members.
- To minimise the leakage the bearings that allow the rollers to rotate are placed inside the rollers reducing the clearance between the roller and the chamber wall.

The roller arrangement within this air lock invention allows for varying thicknesses. To avoid plastic deformation larger rollers are required for increased thickness, this is due to the offset of the roller bending the strip as it passes through. Contact pressure restricts air passing through the steel strip and the roller, this combined with minimal clearance is something important to consider in the state of the art design for minimising leaks and reducing electrical consumption. The clearance of 0.2mm is useful for determining achievable space between a roller and sealing member. A value of 50,000 Pa is given for 1mm thick strip, this is useful information for potential performance characteristics that should be obtained in a new design.

3.5.4 Patent EP 1862567 A2

Title: Method of a sealing chamber and sluice device for a vacuum chamber

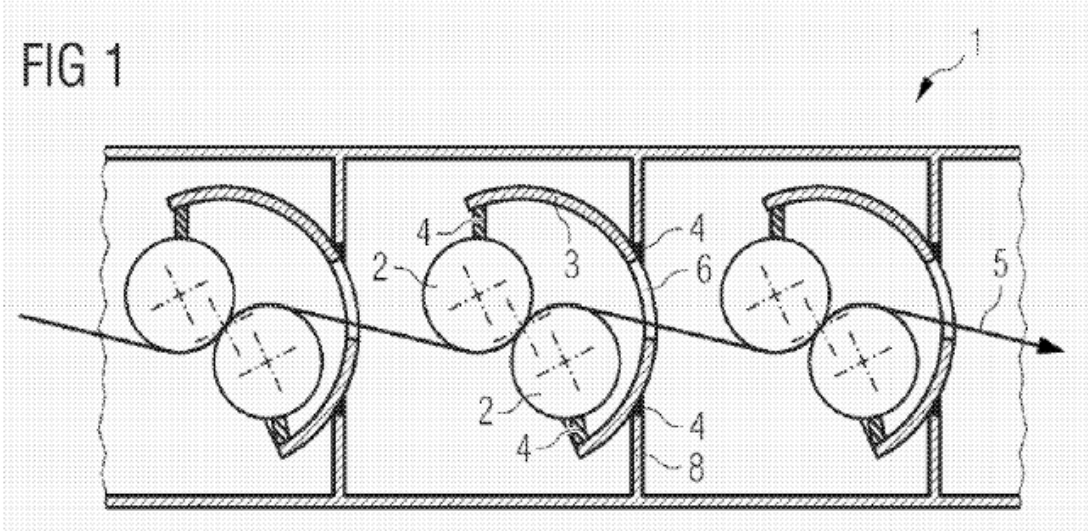

Figure 15: First embodiment of the lock device showing the wrap angle of the substrate around the rollers from Gottsmann et al (2007) [41].

The design in figure 15 shows an arrangement of vacuum locks comprising of multiple sealing rollers that are mounted on rotatable brackets allowing flexible movement. The basic principle of the design is to obstruct air flow by a sealing the gap both between the belt and roller as well as the inlet and outlet container [41]. Sealing rollers can have a rubber or metallic surface. Rollers with a rubber surface have limited thermal stability whereas rollers with a metallic surface have better thermal resilience and can

be water cooled internally. A disadvantage of metallic surface rollers is the required traction between the strip and the roll (the roll driven without external drive passively from the strip). Comparatively thick strip requires a very large roller diameter to avoid damage to the strip due to excessive curvature [41]. Only acceptable tension (material dependent) may be used for thin strip, if values are increased damage can occur. The invention can accommodate varying strip thicknesses including thin strip with low belt pull and large tolerable bending strain and thick strip with high belt pull and low tolerable bending strains.

Important claims of the invention according to Gottsmann et al (2007) [41] are:

- The innovative roller arrangement where:
  - Rollers are rotatably mounted in pairs with strip passing through a respective axis of rotation.
  - Strip passage characterised by the wrap angle between the strip and each roller by rotating the roller pairs.
  - Roller pairs are adjusted relative to the transport direction of the strip so that the forces acting between the strip and the frictional force of the rollers result in rotational movement of the rollers.
  - The transport speed of the strip and the rollers are equal.
- Internal moveable panels allow adjustment of the passage width to the same as the width of the strip, useful for changing strip widths.
- The adjustable sluice makes it possible to open a single lock of the system without having to stop the entire process for maintenance, for example dirty rollers
- In the case of non-uniform strip thickness one roller can apply pressure by using a pneumatic cylinder, configured spring or other suitable means.
- A control system for the rotation of each roller pair can be provided that measures the strain or tensile force of the strip.

This is a more complex design than other traditional locks due to the rollers mounted on a rotating bracket. The system allows for varying strip thicknesses. Internal moveable panels provide resistance to air leaking into the system when changing the

strip widths, the type of feature could be developed in the state of the art design. A sluice makes maintenance of a lock possible without stopping the line ensuring continuous running. It is stated that relatively thick strip requires larger rollers. The dimensions of the varying widths and thicknesses are not revealed. the vacuum pressure achieved by the system is not mentioned.

3.5.5 Patent WO 2008104169 A1

Title: Method and apparatus for the treatment of strip-shaped substrate in a vacuum coating system.

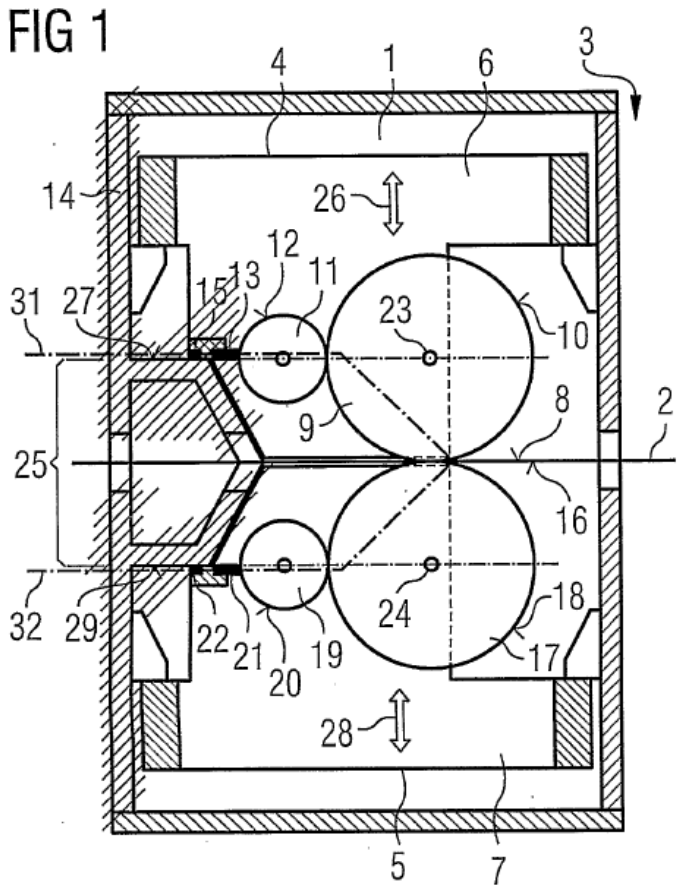

Figure 16: First embodiment with a sealing an intermediate roller and additional sealing surface from Gottsmann et al (2008) [42]**.**

The patent explains in previous inventions a complete lock change is only possible by cutting the substrate and stopping the run. An aim of the invention is to be able to sustain continuous operation, with strip entering from the open atmosphere into the

vacuum and exit after coating [42]. The invention shown in figure 16 allows the upper and lower roller of the lock chamber to be operated separately. All components related to the upper and lower lock systems are mounted on a separate base frame. Contact with the strip can be completely removed during operation if required by moving the locks [42]. The upper lock has an upper base frame and the lower lock has a lower base frame arranged separately from each other. The base frames each respectively accommodate the entire sheath component [42]. Upper and lower locks have a housing seal connected to the base frame. The central axes of the upper and lower sealing roll have a variable distance from one another.

The rollers have a steel surface or other similar hard material that allows the strips to glide through without damaging the surface of the strip [42]. The upper base frame has a top of the substrate sealing roll and on the outer surface of that roller an intermediate sealing roller with an upper sealing strip. Acting on the housing of the upper seal, connected to the lower base frame [42]. The underside of the substrate is sealed by the lower roller with an intermediate roller that has a lower outer sealing strip, the lower seal is connected to a housing. The distance between the lower and upper sealing roll is variable at the central axes and set at the minimum distance depending on the sealing surface of the housing seal [42].

According to Gottsmann et al (2008) [42] the claims of the invention are:

- The upper or lower lock can be changed, without cutting the strip
- It is possible to open the lock during operation without changing parameters of the overall system.
- Contact with the strip can be removed.
- Different substrate widths can be used in production without interruption.
- The lock can be disabled in operation without affecting the substrate.
- The diameter of the wear seal roller is variable even if grinding of the jacket surface of the sealing rollers occurs.
- For rollers with a casing surface of flexible material, remapping of the sealing rolls for flexible material is possible, for example a new rubber coating.

In this invention the design allows larger deviations between strip widths using the additional sealing surface but does not state the exact dimensions of the strip widths. Varying thicknesses are not mentioned although the nature of with the rollers mounted on separate base frames it would it possible to maintain the control of the pressure on different thicknesses, sealing out leaks would then be another challenge. The pressure obtained with this embodiment of lock design was not stated and with the patent.

3.5.6 Patent US 7931750 B2

Title: Sealing lock for a deposition line in vacuum on a flat product

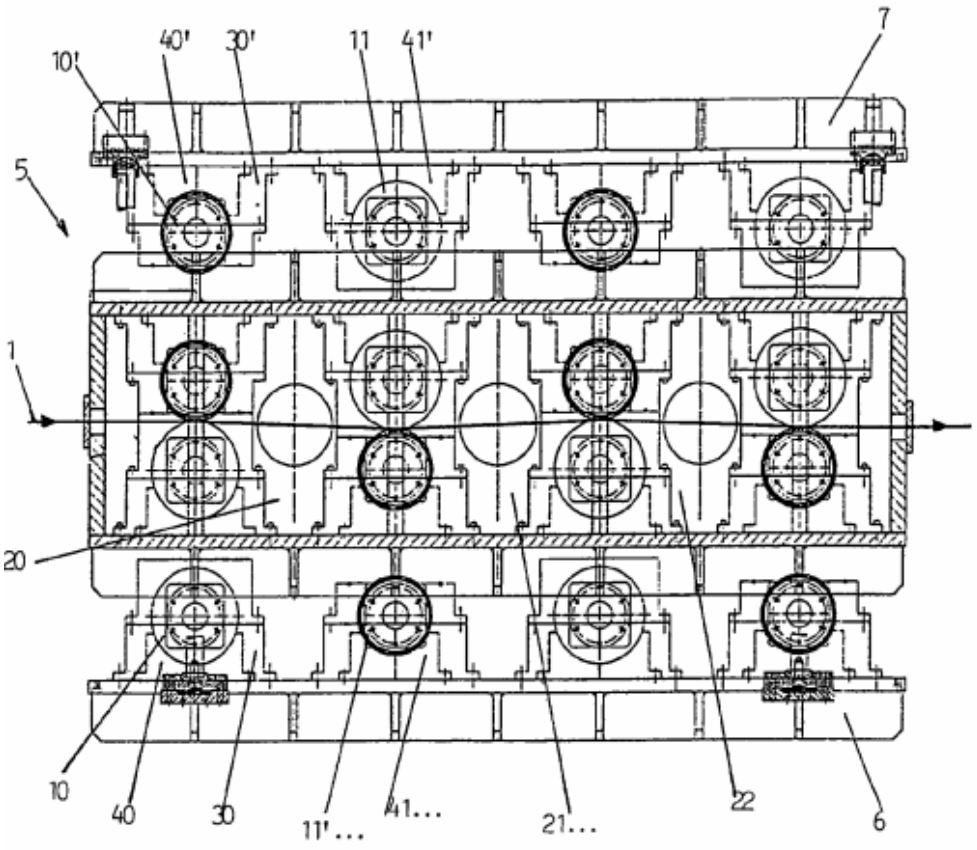

Figure 17: Vertical and longitudinal cross-section view of a sealing lock for a vacuum deposition chamber from Coolen (2011) [36]**.**

The diagram in figure 17, is a sealing lock arrangement of 9 large metal rollers mounted on bearings and fixed to detachable covers. The rollers are arranged in staggered rows establishing 7 sub-chambers each connected to a pumping system. This

is contained inside a vacuum chamber for a continuous deposition process on steel strip [36]. Large metal rollers are mounted on bearings and fixed to the covers (detachable). The adjacent roller of the pair has the axes arranged in the same vertical plane with a smaller diameter (coated with rubber or elastomer). The position of the smaller diameter roller is alternated up and down on passing from one pair to the next pair. The support cradles for the two rollers of the same pair have a lateral projection towards the centre, the spacing of the base to the rollers defines a second gap [36].

Coolen (2011), [36], summarises the claims of the invention as:

- Provides an inlet and outlet sealing lock for a continuous deposition line process for carbon steel or stainless-steel strip.
- Designed to provide low maintenance for insertion of the strip and access to the rollers.
- The nature of how the rollers are placed and the angle direction changes of the strip produces a good seal allowing better pumping performance.
- Enough traction is produced to overcome the difference in pressure between two successive chambers. Significant contact pressure between the roller and the strip avoids the strip lifting off from the roller.
- Eliminates rollers seizing with the expansion of metal parts and prevent wear of the rollers by providing an additional rubber coating
- Reduced electrical energy consumption minimising equipment.
- The invention allows the lowest pressure in a sub-chamber to be lower than 0.01 Pa and can preferably achieve 0.001 Pa.

This invention claims to have achieved the pressure that is required for the EML-PVD process (0.01 Pa), this clearly indicates that it is possible to produce a vacuum lock capable of achieving the required pressure. This is an improvement to the continuous Nisshin Mitsubishi PVD line and similar to the air to air POSCO line. The roller arrangement allows good contact with the steel strip and roller avoiding the steel strip lifting off from the roller, therefore creating a good seal stopping air passing through. It does not state the invention can accommodate varying width or thicknesses of strip.

3.5.7 Patent US 8499784 B2

Title: Lock valve in particular for strip processing unit

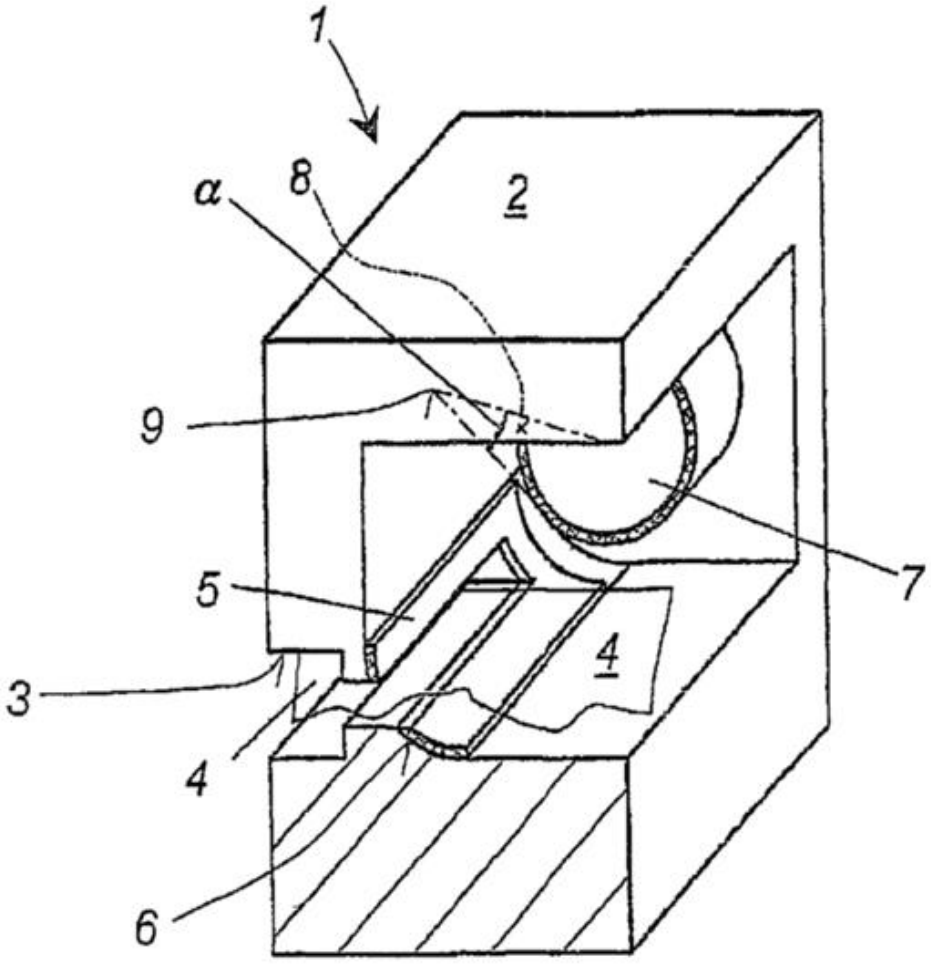

Figure 18: Partial cut through section of the air-lock valve from Hein (2013) [37].

The purpose of the patented invention in figure 18 is to provide an addition air-lock valve for static sealing purposes, in order to reduce or eliminate the problems with previous lock designs [37]. To improve the air-lock valve, a frame like sealing face (label 5 in Figure 18) is formed which surrounds the opening through which the band substrate passes [37]. The Air lock valve is designed especially for band processing plant and Hein (2013), [37] patent claims include:

- It provides closing for a gap-like opening. The air opening gap can be larger. So that with an open valve the substrate is not of risk of contact with the edges of the opening. Damages of coatings and band ruptures are therefore largely excluded.
- Traversed by a flexible band substrate between two different plant sections, with at least one moveable sealable body.
- The body may be pressed upon the sealing surface and/or the band substrate, traversing the opening obstructing it at least to indirect juxtaposition (positioned close together) at the edges of the sealing surface.
- Upon closing the opening, the band substrate is firmly mounted by the roller and the sealing surfaces.
- During closing of the air-lock valve, the sealing surface surrounds the opening in order to close the opening.
- A fluidic pressure operated valve is not required as it was with tube designs. With this type of configuration uneven pressure or too much stress on the substrate can be avoided.
- It is possible to assemble the sealing surface along the corresponding sealing body or valve body, in the operating area (unrolling and rolling up modules) to be periodically ventilated. The atmospheric pressure will press the valve or sealing body correspondingly firmer upon the sealing surface.

The patent gives the embodiment of the design claiming that the sealing face provides good contact with the substrate without damaging it. The sealing between one roller and sealing block has been achieved with this design whereas previously it has not been possible, however this vacuum lock is designed for a flexible band such as plastics, foils, magnetic tapes or films. Steel strip is less flexible. This type of lock design may not be suitable. The patent does not give information on whether this design could accommodate varying widths or thicknesses, an operating pressure is not given and the number of locks are not specified.

3.5.8 Patent US 8926756 B2

Title: Strip passing apparatus for treating surface of strip with the same, and method for treating surface of strip [7].

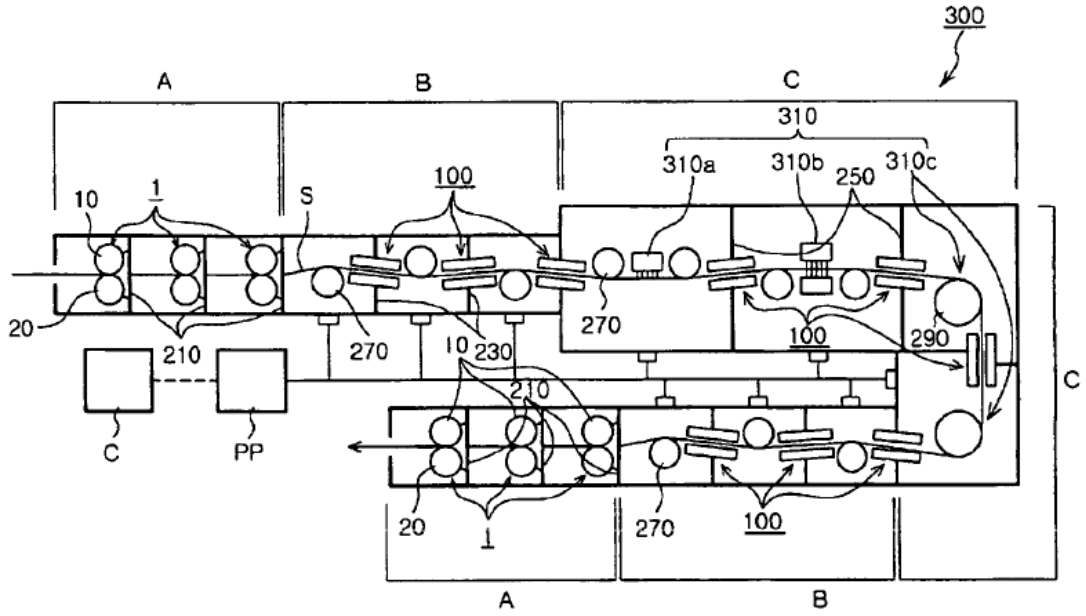

Figure 19: Configuration diagram of a sealing and masking type apparatus from Lee et al (2015) [7]**.**

Vacuum deposition is currently being utilised in the semi-conductor, display, electronic, IT, and solar industries to generate high quality products. Regardless of which material is used the process has to be performed under vacuum conditions, consequently the process has limitations and is difficult to maintain the required conditions [7]. A system where the strip can be continuously coated with deposition by maintaining the vacuum conditions using a sealing mechanism is actively sought. There are existing locks that allow strip to pass from atmospheric pressure into a vacuum at high speed. The conventional sealing locks seal a strip under a vacuum, using sealing rolls within a casing structure and have a multistage arrangement.

The limitation with most conventional designs is that they struggle with continuous variation in widths and gauges of strip. Incomplete sealing of the strip also results in excessive electrical consumption and therefor some existing sealing locks are

uneconomical. It is difficult to use varying widths and gauges of strip in the conventional multistage arrangement of a continuous array of zigzag shaped sealing rolls. The mechanism has a precise structure with narrow gaps between the sealing mechanisms resulting in complicated manufacturing and difficult maintenance and repairs, without providing enough sealing [7].

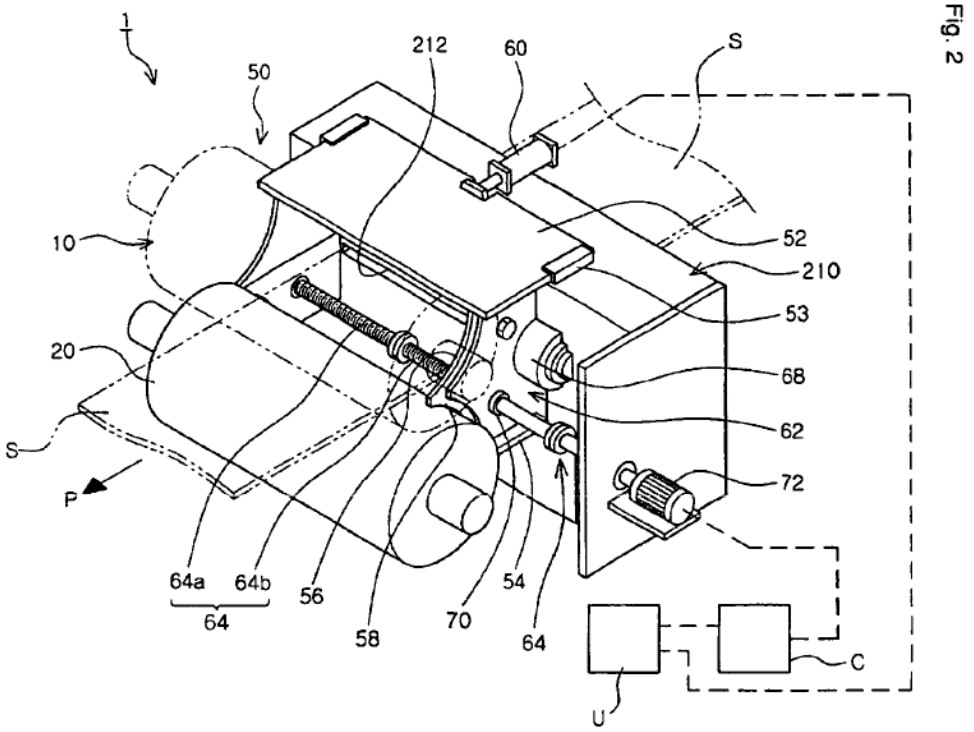

Figure 20: Perspective view of the sealing apparatus from Lee et al (2015) [7]**.**

The invention by Lee et al (2015), [7] shown in figures 19 and 20 consist of upper and lower sealing rolls allowing the transport of varying gauges of strip and a strip sealing unit for variations in width. Lee et al (2015), [7], summarises the invention characteristics as the following:

- The upper sealing roll bearing is connected to a vertical screw bar passing through a gear box, connected to a driving motor allowing movement for the steel of varying gauge to pass.
- A second driving motor is connected to the roll bearing, a vertical driving cylinder and an electrical actuator could be used as the second driving source.

- A strip sealing unit for the varying width and gauge of the strip, with a sealing plate restricting the air space around the strip.
- The sealing plates move as the thickness of the strip changes and remains 5 to 20mm distance away from the edge of the strip.
- The strip sealing unit co-operates with upper and lower sealing rolls to seal the strip through the chamber surrounding the proceeding strip.
- A masking unit covering the gap between the strip and the sealing case for varying widths and gauges.
- The sealing case has a box structure with a hole for the strip to pass through, which varies between an approximate distance of 0.5 and 1mm from the flat surface of the strip.
- A masking plate with a clearance of 3 to 20mm to the edge of the strip (depending on strip speed) restricts clearance for air flow as the width changes.

The claims for the invention from Lee et al (2015), [7], are the following:

- The apparatus for treating the strip can operate across viscous, intermediate and molecular flow regions.
- The present invention allows the strip to pass continuously under vacuum remaining tightly sealed with negligible vacuum loss therefore not requiring continuous or excessive vacuum pumping to maintain the desired pressure.
- The apparatus can be simplified as the strip is sealed in the divided regions between atmospheric pressure and viscous flow, differential pressure and intermediate molecular flow and differential pressure and the vacuum space.
- The strip can continuously pass through the tightly sealed space resulting in improved quality of the deposition, more productivity due to high speed transport and therefore a superior product that is economically feasible.

This invention uses a simple rather than complex arrangement seen in some of the existing vacuum locks. It uses two offset rollers like in the Erbkamm invention. Sealing plates have been used to restrict the space as the strip widths change and the rollers adjust for thickness. The obtaining pressures are not disclosed here but the molecular flow region is mentioned therefore it could be possible to exceed the

requirement of 0.01 Pa, but no evidence is given. The plates would still wear and require maintenance and the interval for this is not disclosed. The claims of the performance of this invention indicate it may be possible to create a state of the art design that complies with Tata Steels requirements as it claims varying width and thicknesses are possible whilst achieving free molecular flow.

3.6 Review of Air Bearing Vacuum Locks

Air bearing locks are used for more delicate substrate that requires minimal or no surface contact. The difference between air bearing locks and traditional locks, is instead of using rollers to transport the substrate, high pressured air bearings are installed within the apparatus that allow the substrate to be transported through without surface contact.

3.6.1 Patent WO 2007/016688 A1

Title: Method and device for depositing a film of material or otherwise processing or inspecting, a substrate as it passes through a vacuum environment, guided by a plurality of opposing and balanced air bearing lands and sealed by differentially pumped grooves and sealing lands in a non-contact matter.

Figure 21 represents an apparatus invented for Coating and deposition of surfaces on a glass or flexible substrate, such as films and thin glass sheets or other similar work pieces [43]. The substrate is transported through small gaps of aero-static or hydrostatic porous media bearings and grooves, which constrain the substrate in a non-contact manner. A natural equalising force provided by the bearings puts the substrate back into equilibrium if displacement occurs [43]. Grooves are axially placed relative to the substrate equally on both sides and are differentially pumped creating a vacuum environment [43]. The bearings accomplish a substantially lower pressure chamber allowing the substrate to be vacuum processed, both chambers (upper and lower) are maintained at 530 Pa [43].

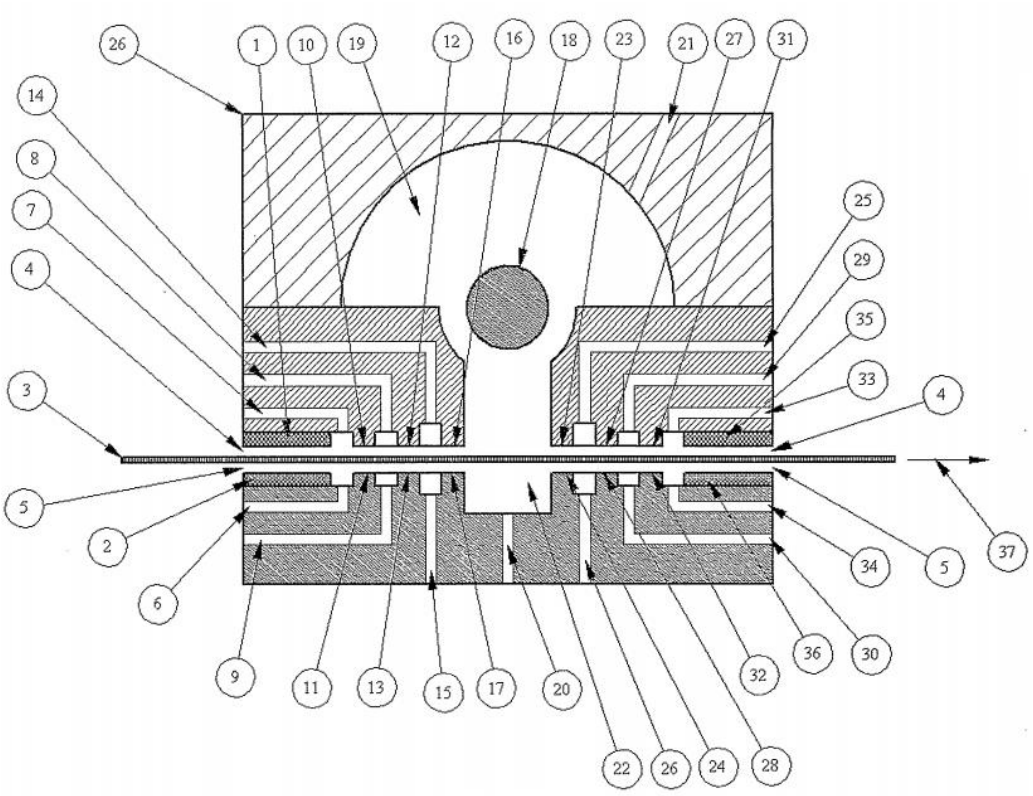

Figure 21: Schematic view of a CVD process with the substrate between vertically opposed aerostatic bearings from Devitt (2007) [43]**.**

The outlet of the chamber is identical to the inlet, the substrate leaves the lower pressure chamber through a series of grooves equal in size and number to the first set, they are arrayed to bring the substrate back to ambient pressure and temperature. At the same time the pressure chamber is sealed from air particles, contamination and fluctuations in temperature [43]. The invention is intended for deposition of glass and delicate materials; however, the design achieves very good coating characteristics.

The maintained pressure of 530 Pa is not low enough for Tata steels 0.01 Pa requirement and higher than values given in the PVD lines. The pressure stated is for the maintained pressure in the chamber but does not state the pressure reductions in consecutive chambers produced by the air bars. Devitt (2007) does claim that the bearings achieve a substantially lower pressure chamber but does not give a comparison. The natural equalising force from the air bearings overcomes uneven pressure applied to the substrates which has been a previous problem. The frictionless free transport also ensures that the coating will not get damaged by abrasion.

3.6.2 Patent US 8123868 B2

Title: Method and apparatus for in-line processing and immediately sequential or simultaneous processing of flat and flexible substrates through viscous shear in thin cross section gaps for the manufacture of micro-electronic circuits for displays.

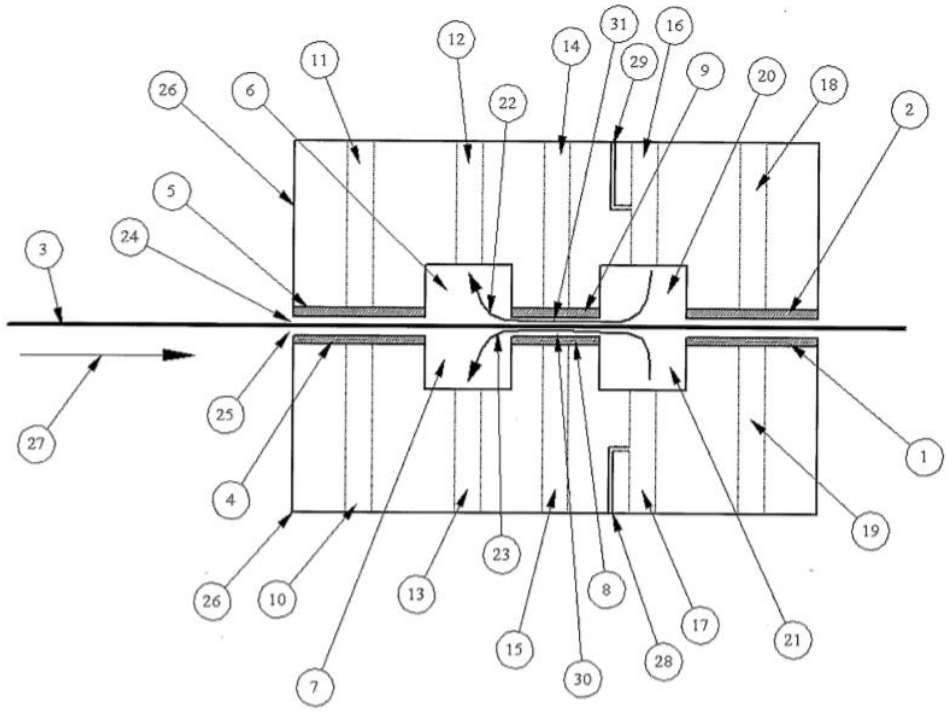

Figure 22: Schematic view of a substrate between vertically opposed hydrostatic bearings from Devitt (2012) [44]**.**

The apparatus in figure 22 is used to clean, dry, coat, bake and etch glass for the flat panel display (FPD), window elements, solar elements, integrated circuit and panel circuit board industries [44]. There are two horizontal inline and vertically opposed porous media or fluid bearings, substantially wider and longer than the selected substrate [44]. Multiple holes and gas passages provide transport for air or fluid to be forced through from behind the porous media. The substrate is constrained using orifice, capillary and step bearings, using different types of fluids. Bearings are situated horizontally and vertically opposed to each other and parallel to create a thin gap, large enough to allow the substrate to flow between them. The porous media bearing used operates at pressures up to 60 psi [44].

The pressured air flow from the porous media on two opposing sides results in the substrate remaining static between the bearings, also non-contact disposition to the porous media. If the substrate displaces off the midpoint towards one of the bearings, there is a natural equalising force due to the pressure lowering as the gap increases and the now smaller opposite gap increases in pressure, this forces the substrate back into equilibrium [44]. There is no deflection or risk of breaking the fragile substrate as the pressure is even on both sides of the substrate. There is a second set of grooves that supply fluid onto the substrate and act as hydrostatic bearings; these have a substantially higher pressure than the first set of grooves.

The invention uses air bearing to reduce pressure for coating but also includes other processes that are specific to the substrates and not used for steel. The coating pressure is not given and the claims are similar to Devitt (2007). The air bearing concept of frictionless transport with an equalising force are something to be considered in the state of the art design. The operating pressure of the air bearings is useful for later on when it comes to simulating the additional added pressure from the air bearings.

3.7 State of the Art Vacuum Lock Requirements

Vacuum locks for continuous substrate coating are a specialist technology. It is therefore unsurprising that there is limited amount of literature available on vacuum locks and most of the literature is in the form of patents. The information in the patents was limited. Patents are supposed to be purposely vague and not give away much information but include enough to hold intellectual property. Copying a patent is known as an infringement, this can be true even if the infringement only falls within in the scope of the patent claims. Care needs to be taken not to infringe on the reviewed patents. In the patent literature there was limited information on achievable pressure. Some values were given for pressure changes between locks, the preceding lock of the coating chamber or the overall achievable pressure by the apparatus. Pressures were given at every individual stage for the Nisshin Mitsubishi lock arrangement in figure 9 which is useful but that is a batch line not fully continuous.

Out of the available literature most of the inventions were the traditional style vacuum locks and there were very few air bearing inventions. The air bearing inventions were

linked to New Way® air bearings. The traditional vacuum locks produced pressures that matched or exceeded Tata Steels EML-PVD requirements for example patent US 7931750 B2 could maintain 0.01 Pa, maintains good contact with the strip, the rollers do not seize and apply even pressure to the strip. A disadvantage of US 7931750 B2 it that there is no claim of being able to accommodate strip of varying width and thicknesses. An invention that claims to provide the varying width and thicknesses of steel strip is patent DE 4240489 C1. The final achievable pressure for this invention was not disclosed. This is also the case for patent US 8926756 B2 that claims to overcome existing problems providing continuous coating of steel strip of varying widths and thicknesses but does not state the achievable vacuum pressure. Although the exact pressures are not defined in all traditional vacuum locks, it is implied that they are suitable to provide suitable vacuum conditions for the vacuum coating chamber.

For maintaining an efficient and sustainable vacuum a sequential connected lock arrangement is seen in all the patents apart from patent US 8499784 B2, however the patent does not state the system will only have one lock. Most patents use two or more rollers to provide adequate sealing between the strip and the roller completely restricting air flow through. Variable thickness has been achieved so far by moveable rollers using springs, mounts, slots or being offset horizontally. The clearances between the edge of the strip and the rollers caused by variable widths are sealed using physical features such as plates, rubber coatings on the rollers or additional band material. Sealing members or housing is used between the circumference of the rollers and the sides of the chamber. The clearance between the side of the roller and the chamber walls are restricted with the bearings inserted into the rollers and some patents use the sealing plates.

The physical features all introduce more mechanical parts into the vacuum lock system that will require for inspection and maintenance. The intervals for this will vary depending on ease of access and the design. The air bearing locks remove the requirement for additional mechanisms due to the tight clearances that can be achieved due to the frictionless transport. The air bearing system has been developed for flexible substates and the stiffness of the steel strip could possibly be an issue if the steel does

not enter the lock parallel to the air bearing and abrasion occurs. This would depend on the roller arrangement, if the steel strip is transported flat and not bent around rollers then there is no reason to consider abrasion of the steel strip against the air bearings. From the literature search a steel strip air bearing lock was not discovered and joining concepts from the traditional inventions combining them with air bearing system for steel strip is understood to be a new direction in the field.

After reviewing the existing inventions. The requirements for a state of the art vacuum locks must be able to accommodate varying widths and thicknesses whilst remaining in continuous operation. Sustain the pressure required for reliable coating. Require minimal maintenance that does not interfere with operation and reduce electrical consumption to maximise efficiency. To develop the state of the art vacuum locks that can fulfil all these requirements. Air bearing technology will be incorporated with computational modelling to evaluate concepts.

4. Theory of Low-Pressure Fluid Dynamics

A mathematical model is required to simulate physical processes computationally. Governing equations are applied in computational simulation software to predict the physical events. Care must be taken to understand the physics that is required to be solved. It is important that the correct boundary conditions and right mathematical models are used to solve the problem. The nature of the gas must be determined to know whether to analyse microscopic or macroscopic behaviour of the system. Microscopic behaviour determines the position, velocity and interaction of every atom or molecule [45]. This level of information is not always required as the macroscopic properties of pressure, temperature and volume are normally sufficient to solve a fluid flow problem. Engineering software tends to aim at solving fluid mechanic problems that occur in atmospheric pressure using the Navier Stokes equations. For example, hot and cold fluids mixing in a pipe or air flow over an aerofoil.

It is improbable that conventional CFD methods are suitable for the low pressure conditions present within the vacuum lock. It was anticipated that the fluid flow problem requires analysis of the microscopic behaviour to determine the flow characteristics. The EML-PVD coating line operates in low pressures containing far less gas atoms and molecules than in atmospheric conditions. To provide an accurate analysis for the state of the art vacuum lock, the theory of low pressure fluid dynamics is reviewed to determine what mathematical models to apply and find suitable engineering simulation software for the analysis. First the characteristic of the gas flow needs to be determined.

4.1 Knudsen Number and Characterisation of Gas Flow

The Knudsen number (K_n) is generally used as the governing parameter for the analysis and the characterisation of gas flow. The Knudsen number is defined as the ratio of the mean free path in a flow to the characteristic length of a body immersed in the flow. [8] [46] [47].

$$K_n = \frac{\lambda}{L} \tag{4.1}$$

λ = Mean free path

L = Characteristic length

Characteristic length is defined as the length that is of most interest or importance in the flow. If the flow is divided up into a grid of mesh. The characteristic length of the mesh is where flow is considered to have the most influence. If there is an area of refined mesh that is of particular interest, the average mesh length in that focused area.

The Mean free path is the average distance a gas particle travels before colliding with another particle shown in equation 4.2 [48] [49].

$$\lambda = \frac{1}{\sqrt{2}\,\pi\sigma^2 n} \tag{4.2}$$

n = Number density (number of particles)

σ = Effective diameter of the molecule

The Knudsen number allows approximate estimation of the flow pattern in a system, by specifying the degree of rarefied gas [46]. Rarefied gas is gas with a pressure much lower than atmospheric pressure. There are less gas atoms and molecules in a low pressured gas. Figure 23 gives a visual representation of how equations of fluid flow are linked to the Knudsen number. The Boltzmann Equation can be applied for all Knudsen numbers whereas the other equations can only be applied to specific values.

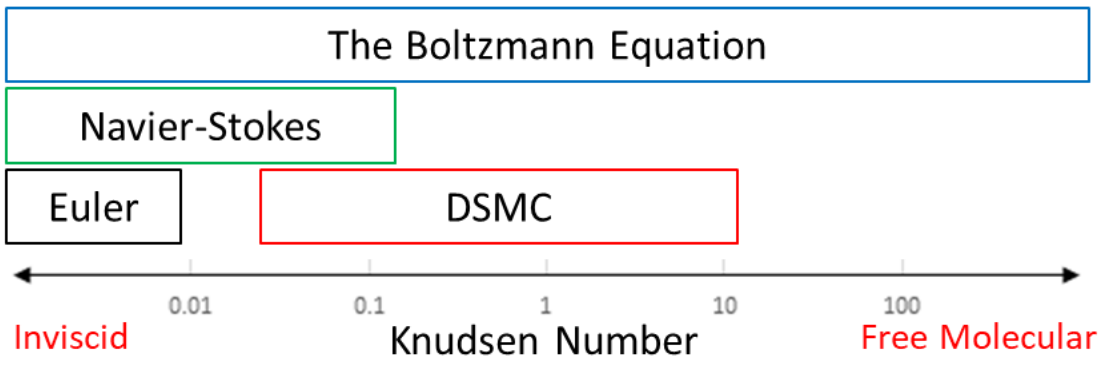

Figure 23: Equations that analyse flow depending on the Knudsen number

4.2 Gas Flow Regime

The Knudsen number can be used to distinguish the regime of gas flow. The flow regime is a description of the fluid behaviour. For lower Knudsen numbers the flow regime can be considered in a continuum medium where all the gas particles are equally distributed in the region occupied. For larger Knudsen number particles can be considered to move independently from one another known as a free molecular flow regime [50]. Table 1 shows the calculation methods that are suitable depending on the Knudsen values and then the flow regimes are explained in more detail.

Table 1: Knudsen range and flow behaviour [51] [52]**.**

Regime	Calculation Method	Knudsen Range
Continuum flow	Navier – Stokes with non-slip boundary conditions	$K_n < 0.001$
Slip flow	Navier – Stokes with slip boundary conditions	$0.001 < K_n < 0.01$
Transition flow	DSMC	$0.1 < K_n < 10$
Free molecular flow	DSMC	$K_n > 10$

4.2.1 Continuum Regime

The Navier-Stokes equations give an excellent approximation for gas flows that are very close to equilibrium. The equations assume that the local macro properties of the fluid are averaged over elements that are large compared to the microscopic structure, but are small enough with respect to the macroscopic conditions to allow differential calculus [53]. At low Knudsen numbers ($K_n < 0.001$), internal flows the molecules rarely collide with the walls and flow is determined by enough intermolecular collisions occurring to reach local thermodynamic equilibrium in a very short time when compared with the macroscopic time scale [53] [54]. This results in the gas being

in local equilibrium and the molecules having a Maxwellian velocity distribution [54]. For a zero Knudsen number, molecular diffusion can be ignored, and the Navier-Stoke equations are reduced to inviscid Euler equations, the transport terms in the momentum and energy equations become negligible [53] [55]. The N-S transport terms that include the coefficients of viscosity, heat conduction and diffusion break down for increased Knudsen numbers [8] [46].

4.2.2 Slip Regime

As the Knudsen number increases, molecule surface interactions become less frequent and non-equilibrium regions start to appear near surfaces. This can be viewed macroscopically and the continuum equations remain valid if the gas velocity and temperature at a surface do no obtain the same values as the surface itself [8] [53]. This is known as velocity slip and temperature jump. If this occurs, the validity of the Navier-Stoke equations can be extended to the slip regime by applying Maxwell's velocity slip and Smoluchowski's temperature-jump boundary conditions [53].

4.2.3 Transition and Free Molecular Regimes

In the transition and free molecular regimes, the non-equilibrium effects are substantial, therefore the conditions are no longer continuum and the Navier-Stokes equations are no longer valid as the shear tensor and heat flux are now unusable (37) [54]. For low pressure flows where the mean free path λ becomes large or flows that have a very small dimension, the molecules travel a significant distance between collisions compared to characteristic length L [54]. For internal flow this means there are more frequent wall interactions and this is an important for description of the flow [54]. In this situation the Boltzmann equation is required to accurately describe the flow behaviour. Examples of this type of flow are micro scale geometries (micro-channels) and hypersonic flows, particularly at low temperatures [53].

PVD coating line pressures range from atmospheric to vacuum levels. The flow regime varies from the entry lock to the coating chamber. One form of analysis for the entire system will not work and both a continuum and free molecular methods are required to simulate the different stages of flow. When the lock is further developed into a

complete system the analysis will require these steps to be taken or a complete experimental rig built and tested to gain results on performance and what vacuum can be achieved.

4.3 Governing Equations of Fluid Flow

Governing equations are used to form the mathematical model of fluid flow. The Boltzmann equation is a traditional mathematical method for solving microscopic gas flows. In kinetic theory molecular flow can be described in terms of position, velocity and internal state of every molecule at an instant. The Boltzmann equation is denoted by equation 4.3 taken from Shang (2013) [56].

$$\frac{\partial(nf)}{\partial t} = c\frac{\partial(nf)}{\partial r} = +F\frac{\partial(nf)}{\partial c} = \int_{-\infty}^{+\infty}\int_{0}^{4\pi} n^2(f^* f_i^* - ff)c_r \sigma d\Omega dc_i \qquad (4.3)$$

n = number density

f = velocity distribution function

c = velocity

f^* = post collision velocity distribution function

c_i = velocity of other molecules

f_i = velocity distribution function of other molecules

c_r = relative velocity

$\sigma d\Omega$ = differential of collision cross section

The Boltzmann equation is complex and hard to solve. The right hand side of the equation is a form of integral-differential that requires 7 variables to be solved simultaneously [45]. The solution is to use computational molecular models that can run direct numerical simulations directly from physical properties of gases [56]. The direct numerical simulations use a numerical method to solve the Boltzmann equation instead of solving it directly. Determining the most suitable

numerical method depends on the Knudsen number and corresponding flow regime.

4.3.1 Navier-Stoke Equations

As previously mentioned Navier Stokes equations are used to solve fluid flow in the continuum region. The kinetic theory of gases considers gas as a large number of molecules in controlled volume. At rest the molecules are in equilibrium, heat is transferred into kinetic energy resulting in constant motion and collisions [57]. The intermolecular collisions are considered perfectly elastic, the molecules are considered as hard spheres that do not deform when colliding [58]. Engineering analysis in general is more concerned with the macroscopic fluid behaviour than individual molecular details. To remove complexity, fluid is considered as a continuum, this is a valid approach when only the macroscopic characteristics of fluid behaviour is required [57].

For fluid flows analysed at a macroscopic level (1μm or larger) the molecular structure and molecular motions can be ignored [59]. The Navier-Stoke equations are used to analyse compressible and incompressible flow. The behaviour of gas is described by its macroscopic properties' velocity, pressure, density and temperature including their space and time derivatives. These might be thought as averages of over large numbers molecules. The governing equations of fluid flow are mathematical representations of the conservation laws of physics [59].

- Conservation of mass of the fluid
- Conservation of momentum – (Newton's second law) The sum of external forces acing on a fluid particle equals the rate of change of momentum
- Conservation of energy – (First Law of Thermodynamics) The Rate of change of energy equals the rate additional heat and rate of work done on a particle of fluid

The physics of fluids and heat transfer of continuum mechanics is well established and can be derived from the first law of thermodynamics as shown in Chung 2010 [60].

Equation (4.4) was derived from the conservation of mass in all directions taken from Versteeg and Malalasekera [59].

Compressible Continuity Equation in Cartesian coordinates:

$$\frac{\partial \rho}{\partial t} + \frac{\partial (\rho u)}{\partial x} + \frac{\partial (\rho v)}{\partial y} + \frac{\partial (\rho w)}{\partial z} = 0 \tag{4.4}$$

The equation can also be written in vector notation using the del operator shown in equation (4.5) [59].

Compressible Continuity Equation:

$$\frac{\partial \rho}{\partial t} + \vec{\nabla}.\left(\rho \vec{V}\right) = 0 \tag{4.5}$$

The momentum and energy equations for compressible flow are not documented here as the analysis is considering incompressible flow, if it is determined that flow is compressible then the literature for the simulation software will be used to cover the different flow conditions. In Newtonian fluids the stress tensor is linearly proportional to the strain rate tensor. In incompressible flow density ρ is constant and flow is assumed to be isothermal (local changes in temperature are small or non-existent, resulting in no requirement for a differential energy equation. Consequently, dynamic μ and kinematic viscosity ν are constant. [61].

For incompressible fluids, density is not a function of time and space if the flow is approximated as incompressible. Density (ρ) from the continuity equation can be taken outside the divergence operator resulting in equation (4.6) from Çengel (2006) [61].

$$\vec{\nabla}.\vec{V} = 0 \tag{4.6}$$

Incompressible Navier–Stokes equation:

$$\rho \frac{D\vec{V}}{Dt} = -\vec{\nabla}P + \rho \vec{g} + \mu \nabla^2 \vec{V} \tag{4.7}$$

The equation above is an Unsteady, nonlinear, second-order, partial differential equation. The equations below are the incompressible continuity and momentum Navier Stokes equations from Çengel (2006) [61].

Incompressible continuity equation in Cartesian coordinates:

$$\frac{\partial u}{\partial x}+\frac{\partial v}{\partial y}+\frac{\partial w}{\partial z}=0 \tag{4.8}$$

Momentum:

x–component of the incompressible Navier–Stokes equation [61]:

$$\rho\left(\frac{\partial u}{\partial t}+u\frac{\partial u}{\partial x}+\ v\frac{\partial u}{\partial y}+\ w\frac{\partial u}{\partial z}\right)=-\frac{\partial P}{\partial x}+\rho g_x+\mu\left(\frac{\partial^2 u}{\partial x^2}+\ \frac{\partial^2 u}{\partial y^2}+\ \frac{\partial^2 u}{\partial z^2}\right) \tag{4.9}$$

y–component of the incompressible Navier–Stokes equation [61]:

$$\rho\left(\frac{\partial v}{\partial t}+u\frac{\partial v}{\partial x}+\ v\frac{\partial v}{\partial y}+\ w\frac{\partial v}{\partial z}\right)=-\frac{\partial P}{\partial y}+\rho g_y+\mu\left(\frac{\partial^2 v}{\partial x^2}+\ \frac{\partial^2 v}{\partial y^2}+\ \frac{\partial^2 v}{\partial z^2}\right) \tag{4.10}$$

z–component of the incompressible Navier–Stokes equation [61]:

$$\rho\left(\frac{\partial w}{\partial t}+u\frac{\partial w}{\partial x}+\ v\frac{\partial w}{\partial y}+\ w\frac{\partial w}{\partial z}\right)=-\frac{\partial P}{\partial z}+\rho g_z+\mu\left(\frac{\partial^2 w}{\partial x^2}+\ \frac{\partial^2 w}{\partial y^2}+\ \frac{\partial^2 w}{\partial z^2}\right) \tag{4.11}$$

P = Pressure

t = Time

ρ = Density

μ = Dynamic Viscosity

x, y, z = Cartesian Coordinates

g = Gravity

The reviewed literature notes that the Navier-Stokes equations assume the gas is in a continuous medium and ignore the discrete molecular nature of a real gas [8] [46]. For optimization of the PVD process it is important to gain detailed characteristics of the neutral gas flow inside the reactor chamber [46]. Therefore, a traditional CFD method such as ANSYS Fluent will not be accurate for vapours with higher Knudsen numbers because Fluent uses solvers based around the Navier-Stokes equations and continuum mechanics.

4.3.2 Monte Carlo Method

Monte Carlo method is the broad term for algorithms that use random numbers to solve numerical problems. There have been multiple variants of Monte Carlo methods developed around the premise of resolving complex problems using random numbers [62]. The methods have been used for a wide range of applications from computational chemistry and material science to biology and quantum physics [63]. The requirement for a large number of calculations means the Monte Carlo method is best suited to using a computer [12]. Monte Carlo methods can be applied to problems involving many degrees of freedom. For example, a deterministic method of numerical integration work by taking evenly spaced samples from a function. This works for functions of one variable however can be very inefficient for functions of several variables.

To numerically integrate a function of an N-dimensional vector (N=100) with a grid of 10 points in each dimension requires the evaluation of 10^{100} points, which is far too many to compute [63]. Monte Carlo method avoids the exponential time increase. If the function is reasonably compliant, it can be estimated by randomly selecting points in N-dimensional space and taking the average function values of these points [63]. Under the central limit theorem, the Monte Carlo method displays $1/\sqrt{N}$ convergence. Quadrupling the number of sampled points will halve the error regardless of the number of dimensions [64]. Monte Carlo methods have been developed for the simulation of ensemble properties (thermodynamic ensembles) for classical simulations of molecular liquids and gases using Metropolis algorithm and later derivatives of that method [62]. The analysis of the vacuum lock is likely to focus on

the constant NPT (Number of particles, Pressure and Temperature) ensemble ignoring diffusion and considering the air to be in equilibrium.

The analysis of the vacuum coating chamber will consider non-equilibrium processes where the metal vapour spreads from the injector nozzles to the substrate and could also spread to chamber walls and into the vacuum locks. In addition to equilibrium properties the Monte Carlo method can also be applied to dynamical properties using the Kinetic Monte Carlo (KMC) method. The method has been developed under different names over decades until it was known universally as KMC [63]. KMC is a prominent method used to analyse transport diffusion, crystal growth, equilibrium and non-equilibrium chemistry. KMC is a method used to overcome the limitation of short time steps required to resolve atomic vibrations in Molecular Dynamics (MD). Molecular dynamics is a fully deterministic method that involves direct solution of the motions of equations at a time step. KMC does not follow particle trajectories instead it exploits the long term dynamics of the system that consists of diffusive jumps KMC does not follow trajectories through every vibrational period, instead KMC simulations assume that transitions from one state to another are Markovian, having probabilities that given the present state, the future is independent of the past [65].

KMC has been used to study the atomic layer deposition of Zinc Oxide and simulation of film growth by physical vapor deposition on rotating substrates [66] [67]. Venkattramen and Alexeenko (2012) states that KMC can simulate the growth of atomic layer deposition of metallic vapour and predict the grain structure of the deposited material on a surface. Another method called Direct Simulation Monte Carlo is used to simulate the surface interaction processes of absorption, diffuse reflection and specular reflection [68]. The surface impact results from a DSMC are used as inputs to the KMC method obtained at a specific location on the substrate. The combined techniques are used to determine optimum deposition conditions with respect to coating uniformity, porosity, and deposition rate [68] [69].

The prediction accuracy of the transport of metallic vapour from the vapour distribution source to the surface depends on the models used in the DSMC method, including the interaction between the gas particles and the particles interaction with the solid surfaces. The DSMC method predicts the number flux and energy

distribution of the atoms at the substrate location [68]. Deposition growth and metallic vapour transport are more relevant to the coating chamber and substrate coating than the pressure requirements of the vacuum lock however the transport of gas particles in lower pressure is an important consideration and the DSMC method has been developed to investigate rarefied gas dynamic problems [55].

4.3.3 Direct Simulation Monte Carlo (DSMC) Method

The DSMC method does not depend on the conventional mathematical models such as the continuum Navier-Stokes or the discrete Boltzmann equations [8]. The DSMC method is applied to non-equilibrium or rarefied gas flows such as those encountered under vacuum conditions [68]. DSMC is a probabilistic Monte Carlo method used to solve the Boltzmann equation for dilute gas flows. DSMC is linked to the kinetic theory of gases and rarefied gas dynamics. Kinetic theory considers gases on a molecular level described statistically in terms of probabilities of the various states of gas molecules in space and time. DSMC is a particle based method like MD, however in DSMC, a single particle represents a large number of real gas atoms or molecules reducing the computational expense of MD [55].

The DSMC method can be utilized for the analysis of flows where the Knudsen number is outside the range suitable for the Navier Stokes equations. Bird (2013) states that the DSMC Method "provides a probabilistic physical simulation of a gas flow by simultaneously following the motion of representative model molecules in physical space" [8]. A simulated molecule represents the number F_N of real molecules, which is a computational variable. The quantity of molecules is very large in a rarefied gas, however there may be a one to one ratio between simulated and real molecules in a dense gas [8]. Millions of molecules are simulated in a typical computation and requires billions of intermolecular collisions and surface interactions. Time is an independent variable and steady flow is developed as the large-time state of a physically realistic unsteady flow [8]. Flow symmetries can be taken to reduce the number of independent spatial variables, though collisions and surface interactions are always considered as three dimensional events [8].

The DSMC method requires a dilute gas, where the molecular mean free path is considerably larger than the molecular diameter [8]. The dilute gas assumption and probabilistic approach allows the molecular motion and collisions to uncouple over a time interval that is small in comparison to mean collision time. This allows DSMC calculations to use real molecular diameters, but requires a mesh or cell network in physical space [8]. In early years of DSMC development, it was found that the simplest of the DSMC method provides a solution to the Boltzmann equation for a time step and grid size tending to zero and molecule number to infinity [70]. Modern DSMC solutions have more intricate procedures and consequently there is concern about their validity [8].

The derivation of the mathematical model of the Boltzmann equation depends on the same physical arguments that led to the DSMC procedures, therefore a simulation model should have the same accuracy as the mathematical model [8]. DSMC method can deal with physical affects that are beyond the scope of the Boltzmann equation and is not limited by the same restrictions of the Boltzmann equation. DSMC method does not depend on the conventional mathematical models such as the continuum Navier-Stokes or the discrete Boltzmann equations [8]. DSMC method is a probabilistic physical simulation of a gas flow by simultaneously tracking the motion of model molecules characteristics in physical space [2]. The DSMC Method involves the microscopic or molecular gas properties that include summing up all the molecules within a volume V [2]. The molecules are defined for a general gas mixture case with s molecular species. For a simple gas only containing a singular molecular species the number density is determined as:

$$n = \sum_{p=1}^{s} n_p \tag{4.12}$$

n_p is the number density per unit volume of species p, the overall number density n is found by the summation over all species s [2]. The average number $\bar{N}$ of molecules within the volume V is $\bar{N} = nV$ subject to statistical fluctuations from the Poisson Distribution [2].

Probability for N of given value is:

$$P(N) = \frac{(nV)^N \exp(-nV)}{N!} \tag{4.13}$$

The distribution becomes indistinguishable from normal or gaussian for large values of N

$$P(N) = \frac{(2\pi nV)^{-\frac{1}{2}} \exp\{(N - nV)^2}{2nV} \tag{4.14}$$

The standard deviation is $1/\sqrt{nV}$ and C is the number of standard deviations. Integrating this distribution gives the probability of an individual density sample falling within $C/\sqrt{n}V$ of the average as erf $(C/\sqrt{nV})$. This means 66.26% of samples occur within one standard deviation, 95.45% within two, 99.73% within three and 99.994% within four standard deviations. These expectations and magnitudes of the of the fluctuations apply to the generally enhanced fluctuations within a DSMC calculation and a real gas [8].

4.3.4 DSMC Variable Hard Sphere Model

Interaction between atoms and molecules is an important parameter required to perform a DSMC simulation. There is a range of Molecular models, the Variable Hard Sphere (VHS) is the most widely used. The VHS model is computationally efficient and has the capability to reproduce the viscosity of various molecules using the reference diameter (d_{ref}) and the temperature coefficient of viscosity (ω) [68]. The equation 4.15 is for mean free path of a VHS molecule, taken from Scanlon et al (2010) [70].

$$\lambda = \frac{2(5 - 2\omega)(7 - 2\omega)}{15}\left(\frac{m}{2\pi kt}\right)^{\frac{1}{2}}\left(\frac{\mu}{\rho}\right) \tag{4.15}$$

ω = Temperature coefficient of viscosity

m = Atomic mass

k = Boltzmann constant

μ = Dynamic viscosity of the gas

ρ = Gas density

One of the most important inputs of a DSMC simulation is the molecular interactions. The most common molecular interaction models used in DSMC are the hard sphere and Variable Hard Sphere models. Both neglect the large range attractive force that exists between molecules [71].

- Essential to simulate particle collisions in DSMC
- Cross-section collisions (d_{ref}) derived from coefficients of viscosity (μ_{ref})
- Angular scattering
- Theoretically determined from the VHS method

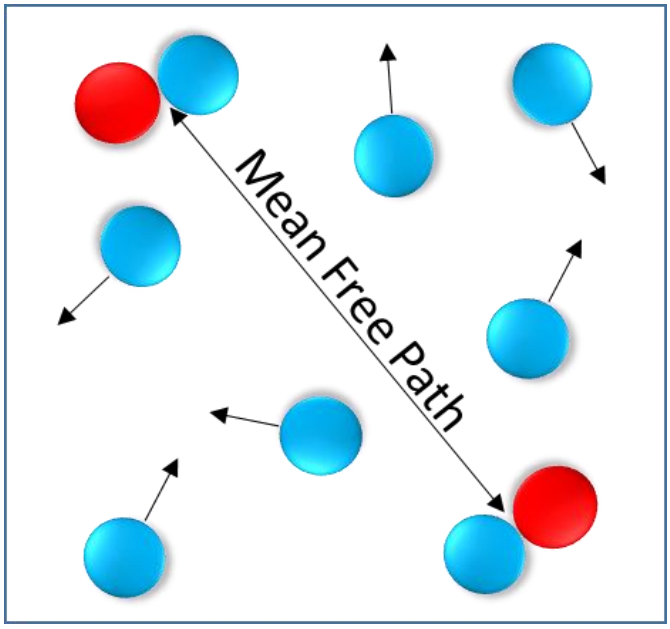

Figure 24: Intermolecular collisions in a dilute gas – kinetic scale

Figure 24 is a diagram that visualises the intermolecular collisions on a kinetic scale within a fixed area. In the Boltzmann equation the position, velocity and interaction of every particle in the region of interest are known. DSMC is a probabilistic method that uses random events to predict the same behaviour. Instead of tracking every

particle DSMC tracks a parcel which is a large sample of particles modelled as one. The interest of region is split up into a grid. The interactions are measured as the possibility of a particle sharing the same space in the same grid at the same time. The position of the particles could have velocities in different directions but if the velocity of two particles are high enough in a close enough space as the same time an interaction is recorded. This simplifies the requirement for the knowledge of every single particles velocity and position and uses random numbers to predict the outcome [45]. The velocities of the particles are predicted from a Maxwell-Boltzmann distribution.

Figure 25 shows the intermolecular collisions on a quantum scale, m1 and m2 represent two gas molecules of different sizes. It can be seen here that the reference diameter (d_{ref}) is measured from centre to centre of m1 and m2 and that the molecules are hard spheres and they have not deformed in the collision as in accordance to the hard sphere model.

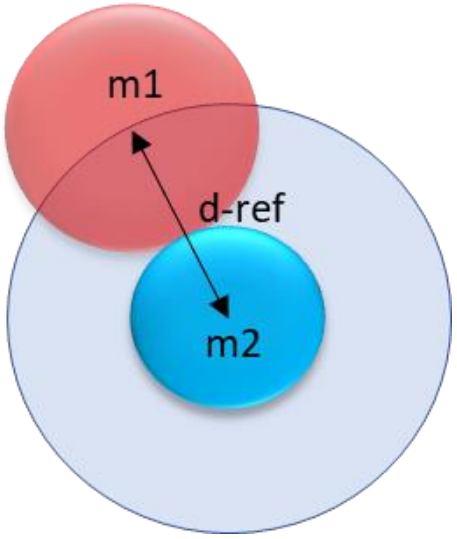

Figure 25: Intermolecular collisions in a dilute gas – quantum scale

In chapter 6 DSMC method will be used to run a simulation using a software called OpenFOAM. To run a DSMC simulation in OpenFOAM, the DSMC properties dictionary file must be populated with accurate data about the gas being analysed. The equations 4.17 to 4.19 taken from from Bird (1994), [72] can be used to determine theoretical values for reference viscosity and reference diameter, these are important

values required within the DSMC method calculation or simulations as they are linked with the molecular model used in this case the VHS model.

The diameter of a hard sphere gas with a coefficient of viscosity u_{ref} at temperature T_{ref} is:

$$d_{HS} = \left(\frac{\left(\frac{5}{16}\right)\left(\frac{mkT_{ref}}{\pi}\right)^{\frac{1}{2}}}{u_{ref}} \right)^{\frac{1}{2}} \tag{4.16}$$

VHS coefficient of viscosity

$$\mu_{ref} = \frac{5m\left(\frac{RT}{\pi}\right)^{\frac{1}{2}}\left(\frac{2mRT}{k}\right)^{\frac{2}{(\eta-1)}}}{8A_2(\eta)\Gamma\left(4-\frac{2}{\eta-1}\right)} \tag{4.17}$$

$A_2(\eta)$ is a numerical factor defined by

$$A_2(\eta) \equiv \int_0^{\infty} \sin^2 x\, W_0 dW_0 \tag{4.18}$$

VHS relative diameter equation:

$$d_{VHS} = \left(\frac{\left(\frac{15}{8}\right)\left(\frac{m}{\pi}\right)^{\frac{1}{2}}\left(kT_{ref}\right)^{\omega}}{\Gamma\left(\left(\frac{9}{2}\right)-\omega\right)\mu_{ref}\epsilon_t^{\omega-(1/2)}} \right)^{\frac{1}{2}} \tag{4.19}$$

For the vacuum lock the gas mainly considered is air due to the investigation focusing on the pressure. In the vacuum coating chamber zinc-magnesium vapour particle transport is the focus. There is little data available for metallic vapour however there is data for gas properties in Bird (1994) and Bird (2013) originally sourced from Chapman and Cowling (1970). The values in figure 26 below are linked with the VHS model and have already been determined, therefore the equations above do not need

to be used, however the equations above or experimental research is required in order to provide values for metallic vapour. In chapter 6 the reference diameter is one of the inputs for the DSMC+ solver in OpenFOAM. The DSMC+ solver will be explained in Chapter 5.

Gas	Rotational degrees of freedom	Molecular mass (10^{-27} Kg)	Diameter at 273 K (10^{-10} m)	Viscosity-temperature index
Hydrogen H_2	2	3.34	2.92	0.67
Helium He	0	6.65	2.33	0.66
Neon Ne	0	33.5	2.77	0.66
Carbon monoxide CO	2	46.6	4.19	0.73
Nitrogen N_2	2	46.5	4.17	0.74
Nitric oxide NO	2	49.9	4.20	0.79
Oxygen O_2	2	53.1	4.07	0.77
Argon Ar	0	66.3	4.17	0.81
Carbon dioxide CO_2	3	73.1	5.62	0.93
Nitrous oxide	2	73.1	5.71	0.94

Figure 26: Information for VHS model reference diameter from Bird (2013), [8]

4.4 Gas Properties

It is important to know the flow regime before performing analysis on the flow problem to adopt the correct boundary conditions and analysis method. Pressure and temperature and number density need to be known to determine the mean free path and Knudsen number. The following equations include constants required for the calculations of the mean free path. Avogadro's constant is the number of molecules in one mole of gas, $N_A = 6.023 \times 10^{23}$ molecules [72]. In kmoles that number becomes $N_A = 6.023 \times 10^{26}$ molecules. Avogadro's law states the volume occupied my one mole of any gas at a certain temperature and pressure is the same for all gases [72].

4.4.1 Avogadro's Law

$$n = \frac{N}{N_A} \tag{4.20}$$

N = Number of particles

n = Number of moles

N_A = Avogadro's constant

R_U = Universal gas constant

R_S = Specific gas constant

m = Mass (single molecule)

M = Molecular weight (relative atomic mass)

Mass m, of a single molecule is found by dividing the molecular weight M of the gas by the Avogadro's number.

$$m = \frac{M}{N_A} \tag{4.21}$$

Example mass of a single molecule of Air:

$$m = \frac{28.97}{6.023e + 26} = 4.081e - 26kg \tag{4.22}$$

Relative atomic mass (molecular weight) M, is the ratio of the average mass per molecule to 1/12 of the mass of Carbon-12 [73]. The molecular weight is calculated by the sum of the relative atomic mass of all atoms that a molecule comprises of [73]. The number of grams per mole of an element can be obtained from the periodic table (atomic mass). Air is a mixture; therefore, the molecular weight must be calculated from adding the molecular weights of the individual gasses. The calculated value for dry air is 28.97 [74].

Using SI units, values containing grams are changed to kilograms (kg).

$$M = M\frac{[g]}{[mol]}\frac{[1000].[mol]}{[kmol]}\frac{[kg]}{[1000].[g]} = M\frac{[kg]}{[mol]} \tag{4.23}$$

Example molecular mass of Air: [75]

$$M = M\left(\frac{28.97g}{mol}\right)\left(\frac{1000mol}{kmol}\right)\left(\frac{kg}{1000g}\right) = 28.97\frac{kg}{mol} \tag{4.24}$$

4.4.2 Ideal Gas Law

$$PV = nR_UT \tag{4.25}$$

P = Absolute Pressure

V = Volume the gas is contained in

n = Number of kmoles

T = Absolute Temperature

$$R_u = 8.314\frac{[kJ]}{[kmol].[K]} = 8314\frac{[J]}{[kmol].[K]} \tag{4.26}$$

The specific gas constant depends on the specific gas being considered and is not universal, [75]:

$$R = \frac{R_u}{M} \tag{4.27}$$

$$R_{air} = \frac{R_u}{M} = \frac{8.314\frac{[kJ]}{[kmol].[K]}}{28.971\frac{[kg]}{[kmol]}} = 0.287\frac{[kJ]}{[kg].[K]} = 287.058\frac{[J]}{[kg].[K]} \tag{4.28}$$

Specific gas constant = 287 J.kg.K^{-1}

Using this value of R allows the ideal gas law equation to be written as:

$$PV = mR_sT \tag{4.29}$$

Density calculated from the ideal gas law

$$\rho = \frac{m}{V} \therefore V = \frac{m}{\rho} \tag{4.30}$$

$$PV = mR_sT \rightarrow P\frac{m}{\rho} = mR_sT \rightarrow \rho = \frac{Pm}{R_sTm} \tag{4.31}$$

$$\therefore \rho = \frac{P}{R_sT} \tag{4.32}$$

Example density of air at atmospheric pressure (101,325 Pa), zero degrees centigrade temperature (273 Kelvin) and using the specific gas constant calculated above is:

$$\rho = \frac{101.325 \times 10^3}{287.058 \times 273} = 1.293 kg.m^{-3} \tag{4.33}$$

4.4.3 Number Density

The number density n (molecules per unit volume), of a gas depends on the temperature and pressure, however it is independent of the gas composition [72].

$$n = \rho\frac{N_A}{M} \tag{4.34}$$

$$n = 1.293 \times \frac{6.023 \times 10^{26}}{28.97} = 2.69 \times 10^{25} m^{-3} \tag{4.35}$$

n = Number Density

M = Molecular Mass

N_A = Avogadro's Number

ρ = Density

4.4.4 The Boltzmann Constant K_B

The Boltzmann constant is the ratio of the universal gas constant to the Avogadro's constant, therefore can be referred to as the gas constant per molecule [73].

$$K_B = \frac{R_u}{N_A} = \frac{8.314}{6.023 \times 10^{23}} = 1.38 \times 10^{-23} \quad (4.36)$$

4.4.5 Loschmidt Constant

The standard number density n_o at atmospheric pressure and zero degrees centigrade temperature is known as the Loschmidt number. The Loschmidt number is the number of molecules in one cubic centimetre is 2.68684 x 10^{19} molecules and can be regarded as a physical constant [72].

$$n_o = \frac{P}{K_B T} \quad (4.37)$$

$$n_o = \frac{101325}{1.38 \times 10^{-23} \times 273} = 2.69 \times 10^{25} m^{-3} \quad (4.38)$$

The volume of one kmole of an ideal gas at atmospheric pressure is N/n_o or 22.414 m^3. Number density is the number of particles in 22.4 cubic metres of volume for any ideal gas. The Loschmidt constant is normally used for number density at atmospheric pressure, however as the pressures fluctuate in the vacuum lock system the number density will be calculated using equation (4.37).

4.5 Gas Properties in Vacuum Lock Revision 7

Calculations were performed to determine the Knudsen number and associated flow conditions within the vacuum lock. Although Sutherlands viscosity law states that viscosity is a function of temperature [76]. As a simplification temperature and viscosity are assumed constant when calculating the mean free path, Knudsen and Reynolds numbers within the vacuum lock. Table 2 shows an estimation for the molecular diameter of air by taking an average of the mixture of molecules that make up air. The molecular diameter of air is required to calculate the mean free path of air molecules in the vacuum lock.

Table 2: Calculation of the molecular diameter of air

Gas	Percentage by Volume	Mole ratio	Molecular Diameter at 273k (10^{-10}m)	Averaged molecular diameter (10^{-10}m)
Nitrogen	78.084	0.78084	4.17	3.2561028
Oxygen	20.9476	0.209476	4.07	0.85256732
Carbon Dioxide	0.0314	0.000314	5.62	0.00176468
Methane	0.0002	0.000002	3.17	0.00000634
Air				4.11044114

The equations below show how mean free path is calculated.

Avogadro's Law Equation (4.20)

$$n = \frac{N}{N_A} \tag{4.20}$$

Number of molecules per unit volume, divide by volume.

$$\frac{nN_A}{V} = \frac{N}{V} \tag{4.39}$$

Mean free path Equation (4.2)

$$\lambda = \frac{1}{\sqrt{2}\,\pi\sigma^2 n} \tag{4.2}$$

$$V = \frac{nR_U T}{P} \tag{4.40}$$

$$\frac{N}{V} = \frac{nN_A}{\frac{nR_U T}{P}} = \frac{N_A P}{R_U T} \tag{4.41}$$

Mean free path combined with ideal gas law equation, defined in reference [77].

$$\lambda = \frac{R_U T}{\sqrt{2}\,\pi\sigma^2 N_A P} \tag{4.42}$$

Using equation (4.42), the mean free path is calculated for the vacuum lock to obtain the Knudsen number and produce the graph in figure 27. It is assumed that temperature is constant at 288 K. Avogadro's constant per mole is 6.023×10^{23} and the molecular diameter of air is 0.411 nanometres taken from Table 2. The characteristic length within the vacuum lock was taken as the 1mm clearance between the roller and the surrounding sealing block. The width of the lock is a common flow path, however higher Knudsen values are more likely with a small characteristic length. Figure 27 shows the Knudsen numbers occurring in the lock at varying pressure. It is clear to see that the Knudsen increases as pressure decreases.

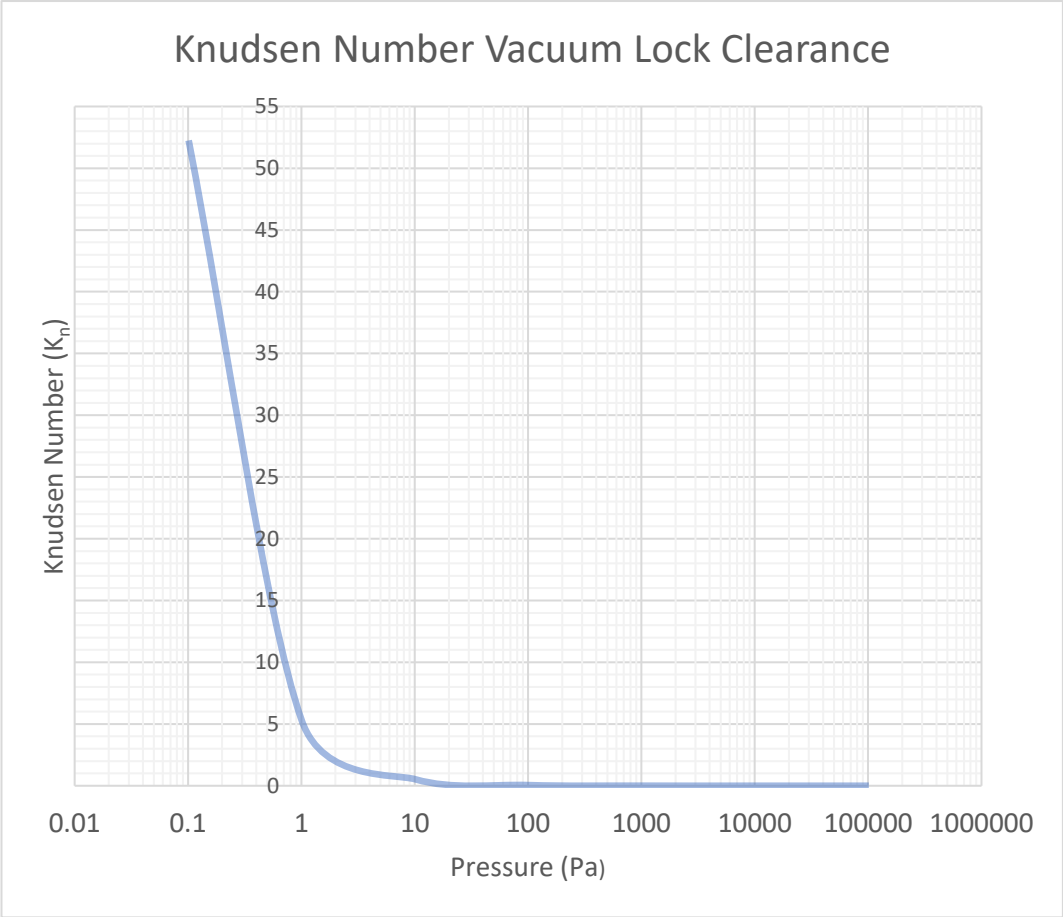

Figure 27: Knudsen number compared against pressure in the vacuum lock

Free molecular flow does not occur until the pressure is less than 1 Pa. It is not clear from the graph in figure 27 where slip and transitional flow occur but with interpolation in excel, slip flow occurs approximately between 1000 Pa and 100 Pa as the corresponding Knudsen number are less than 0.001 and transitional flow between

100 Pa and 10 Pa as the corresponding Knudsen number are between 0.1 and 10. When the pressure is 1000 Pa or more, the Knudsen number is less than 0.001 and the regime is continuum flow in that region. Figure 27 can be used as a guide for the vacuum lock to determine the nature of the gas flow and apply the appropriate analysis tools to simulate the behaviour. If area of interest changes then a different characteristic length can be used and a new graph formed to identify the gas rarefication in the area of interest.

4.5.1 Mass Flow Rate

Mass flow rate is calculated to show how changing the geometry the air is flowing through effects the velocity of the flow. This follows Bernoulli's principle that when there is an increase in the speed of air the static pressure decreases; this is only true for isentropic incompressible flow.

The mass flow rate is given by, [78]:

$$\dot{m} = \rho_1 A_1 V_1 = \rho_2 A_2 V_2 \tag{4.43}$$

Volume of gas in the chamber of revision 7 = 0.0191 m^3 (Taken from Solidworks)

$$V_2 = \frac{\dot{m}}{A_2 * \rho_2} \tag{4.44}$$

$$V_1 = \frac{0.1\ kg/s}{0.001963495m^2 * 1.225} = 4.157516881ms^{-1}$$

Total initial air mass in chamber

$$PV = mR_sT \tag{4.29}$$

Rearranging Equation (4.29) for m

$$m = \frac{PVM}{R_sT} \tag{4.45}$$

$$m = \frac{PVM}{R_sT} = \frac{101325\ Pa\ \times\ 0.0191\mathrm{m}^3\ \times\ 0.02897kmol^{-1}}{8.31\ Pa.m^3.mol^{-1}288K^{-1}} = 0.0234\ kg\ Air$$

The inlet area of the lock is 450 mm by 10 mm which is 0.00450 m^2, the density of air is considered constant 1.225 kg/m^3 and the outlet area 0.00196 m^2 (Area of a 25mm diameter outlet) This is taken from the vacuum lock revision 7 design that was used for the final simulations. Figure 28 shows the smaller geometry of the outlet in comparison to the inlet results in a higher velocity. This is a simplification as it does not take into consideration the changes the rollers and internals components will have on the flow through the lock from the inlet to the outlet but still shows that changing the area the air flows through does have an effect on the velocity of the flow. It is important to consider the clearances later in the simulations. In a closed system the mass flow rate could be used to identify how long it would take to remove the volume of the system for example emptying a tank of water. In an open system the mass entering the system whilst mass is flowing out of the system needs to be considered. To reduce the air in the vacuum lock and lower the pressure, the air needs to be pumped out faster than it leaks in.

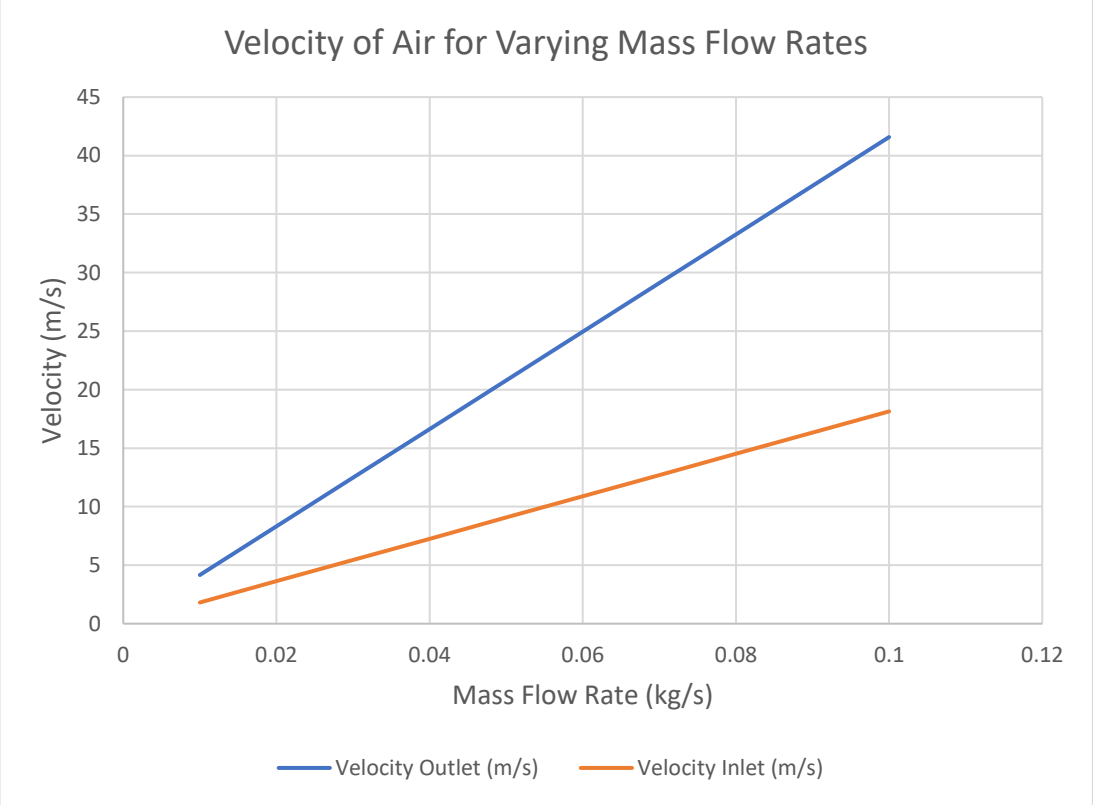

Figure 28: Mass flow at the inlet to the vacuum lock and outlet to vacuum pump

4.5.2 Reynolds Number

The tighter clearances result in a higher velocity. This is likely to increase the occurrence of turbulent flow due to higher Reynolds numbers. Reynolds number is the ratio of inertial to viscous forces and the type of turbulent flow is determined by the Reynolds number shown in Table 3. Reynolds number [79].

$$R_E = \frac{\rho V L}{\mu} \tag{4.46}$$

Table 3: Type of flow at different Reynolds numbers

Laminar	Re < 2000
Transitional	2000 > Re < 4000
Turbulent	Re > 4000

μ = Dynamic viscosity (N.s/m^2)

ρ = Density (kg/m^3)

L = Characteristic Length

V = Flow Velocity

The diameter and width of channels are used as the characteristic lengths for calculating Reynolds numbers. The diameter of the outlet of 25mm was used and 10mm for the height of the inlet. Density of air is considered constant at 1.225 kg/m^3 as well as dynamic viscosity of air at 1.83×10^{-5}. Figure 29 shows that the increased velocity at the outlet has higher Reynolds numbers and the flow is more turbulent than at the inlet. This is only an indicator and is dependent on whether the correct assumption has been made for the characteristic length. To produce a vacuum in an open system means it is very likely that the mass flow rate of air removed from the vacuum lock by a pump will result in higher velocities and turbulent flow. When running simulations on the system turbulence will need to be considered. The mass flow rate at the outlet is provided by a vacuum pump. Pumping capacity is important to know for the power of the pump required.

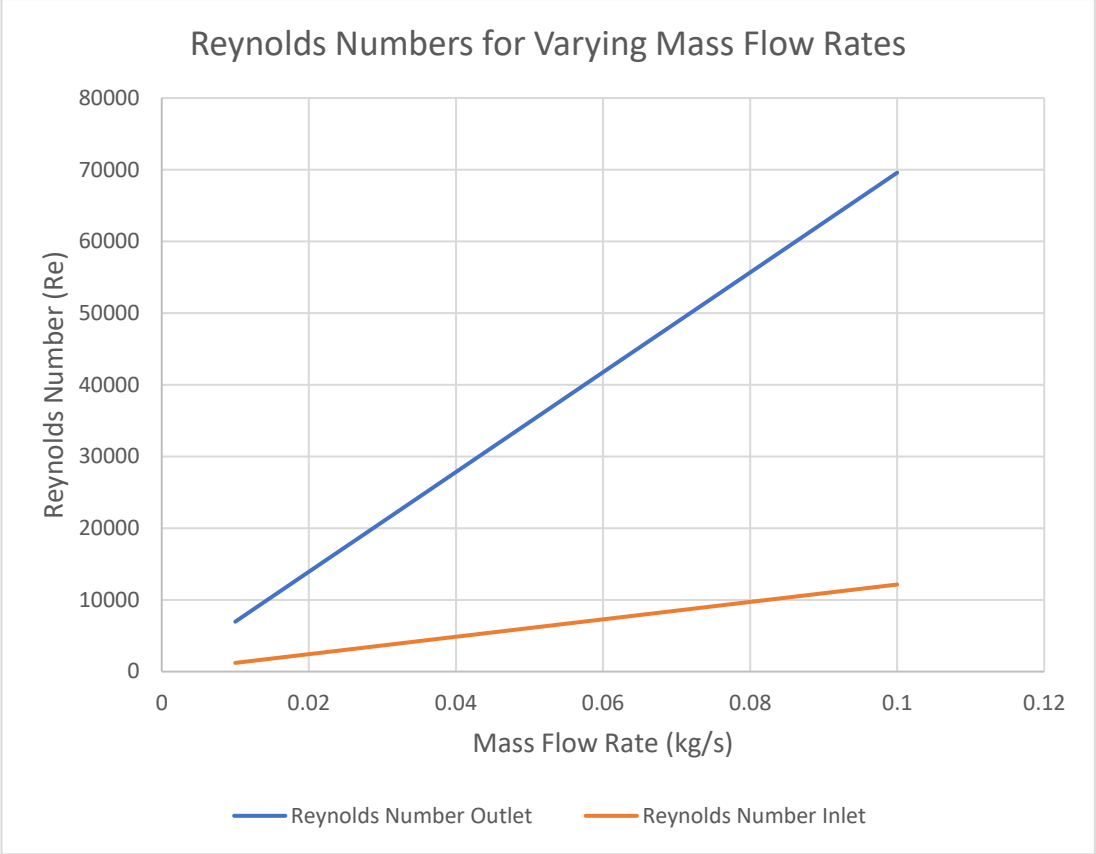

Figure 29: Reynolds numbers for varying mass flow rates

4.6 Pumping Capacity of Vacuum Lock

One of the deliverables in producing a state of the art vacuum lock is to determine the required pumping capacity to achieve a certain pressure. Pumping Capacity (Q) is the throughput of gas moved by a pump over unit time, equal to the mass flow through the pump intake port [32] [33].

$$Q = \frac{m}{t} = \frac{PV}{t} (Pa.m^3.s^{-1}) \tag{4.47}$$

The pumping capacity depends on the pumping performance of the pump. Pump performance curves are produced experimentally by plotting pumping speed against pressure, [80]. The pumping speed of a pump is measured in ideal conditions and therefore any connections in a system will reduce this value, [80]. Pumping speed is

the transportation capacity which the pump makes available in a specific time. Typical units are m^3/h or l/s, [33], [81].

4.6.1 Pumping Speed

Pumping Speed, S, is the volumetric flow through the intake port, [33]:

$$S = \frac{\Delta V}{\Delta t} \tag{4.48}$$

If pressure and volume are constant at the intake, the pumping capacity can be expressed as, [33]:

$$Q = SP \tag{4.49}$$

Equation (4.49) is the usual form of expressing pumping capacity describing the quantity of gas flow for the volumetric flow rate at a certain pressure, [81]. Pump capacity is very important and should not be confused with pumping speed. The throughput value is used to determine the size of a vacuum pump with which it is connected in series in order to ensure that the backing pump will be able to remove the gas moved by the vacuum pump [33].

4.6.2 Conductance

Connection in the vacuum system obstructs the flow, this resistance to the flow is known as Conductance, also having the same dimensional units as volumetric flow, (volume per time) normally measured in litres per second [81]. For a gas, conductance is expressed as equation (4.50) defined in reference [33]:

$$C = \frac{Q}{P_1 - P_2} \tag{4.50}$$

For a pipe this is the difference between upstream (P_2) and downstream (P_1) pressures that connect two volumes (40). It can be re-written for throughput equation (4.51) defined in reference [33]:

$$Q = C(P_1 - P_2) = (m^3 s^{-1}) \tag{4.51}$$

Conductance depends on the geometry. The flow is affected by any section such as hoses, nozzles, gaps, clearances, etc. Conductance is said to be like the "Ohm's law of vacuum technology" [33], the resistance behaves in an inverse way to that of electrical circuits though [81]. If pipes are in parallel or series the conductance acts as follows:

In parallel:

$$C = C_1 + C_2 + C_3 \tag{4.52}$$

In series:

$$C = \frac{1}{C_1} + \frac{1}{C_2} + \frac{1}{C_3} \tag{4.53}$$

In a high vacuum conductance is constant and therefore independent of pressure. In a medium vacuum conductance is dependent on pressure and calculation must be conducted separately for the individual pressure ranges, [82]. Conductance has the greatest effect in the viscous region and is least in the molecular flow region [82]. Conductance has to be calculated according to which regime the flow is in [83]. It is very difficult to calculate conductance for complex geometries, formulas for annular and rectangular cross sections for short and long tubes can be found in literature [83] [84].

Other important obstructions or losses in a vacuum system are leaks and outgassing. Any crack, gap or hole that allows gas into the system will cause a leak to atmospheric pressure. Units for leak rate are (mbar.l.s^{-1}). A leak is often measured or indicated with atmospheric pressure prevailing on one side of the barrier and a vacuum at the other side [33]. Outgassing is a release of gases and vapours from the walls of a vacuum chamber or other components inside the vacuum system [32] [33]. Conductance, leaks and outgassing will reduce the performance of the vacuum system, reducing these factors in the system design will determine what pumping is required to sustain a stable vacuum in the system [82].

5. Computational Modelling Software

This section includes the boundary conditions and solvers used in the software. It is important to understand which solvers should be used to solve the physics of the vacuum lock for the defined boundary conditions. For example, SIMPLE is a pressure based algorithm that is predominantly used for incompressible flow. A typical boundary condition used for the SIMPLE algorithm would be a velocity inlet and pressure outlet. If the velocity of air flow caused by a leak into the vacuum lock is known and the pressure at the outlet, these boundary conditions and the SIMPLE algorithm could be used. If the flow is compressible then a density based algorithm such as PISO would be used. The boundary conditions in this case could be a pressure inlet and pressure outlet. This arrangement could be used if the flow of air has an increased velocity and the inlet and outlet pressure is known. If the incorrect solver is used with the boundary conditions then the solutions will most likely not converge, sometimes errors will be posted by the software. The vacuum lock system will experience air at different pressures, starting with atmospheric pressure down to free low/medium vacuum and therefore the gas regime will vary. It is unlikely that one engineering software will cover all the different gas regimes and to simulate the vacuum lock three different computational engineering software's are investigated.

Engineering software uses a process called discretisation to solve the governing equations that have been applied to the domain. Discretisation is the process of numerical approximation of the partial differential equations (PDE's) used to solve engineering problems such as structural or fluid mechanics. Three established methods used for the discretisation of the governing PDE's of fluid flow are Finite Difference (FD) Finite Element (FE) and Finite Volume (FV). Finite Difference requires a structured mesh that is equality spaced and is not easily applied to irregular geometries unlike Finite Element and Volume methods that can be applied to unstructured complicated geometries and more commonly used for engineering problems. The vacuum lock has tight clearances and geometries that require an unstructured mesh. A mesh is the name for the division of the geometry when divided into elements, this is explained further in the chapter 8. ANSYS Fluent and OpenFOAM both use finite

volume method (FVM) and COMSOL uses finite element method (FEM). FVM is typically used in CFD, whilst FEM in solid mechanics [85]. This chapter provides background information on the engineering software to show what algorithms and solvers are used. There is also a focus on what boundary conditions are required for the solvers.

5.1 ANSYS

ANSYS uses finite volume method to solves partial differential equations (PDE). ANSYS Fluent has five pressure-velocity coupling algorithm-based solvers:

- SIMPLE – Semi-Implicit Method for Pressure Linked Equations
- SIMPLEC – Semi-Implicit Method for Pressure Linked Equations Consistent
- PISO – Pressure-Implicit with Splitting of Operators
- COUPLED
- NITA – Non-Iterative Advancement

The algorithms are used to solve the physics in the simulation. Boundary conditions give the solver the initial conditions required to calculate a solution. From the ANSYS User Guide, the following statements explain how the algorithms work and limitations. “The SIMPLE algorithm uses a relationship between velocity and pressure corrections to enforce mass conservation and to obtain the pressure field”. [9]. “One of the limitations of the SIMPLE and SIMPLEC algorithms is that new velocities and corresponding fluxes do not satisfy the momentum balance after the pressure-correction equation is solved” [9]. “To improve the efficiency of this calculation, the PISO algorithm performs two additional corrections: neighbour correction and skewness correction” [9]. Coupled and NITA are both used for unsteady simulations more information on the solvers can be found in the ANSYS theory guide [9]. In addition to the algorithm another consideration in ANSYS Fluent in particular is the upwind scheme used for the discretisation. The upwind scheme considers the flow direction when determining the value of a cell face. The cell is a division of the

geometry known as a mesh element. The value at a cell face is taken as equal to the value of the upstream node [59]. There is a first and second order upwind scheme. First order considers a field value to represent the cell average value throughout an entire cell and second order computes the quantities at cell faces using a multidimensional linear reconstruction approach [86]. The second order upwind scheme is more accurate however is more computationally expensive.

5.1.1 ANSYS Boundary Conditions

Appropriate boundary conditions need to be applied in order to solve the Navier-Stokes equations that are used within the FLUENT solvers [87]. Pressure at the inlet and the outlet are known. The velocity at the inlet and outlet is not defined as it will be a result of achieving the desired pressure at the exits of the locks. The mass flow of air at the inlet and outlet is also undefined. Inlet and Outlets are external boundary conditions. As the only known properties at the boundaries are the pressures, the boundary conditions in FLUENT can be modelled as a pressure inlet and pressure outlet, as shown figure 30.

ANSYS uses pressure-based or density-based solvers depending on the boundary condition. The pressure-based solver is used when there is a velocity inlet and a pressure outlet. The pressure-based solver uses an algorithm from a general class of methods known as the projection method [9]. In the solver the continuity of the velocity field is achieved by solving a pressure equation. The pressure equation is derived from the continuity and momentum equation, so the pressure corrected velocity field satisfies the continuity (mass conservation). The governing equations are non-linear, coupled and segregated, therefore are solved repeatedly until the solution converges [9].

If the boundary condition contains a pressure inlet and pressure outlet then the density-based solver must be used, this set up is normally used for compressible flows with ideal gas properties [9]. The density-based solver solves the governing equations of continuity, momentum and energy coupled together as a vector of equations. The additional scaler terms are solved afterward separately from one another and the coupled sets [9]. Using the right solver here is important as the governing equations

are solved differently depending on what boundary conditions are used. There must be the same number of terms in the boundary conditions that the solvers require to solve the Navier-Stokes equations.

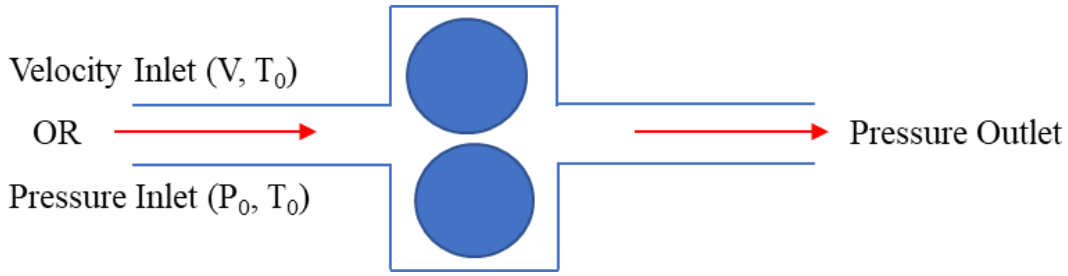

Figure 30: Common boundary conditions used in ANSYS

These conditions are useful for when the flow rate and the velocity are unknown. When a computational model is set up with a pressure inlet, a pressure outlet is usually used. Figure 30 shows typical boundary conditions in ANSYS at an inlet and outlet.

Pressure Inlet

At the pressure inlet, the temperature, pressure and density are fixed; the velocity is unknown [88]. Pressure inlets are a suitable boundary condition for both compressible and incompressible flows. Static pressure and velocity at the inlet is calculated by FLUENT [89]. Total gauge pressure is required when the flow is subsonic and static pressure is ignored [90].

Pressure Outlet

At the pressure outlet, the pressure is fixed whereas the temperature and velocity are unknown [88]. Pressure outlets are a suitable boundary condition for both compressible and incompressible flows. Static gauge pressure is required (pressure of the flow exit environment). For compressible flow (ideal gas) non-reflecting boundary conditions (NRBC) are available [89]. For the Navier-Stokes equations to solve, the analysis must use a density-based solver and the fluid is modelled as an ideal gas. Boundary conditions for pressure require static gauge pressure inputs. The operating pressure is set separately [87].

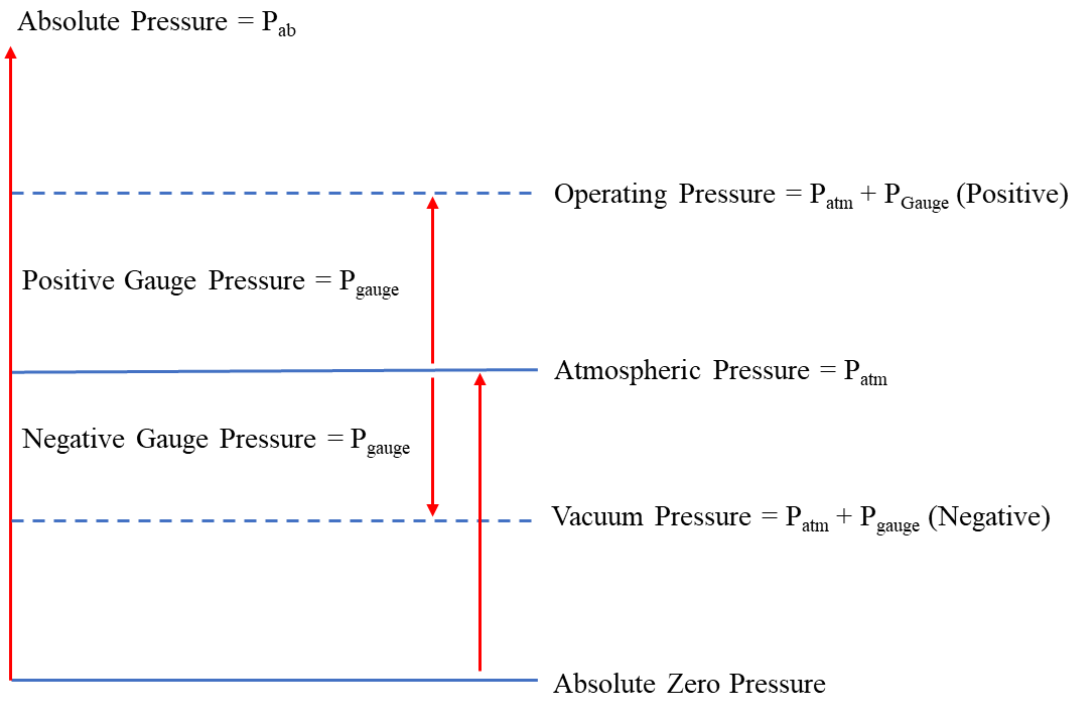

Figure 31: Pressure diagram [87]

The absolute pressure starts from zero and atmospheric plus any additional pressure is added to it denoted by equation (5.1). Gauge pressure is a relative pressure because it is measured relative to atmospheric pressure (figure 31). If a vessel is pressurised by pumping a fluid into it then the operating pressure will be the gauge pressure of the vessel plus the atmospheric pressure. In the case of a vacuum vessel the fluid is removed by pumping and the gauge pressure is negative when measure against atmospheric pressure. The vacuum pressure is atmospheric pressure plus a negative gauge pressure. Static pressure is used in ANSYS as a pressure measurement relevant to the operating pressure which is usually set as atmospheric pressure in ANSYS but can be changed. If operating pressure in ANSYS is set at absolute zero, then the Static pressure results are the absolute pressure or vacuum pressure.

$$P_{absolute} = P_{gauge} + P_{atmosphere} \tag{5.1}$$

5.2 COMSOL

COMSOL uses finite element method to solve partial differential equations (PDE) [10]. This is different from other CFD simulation software that uses the finite volume method. In finite element methods it is common to deal with very large matrices where only a few coefficients are different from zero [91]. The solvers are a library for solving sparse real and complex linear systems of equations [91]. COMSOL automatically detects and choses the best solver, based on the physics [91].

The direct solvers in COMSOL are:

- PARDISO – Parallel Direct Sparse Solver Interface
- MUMPS – MUltifrontal Massively Parallel sparse direct Solver
- SPOOLES – SParse Object-Oriented Linear Equations Solver

These are different to the solvers used in ANSYS and OpenFOAM. More information can be found in the COMSOL user guide [91]. COMSOL has a GUI and Multiphysics can be loaded in of varying modules depending on what the user is trying to solve. The boundary conditions are set very similar to ANSYS, for example setting the velocity at the inlet and pressure at the outlet or mass flow rate.

5.3 OpenFOAM

OpenFOAM uses finite volume method to solve partial difference equations (PDE) the same as ANSYS Fluent. OpenFOAM stands for Open Source (Field Operation and Manipulation) it is freely available software under GNU general public licence [11]. OpenFOAM consists of a C++ library built of precompiled applications, users have the access to create or modify existing code to adapt it to their requirements [11]. Figure 32 is an overview of the OpenFOAM libraries, it shows the applications are split into two categories:

- Solvers – solve CFD and other engineering mechanics problems [92].
- Utilities – perform data manipulation, visualisation and mesh processing tasks

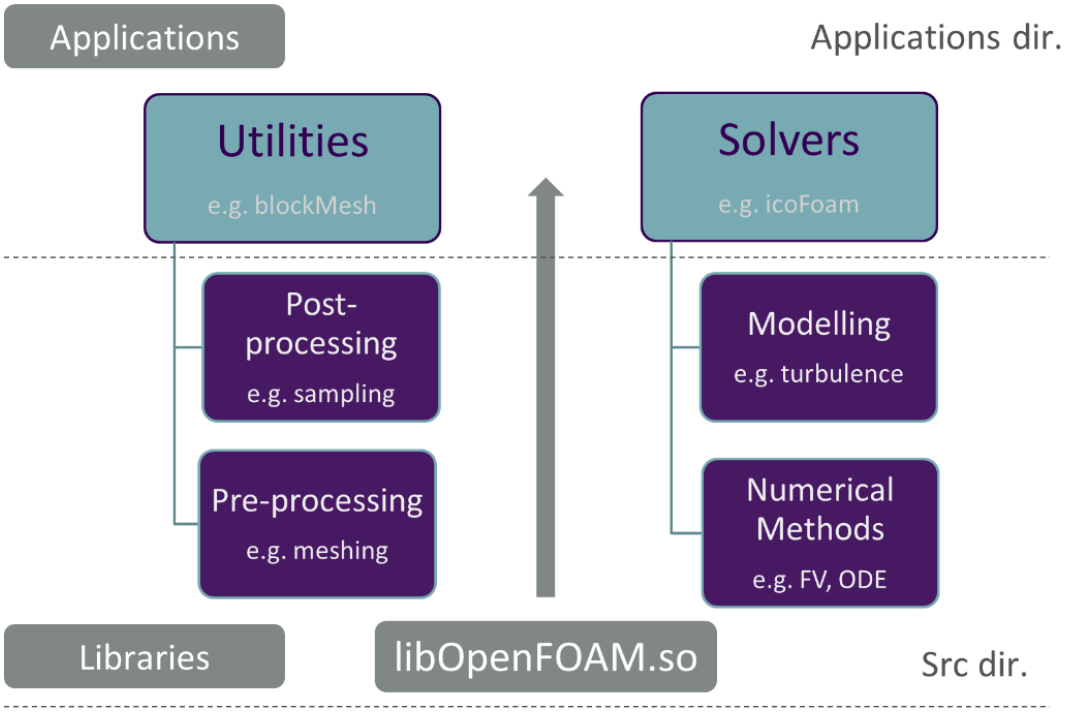

Figure 32: OpenFOAM library folder overview [92].

5.3.1 Solvers

The OpenFOAM library includes a large range of solvers with varying equations and algorithms depending on the type of analysis required. OpenFOAM uses similar standard solvers to ANSYS Fluent, the OpenFOAM user guide (2015) [11], lists the common solvers used for incompressible flow as:

- "icoFOAM – Transient solver for incompressible, laminar flow of Newtonian fluids".
- "pimpleFOAM – Transient solver for incompressible, turbulent flow of Newtonian fluids on a moving mesh".
- "pisoFoam – Transient solver for incompressible, turbulent flow, using the PISO algorithm".
- "simpleFoam – Steady-state solver for incompressible flows with turbulence modelling".

Although the word FOAM is added to the end of the solver name the solvers are the standard algorithms, for example PISO and SIMPLE. An example of commonly used compressible solvers in OpenFOAM taken from the OpenFOAM user guide (2015) [11], are:

- "rhoCentralFoam – Density-based compressible flow solver based on central-upwind schemes of Kurganov and Tadmor".
- "rhoPimpleFoam – Transient solver for turbulent flow of compressible fluids for HVAC and similar applications, with optional mesh motion and mesh topology changes".
- "rhoSimpleFoam – Steady-state solver for turbulent flow of compressible fluids".

These again use the same algorithms but set up for compressible flows. Another very useful aspect of OpenFOAM is the built-in ability to do particle-based analysis, therefore OpenFOAM can be used to analyse rarefied gas conditions. The solver used to do this is called dsmcFOAM. dsmcFOAM is a DSMC solver for transient, multi-species flows.

5.3.2 OpenFOAM Boundary Conditions

OpenFOAM has built in meshing tools called blockMesh for simple geometries and SnappyHexMesh for more complex geometries. There is also a Mesh translation function within OpenFOAM that coverts externally produced meshes into a coded file that can be read in OpenFOAM. Geometry can also be imported as STL files if the user wishes to perform the meshing within OpenFOAM. The built in CheckMesh function is useful for checking if there is poor mesh in the imported file. Unlike ANSYS and COMSOL, OpenFOAM does not have its own GUI and uses a third party post processing software called ParaView, this is a powerful tool that is also utilised by other open source programs. Gas properties such as velocity, temperature, number density, etc., are set at the boundaries [93]. Selecting the appropriate boundary condition is vital for the simulation to be successful and incorrect boundary conditions will result in physically incorrect predictions and potential solver failure [11].

5.3.3 dsmcFOAM

The OpenFOAM solver dsmcFOAM, is code developed by the authors of OpenFOAM by modifying the existing molecular dynamics (MD) code [93]. dsmcFOAM is a solver for 3D, transient, multi-species flows [11]. Separating the computational domain into a collection of grid cells is required to implement DSMC [93]. Once molecular movement has occurred, the particle collisions are simulated in each cell stochastically. DSMC simulator particles can reach as high as 10^8 in large 3D simulations, however smaller practical 2D geometries can provide modest solutions and can be run on a standard desktop computer [93]. DSMC method particles are known as Parcels, 1 DSMC Parcel represents approximately $10^6 – 10^{18}$ physical gas particles. All the parcels in the simulation are termed as a cloud.

The following fundamental features of the existing MD code are featured in the dsmcFOAM capability:

- Particle initialisation
- Arbitrary geometries
- Particle tracking in unstructured, arbitrary polyhedral meshes [93].

Scanlon (2010) [93], states the dsmcFOAM current features include:

- Steady and Transient Simulations.
- Unlimited parallel processing capability (splits the simulation into patches and assigns processing power to each one which reduces the computation time.
- Arbitrary 2D/3D geometries.
- Automatic sub-cell generation to promote nearest neighbour collisions.
- Arbitrary number of gas species.
- VHS collision model.
- Larsen-Borgnakke internal energy redistribution model.
- Diffuse or specular wall reflection boundaries.
- Cyclic (periodic) boundaries.

The diffuse or specular wall interaction model is currently missing code that allows prediction of particles being absorbed at the wall and tracking the amount of material deposited. To produce an absorbing wall interaction model, a new boundary is required to be programmed by copying and pasting parts of the code from other boundary conditions. The code within these library files will contain those parts to be copied, additional code writing may also be required.

5.3.4 dsmcFOAM+

dsmcFoam+ is an adapted version of the standard Direct Simulation Monte Carlo (DSMC) solver in OpenFOAM. The dsmcFoam+ solver is designed entirely with OpenFOAM's C++ object orientated framework which benefits from flexibility to adapt and change the code as required [53]. dsmcFoam+ relies on the standard OpenFOAM directory, therefore pre and post processing capabilities are unchanged from the standard solver. The dsmcFoam+ has many additional features that are not included in the standard dsmcFoam [53].

White (2017) [53], states that the additional features include:

- Molecular vibrational and electronic modes
- Chemical reactions
- Subsonic pressure conditions
- Arbitrary axisymmetric geometries
- Mass flow rate measurement
- Simulation quality reports

The algorithm in figure 33 is the basic time integration scheme for DSMC within openFOAM and is also used for dsmcFOAM+. The pre request for the simulation is the user enters macroscopic values for temperature, velocity and density, which are then used to insert the particles with energies and positions [53].

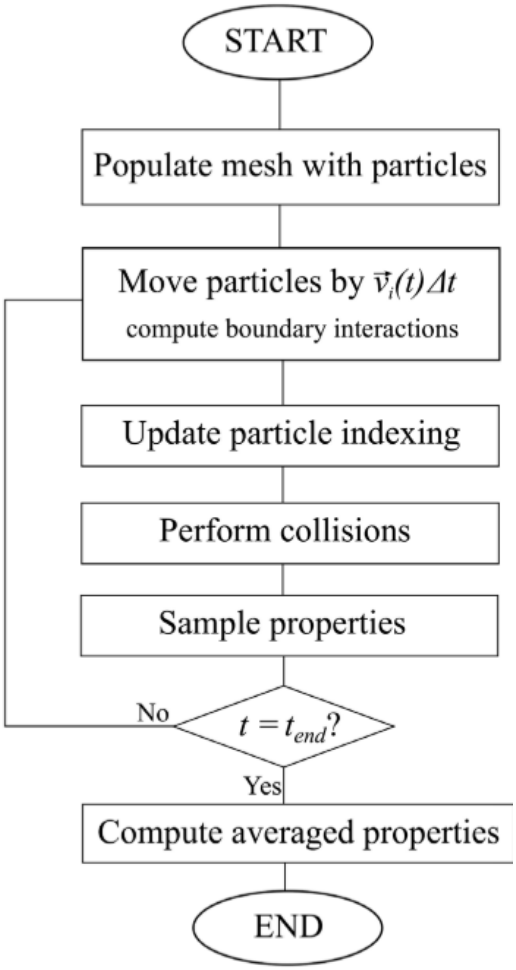

Figure 33: Flow chart of the basic DSMC time-integration scheme. White et al [53].

The algorithm runs as follows

1. Mesh is populated with particles
2. Movement of particles are tracked of their new position in the mesh
3. The list of particles is updated and re-indexed and set the number of collisions to attempt (37).
4. Number of collisions computed probabilistically in each computational cell
5. Sample the time averaged particle properties to calculate macroscopic fields
6. Repeat until the end of the simulation time steps

OpenFOAM is a prevalent analysis tool found in research papers to conduct DSMC analysis of physical vapour deposition. It is possible to produce hybrid method by patching Navier-Stokes models together with DSMC replicating rapidly rarefying conditions. Gott (2015) developed a hybrid method using OpenFOAM to simulate rapidly rarefying flow fields experienced in vapour deposition of Titanium [94]. The engineering software available for this research has been investigated in this chapter. Looking at what boundary conditions are required for the solvers and what algorithms the solvers use, to gain an understanding of what the capabilities are. ANSYS and OpenFOAM methods overlap whereas COMSOL uses different methods. To investigate the software suitability further, the next chapter focuses on some benchmarking exercises. This is the build confidence in the performance of the opensource software OpenFOAM and how well it performs in comparison to the well established software ANSYS. It is also conducted to gain information on the suitability these engineering programs have for simulating the fluid flow of the vacuum lock.

6. Benchmarking of Continuum and Particle Based Fluid Flow Models

To simulate the vacuum lock requires an understanding of the theory that can be applied to analyse the system and suitable computational modelling software to solve the problems. So far chapter 4 has covered theory applied to gas flow across a range of gas regime and chapter 5 has introduced computational modelling software. To reproduce the physical conditions of a vacuum locks is difficult due to the varying pressure. The pressure starts at atmospheric pressure at the inlet to the entry lock and reduces changing through continuum conditions to molecular flow near the coating chamber. The next action is to investigate some existing analysis methods to discover if they are suitable to simulate the behaviour of the fluid flow in the vacuum lock and produce a solution that will determine what pumping capacity is required to sustain a certain pressure within the vacuum lock. Incompressible flow is possible in the larger spaces in the vacuum lock chamber, but there are also clearances that provide tight gaps for air to travel through therefore compressible flows are considered. Metal vapour transport is also a consideration and rarefied gas flow at pressures lower than 1 Pa. Commercial software will be used as analysis tools as it is well established as well as OpenFOAM because it can be used for particle based methods which is convenient for the low pressure analysis. OpenFOAM is an open source software that has less papers and proven track record than mainstream software. Benchmarking OpenFOAM against existing commercial software such as ANSYS and COMSOL can investigate the accuracy of the software, how user friendly it is and the suitability to analyse the flow within the completed vacuum lock design.

6.1 Lid Driven Cavity

The Lid Driven Cavity problem looks at isothermal, incompressible flow in a two-dimensional square cavity [11]. The two corners where the moving lid passes the walls of the chambers form a sharp angle creating singularities. This causes numerical challenges resulting in difficulty in obtaining an exact solution [95]. Despite the singularities the lid driven cavity analysis has been frequently used for testing and

evaluating numerical techniques [96]. The lid driven cavity problem does not include low-pressure conditions but is a good place to start with computational fluid dynamics to build an understanding of fluid flow in the viscous region with continuum flow. It is also good for seeing how different types of engineering software can be used to analysis flow problems.

These are 2D simulations. The accuracy of 2D recirculating flows has been investigated and Shankar states "The study of 3-D cavity flows is difficult, no matter whether analytical, computational, or experimental techniques are used. In fact, hardly any work existed until the pioneering experimental work of Koseff & Street and coworkers at Stanford in the early 1980s. Their studies, however, changed the whole picture because they clearly showed that cavity flows were inherently 3-D in nature. Not only are 2-D models inadequate, they can be seriously misleading" [97]. Great care needs to be taken if a 2D simulation is produced to solve a 3D physical problem, without validation the results could overlook the difference between a 2D and 3D flow problem.

In order to understand the conditions within a chamber at atmospheric pressure with a sheet sliding through air, an initial investigation was carried out using tutorials in OpenFOAM, ANSYS Fluent and COMSOL for a Lid Driven Cavity problem. The reason for this simple analysis was to familiarise using the software, gaining an understanding that can be built upon to produce a much more complicated analysis as the research progresses. OpenFOAM is an open source software so this process also checks the performance of OpenFOAM against paid software. The geometry is shown in Figure 34 in which all the boundaries of the square are all 1 metre walls. The top wall moves in the x-direction at a speed of 1 ms^{-1} while the other 3 are stationary. The flow was assumed laminar and was solved for laminar, isothermal, incompressible flow.

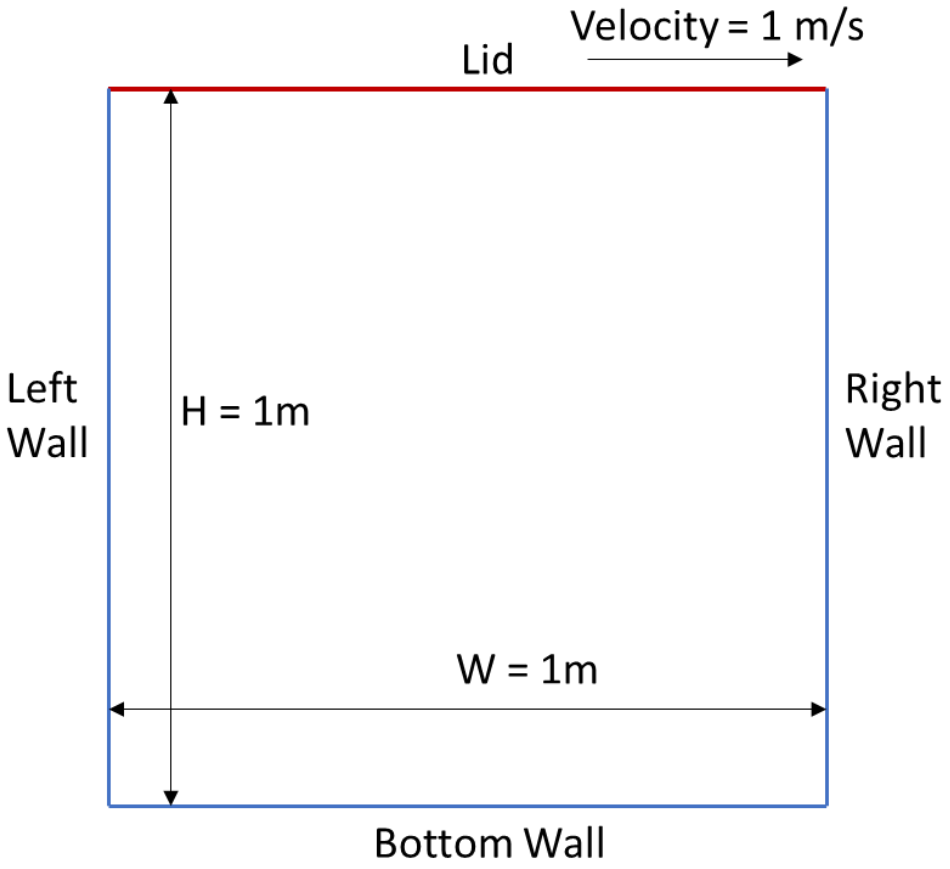

Figure 34: Lid driven cavity 2D diagram

The results in Ghia el al 1982 are for Reynolds numbers of laminar, transitional and turbulent flow. Reynolds numbers used are 100, 400, 1000, 3200, 5000, 7500 and 10000. The flow is considered as incompressible laminar flow, that is a fair assumption for Reynolds numbers under 2000, however the value of 3200 will have a mixture of laminar and turbulent flow and above 4000 will have turbulent flow. For the purpose of this study the tutorials for OpenFOAM [98], ANSYS Fluent [99] and COMSOL Multiphysics [100] were used and the results compared with Table 1 from Ghia et al (1982), which are velocity u along the vertical line through the geometric centre of the cavity [96]. Results were obtained in OpenFOAM and ANSYS Fluent and COMSOL are showed visibly in the figures 35. 36 and 37.

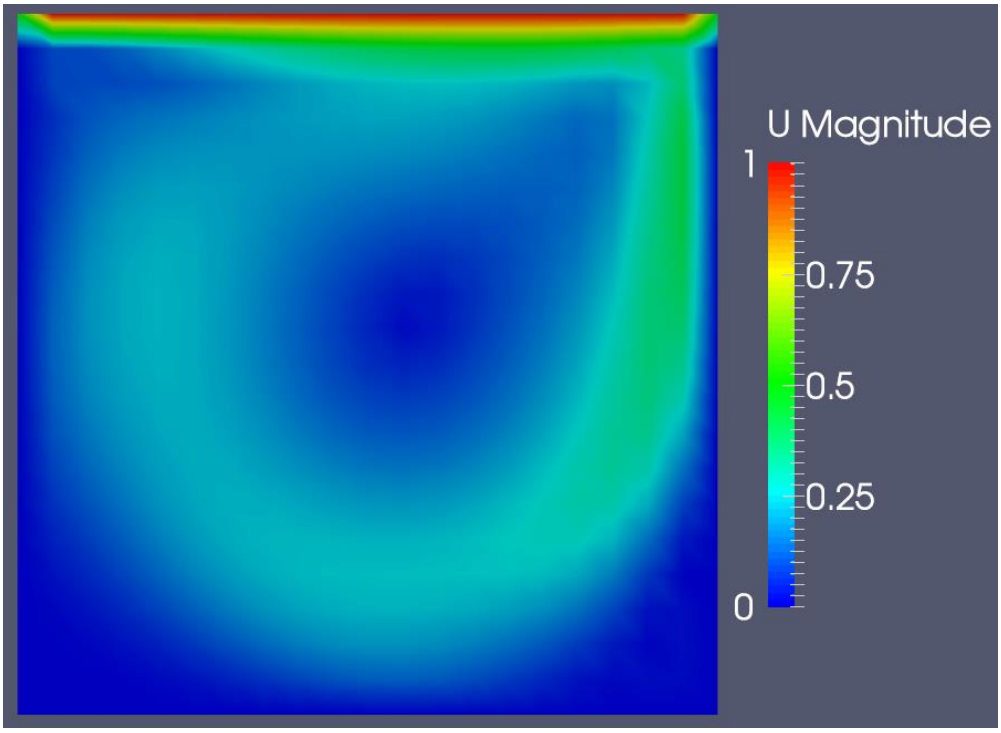

Figure 35: OpenFOAM lid driven cavity velocity result for Reynolds 1000

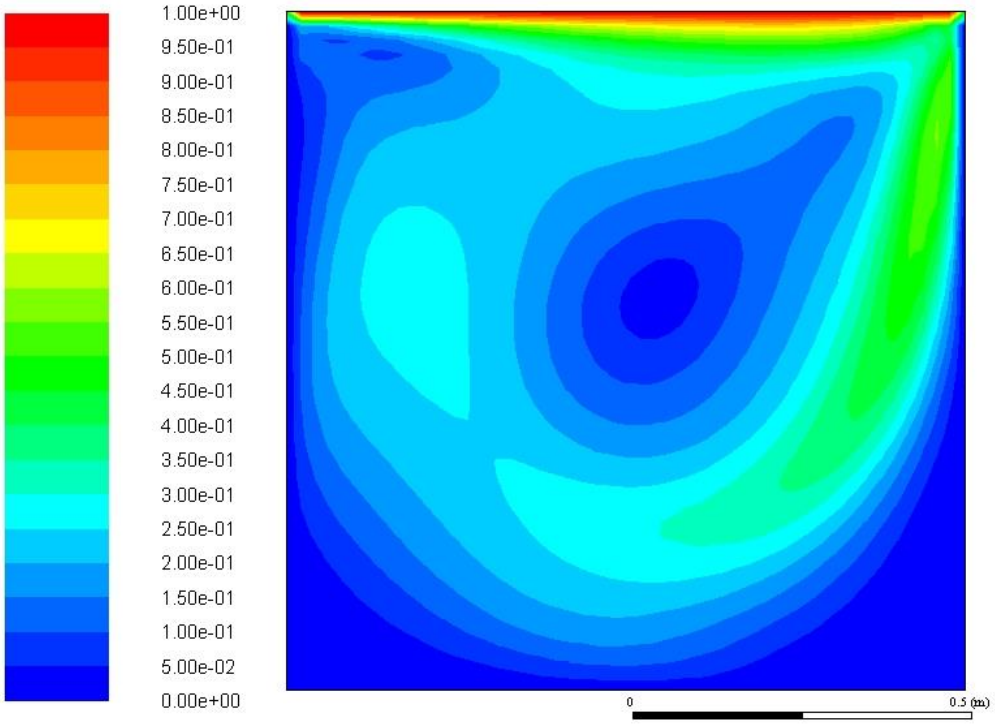

Figure 36: ANSYS Fluent lid driven cavity velocity result for Reynolds 1000

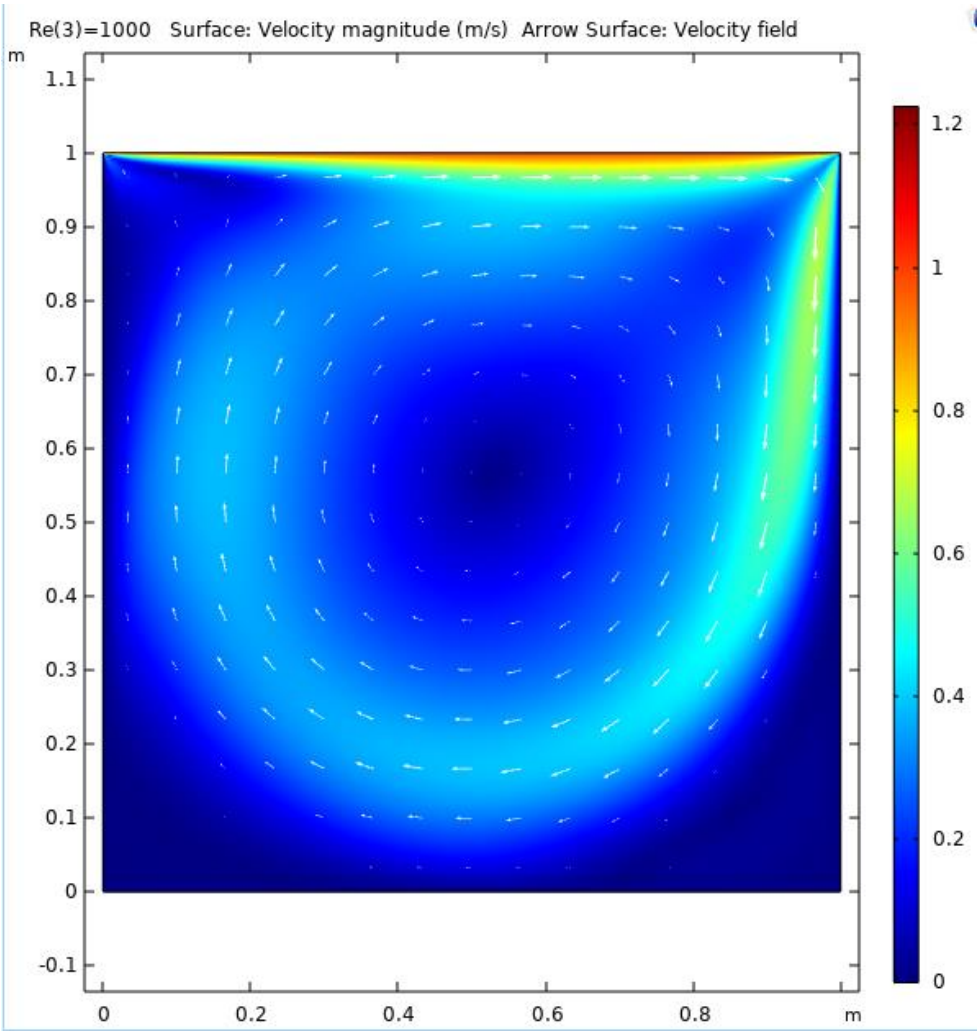

Figure 37: COMSOL lid driven cavity velocity result for Reynolds 1000

The Lid Driven Cavity simulation results for laminar flow were compared with numerical results from the benchmark data of Ghia et al (1982). The results shown are the velocity across the centre (y-axis) of the lid driven cavity. The results in figure 38, 39 and 40, show very close correlation. Further investigation was made into the transitional and turbulent flow within the Lid Driven Cavity by increasing the Reynolds Number. The results were again compared with the work from Ghia et al (1982). Shown in figures 41 to 44.

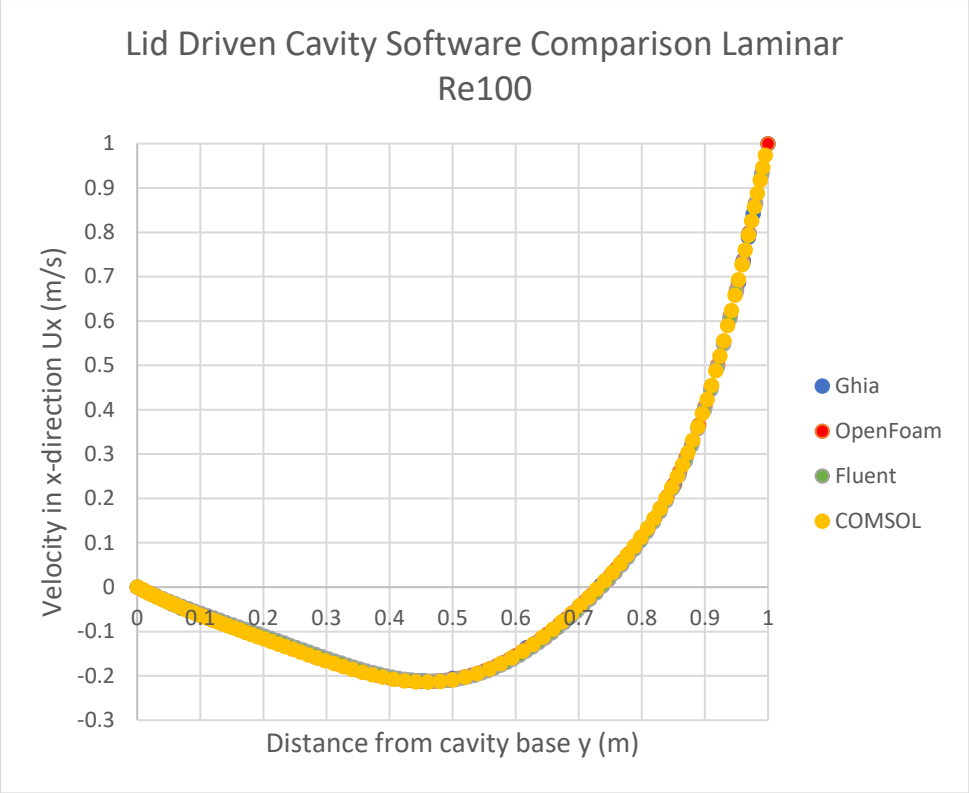

Figure 38: Lid driven cavity comparison results Reynolds 100

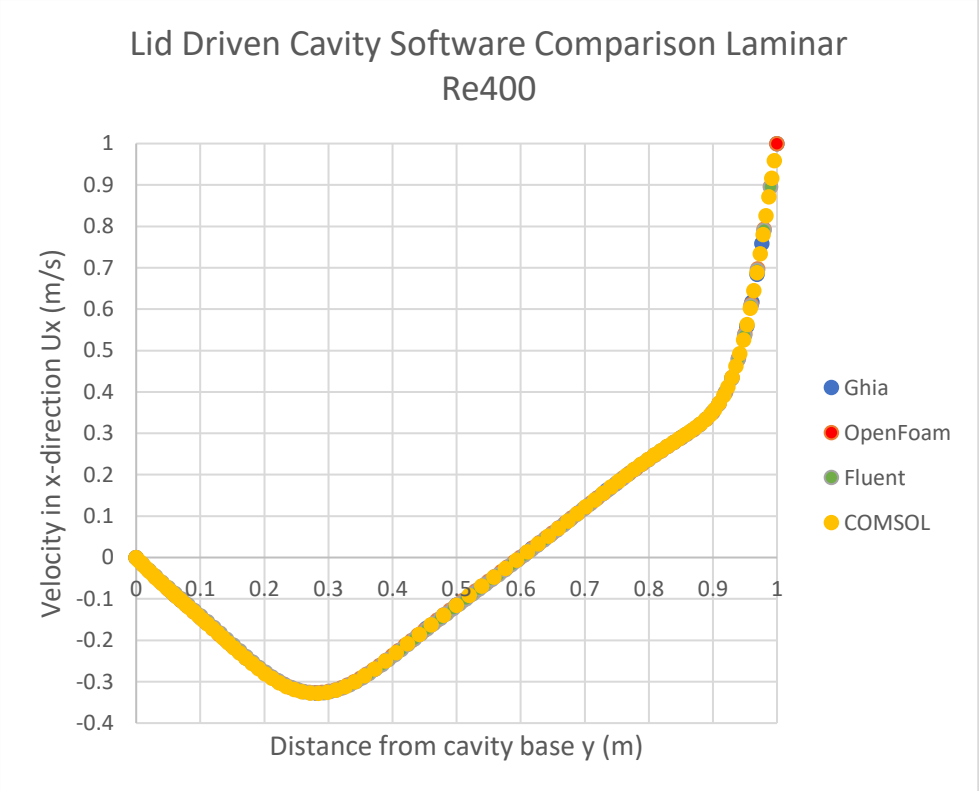

Figure 39: Lid driven cavity comparison results Reynolds 400

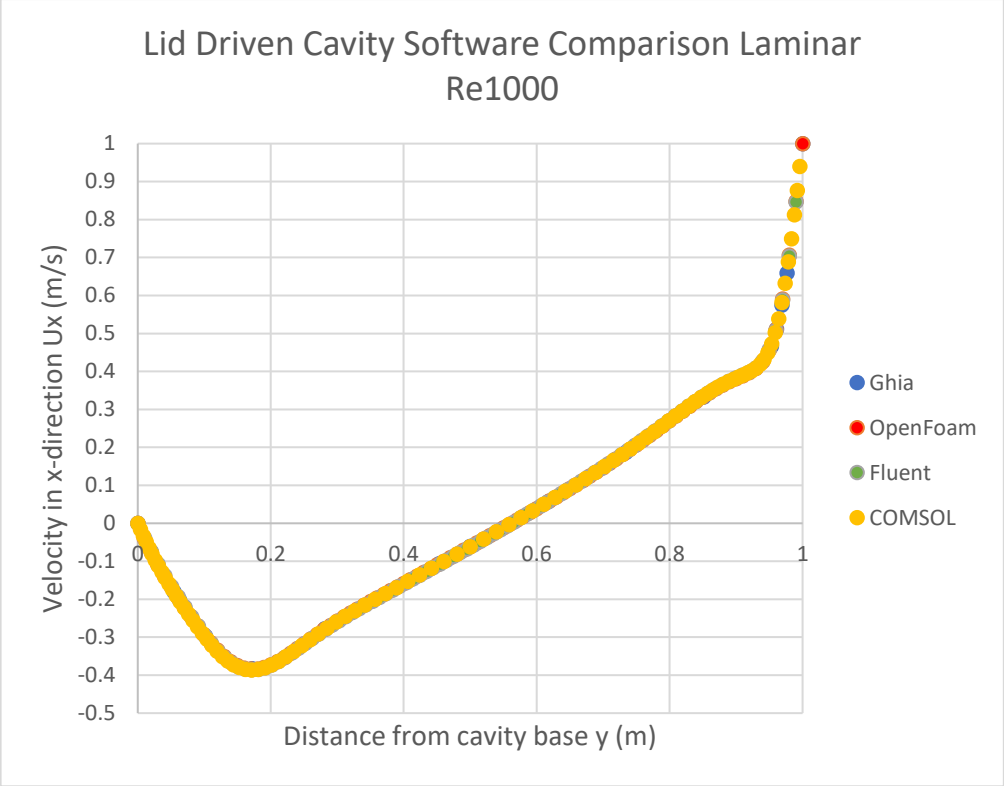

Figure 40: Lid driven cavity comparison results Reynolds 1000

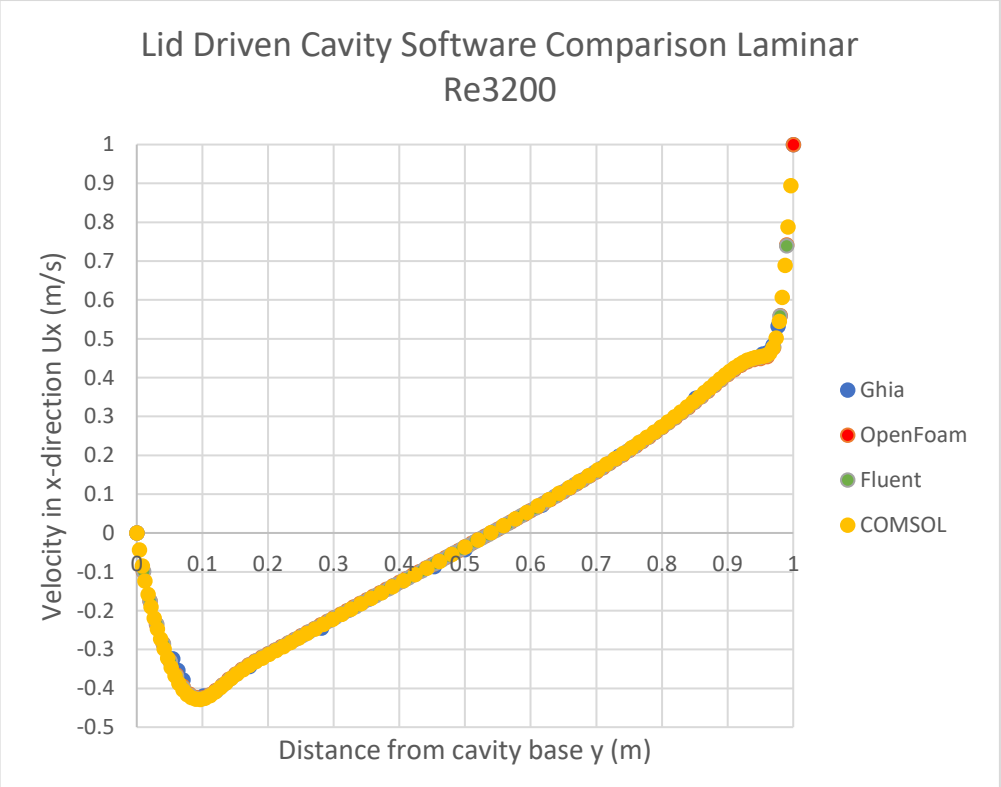

Figure 41: Lid driven cavity comparison results Reynolds 3200

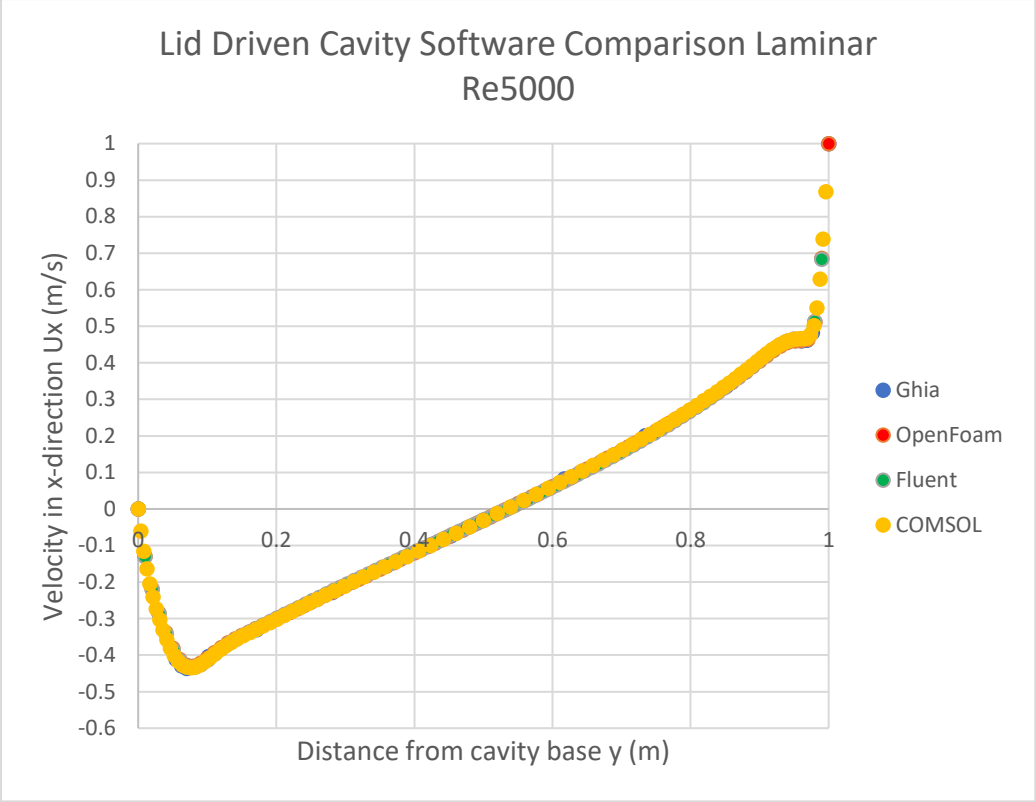

Figure 42: Lid driven cavity comparison results Reynolds 5000

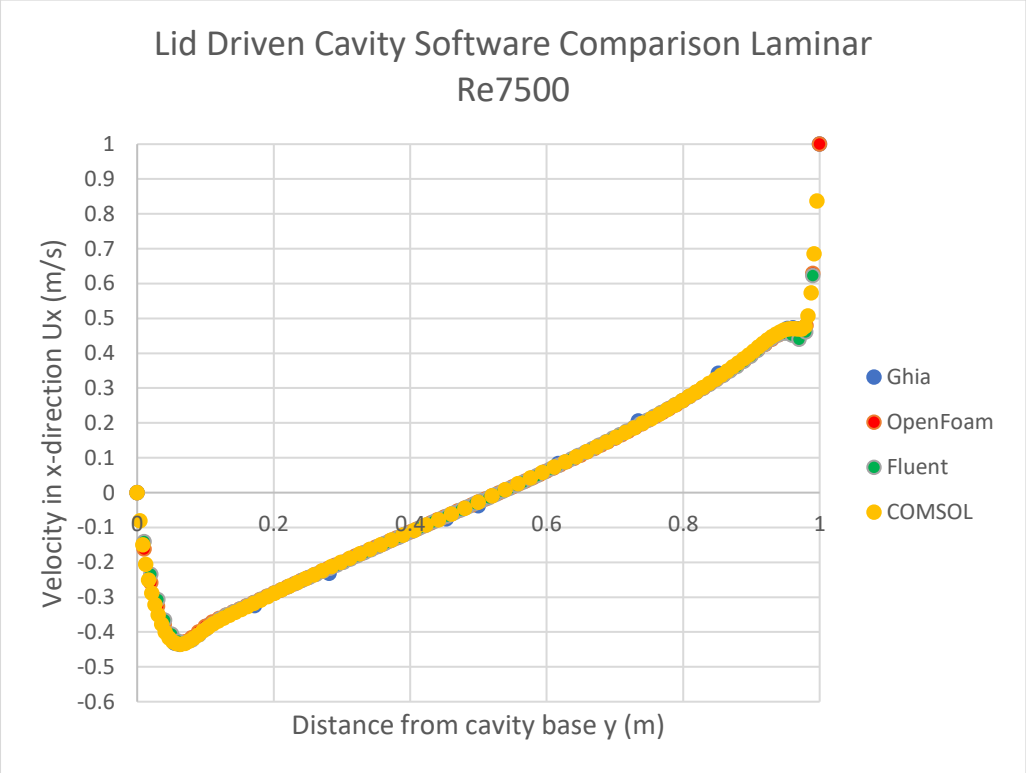

Figure 43: Lid driven cavity comparison results Reynolds 7500

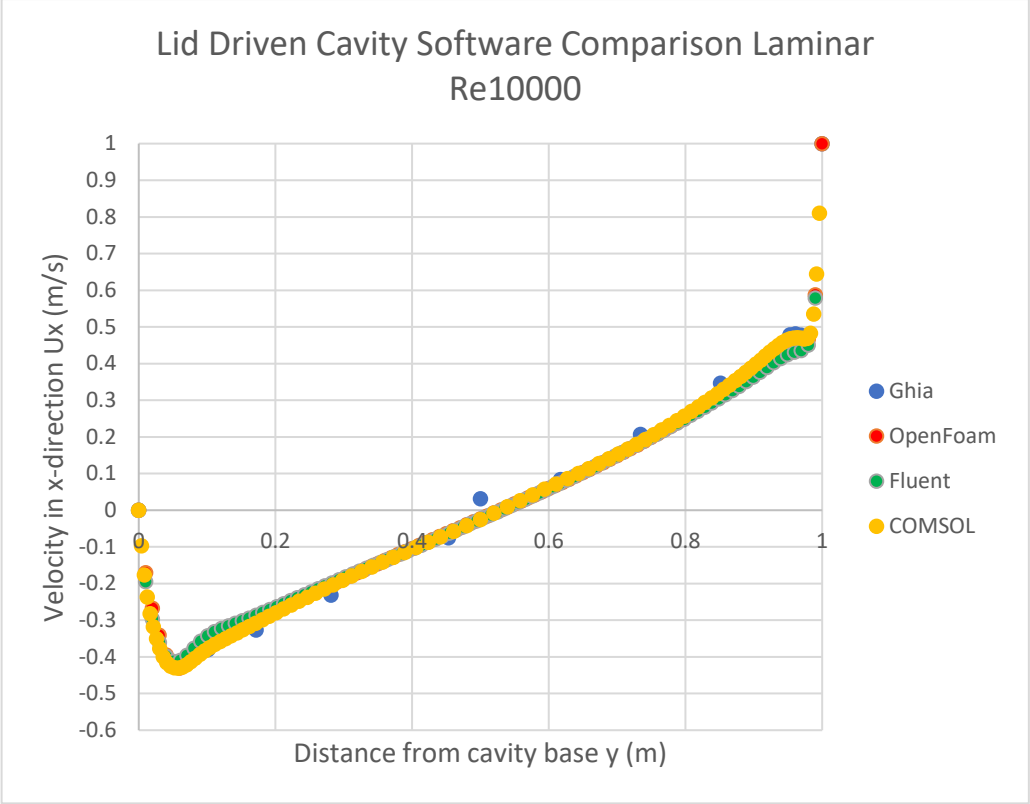

Figure 44: Lid driven cavity comparison results Reynolds 10000

All the engineering software matched closely to the results from Ghia et al (1982). The software did not match up quite as closely at the higher Reynolds numbers, singularities might be more problematic depending on how the problem is being solved. Turbulence models and enhanced near wall treatment could be applied to get the more accurate results of the CFD problem, however the results from Ghia et al do not take into consideration turbulence modelling in the results published in the paper. The pressures within a vacuum lock stay similar regardless of line speed [2]. This has been mentioned through several of the patents and the effect of the strip moving over evacuated air is unlikely to result in the same flow patterns as the lid driven cavity which is at atmospheric pressure. Turbulence is highly likely because of the powerful pumping that will be required. The lid driven cavity problem has provided confidence of OpenFOAM and accuracy of results but will not cover the analysis required for the lock. Further investigation is required.

6.2 De Laval Nozzle

The air flowing into the vacuum lock is restricted by reducing the clearances for air to flow through. Nozzles are designed to reduce the area from the inlet to the outlet to increase the velocity of the flow. This behaviour could be experienced in the vacuum lock as the geometry reduces from larger areas to smaller areas in several places. High velocity flow involves significant changes in density, this type of flow is considered compressible. Compressible flow is a combination of fluid dynamics and thermodynamics. [101]. The geometry of the vacuum lock also increases after the small clearances therefore diverging sections are also present within the structure. A converging-diverging nozzle chokes the fluid at the throat of the converging section of the nozzle and then accelerates the fluid in the diverging section [101]. In some of the initial simulations of the vacuum lock, high velocities were observed, therefore investigation was made to understand the nature of the flow.

A converging nozzle velocity is restricted to sonic velocity (Ma = 1) occurring at the chocked outlet (throat) of the nozzle. Adding a diverging section after the throat of the nozzle, can result in accelerating the fluid to supersonic velocities (Ma > 1). There is no guarantee that forcing fluid through a converging-diverging nozzle will result in fluid accelerating to supersonic velocity [101]. If the back pressure is incorrect the velocity can actually reduce in the diverging section [101]. The following analysis of a de Laval nozzle was performed in OpenFOAM and ANSYS Fluent and then compared with analytical results to show similarities between simulation and numerical results. A visual representation of the simulation contours can be seen in figure 45. The geometry for the nozzle and pressures used were taken from the paper on flow through a de Laval nozzle written by Connor Robinson [102]. The radius of the de Laval nozzle was calculated using the following formula from the Robinson paper [102].

$$r = 1 - 0.868z^2 + 0.432z^3 \tag{6.1}$$

Values of 0 to 2 were used for z and the equation was input into Solidworks to form a 3D model, an axisymmetric model could have been used, but a 3D model was used to investigate results against the wedge model used in the Robinsons paper. For the

analytical calculations the following equations were used from the Robinson paper, the equations ignore viscosity and gravitational effects, assume steady state and laminar flow. The equations are for both subsonic and supersonic conditions

$$\frac{A}{A^*} = \frac{1}{M}\left(1 + \frac{\frac{\gamma-1}{2}M^2}{\frac{\gamma+1}{2}}\right)^{\frac{\gamma+1}{2(\gamma-1)}} \tag{6.2}$$

$$\frac{T0}{T} = 1 + \frac{\gamma-1}{2}M^2 \tag{6.3}$$

$$\frac{P0}{P} = \left(1 + \frac{\gamma-1}{2}M^2\right)^{\frac{\gamma}{\gamma-1}} \tag{6.4}$$

To rearrange and solve equation (6.4) for M (Mach number), a bisection method can be used, a pre-existing MATLAB code was used to do this and was checked against the NASA isentropic flow calculator [103] [104]. The A/A* ratio used the length values from ANSYS. The cross-sectional area at the throat of the nozzle, A*, is calculated from the minima z value, given in the Robinson paper as 0.658 where subsonic flow transitions into supersonic flow. The specific heat ratio (γ) for air is given as 1.4 [101]. Using this value and rearranging the equations Analytical Pressure, Velocity and Temperature could be calculated. The following charts represent the data calculated and simulated. The pressure at the inlet to the Nozzle is 101,325 Pa (atmospheric) and the outlet is 2533 Pa.

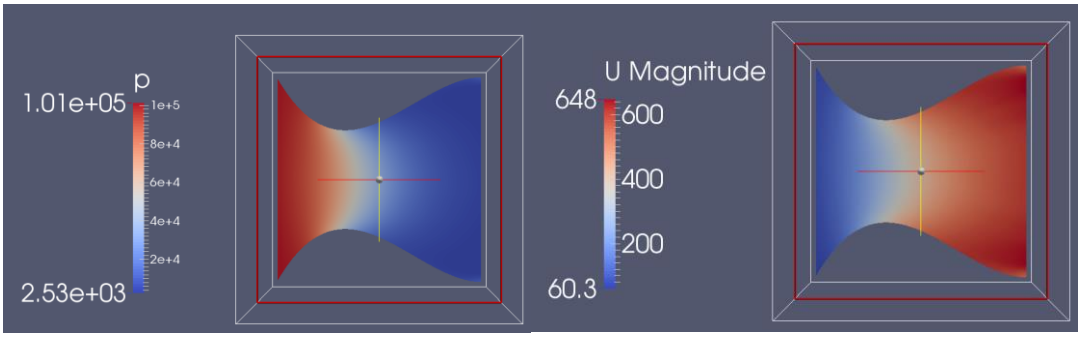

Figure 45: de Laval results in OpenFOAM for pressure and velocity

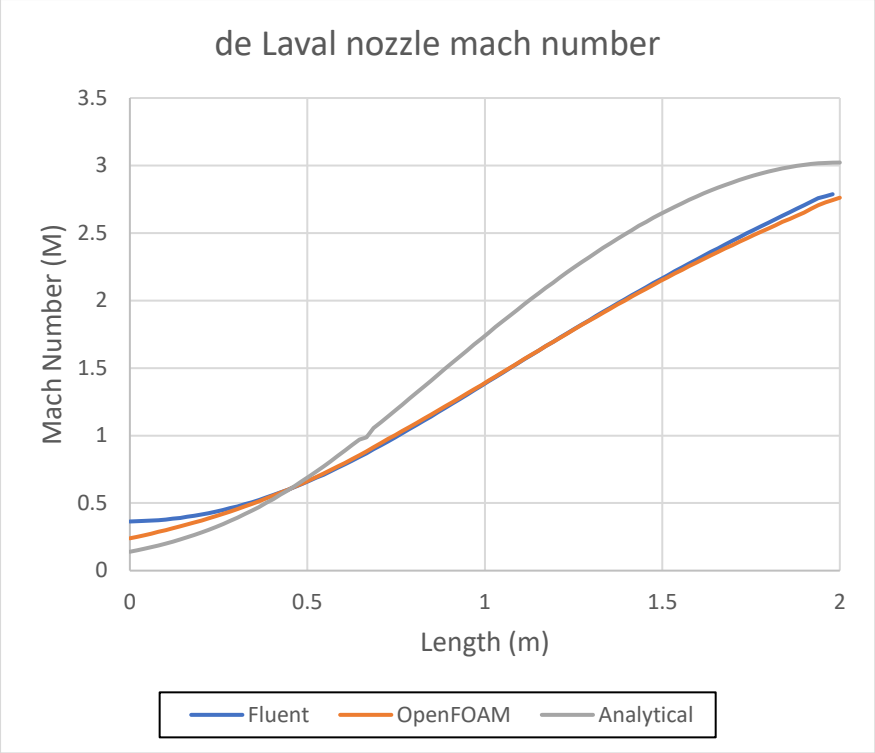

Figure 46: de Laval nozzle Mach number comparison

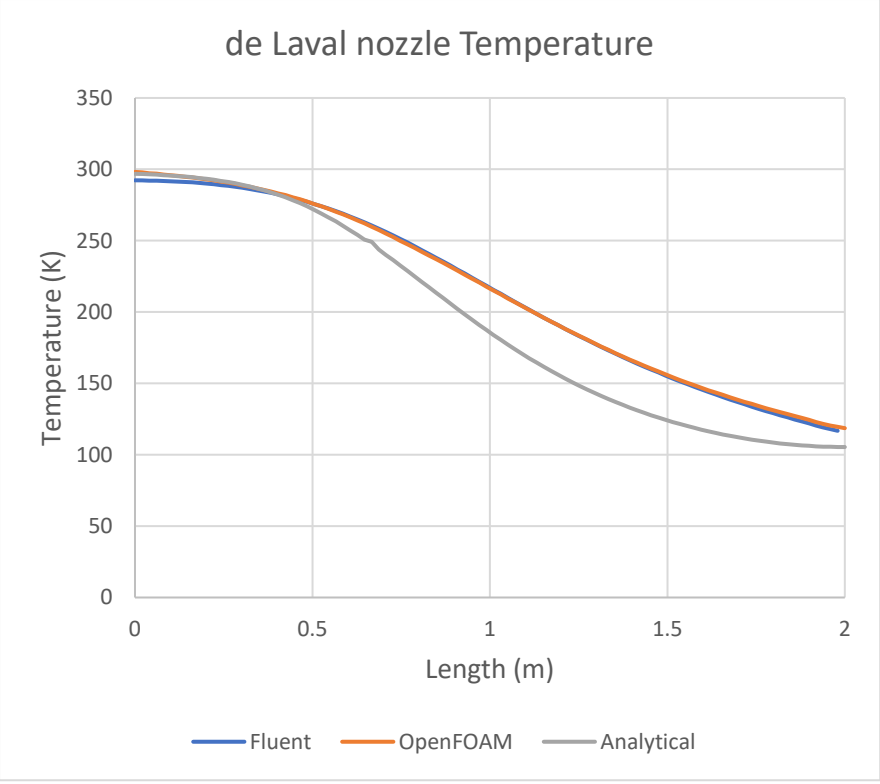

Figure 47: de Laval nozzle temperature comparison

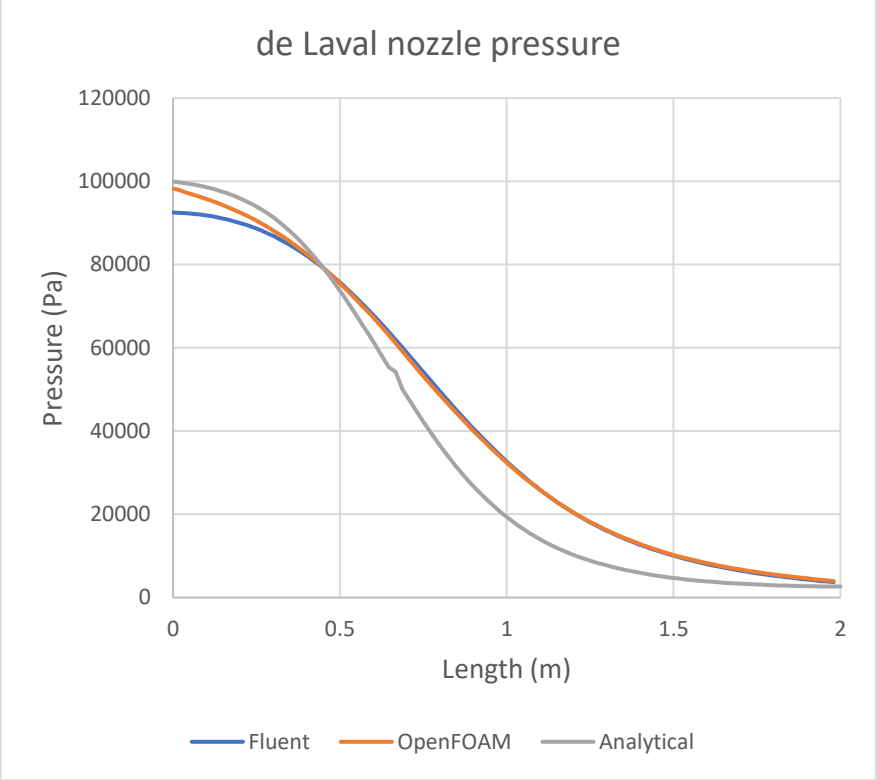

Figure 48: de Laval nozzle pressure comparison

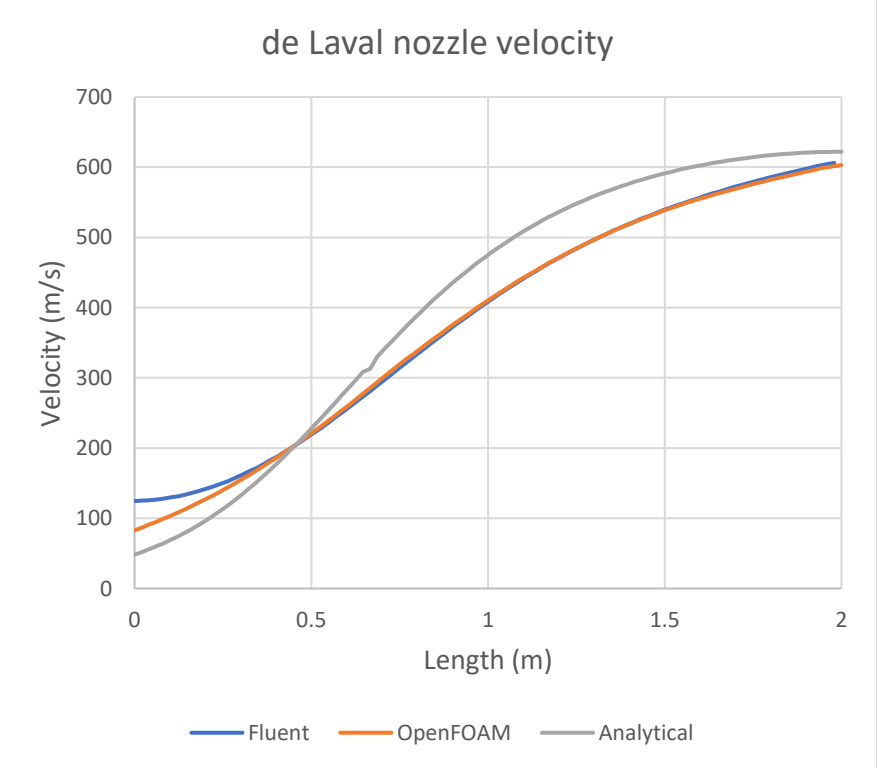

Figure 49: de Laval nozzle velocity comparison

The figures 46 to 49 show the results of the ANSYS and OpenFOAM simulations compared to analytical values. The results from the de Laval nozzles simulations are very similar although both differ slightly from the analytical results however that was the same in the Robinson paper and is most likely due to ignoring viscous terms (inviscid simulation). Some preliminary vacuum lock simulation results included high velocities indicating that there could be compressible flow and similar chocking of flow in the vacuum lock to the de Laval nozzle problem. OpenFOAM again showed good results in this benchmarking exercise and this time it is indicated that this analysis method could be used to form the analysis of the vacuum lock from atmospheric pressure down to a lower pressure. From chapter 4, the pressure could not reasonably be lower than 1000 Pa at the outlet due to the gas regime.

6.3 Metal Vapour Deposition Under Vacuum

The last benchmarking exercise investigates metal vapour deposition under vacuum conditions. This is more relevant to the vacuum coating chamber, however, is an important consideration in the EML-PVD coating system. The benchmarking exercise this time does not compare different software. A level of confidence in OpenFOAM has now been achieved by the existing benchmarking and there is some completed metal vapour deposition research to compare results. The purpose of this benchmarking exercise to build confidence in the DSMC solver within OpenFOAM by matching existing analysis and the potential to build upon this to apply it the zinc-magnesium vapour deposition. ABB investigated copper vapour deposition within vacuum interrupters. Vacuum interrupters are used in high voltage networks to interrupt short circuit currents. A vacuum interrupter consists of an evacuated chamber with two open contacts with an arc forming between them at the time of current interruption [12]. During arcing a copper vapour is produced from strong evaporation of the contacts and can deposit anywhere in the chamber. In regular use the component fails to withstand the large voltage applied across it due to a build-up of deposited copper vapour especially on the ceramic body of the container [12].

Hencken (2014), [12], conducted an analysis of metallic vapour condensation in a Vacuum Interrupter using FOAM, to understand the deposition of the copper vapour

tracking the locations and behaviour of the copper particles. The investigation included an adaption of the OpenFOAM code for the absorbing and reflecting boundary conditions [12]. Hencken (2014), [12], adapted the MixedDiffuseSpecular wall interaction model to implement a new absorbing wall class that allow for removal of particles from surfaces using fixed absorption coefficients for both ceramic and metal surfaces. Additionally, ABB obtained the parameter for the VHS interaction model from integrals and compared them with literature.

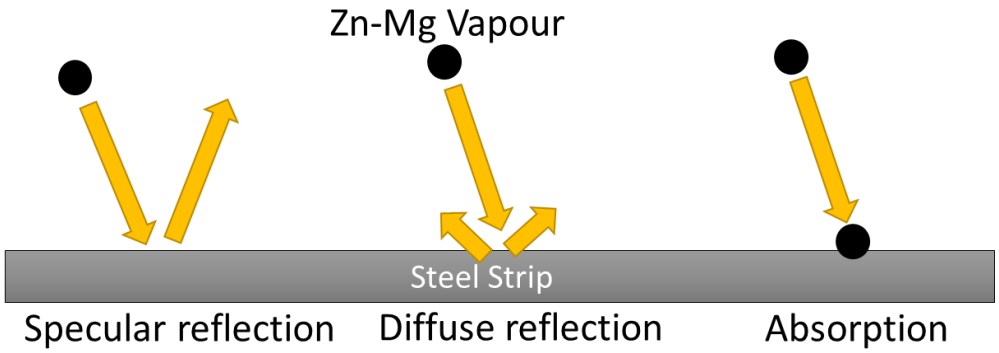

Figure 50: Wall interaction particle behaviour

Figure 50 shows the wall interaction behaviour when the metallic particles collide with the surface. Three main events can occur:

- Absorption – The particle is absorbed by the wall and chemically bonds to it.
- Specular reflection – The particle collides with the wall and is reflected at the same angle.
- Diffuse reflection – The particle collides with the wall but reflects in a random direction.

Another possibility is surface diffusion. This is where the particle collides with the wall and jumps along the surface before being absorbed, this would be a more complicated version of wall absorption. The analysis work conducted for the ABB Vacuum Interrupter is very similar to the analysis required to simulate metallic particle movement within the vacuum distribution box (VDB) developed by TATA and the vacuum conditions within the chamber and vacuum locks. Benchmarking this existing work is a starting point to gain a working DSMC simulation in OpenFOAM yielding

sensible results. It builds upon the work of Venkattraman and Alexeenko, [71], where a DSMC molecular model was produced for electron beam physical vapour deposition EBPVD of thin copper films. Choosing a suitable molecular model for the vapour is required for accurate DSMC modelling of vapour flows. The collision models use measurements of transport properties of the material such as coefficient of viscosity or thermal conductivity of the gas phase [71]. It is difficult to perform these measurements on non-volatile materials in this case metal vapours, [71].

Measurement of the transport properties for metal vapours at high temperature is difficult to obtain because of many unavoidable sources of error. Except for alkali metals, no viscosity data are available for metal vapours such as yttrium, barium and copper and few studies address the collision cross-sections for metal vapours [105]. The molecular model specifies the interaction between the simulated particles and is a very important input to modelling using the DSMC method [71]. The most commonly used molecular models with the DSMC method are the hard sphere (HS) and VHS models. They neglect the large range attractive force that exists between molecules.

Venkattraman and Alexeenko, [106], provide a reference diameter d_{ref} for copper of 0.45 nm, an exponent $\alpha = 0.42$ and a reference temperature $T_{ref} = 300K$. ($\alpha = \omega - 0.5$). These values will change depending on the molecular model used and the temperature. The VHS molecular model determined for Copper is to be used in axisymmetric DSMC simulations of a practical EBPVD vacuum deposition system using EVCFABEB-13 source [68]. The geometry used in the vacuum interrupter analysis is not public knowledge, therefore it had to be estimated. Some dimensions of a vacuum interrupter were detailed in an ABB article on 'new vacuum interrupters for contactors and switches' [107]. This gave a diameter of 51 mm and length of 96 mm, however this looked different to the one used in the work from Hencken (2014), [12], and has no internal dimensions.

The mesh image shown in figure 51 was used to determine the geometry by counting the mesh elements and then comparing with the dimensions of the similar component mentioned above. The areas where the mesh is refined are approximately half the

width. Considering a cell width of 1mm, that makes 106 mm wide and 56 mm in height. The values are reasonable as they are similar to the dimensions given.

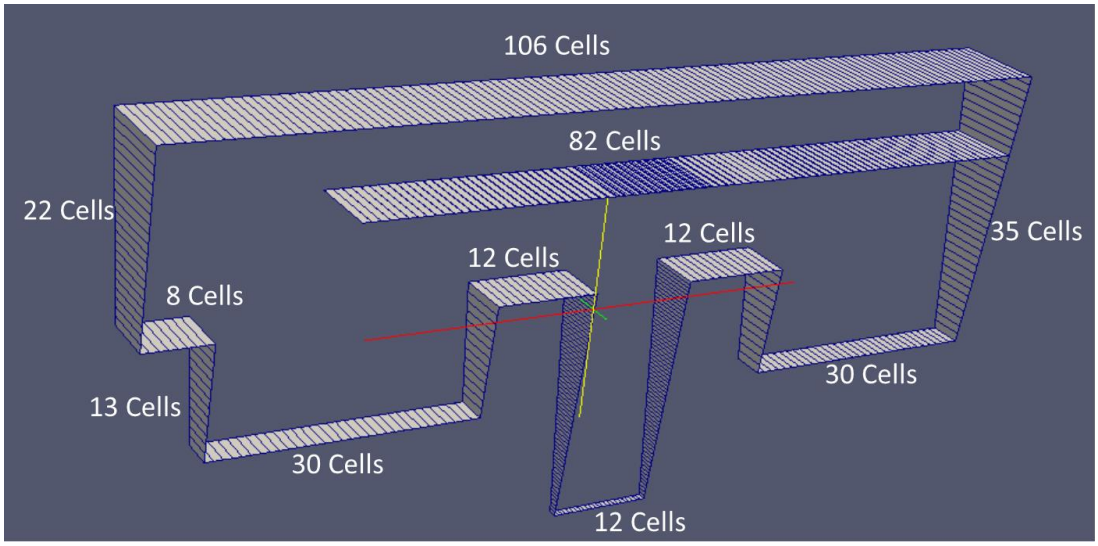

Figure 51: Adapted mesh image from Hencken (2014), [12]**.**

Figure 52 shows the geometry created in ICEM to include the strip surface; this is an axisymmetric model with defined surfaces produced to match the ABB model. Figure 53 is the corresponding mesh created from the geometry in ICEM.

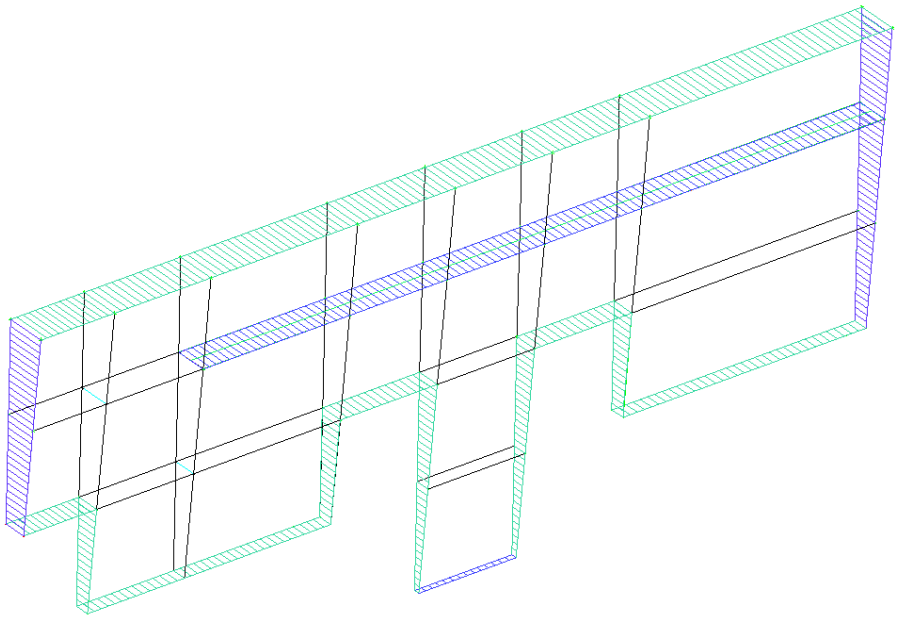

Figure 52: Vacuum Interrupter geometry created in ICEM

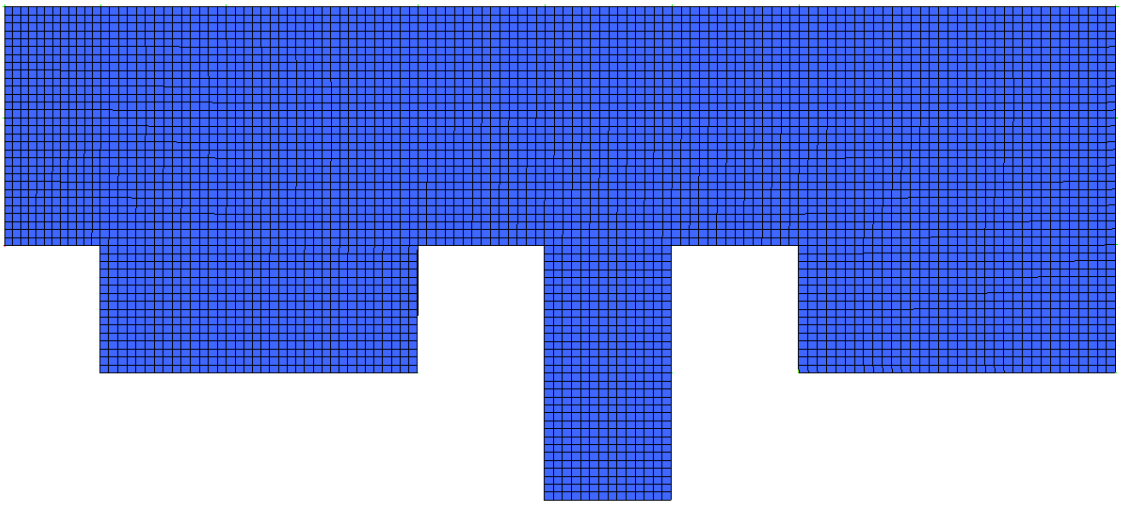

Figure 53: Meshed vacuum interrupter in ANSYS ICEM

6.3.1 Copper Calculation

The vacuum interrupter is evacuated to 10^{-8} mbar (10^{-5} Pa) inside the component. Temperature is likely to be higher as the current passes through the component and copper is vaporised, there are no values available for this. A way to consider the number density of the copper vapour is to calculate the dislodged copper particles by the charge applied to the vacuum interrupter when breaking the circuit. The vacuum interrupter rated short circuit breaking currents of up to 63kA kC/s Charge separation (assumed at 1 second)

- The elementary charge, e = 1.602×10^{-19} C (coulombs)
- Coulomb (C) = SI unit for electric charge. The charge transferred by a current of one ampere in one second [73].
- Ampere (A) = SI unit for electric current. Charge of one coulomb past a point in one second.
- Copper ionic formula Cu^{2+} (2 ions)
- Atomic Weight Copper = 63.54 g/mol or kg/kmol
- Density solid at 300K = 8.96 g/cm^3

$$Number\ of\ Electrons\ = \frac{I}{C}\ = \left(\frac{63000}{1.602 \times 10^{-19}}\right) \rightarrow 3.933 \times 10^{23} \qquad (6.5)$$

$$Number\ of\ Ions = \frac{1}{C}/2 = \left(\frac{63000}{1.602 \times 10^{-19}}\right)/2 \rightarrow 1.966 \times 10^{23} \qquad (6.6)$$

$$Number\ of\ Moles = \frac{Number\ of\ Ions}{Avogadros\ Number}\ = \frac{1.966 \times 10^{23}}{6.023 \times 10^{23}} = 0.326 \qquad (6.7)$$

$$Copper\ Mass = \ Number\ of\ Moles\ \times Atomic\ Weight\ Copper$$
$$= \ 0.326\ \times\ 63.546 = 20.7\ gs^{-1} \qquad (6.8)$$

The mass of copper particles deposited is approximately 20 grams per second. This is assuming maximum current flowing through the vacuum interrupter and the deposition lasting a full second; this is unrealistic.

$$Mass\ of\ One\ Copper\ Molecule = \frac{Atomic\ Weight\ Copper}{Avogadros\ Number} \qquad (6.9)$$

$$\frac{63.546}{6.023 \times 10^{23} \times 1000} = 1.06 \times 10^{-25} kg$$

number of Copper particles for 20 grams of Copper in one second is found from rearranging equation (4.20)

$$N = n \times N_A$$

$$N = \ 0.326 * \ 6.023\ \times 10^{23} = 1.96 \times 10^{23}$$

According to ABB the current needs to be interrupted within 10 milliseconds (one half-cycle) [12]. The Coulomb is charge transferred by current of one ampere for one second, due to the vapour being produced in a shorter time, there is less copper mass, therefore the mass can be considered as approximately 0.2 grams of copper particles.

$$\frac{20\ grams}{100} = 0.2\ grams$$

This reduces the number density of the copper particles as the mass of copper has reduced. Using basic chemistry equations known as Stoichiometric calculations in figure 54 and 55 the new number density can be calculated [108].

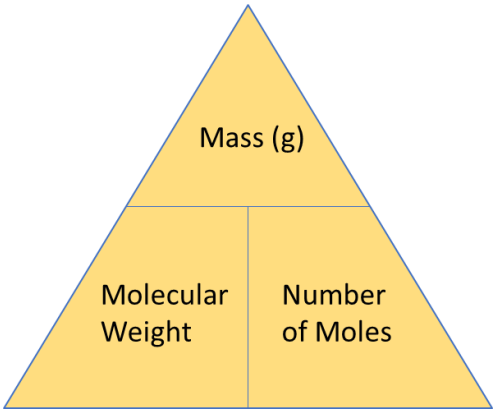

Figure 54: Number of moles stoichiometric calculation triangle

$$Number\ of\ Moles\ (n) = \frac{Mass\ of\ Substance}{Molecular\ Weight} = \frac{0.2}{63.546}$$

Then using Equation (4.20) the number of Copper particles for 0.2g of Copper can be calculated.

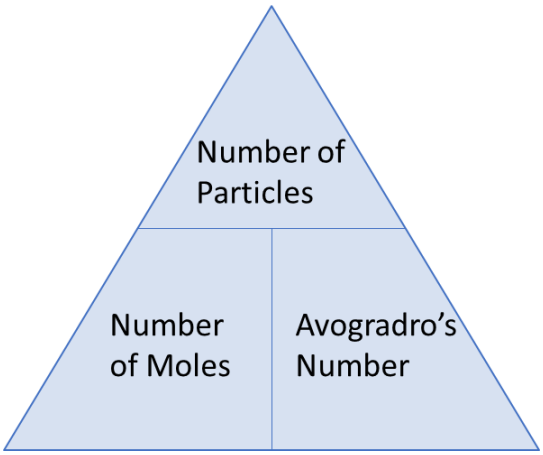

Figure 55: Number of particles stoichiometric calculation triangle

$$\frac{0.2}{63.546} \times 6.023 \times 10^{23} = 1.90 \times 10^{21}$$

6.3.2 Copper Vapour Properties

Measurement of the transport properties for metal vapours at high temperature is very difficult to obtain because of many unavoidable sources of error [105]. No viscosity data are available for transition metal vapours apart from alkali metals. Very few studies theoretically address the collision cross-sections for metal vapours. Six

molecular models for copper vapour are compared in the paper 'Molecular Models for DSMC Simulations of Metal Vapor Deposition' by Venkattraman and Alexeenko. It was found in the DSMC simulations that only molecular model 3 agreed well with experiments [71]. Therefore model 3 values were used in the analysis taken from figure 56.

Model No.	Model Type	d_{ref} (nm)	T_{ref} (K)	α
1	HS	0.234	300	0.000
2	HS	0.357	300	0.000
3	VHS	0.450	300	0.420
4	VHS	0.550	300	0.310
5	VHS	0.570	300	0.420
6	VHS	0.627	2000	0.349

Figure 56: Summary of molecular models used in DSMC simulations from Venkattraman and Alexeenko (2011) [71]**.**

Model 3 values:

$\alpha = 0.420$

$\alpha = \omega - 0.5$ [71]

$\omega = \alpha + 0.5 = 0.920$

$d_{ref} = 0.450$ nm

$T_{ref} = 300$

$P_{inside} = 1 \times 10^{-5}$ Pa

α = Angular scattering parameter

ω = Temperature dependence

d_{ref} (nm) = Reference diameter (VHS)

T_{ref} (K) = Reference Temperature

Mean free path – For the reference viscosity μ_{ref} at the reference temperature T_{ref}, The mean free path λ, for the VHS model is given in equation (6.10) [72].

$$\lambda = \frac{1}{\sqrt{2}\pi n d_{ref}^2 \left(\frac{T_{ref}}{T}\right)^{\alpha}} \tag{6.10}$$

Assuming no there is no temperature change this becomes

$$\left(\frac{T_{ref}}{T}\right)^{\alpha} = 1$$

$$\lambda = \frac{1}{\sqrt{2}\pi n d_{ref}^2}$$

$$\lambda = \frac{1}{\sqrt{2}\pi \times 1.9 \times 10^{21} \times (0.45 \times 10^{-9})^2} = 0.59\ mm$$

Knudsen number (Equation 4.1)

$$K_n = \frac{\lambda}{L} \tag{4.1}$$

$$K_n = \frac{0.59\ \times 10^{-3}}{46 \times 10^{-3}}\ 0.013$$

Continuum flow. $K_n < 0.001$ therefore this is in the region outside continuum flow, however it is not free molecule flow, $K_n > 10$.

Most probable velocity

$$v_{mp} = \sqrt{\frac{2k_b T_\infty}{M}} \tag{6.11}$$

$$v_{mp} = \sqrt{\frac{2 \times 1.38 \times 10^{-23} \times 300}{1.06 \times 10^{-25}}} = 280\ ms^{-1}$$

Particle thermal velocity

$$v_p = v_\infty + v_{MPV} \tag{6.12}$$

v_∞ is unknown but likely subsonic, use speed of sound as worst-case scenario.

$$v_p = 340 + 280 = 620$$

Mean collision time

$$\frac{\lambda_\infty}{v_{MPV}} \tag{6.13}$$

$$\frac{59 \times 10^{-3}}{280} = 210 \times 10^{-6}\, s$$

System volume

$$Volume = 1.32 \times 10^{-5}\, m^3$$

Number of cells

$$No.Cells = 42075$$

Average cell size

$$Cell\ size = \frac{Volume}{No.Cells} \tag{6.14}$$

$$= \frac{1.32 \times 10^{-5}\, m^3}{42075} = 3.14 \times 10^{-10}$$

Recommended DSMC procedure suggests that typical cell size should be a fraction of the mean free path [93].

Residence time

The resistance time equals the mean free path divided by the particle velocity

$$t_{res} = \frac{\lambda}{Vp} \tag{6.15}$$

$$t_{res} = \frac{0.59 \times 10^{-3}}{620} = 0.95 \times 10^{-6}\ s$$

Time step

The time-step should be a fraction of the mean collision time of gas molecules [72]. Mean collision time halved to adhere to this recommendation.

$$t_{step} = \frac{t_{res}}{5} \tag{6.16}$$

$$= \frac{0.95 \times 10^{-6}}{5} = \times 0.19 \times 10^{-6} s$$

Number of particles

For particle initialisation there needs to be at least 20 DSMC particles per cell

$$\text{Number of cells} \times 20 = 42075 \times 20 = 8.42 \times 10^{5}$$

nEquivalent particles

$$nEquivalentParticles = \frac{n_{\infty} \times System\ Volume}{Number\ of\ particles} \tag{6.17}$$

$$nEquivalentParticles = \frac{1.96 \times 10^{21} \times 1.32 \times 10^{-5}}{\times 10^{5}} = 2.98 \times 10^{10}$$

6.3.3 dsmcFOAM+ Simulation

Now all the properties required to run the simulation have been calculated the simulation can be run. The mesh produced in ANSYS ICEM was saved as a fluent mesh ASCII file that can be used in OpenFOAM. Mesh produced in ANSYS can be created in OpenFOAM using the function fluent3DMeshToFoam to create the OpenFOAM mesh format. Once the mesh was generated, the polyMesh folder was populated and the boundary conditions are generated as they were specified in the original mesh file. Depending on how they are specified, they will be named as wall, patch, symmetry, wedge, etc. The applicable boundary conditions are entered to the fields within the 0 folder [93]. After the boundary conditions have been correctly

specified and other variables have been input (time-step, hard sphere model, number of particles, etc.) the dsmcFOAM solvers are run.

The pre-processing utility dsmcInitialise is run first to create initial configurations of DSMC particles in arbitrary geometries [93]. Once pre-processing is complete, the dsmcFOAM solver runs until a solution is obtained. Following the solver the post processing utility dsmcFields is run to calculate the intensive fields (temperature, velocity and density) from extensive fields (mass, momentum and energy) [93]. The open source visualiser tool ParaView is used to carry out all post-processing of the simulations including the visual representation shown in figure 57. Predictive modelling is important for thin film coating applications as there are high costs of optimising deposition conditions due to the low pressures or ultra-high vacuum (UHV) conditions [68].

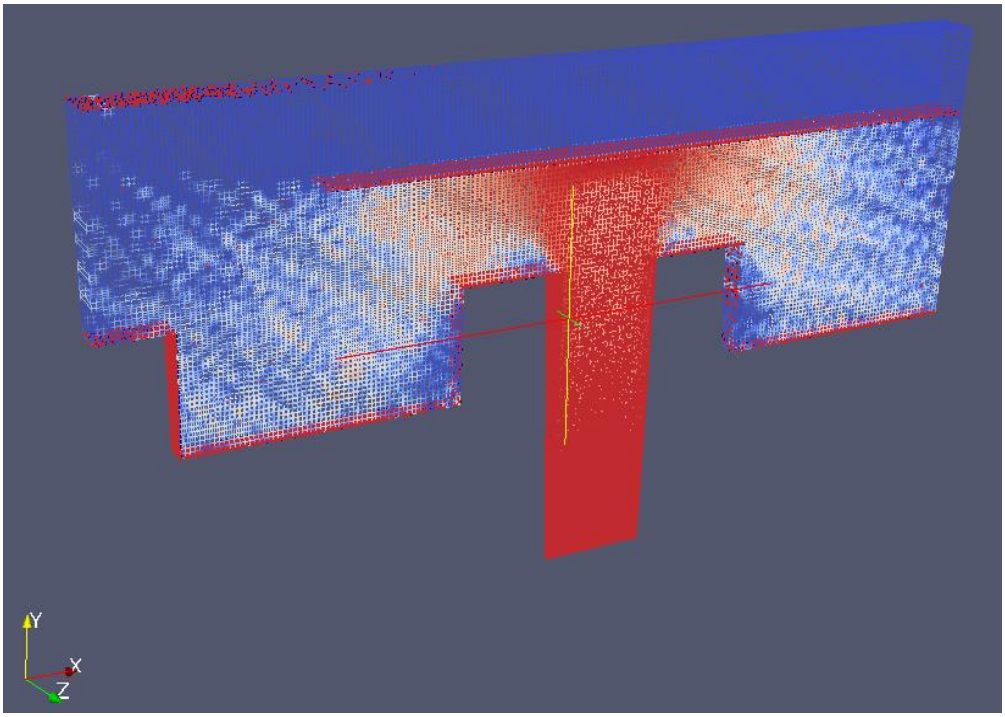

Figure 57: Vacuum interrupter copper particles visualisation in ParaView

With the absorbing wall function added to the wall interaction model, a graph of the material deposited on the wall has been produced and compared with the existing analysis by ABB. The sticking wall function within dsmcFOAM+ now makes it possible to produce a simulation of copper particles that are stuck to surfaces of the

vacuum interrupter. Plotting the particles sticking on the condensing shield, requires the fields to be written out as a surfaceScalarField for the plot data filter to be able to read it. Implementing this in the repository has not currently been achieved. The results can be saved as a csv file, this was then loaded into a program called liquid studio to delete the top line. Excel could not process the file as it had over 3 million rows. The file was than saved as a csv file again and imported into MATLAB to process the results.

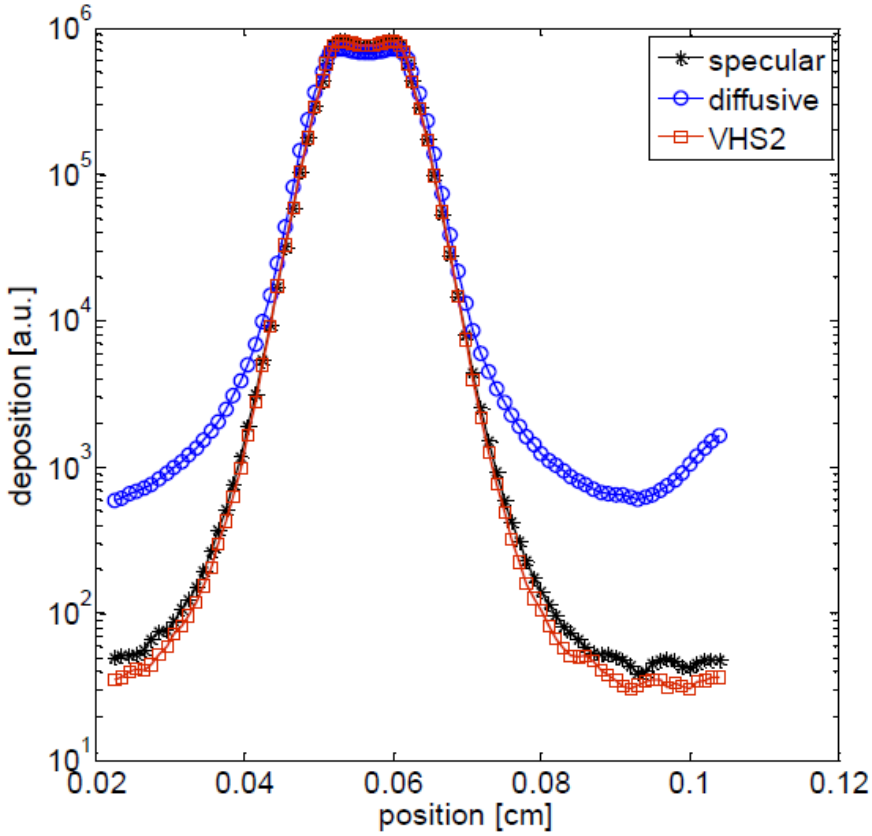

Figure 58: Results of material deposited on the condensing shield from Hencken (2014) [12]

The MATLAB code first removes unwanted columns from the CSV file leaving a matrix only containing the columns 13 to 15, which hold the stuck particles. It then uses nnz to determine the number of non-zero values in the specified column, equal or above 0.060 metres for the top and equal to 0.050 metres for the condensing shield. The code then samples along a 0.001 metre slit across the vacuum interrupter and separates the XYZ values so X can be plotted giving the correct scatter chart of the results. The data obtained provides the particles that were stuck on the condensing

shield and the top of the vacuum interrupter casing [109]. The comparison of the two plots in figures 58 and 59, show very similar profiles. The number of stuck particles is smaller in the benchmark having an approximate maximum of 10^5 instead of 10^6, reasons for this could be a higher number density used, faster particle movement or particles being absorbed for a longer time. The profiles do show a very similar shape and absorption between 10^1 and 10^2 on both. The original work shows a wider spread of 60 mm across the profile and the benchmark is 40 mm, so the geometry was estimated smaller than the original.

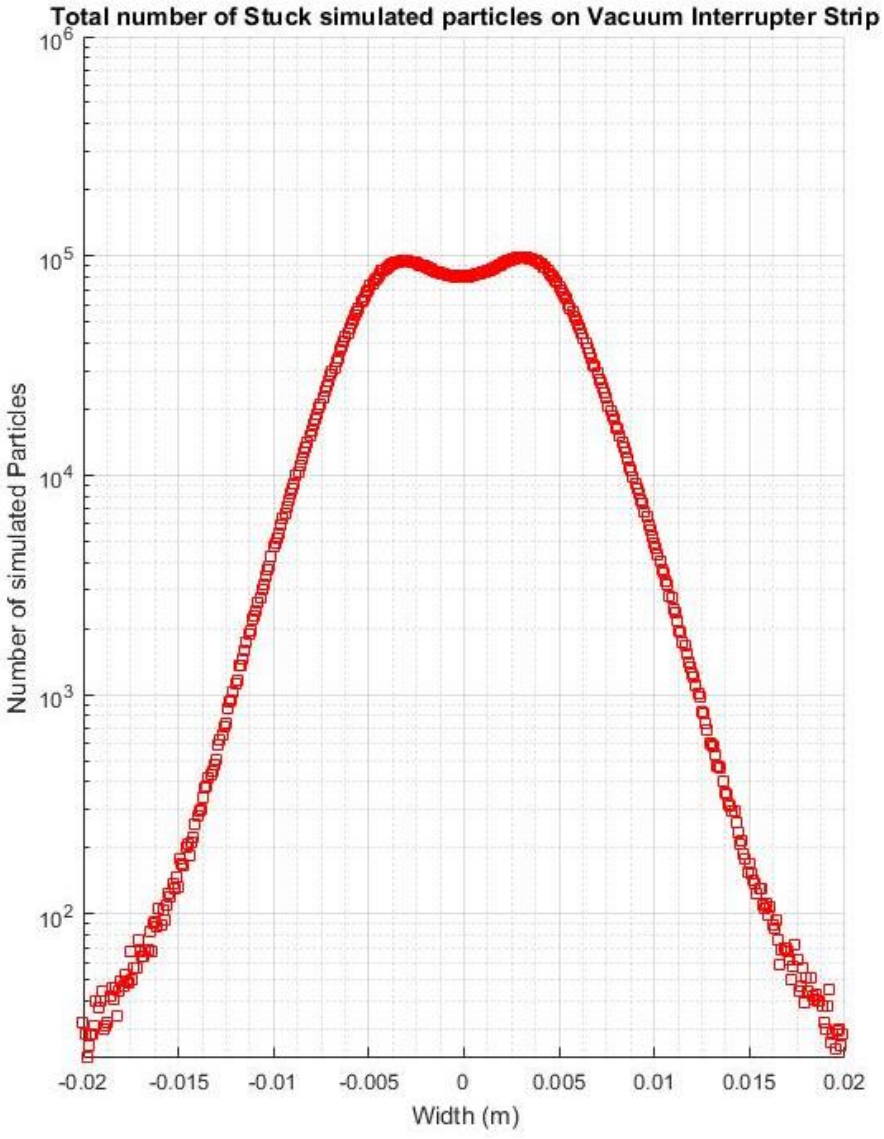

Figure 59: Benchmark results: Total number of simulated deposited copper particles on the vacuum interrupter strip

There are much fewer particles that accumulate on the top of the casing in the benchmark model, reasons for this will be due to particle density, average velocity and possibly temperature. The profiles show similar patterns for the absorption of the particles increasing as they move away to the left of the condensing shield. There may be an error on x-axis label of both original plots as 0.1 cm is only 1mm, which is incorrect as the component would be much smaller than its actual size.

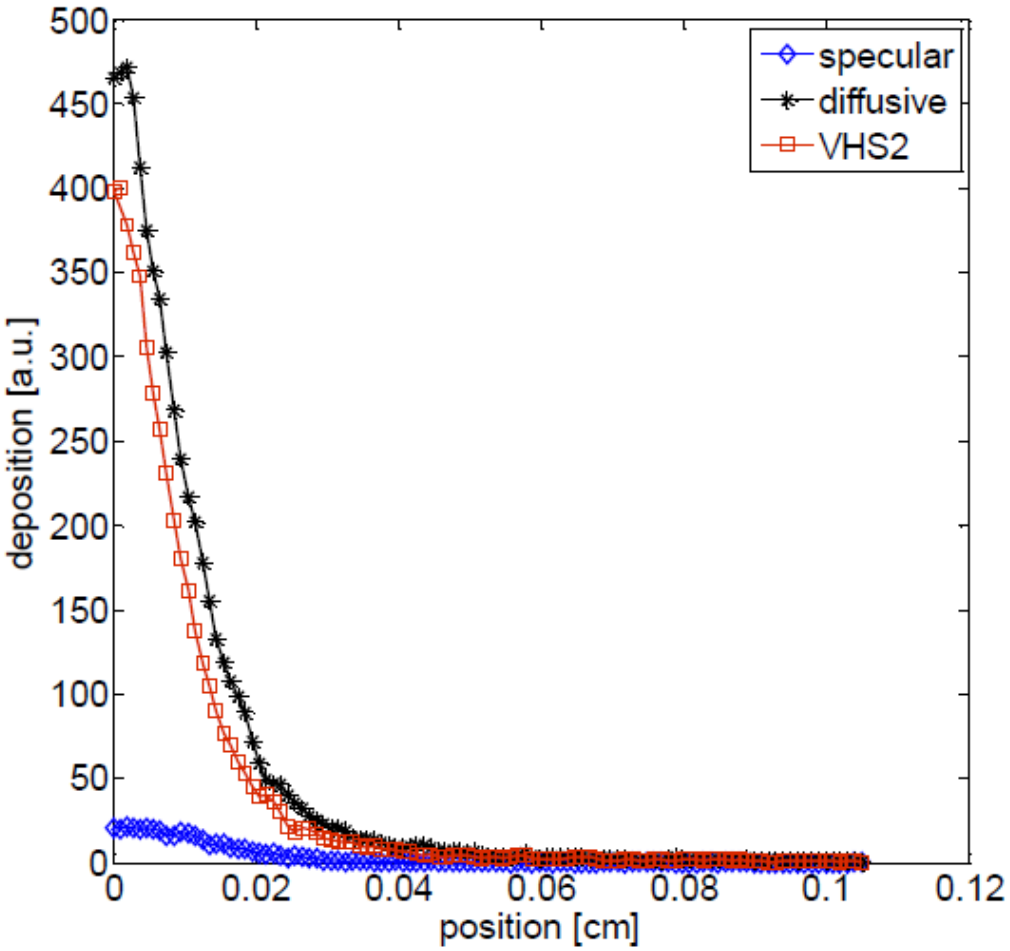

Figure 60: Results material deposited on the casing surface Hencken (2014) [12]

The deposition in figure 61 is not as defined as figure 59 and the profile does not match as accurately. The lower number of particles or analysis runtime could be the reason for this. The OpenFOAM library code used by ABB is likely to had adaptions that also differs from the dsmcFOAM+ library code used. The geometry and analysis set up could not be matched perfectly due to not being known. The simulated particles

interaction with surfaces are only measured by absorption only in this model, the simulated deletes the particle when it collides with a surface and a record of the interaction is recorded. More adaption of the library code is required to add the nature of the surface interactions like specular or diffuse reflection as well as absorption.

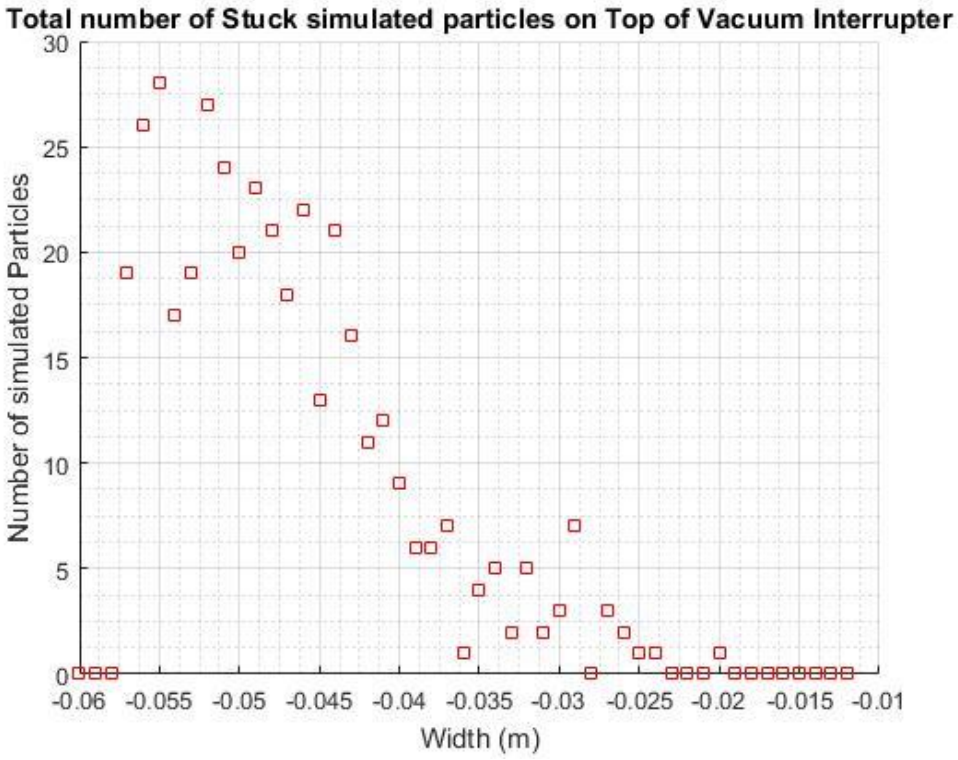

Figure 61: Benchmark results material deposited on the casing surface

The analysis forms a basis for the vapour deposition transport and dsmcFOAM can also be used for analysing the vacuum lock under free molecular flow conditions. The knowledge gathered from the vacuum lock patents, theory and computational simulation software now needs to be brought together to design a state of the art vacuum lock using what has been learnt. To introduce a new state of the art invention in the field of vacuum lock machinery will require using the computational modelling software to add a new way of designing and introducing air bearings that have currently not been utilised for steel strip applications.

7. Vacuum Lock Design

The patent review revealed that most vacuum lock designs have a roller system inside. The reviewed air bearing lock patents do not have rollers inside and are currently used for a delicate substrate such as glass. Rollers are required to transport the steel strip into and out of the coating system. Keeping rollers within the lock is good for close contact between the strip and rollers stopping air passing through this area. Tata Steel's design requirements are for varying strip widths and thicknesses with a maximum strip width of 2 metres and maximum strip thickness of 2mm. A vacuum lock system has mechanical rotary pumps attached to the entry lock, in the consecutive locks diffusion and molecular pumps are required to be used due to rarefied gas conditons. The different pumps are used to pump down to the desired vacuum conditions for the correct pressure required in the vacuum chamber. The pressure in the coating chamber is required to be maintained at 0.1 Pa. In the literature section the POSCO line has 6 entry locks and 7 exit locks [2]. It is desirable to reduce the number of locks required to obtain the desirable pressure because the more efficient the locks are, the more savings on electrical consumption. The pressure reduction for a system of four vacuum locks may be considered as follows:

- Pressure drop in first lock = 101,325 Pa to 1000 Pa (Continuum Flow Regime)
- Pressure drop in second lock = 1000 Pa to 100 Pa (Slip Flow Regime)
- Pressure drop in third lock = 100 Pa to 10 Pa (Transitional Flow Regime)
- Pressure drop in forth lock = 10 Pa to 0.1 Pa (Free Molecular Flow Regime)

The large drop on the first lock is because removing air from a chamber to vacuum is exponential. It is more difficult to evacuate gas at lower pressures after the initial drop down. A range of original vacuum lock creations were developed by the author of the research. The design revision process used the patents and theory section as guidance as well as preliminary computational modelling to show flow patterns and potential achievable pressures. The results of the preliminary simulations were not completely conclusive therefore have not been included in the design revision section until later where the prototype designs had convergence and more accurate results. Findings

from the patents aided logical reasoning and guidance on the design evolution. The final prototype must adhere to the essential design criteria:

- The clearance should be as small as physically possible in order for the flow resistance to increase.
- The flow resistance allows a pressure gradient to form between atmospheric pressure and the coating chamber.
- A differential evacuation system used to produce subsequent pressure drops, reducing power consumption that is not obtained by a single-phase system.
- The substrate must be transported continuously into and out of the vacuum without significant pressure change.
- Must be able to accommodate varying widths and gauges.

7.1 Vacuum Lock Design Revision Process

All of the designs were produced by the author using SOLIDWORKS. Tata did not have a prototype design for the vacuum lock. Patents were used to aid the roller configuration and the sealing members, but as the design evolved careful consideration was made not to copy the existing designs. The prototype arrangement of rollers and sealing members has been designed to try and differ from existing patents. The designs were reviewed by Tata alongside the simulation results. Tata's input into the design was added at a later stage when a partner steel producer shared information about the Teflon blocks used in their design to restrict air. This however was not utilised in the prototype and the air bearing system designed by the author was used instead.

7.1.1 Vacuum Lock Design Revision 1

The initial design was produced to start a design process and develop a computational model. It was kept simple to avoid complex meshing and allow trial with the different boundary conditions in ANSYS Fluent starting with a pressure inlet and pressure outlet. This will be further explained in chapter 8. The steel strip in the initital design is 300mm wide and 2mm thick, these dimensions represent a starting point and a design revision is conducted until a state of the art working model is produced. The

initial vacuum lock design (Figure 62) is a static model of a chamber with no moving parts. Within the chamber there are two rollers with steel strip sandwiched between them. The rollers are tight on the steel strip surface to stop air passing through. There is an inlet to allow the steel to enter the chamber, an outlet for the steel to exit to the next vacuum lock and an outlet on top where the pump is connected.

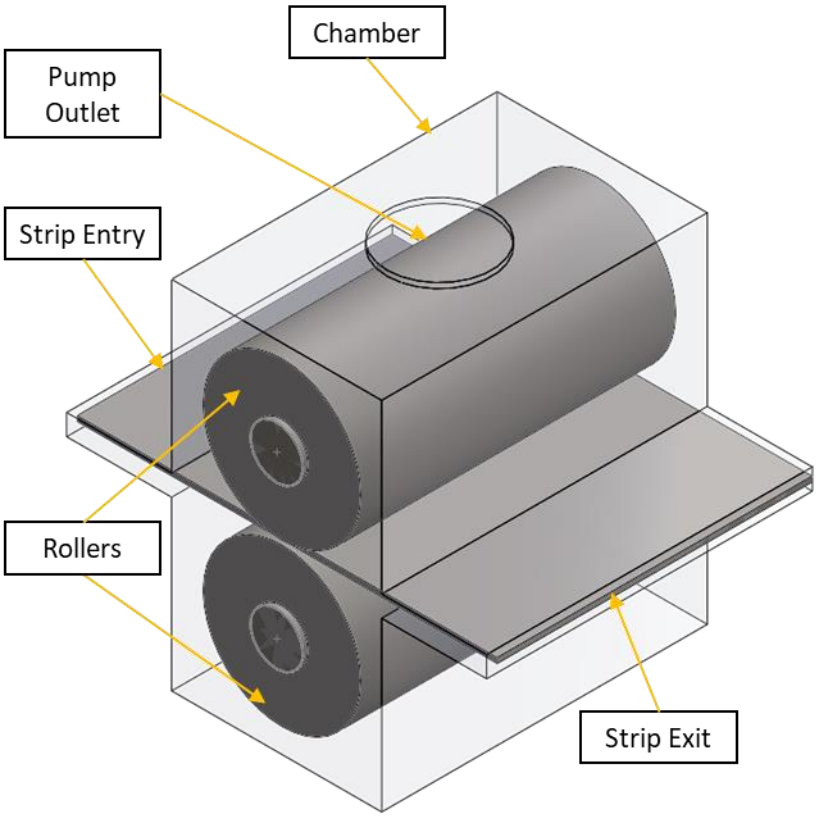

Figure 62: Revision 1 – Initial vacuum lock design

The feedback for the initial design was to move the outlet as it is too close to the internal rollers and will cause obstruction, restricting the pumps performance. There is not much room in the lock if maintenance is required and to look into connecting more than one lock. The outcome of simulations will be discussed in chapter 8.

7.1.2 Vacuum Lock Design Revision 2

The next vacuum lock design included two locks joined together and pump outlets placed further away from the internal rollers shown in figure 63. Connecting the two locks did show a pressure drop between them however the pressure achieved was very similar to Revision 1 therefore it was agreed between the author and Tata that it would it is more important to develop the design of the first lock before moving on to coupling them together.

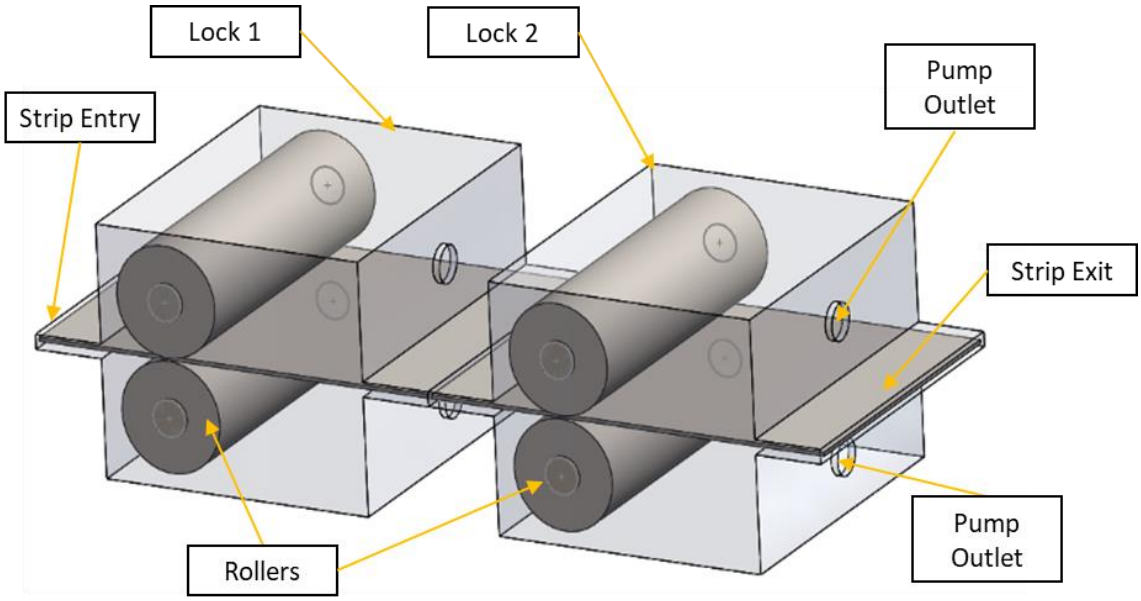

Figure 63: Revision 2 – Coupled vacuum locks

7.1.3 Vacuum Lock Design Revision 3

In Patent DE 4240489 C1 Erbkamm offset the rollers and this has been seen in most of the consecutive vacuum lock patents since whether it is two or more rollers. Offsetting the rollers provides better contact with the steel strip and reduces the chance of air leakage passing between the strip and the roller. In design revision 3 the rollers have been off set and a third roller added. Sealing members (blocks) have been added surrounding the circumference of the roller to reduce the gap for air to flow between

the chamber wall and the rollers. The design is 3D with a 300mm wide steel strip to start with and a 450mm chamber. The chamber has been widened to allow different widths of strips to be used. The configuration of the design can be seen in figure 64. The pump outlet has also been moved to a place in the lock where it can draw the air without restriction of immediate components obstructing the outlet.

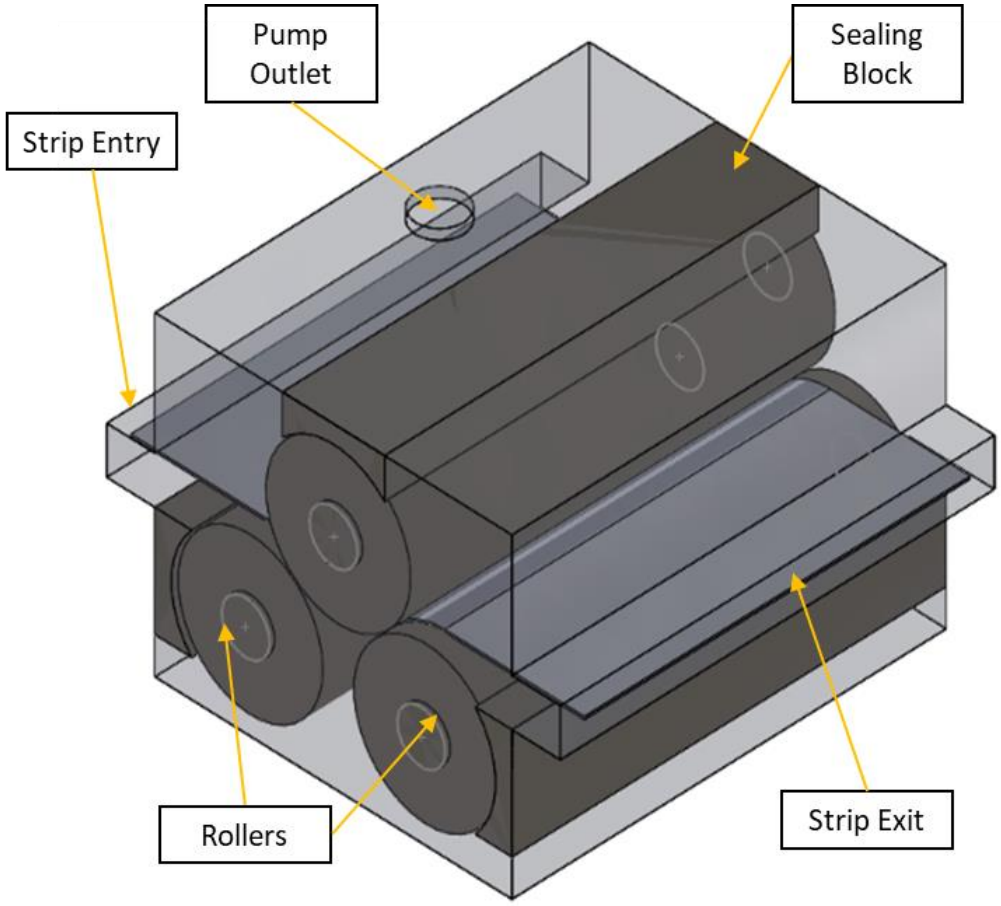

Figure 64: Revision 3 – Offset rollers and sealing blocks horizontal design

Design revision 3 was better at obstructing the air through than the first 2 revisions and the simulation of the flow through revision 3 showed the areas of leakages more clearly.

7.1.4 Vacuum Lock Design Revision 4

Revision 4 is effectively the same as revision 3. Tata requested the design to be turned vertically for a different direction of strip travel and to see if this would change any of the physics. It did not affect the flow.

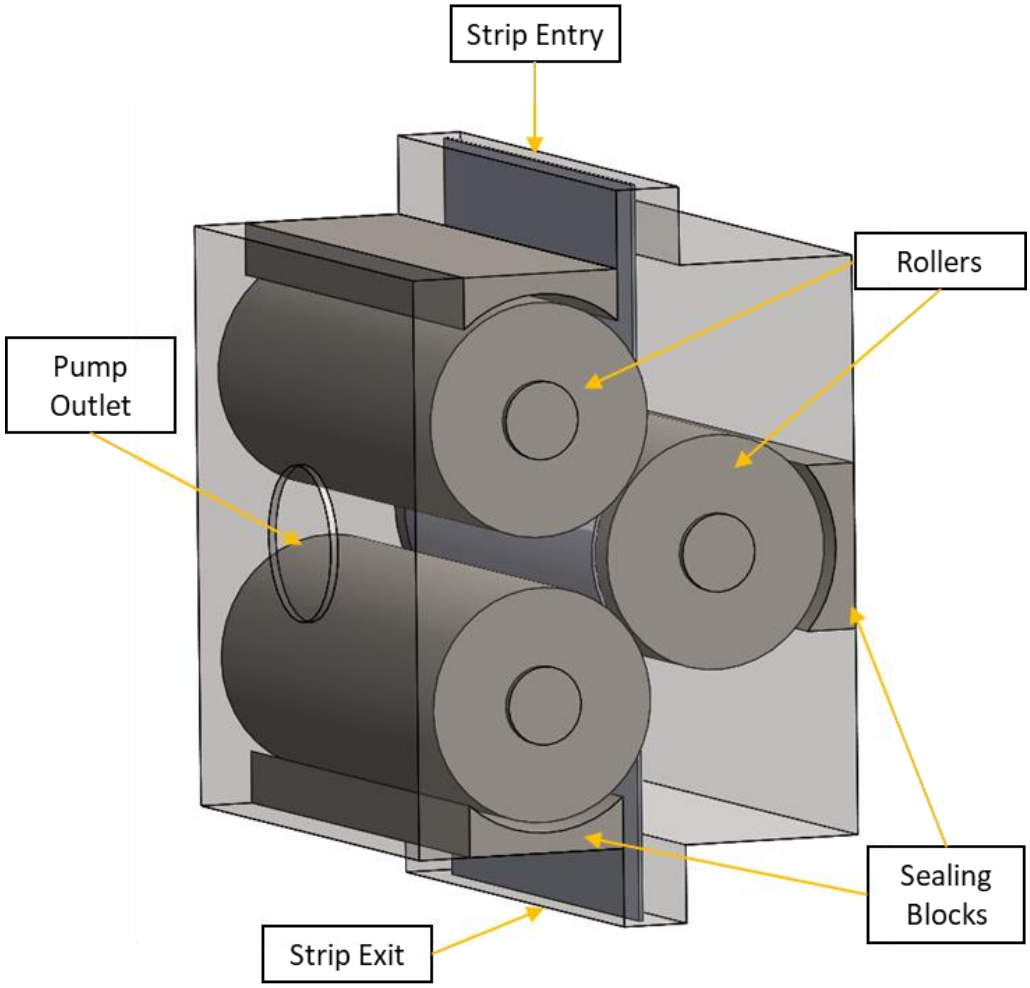

Figure 65: Revision 4 – Offset rollers and sealing blocks vertical design

Like revision 3, the revised design revision 4 (figure 65) reduces some areas where the air can get into the lock, however some remain. The following air leakage areas shown in figure 66 are difficult to eradicate. The clearance between the roller and the chamber wall is essential to stop abrasion and is unavoidable, however it can be minimised as the rollers should have minimal thermal expansion and longitudinal

movement. The gap between the rollers and the edge strip is potentially a large gap as the lock is required to cope with a thickness of up to two metres and 2mm thick, so for example if a strip of 800mm wide 2mm thick steel was running on the PVD coating line, a gap of 600mm by 2mm could be left on either side of the strip. Some of the patents have a band of material or plates to cover these areas.

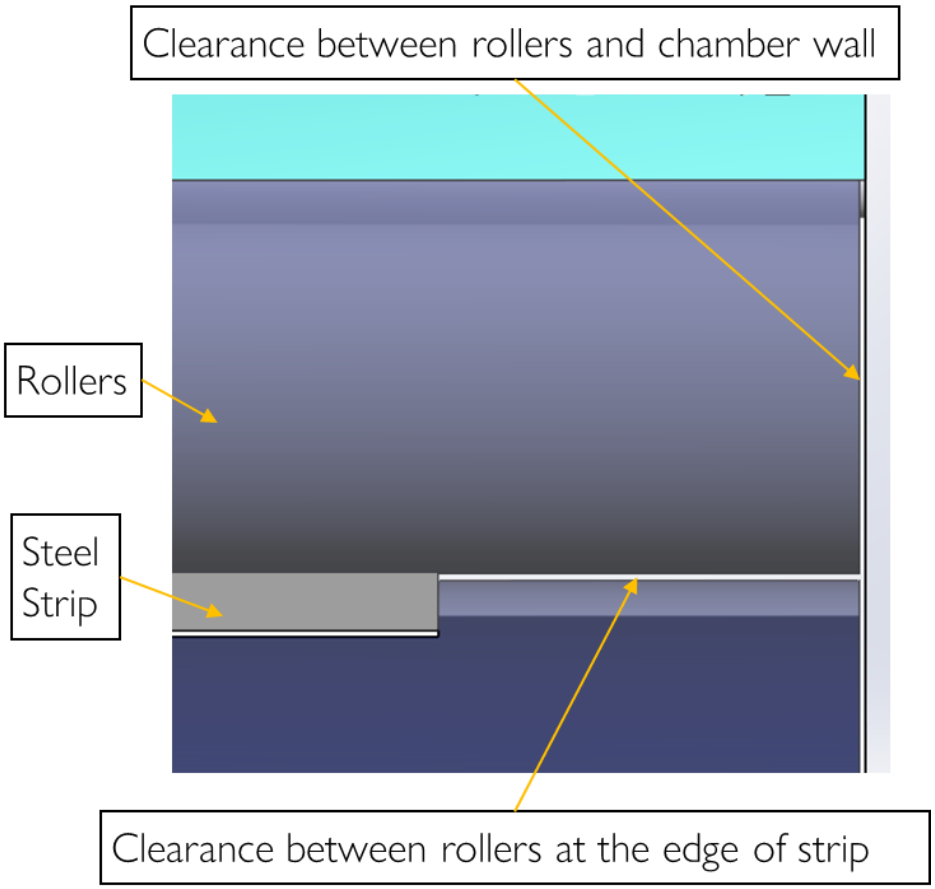

Figure 66: Air leakage into vacuum lock chamber

7.1.5 Vacuum Lock Design Revision 5

Revision 5 changes the roller back to two offset rollers as seen in Patent DE 4240489 C1 and the most recent Patent US 8926756 B2. The reason for this is the strip width can be changed without a mechanism to move the roller because the way they are

offset which is more useful for a static design. Revision 5 includes Tata Steel's partner company lock design information of adding Teflon blocks that push against the rollers to restrict air flow that managed to pass between the rollers at the edge of the strip. This ensures a physical barrier that reduces air flow. Revision 5 incorporates Tata's Teflon block shown in Figure 67.

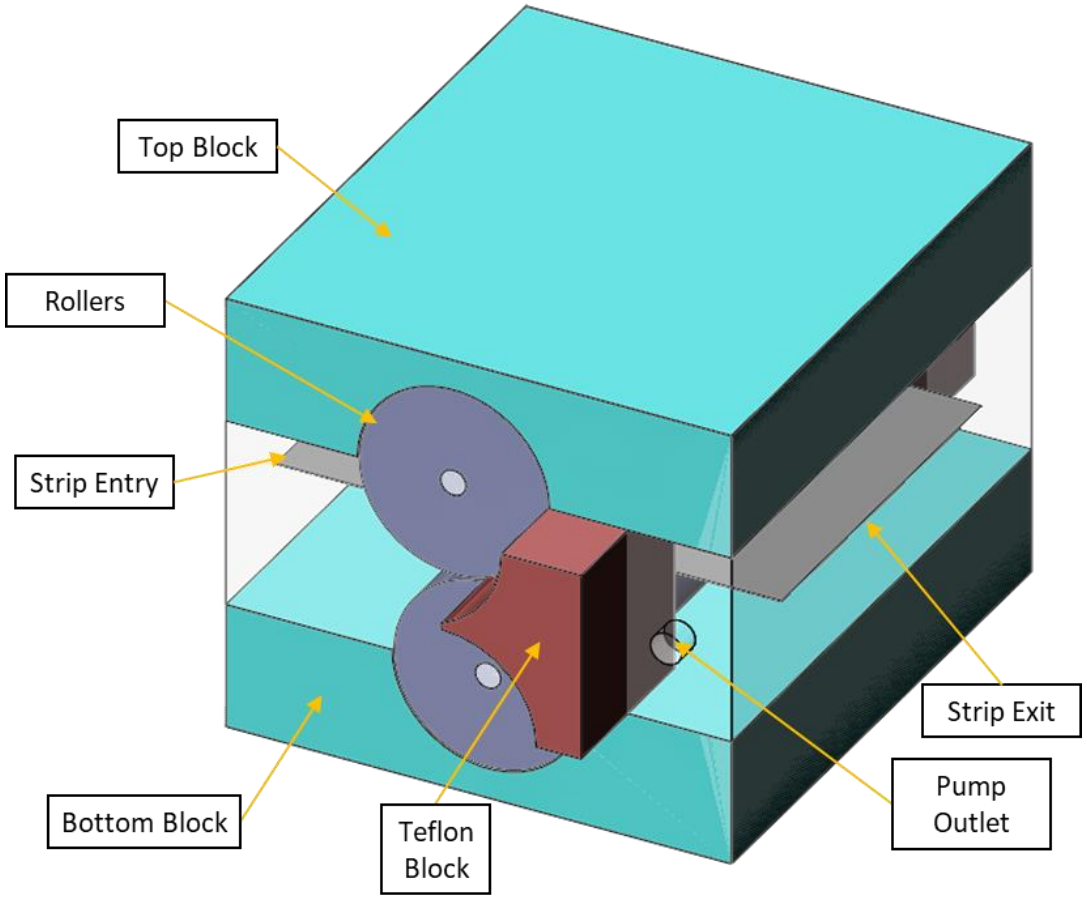

Figure 67: Revision 5 – vacuum lock with Teflon block

The Teflon block will close most of the gap, however because the strip may have some side to side movement as it transports through a clearance must remain to allow for this, otherwise the block could contact the side of the strip and cause damage or buckling. Therefore, leakage area between the edge of the strip and block remains. The Teflon blocks are fed in from the side of the lock, shown by the arrow in figure 67. there is a requirement to add the feeding mechanism and blocks to the chamber,

so no further leakage occurs. With the new design, there is a top and bottom block, which only allows air to channel through three places:

- Clearance between the roller and the chamber wall
- Clearance between the roller and sealing block
- Clearance between the edge of strip and roller

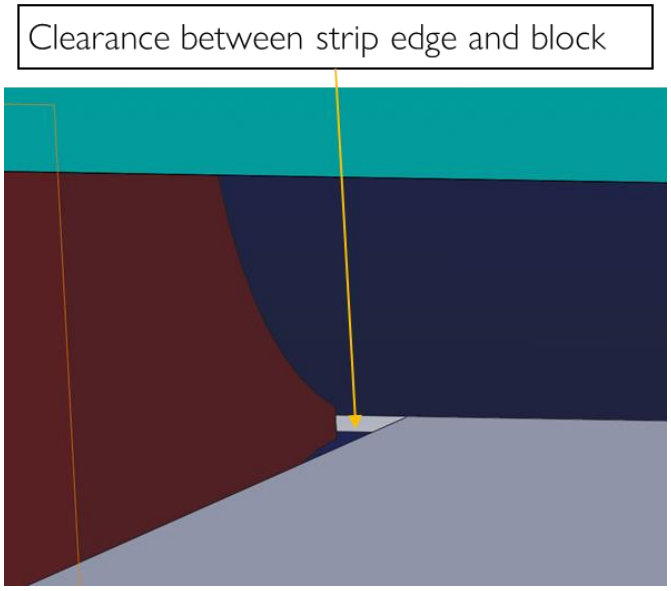

Figure 68: Clearance between strip edge and teflon block

These clearances shown in figure 66 with the added further reduction provided by the Teflon block shown in figure 68. The more space for air to leak into the lock the more pumping that will be required and the less effective it will be. The design tries to limit the paths for air to travel into the system as much as physically possible whilst still allowing the strip to travel through and the rollers to turn. The problem is the Teflon blocks is that they wear out and need replacing, therefore time is lost due to maintenance and there is also a financial impact. Design iterations were conducted to find a solution of how to incorporate air bearings into the lock design was conducted until a prototype design was achieved.

7.1.6 Vacuum Lock Air Bar Design

The design so far has been traditional vacuum lock design and to produce a vacuum lock that is state of the art requires more innovative ideas. The introduction of air bearing technology into vacuum lock design should produce a more efficient and state of the art vacuum lock. The author created a range of design solutions until two chosen designs were produced in Solidworks and then critiqued with the best design chosen to be incorporated into the prototype lock design.

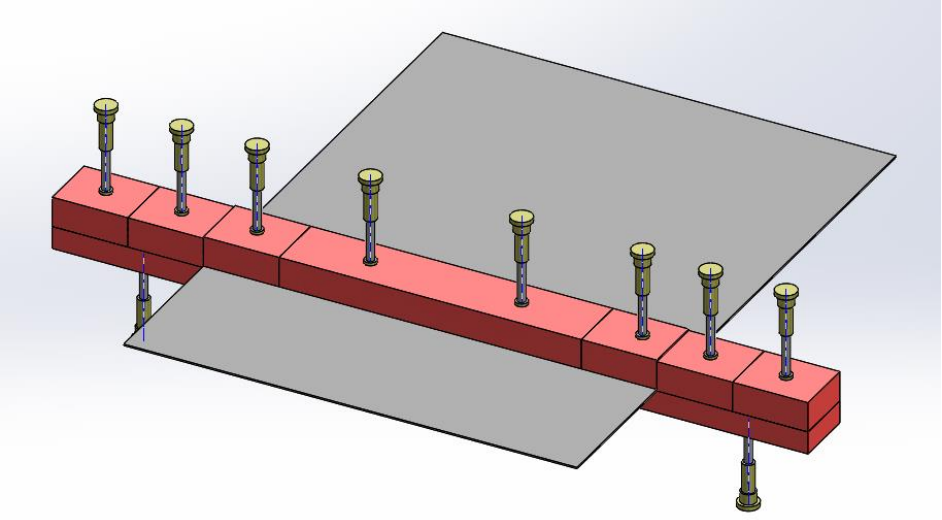

Figure 69: Varying air bearings keys design

The air bearing keys design shown in figure 69, was chosen to close the clearance when the strip changed width, if a small width is used the air bearings move down to close the gap against the air bar. The problem with this design is that it would be expensive and require a lot of moving parts depending on the variation in width of gauges used. The final air bearing design in figure 70 uses air bars, the top air bar can move up and down for the change in strip gauge and the sliders move in from the side on a frictionless rail system to cover the gap caused by reducing the strip width. The sliders connect magnetically and can be changed quickly for variation in gauge.

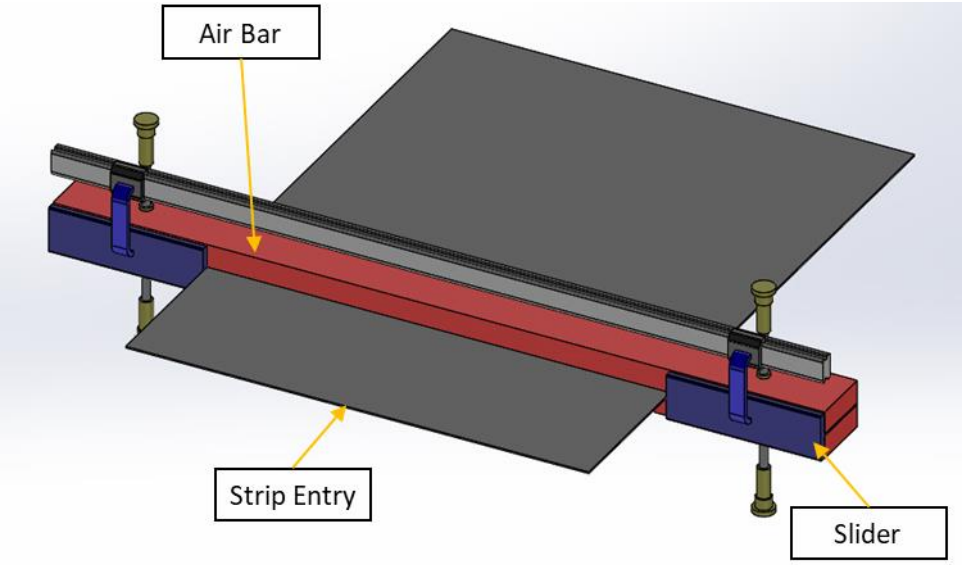

Figure 70: Final air bar design with sliders

A traditional air bearing design consists of a single orifice with no grooves. This technology has been surpassed with a porous media air bearing developed and patented by New Way® air bearings. In a porous media air bearing it has the advantage of millions of micro-sized holes that occur naturally in the substrate such as microporous carbon brick or carbon foam [110]. These holes are passageways where the air must flow and reach a bearing force, this provides a much greater control of air flow through the gap and supplies an equal air pressure across the entire surface of the air bearing. Simultaneously it restricts and damps air flow [110]. This air bearing technology is present in Patent US 8123868 B2. New Way® air bearings also produce air bars which use the same micro porous technology. It was not in the scope of the project to design and produce air bearings therefore a suitable of the shelf product was used.

In sourcing the air bars for the chosen final air bearing design, IBS Engineering were contacted to supply a suitable product. IBS Engineering are a third-party seller for New Way Air Bearings and a meeting was set with IBS Engineering to look at the design and provide a suitable product. A suitable product was the New Way® PA-Rail air bar. The product is designed for glass but is suitable for metal. The substrate can float as close as 100 microns above the bar without risk of damage, allowing a very

tight gap to be produced entering the lock. The air flow is 50 litre per metre of rail [111].

7.1.7 Vacuum Lock Revision 6 and 7

The air bar system was added into the design and a prototype was achieved shown in figure 71. The design is very good at restricting the air into the lock and simulations and experimental validation will be performed to evaluate the design performance.

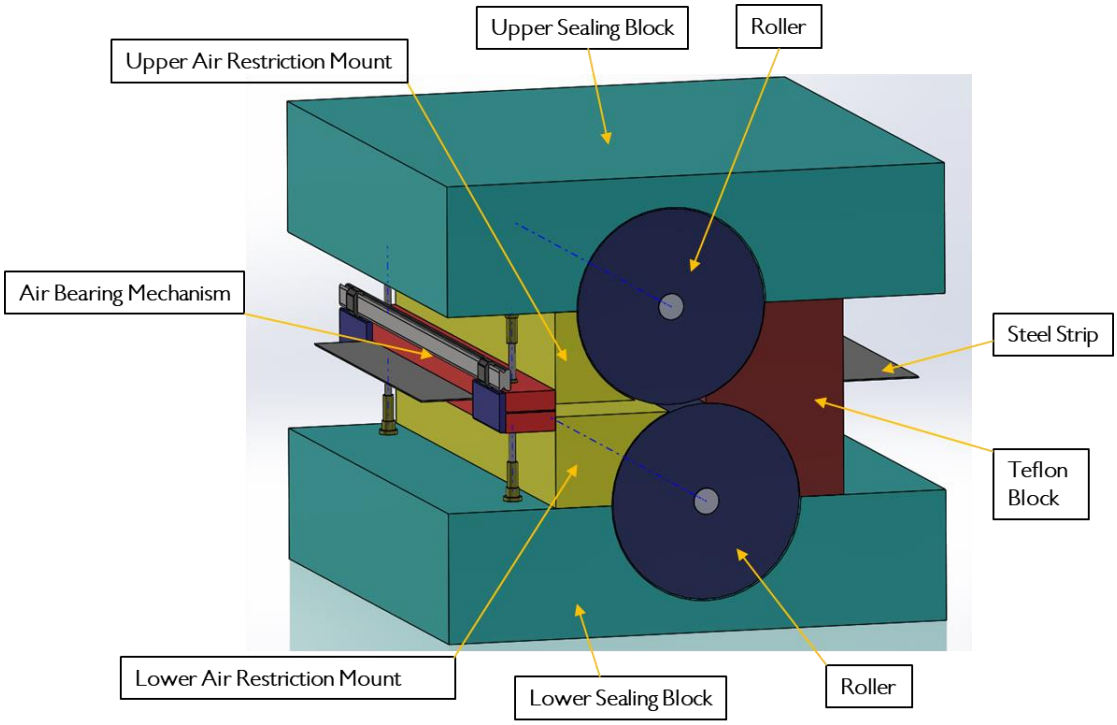

Figure 71: Revision 6 – Prototype Design with Teflon Blocks

Alterations were made at the experimental stage. The air bars provided by New Way required more space, so the upper and lower sealing blocks sizes were reduced shown in figure 72. The path of the air will still be restricted with the smaller sealing blocks as the clearance for the air to travel through is unchanged and weight is reduced. The Teflon blocks were not produced as the air bar system was deemed sufficient enough to reduce air travelling through and the mechanical wear of the internal blocks would be counterproductive. The design of revision 6 and 7 was the work of the author. The information of the Teflon blocks design was from supplied from Tata. The Teflon blocks could be added back in at a later stage to measure the additional effect the

blocks would have on the system. Whether the additional entry chamber to feed the blocks in and out system and the additional wear is practical is another consideration that is not covered in this thesis.

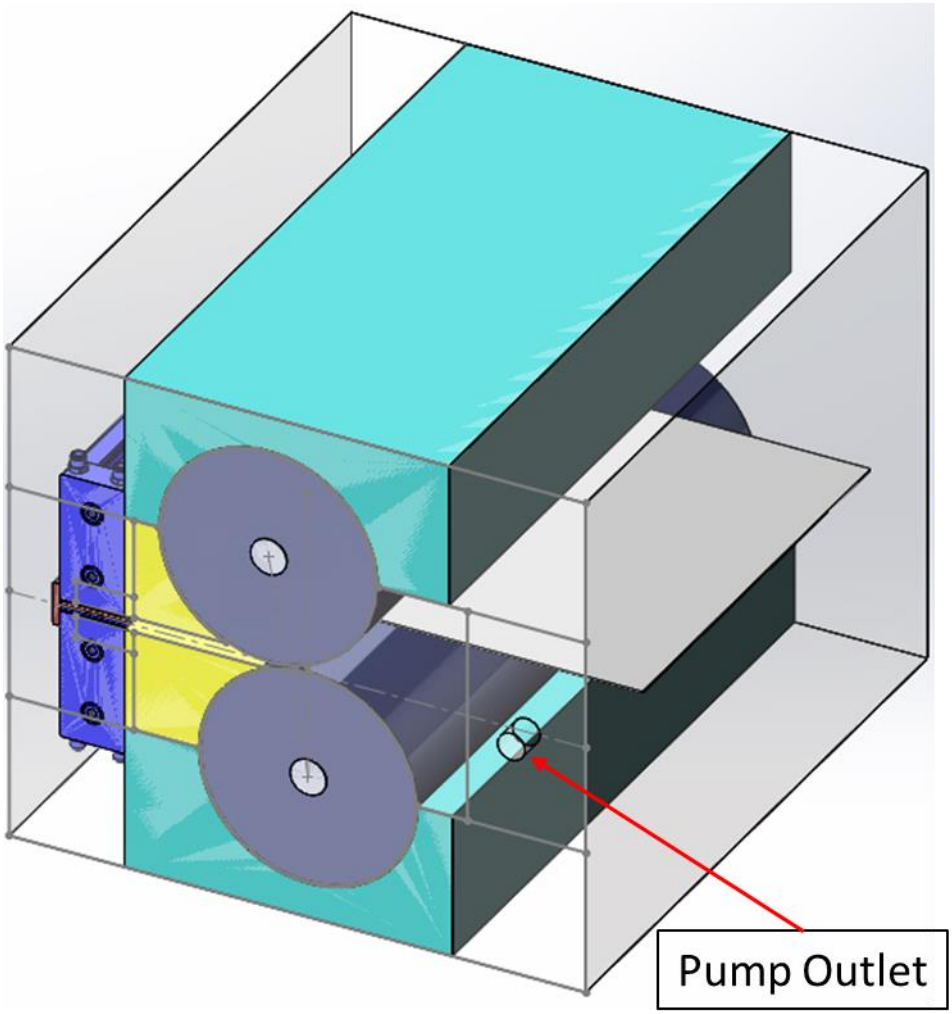

Figure 72: Revision 7 – Prototype with Teflon blocks removed, and New Way air bars added

8. Simulation Based Design of a Vacuum Lock

Modern engineering utilises computational simulations to predict or approximate real-life conditions which can then be verified with experiments or prototypes. The vacuum lock model was simulated in order to identify the pathways air is likely to travel through the geometry therefore indicating potential leak areas and the pressures that are likely to occur within the lock under pumping conditions. The design revision geometries were imported from SOLIDWORKS into ANSYS Workbench and then meshed with simulations performed to gain an understanding of performance. The geometry can be updated and changed, and further simulations run to optimise the design this has the potential to improve upon existing technology that uses general vacuum physics design theory based on simple geometry and equations. Different design configurations, boundary conditions and pumping rates can be simulated. A parametric study of varying the pumping capacity can be used to determine the effect the pumping capacity has on the pressure within the vacuum lock. This fulfils the requirements of deliverable 1. At the time of this research no published computational modelling literature could be found specifically for a vacuum lock. To the authors knowledge using simulation to aid the design of vacuum locks is a new addition to the field. This does not mean that no simulation of vacuum locks has been conducted, if such literature does exist it could be industrial sensitive and has not been published in the public domain.

8.1 Vacuum Modelling Literature ANSYS

For setting up analysis for the vacuum lock, research was conducted on similar computational modelling involving vacuum conditions. The following literature provides information on what ANSYS analysis tools were used including boundary conditions, solvers and turbulence models. This information will be used in collaboration with the theory and benchmarking to build an analysis model.

Kale et al (2016) investigated the aerodynamic performance of an exhaust muffler using CFD method. The boundary conditions used for simulations were a velocity inlet

of 35.47 m/s, a pressure outlet open to atmospheric pressure and flow was considered as turbulent. The muffler was meshed using ANSYS ICEM using tetrahedral elements due to the muffler's small wall thickness, which could have caused problems during mesh generation hence hexagonal mesh was avoided. The performance of a muffler is mainly dependent on the backpressure. The CFD results showed pressure drop, which is the backpressure. The paper does not say what CFD software was used but as the muffler was meshed using ICEM it is likely to be an ANSYS software program such as CFX or Fluent [112]. This paper indicated what meshing can be used and boundary conditions.

Hesse et al (2016) used CFD to simulate a dry scroll vacuum pump including leakage flows. Simulation of a dry scroll pump has some complex flow characteristics including the chamber volume that varies with time and leakage flows through radial and axial gaps in between the rotors and housing. The CFD analysis was performed using ANSYS CFX due to its ability to solve complex flow characteristics. Fluid is considered as a compressible ideal gas, turbulence and heat transfer effects are included. For viscous flow a no slip wall condition is used, which is correct for Knudsen values of less than 0.01. An SST turbulence model was used to consider zero kinetic energy in the clearances. The paper did not clearly specify the boundary conditions used for inlet and outlet but did say that the pressure and temperature were set at the inlet and outlet, so it is possible a pressure inlet and pressure outlet was used. "The transient scheme is second order backward Euler" [113].

Son et al (2018) states the importance of experimental validation of computational analysis "It is difficult to grasp the flow through each element in a fan motor unit; thus, only the overall performance and flow characteristics of a fan are obtained through experimental results for real applications". Three common turbulence models are K-epsilon (k–ε), K-Omega (k–ω) and Shear stress transport (SST). The flow outside the boundary layer can be predicted with accuracy using the K-epsilon model and the flow inside the boundary layer can be accurately predicted using the K-Omega model. The SST turbulence model joins the K-epsilon and K-omega models with blending functions in ANSYS CFX utilising the K-epsilon in the areas of fully developed flow and K-omega near-wall. Using the correct turbulence model will take some trial and

error depending on whether turbulence is being predicted outside the boundary layer, near the wall or a combination. The paper does not disclose the boundary conditions used, the small vacuum cleaner was optimised using CFD and a design of experiments (DOE) [114].

Lai (2011) conducted research on duct flow field optimisation of a robot vacuum cleaner. The duct of the robot vacuum cleaner is the flow channel from the inlet of the rolling brush blower to the outlet of the vacuum blower. The PISO (Pressure Implicit with Splitting of Operators) algorithm in ANSYS Fluent was used to cope with the pressure drop of the duct flow. PISO is a pressure-velocity algorithm that uses one predictor step and two corrector steps. The PISO algorithm uses more computational expense as it solves the pressure correction equation twice. The fluid was treated as incompressible and a K-epsilon model selected to predict turbulence. The duct inlet is as a flow inlet so that data can be obtained experimentally, and the outlet is a pressure outlet. The temperature, pressure and viscosity are standard for air at atmospheric pressure. The speed of the blower is 700 rpm, the paper does not say if this was used as a moving wall, rotating to produce the flow in the simulation, however this is a commonly used method with this type of analysis [115].

Apart from this last paper, the literature does not contain information for the algorithm used and none mention the upwind order. The papers will act as a guide in the simulations of the vacuum lock but do not give an exact method to use as they are for different problems. The boundary conditions of a pressure inlet and outlet was mentioned in Hesse et al (2016), also the de Laval analysis in chapter 6 used these boundary conditions therefore for compressible flow with higher velocity this method could prove to be useful. The different turbulence models (K-epsilon, K-omega, etc.) and solvers (SIMPLE, PISO, etc.) can be interchanged in ANSYS Fluent to determine what gives the best convergence of solution and prediction of the flow.

8.2 Meshing of the Vacuum Lock Designs

Before the simulations are run the geometry is meshed to provide cells for the partial differential equations to be applied to. When the simulation is run the equations are solved for every mesh cell, the larger the number of mesh cells the more computation

time required. A mesh sensitivity study is normally applied to determine the optimum mesh size. Coarse meshes tend to be less accurate than fine mesh but in areas where there is less activity occurring coarser mesh can be used. Fine meshes are needed for small areas and areas where there is significant information. As the geometry ranges from large and small areas the mesh varied and instead of a mesh sensitivity study the meshing was conducted to get as much quality as possible.

Meshing is important for gaining accurate results from a simulation. Poor mesh can result in unrealistic results, simulations not running and errors. The vacuum lock was difficult to mesh due to very small areas purposely created to represent the clearances. The physical parts of the lock are cut away from the geometry leaving just the geometry of the air, the boundaries are walls around the fluid surface. Due to nature of the design the mesh has some very fine geometry where the steel strip contacts the roller (figure 73) and then much larger areas of air in comparison in the empty space of the chamber. As there is such a variation in geometry, the very fine areas are difficult to mesh, therefore have poor mesh quality and could cause divergence in the simulation . These were removed by adding a chamfer in ANSYS design modeller, as the air will not be passing through the closed gap caused by the rollers pushing firmly against the steel (figure 74).

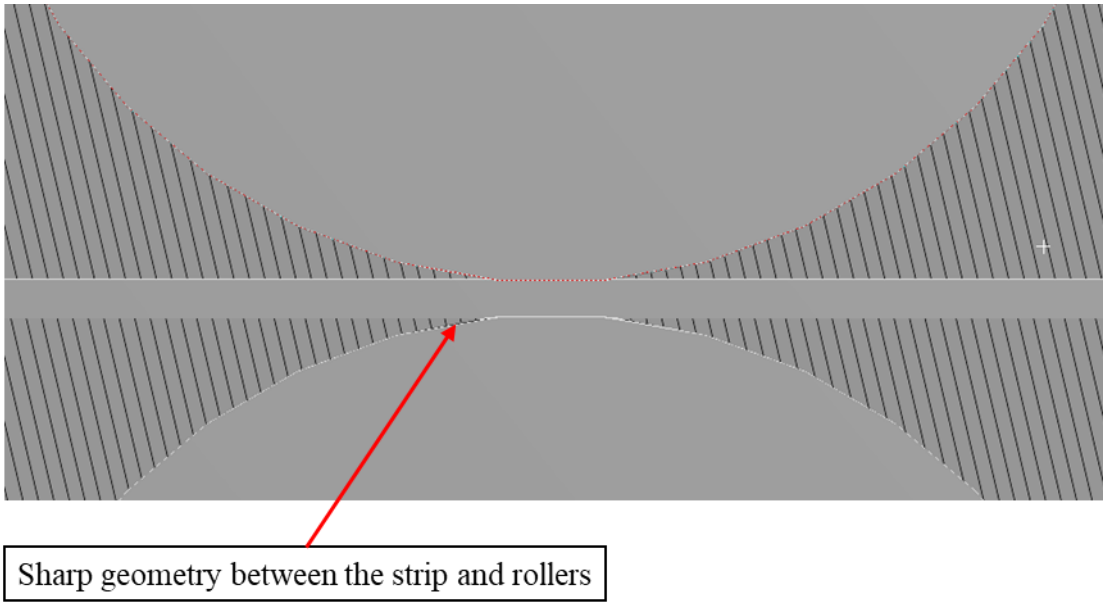

Figure 73: Diagram of the sharp edges formed between the rollers and the strip

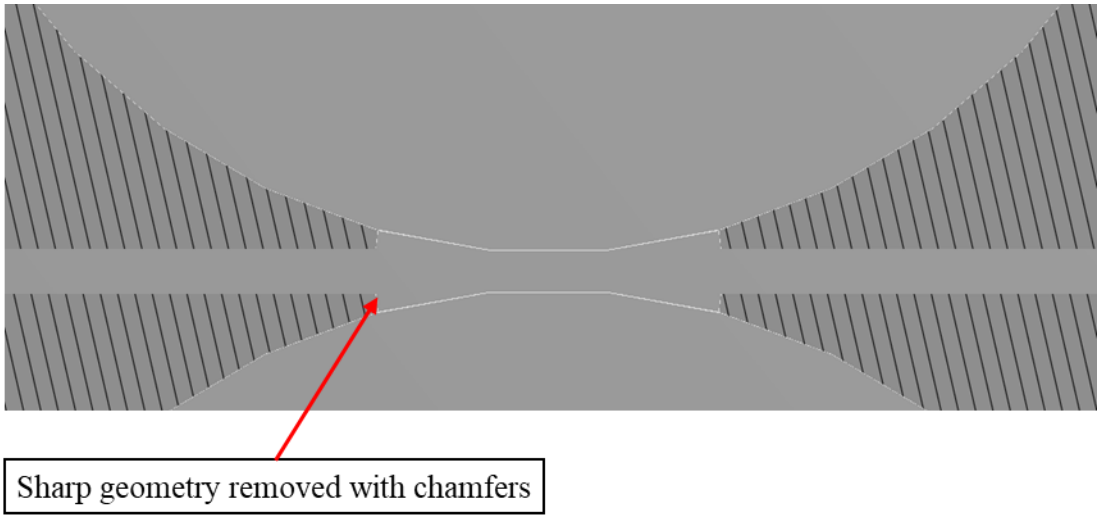

Figure 74: Diagram of the sharp edges removed with chamfers

For CFD simulations there needs to be at least 3 mesh elements across any gap where fluid moves through. The geometry was split into different sections within ANSYS design modeller and the air around the rollers was a hexahedral mesh, the preferred meshing element for CFD. Due to the irregular shapes the rest of the lock was meshed with tetrahedral elements. The quality of the mesh was checked for skewness and orthogonal quality. The check mesh function was used in both ANSYS and OpenFOAM to ensure there was no poor elements that would cause problems for the simulations. As the design increased in complexity so did the meshing required for the simulation and resulting simulation times.

8.3 Vacuum Lock Revision 1 Simulation Results

The initial vacuum lock from revision 1 is changed from a design model into a geometry of air the grey areas are the solid interfaces that still exist to show the boundary between the air and the physical features (figure 75). This model is then uploaded into ANSYS workbench where any geometry is repaired by removing sharp edges or overlapping features and then meshed ready to perform analysis on it (figure 76). As mentioned in the meshing description the sharp geometry between the rollers and strip will cause poor mesh elements as can be seen in figure 77 because the geometry is so sharp the mesh in that gap is only 1 element thick as well which will not allow a prediction of the flow in that area.

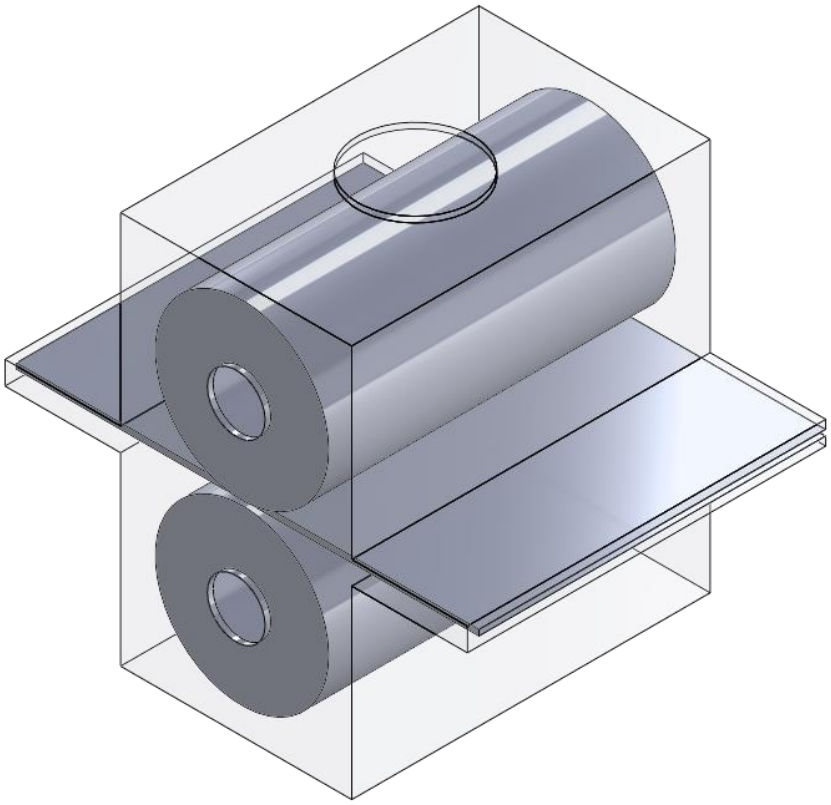

Figure 75: Vacuum lock design revision 1 air geometry

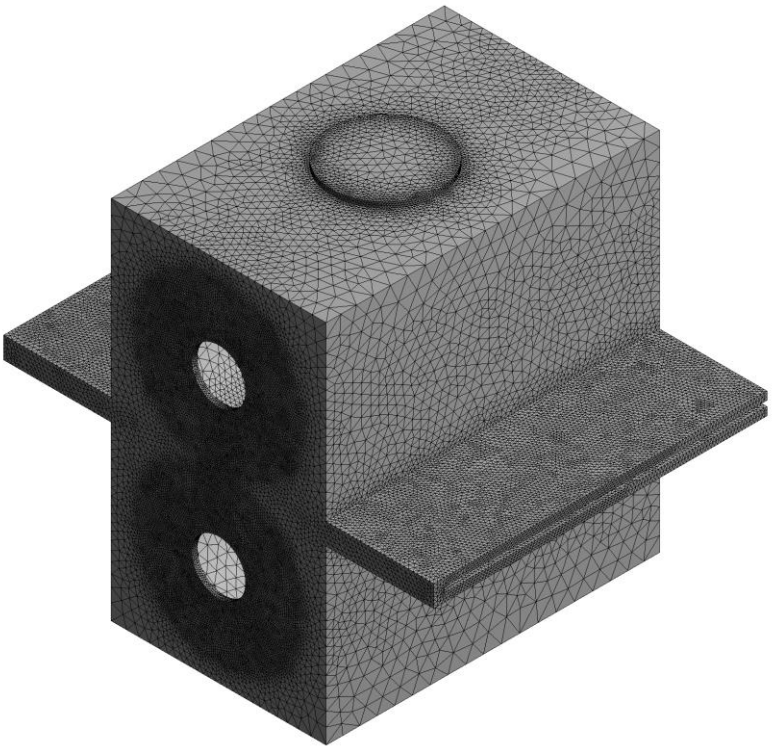

Figure 76: Vacuum lock design revision 1 air mesh

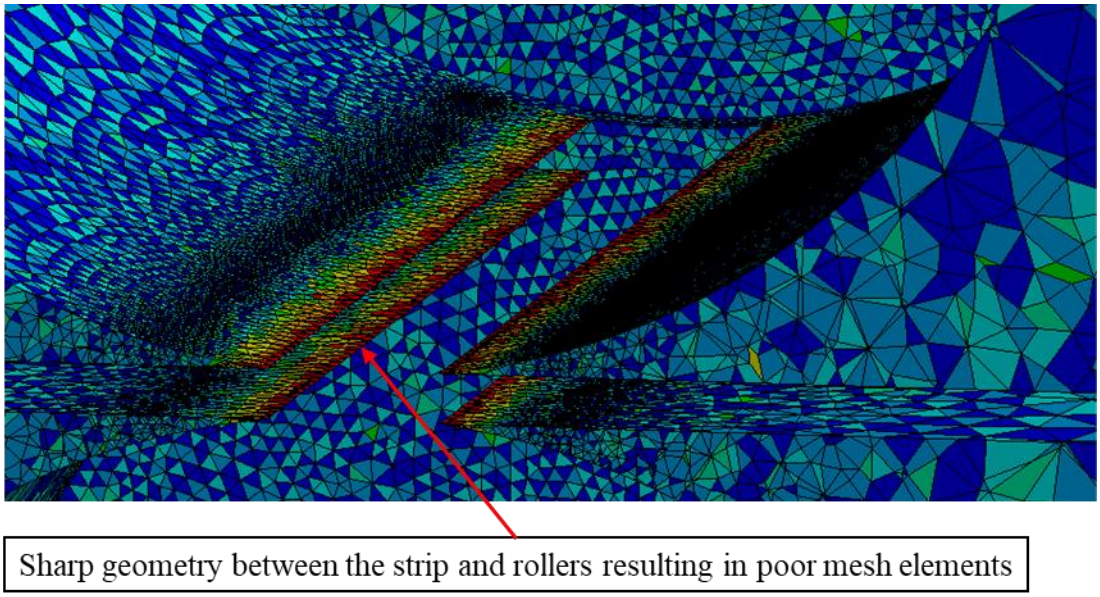

Figure 77: Sharp geometry between the strip and rollers resulting in poor mesh elements

The air will not move through this area as the contact between the roller and strip prevents it and this has been confirmed in the patent literature. The sharp geometry is removed which allows a better quality of mesh to be produced and more than 3 elements across the boundary are achieved.

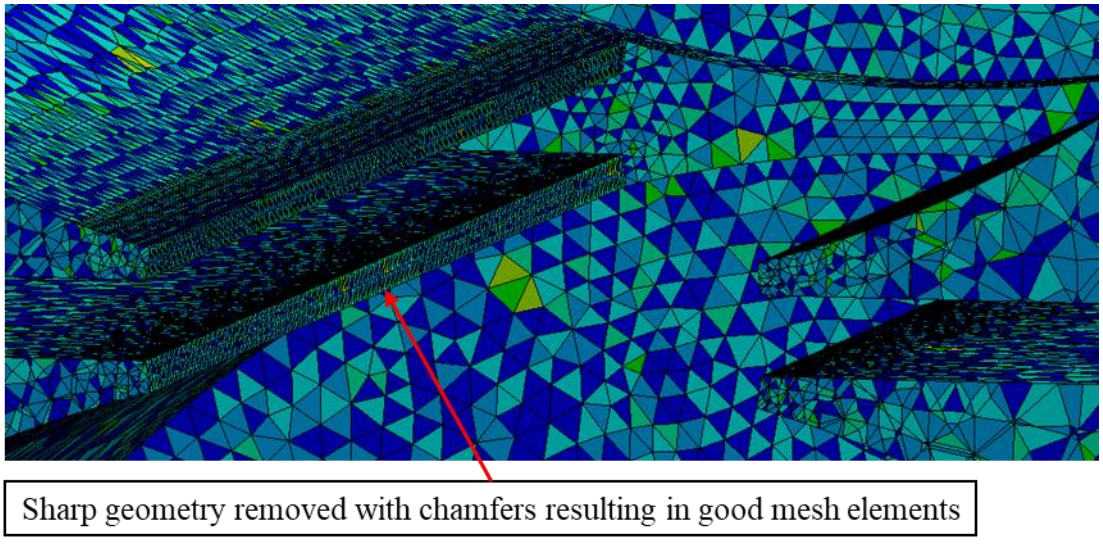

Figure 78: Sharp geometry removed with chamfers resulting in good mesh elements

The following conditions were initially used in the simulations for the vacuum locks:

- Inlet Pressure 101,325 Pa (Atmospheric pressure)
- Outlet Pressure Exit to Lock 2: 10000 Pa
- Outlet Pressure to Pump: 1000 Pa

A pressure for the second lock had to be assumed as it was not possible to know what pressure could be obtained without knowing the performance of the first lock. The pressure the pump would produce was also initially assumed. This was for the purpose of a starting point. The initial pressure is known at the inlet as atmospheric pressure 101,325 Pa. The pump will be evacuating the chamber therefore a much lower pressure will be observed at the outlet where the pump is attached. The idea is to perform adequate pumping of the air to lower the pressure in the chamber and the pressure at the outlet to the next vacuum lock chamber reduced significantly.

The Knudsen number will reduce as the mean free path changes of the gas molecules at lower pressures, ANSYS Fluent and continuum methods can be used to predict flow behaviour at the lower Knudsen numbers in the first lock, however as the Knudsen number increases the DSMC method will have to be used to analyse the flow in the lock near the chamber and a hybrid method of the two methods where transition is occurring, which is likely to occur in the locks between the first lock and final lock. The initial velocity at the inlet to the vacuum lock is not known, it depends on the movement of air due to the change in pressure from static atmospheric pressure at the inlet and the rate of the air pumped out from the chamber, there are also internal components in the path of the airflow as well.

If the combination of both pressure inlet and pressure outlet are used as the boundary conditions, the flow is modelled as a compressible ideal gas in ANSYS Fluent. The simulation has been conducted like this for now, however after the vacuum lock chamber is constructed and tested it will be possible to gain values for the mass flow at the outlet, changes may be required to gain an accurate analysis. The values for the pump need to be defined and as the lock chambers are subsequently reducing, the pressure in the following chamber is not as low as the coating chamber but drops down

in stages. Figure 79 shows the high pressure focussed on the area where the inlet air is blocked by the rollers and strip.

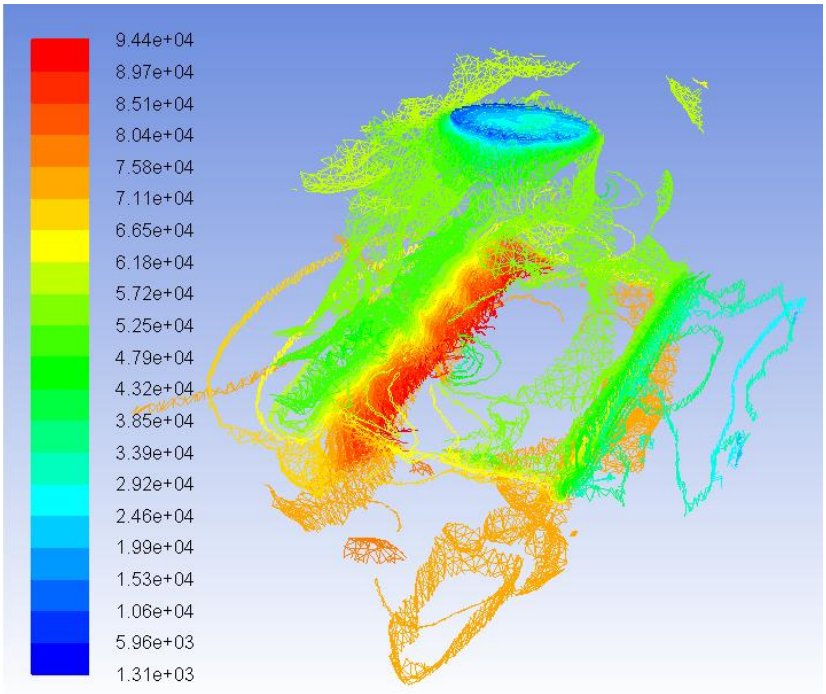

Figure 79: Static pressure (Pa) contours of air within vacuum lock revision 1

Figure 79 shows the high pressure indicated by the red contour at the inlet reduces significantly due to the pumping out of the air at the outlet on the top of the lock. The higher pressure is trapped air that cannot move pass the roller and strip. The values in figure 79 and 80 represent pressure, however they have not been validated as this will be done through experimentation with the final design. In figure 81, the velocity contours show very high flow speed 649 m/s this is nearly double the speed of sound (343 m/s) and is not realistic. The pumping will cause more air to be sucked in at the inlet unless there is something to obstruct the air leaking in, the air will be chocked in areas causing higher velocities, but these values are very high, even when compared to the de Laval Nozzle velocities.

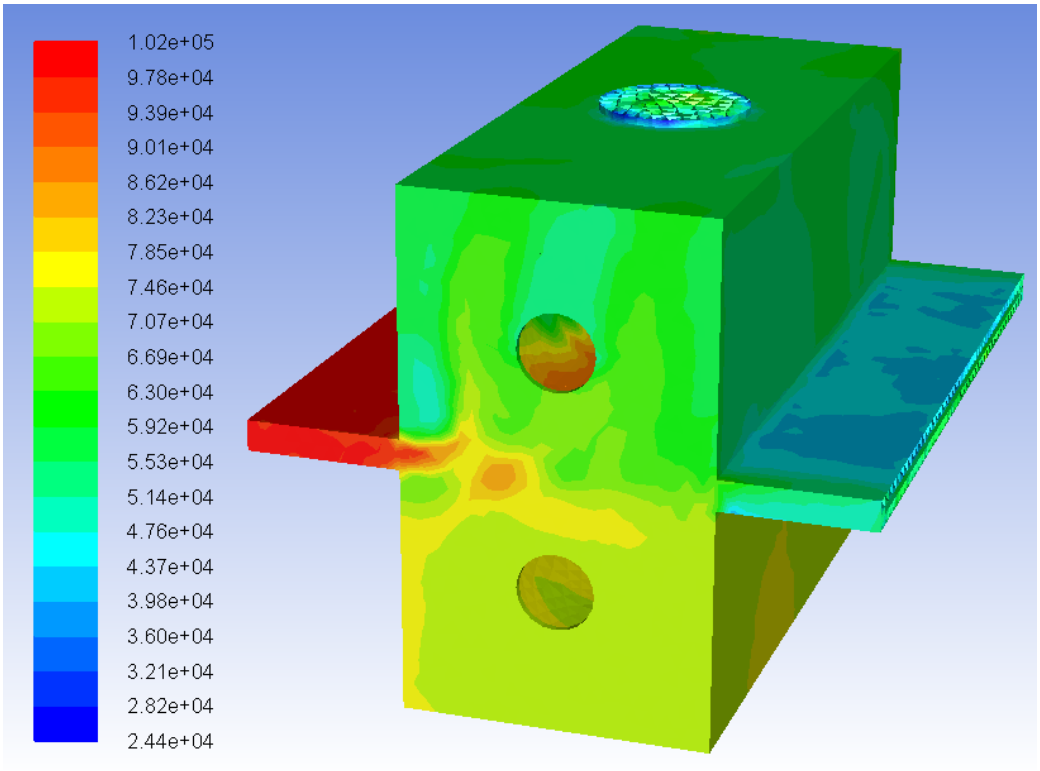

Figure 80: Static pressure (Pa) of air in vacuum lock revision 1

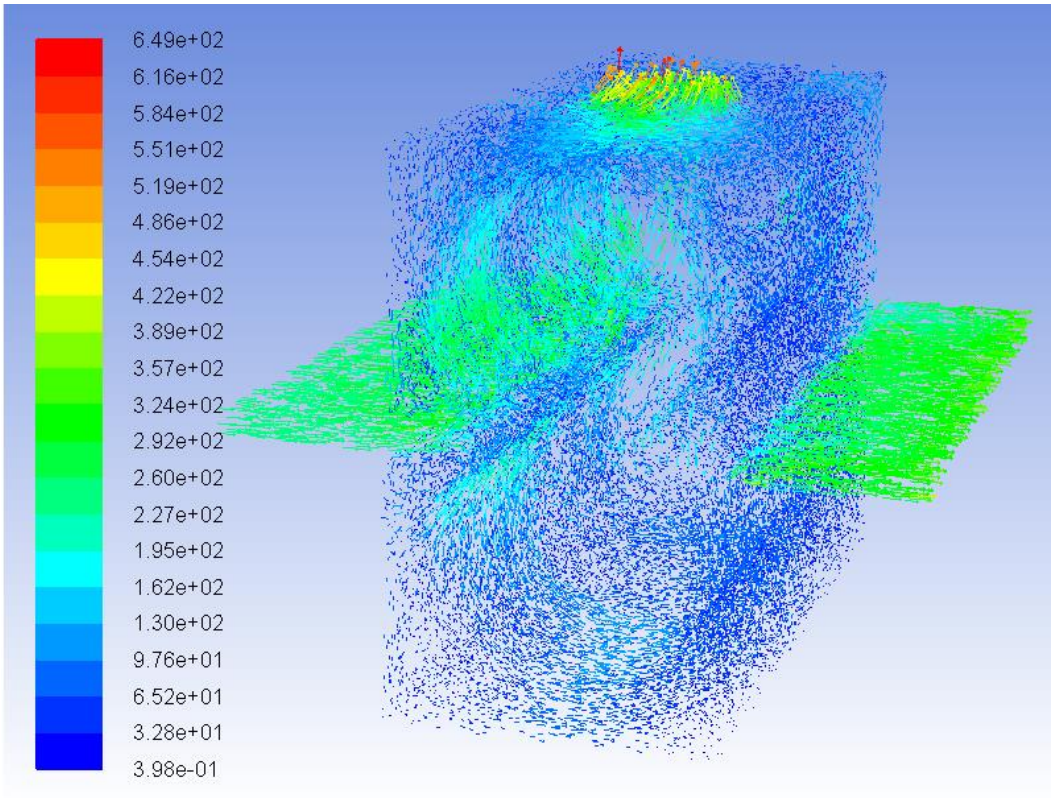

Figure 81: Velocity vectors (m/s) of air within vacuum lock revision 1

The current boundary conditions set in ANSYS Fluent considers air as an ideal gas and has a pressure inlet and outlet. Due to the velocity term missing from the continuity and momentum equation this could be incorrect and not provide accurate results even with using a density-based solver. Using a mass flow outlet boundary condition may be more suitable, more investigation on this is required. Once the vacuum lock design and simulation provide sensible results, they can be compared with an experimental rig for accuracy.

8.4 Vacuum Lock Revision 4 Simulation Results

The simulation moves on from the first revision to revision four. Revision two was deemed ineffective as it didn't perform any better than revision one and the design needs to be completed before producing several locks. Revision three is the same as revision four but just orientated horizontally with no effect on the results. Figure 82 shows the new air geometry and figure 83 shows the new mesh.

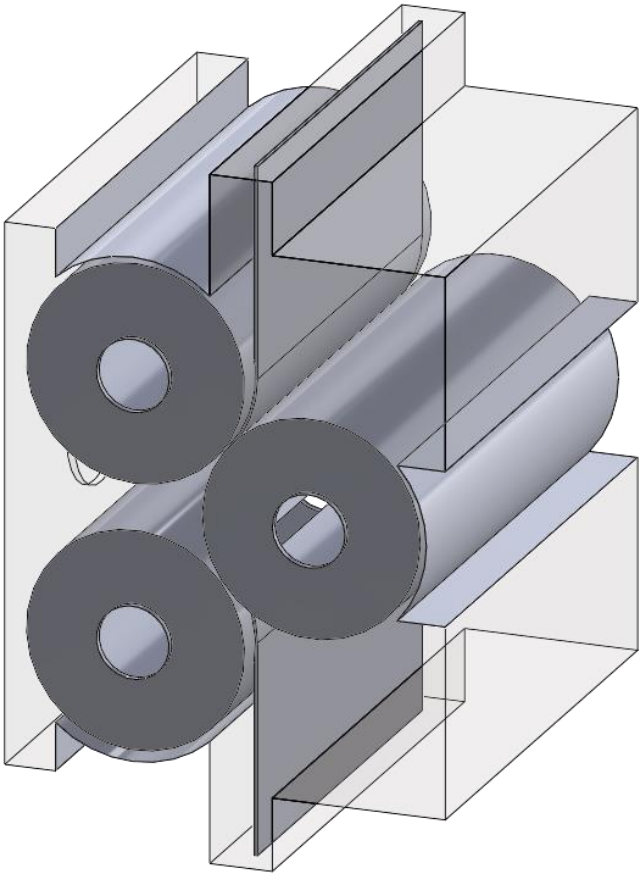

Figure 82: Vacuum lock design revision 4 air geometry

There are now more mesh elements because the geometry is more complex and smaller geometry areas due to the addition of another roller and sealing blocks (figure 83). The sharp elements between the strip and rollers have been removed again by adding a chamfer.

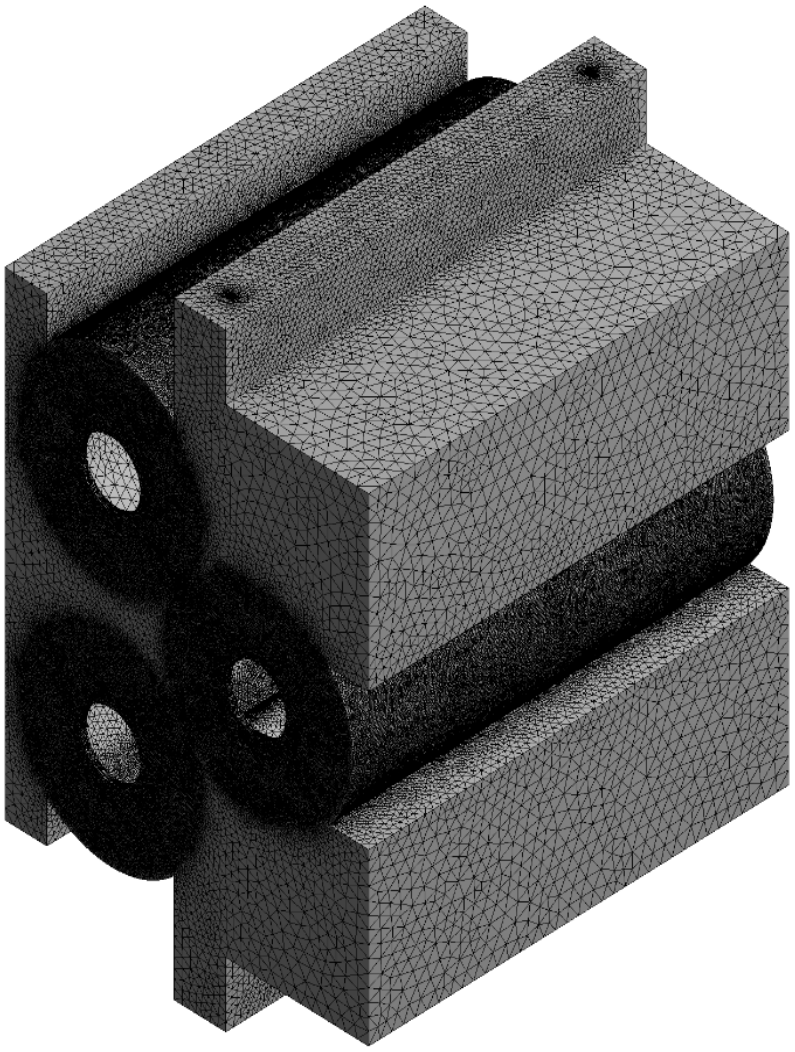

Figure 83: Vacuum lock design revision 4 air mesh

The same pressures were used as the first vacuum lock revision:

- Inlet Pressure 101,325 Pa (Static Atmospheric pressure)
- Outlet Pressure Exit 10000 Pa
- Outlet Pressure Pump 1: 1000 Pa

The new design makes it more difficult for air to pass through the vacuum lock and it can be seen in figure 84 that the higher air pressure is trapped in the top right corner. The simulation currently does not converge and has errors, the velocity results have high magnitude (figure 85) and it is unlikely that the air will travel at this velocity when a vacuum pump is attached. The pressure inlet and outlet boundary conditions are known to be difficult to converge [90]. The mass flow rate is known for pumps available on the market therefore it would be a more beneficial boundary condition to use. Investigation into boundary conditions that are suitable for a converging solution is required to gain more accurate results.

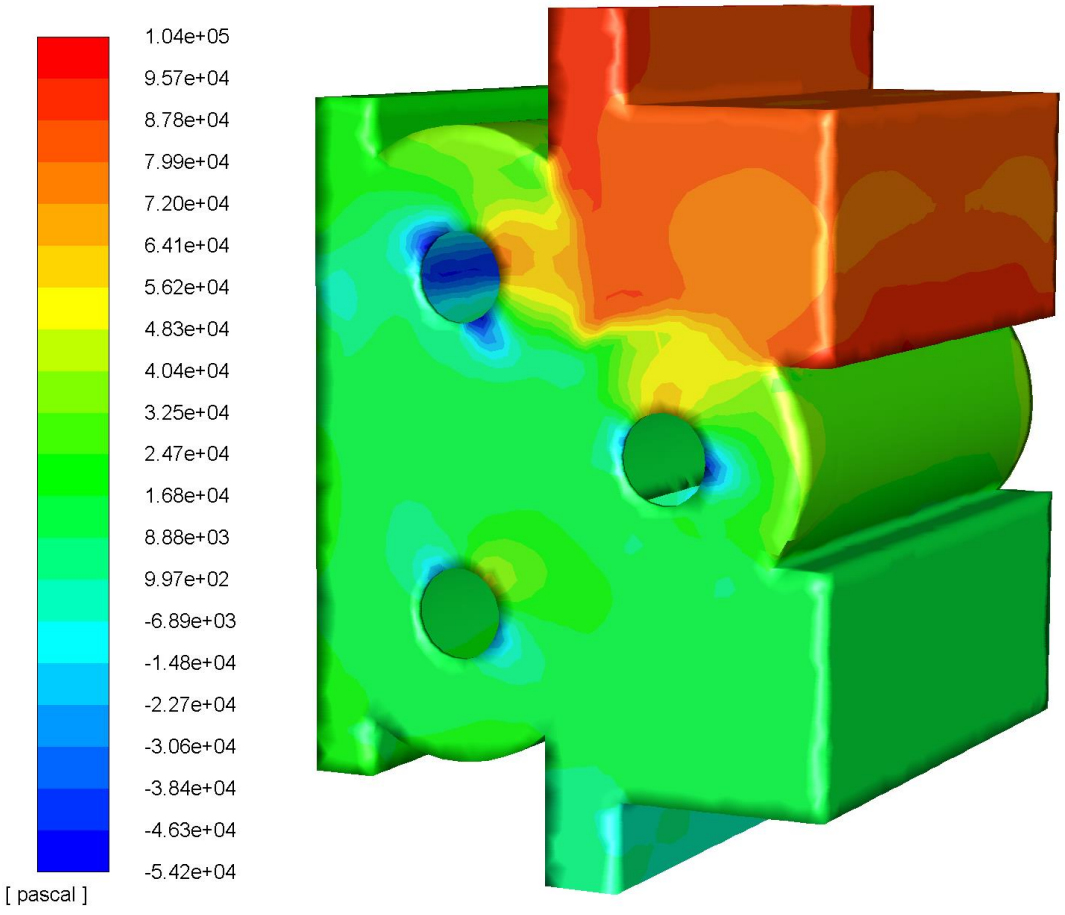

Figure 84: Static pressure within vertical vacuum lock

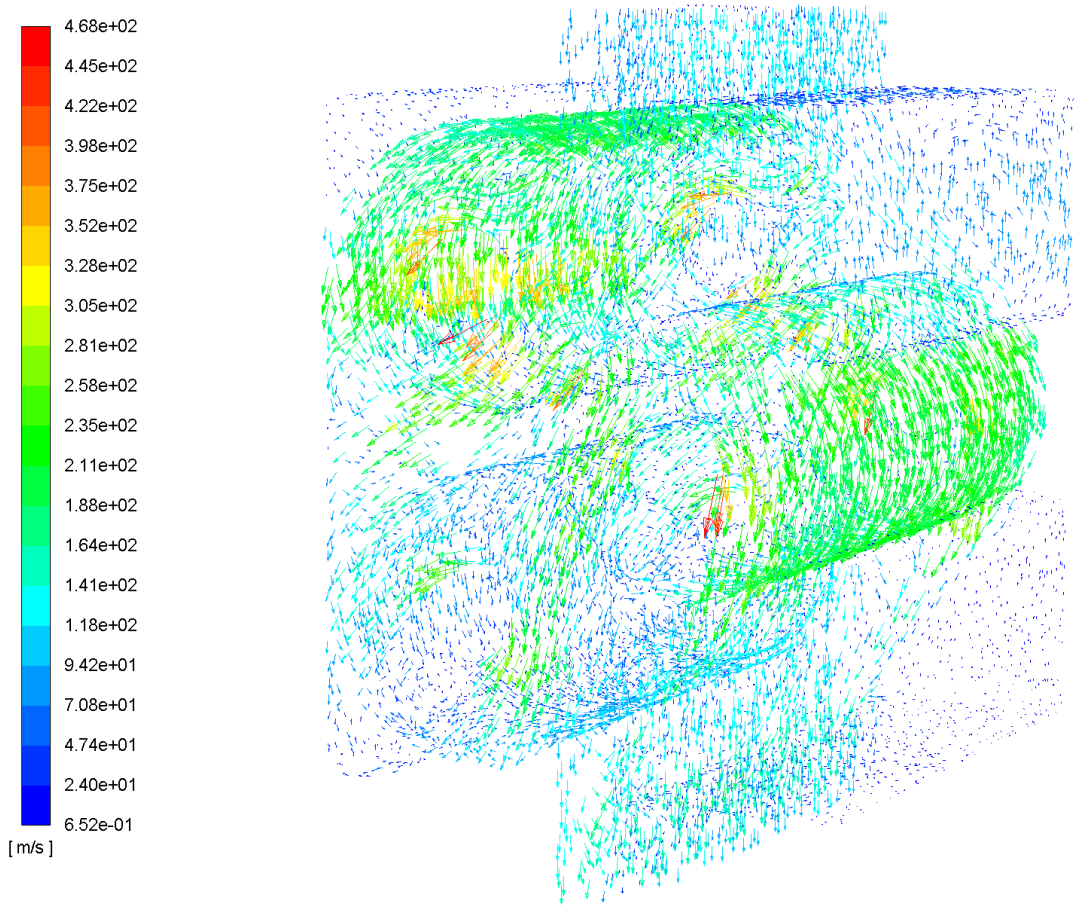

Figure 85: Velocity vectors within vertical vacuum lock

Figure 85 again shows high values for values for velocity, but they have reduced in comparison to figure 81. A value found for speed of air in a vacuum cleaner was a velocity inlet of 35.47 m/s in Kale et al (2016) [101]. The vacuum lock will have more powerful pumping than a vacuum cleaner and no values were observed in literature for the speed of air travelling through a vacuum coated system. Supersonic air speed is very high and from chapter four, figure 28 shows much lower expected velocity values calculated by rearranging the mass flow rate equation. Although there is concern about the high velocity vectors, the simulation does show the leakage occurring down the side of the rollers, which is what is expected. Leakage occurs in areas where there is clearance. In the case of this lock design, the gap at the sides the rollers provide an unwanted path for air to flow through, shown in figure 86.

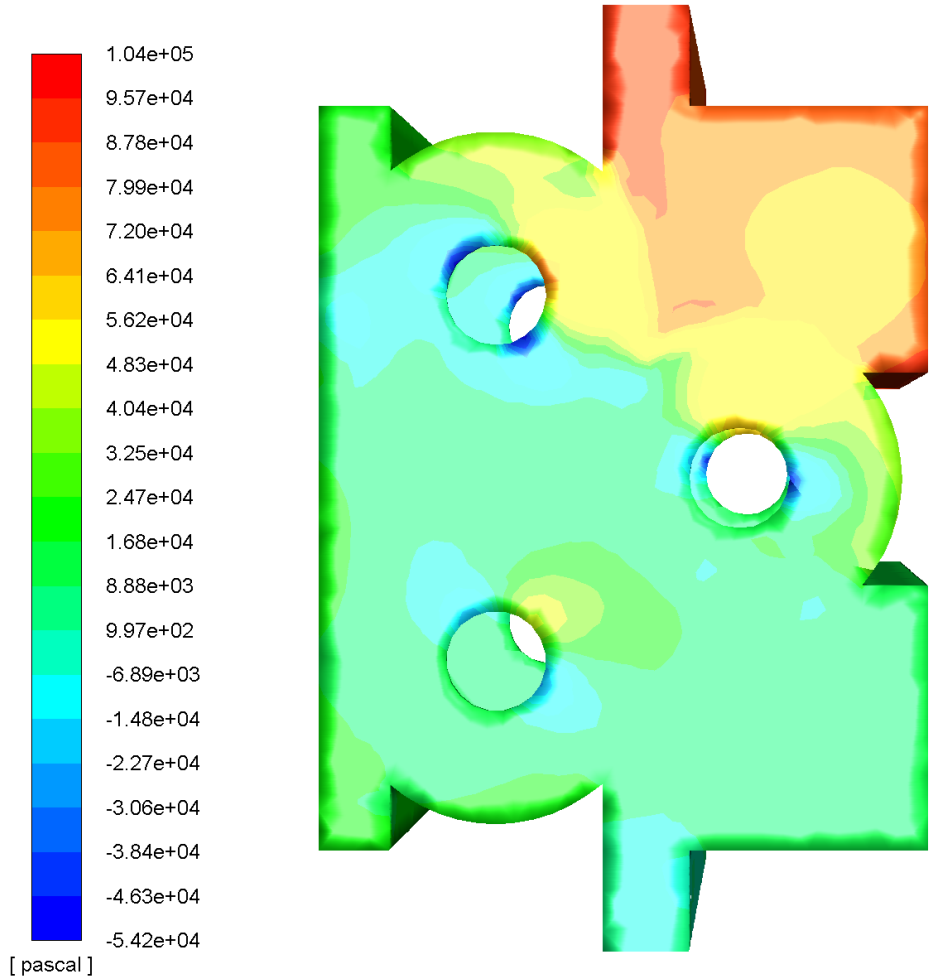

Figure 86: Leakage occurring between the roller and wall of the chamber

US Patent number 6,334,751 B1 states that clearance is inevitable and is dealt with by the vacuum pumps [40]. The rollers are required to be contained within the chamber and must have clearance from the chamber wall, so leakage will occur, the vacuum pumping is used to remove this leakage as well as evacuating air from the chamber. Making the clearances as small as possible in all areas of the lock will reduce the pumping requirements and electrical consumption, it is important however to have enough room for maintenance procedures and enough clearance to allow components to move without unwanted wear or damage.

8.5 Vacuum Lock Revision 6 Simulation Results

It is difficult to determine the flow conditions within the vacuum lock, there are no previous simulations that have been performed or literature available. There are tight clearances that could cause chocking to occur in the flow like the de Laval nozzle investigation, the flow could be compressed, and it is possible that there are areas of higher velocity in the tight gaps. Different boundary conditions were tried to produce a computational model that achieves convergence in the scaled residuals and produce reasonable approximations of the pressure when compared to existing vacuum locks as they give a baseline of what is likely achievable for the first lock. To reduce computational expense a half model was used in the simulations of revision 6 and 7.

8.5.1 Pressure Inlet Pressure Outlet

Changing the geometry resulted in even tighter gaps for the air to travel into the lock. As the volume of air is travelling from a small inlet to tight gap and then larger area it was thought that the physics could be similar to the de Laval nozzle problem therefore the same conditions were used. The viscous model was chosen as this simplifies the problem by ignoring the viscous terms and turbulence. The air is modelled as an ideal gas. As there is a pressure inlet and outlet the density based solver must be used which solves the governing equations of continuity and momentum and the scalers are solved separately using coupled implicit formulation. There is no initial velocity with this set up so the SIMPLE, SIMPLEC, PISO algorithms are not used. The pressure inlet was set at atmospheric pressure and the outlet was set at 1000 Pa. The air geometry and meshed model used are shown in figures 87 and 88.

Before the residuals start to diverge shown in figure 90, the residuals are converging and when checked in the simulation pressures looked reasonable, however after divergence occurred it can be seen in Figure 89 shows that higher static pressures are recorded than given to the system in the boundary conditions. This is because divergence occurred resulting in inaccurate results. This was also the case in earlier simulations which would run for 200 iterations and only converged to $1e^{-1}$ but if run for longer the residuals diverged. A CFD simulation should converge to at least $1e^{-3}$ and preferably lower [99].

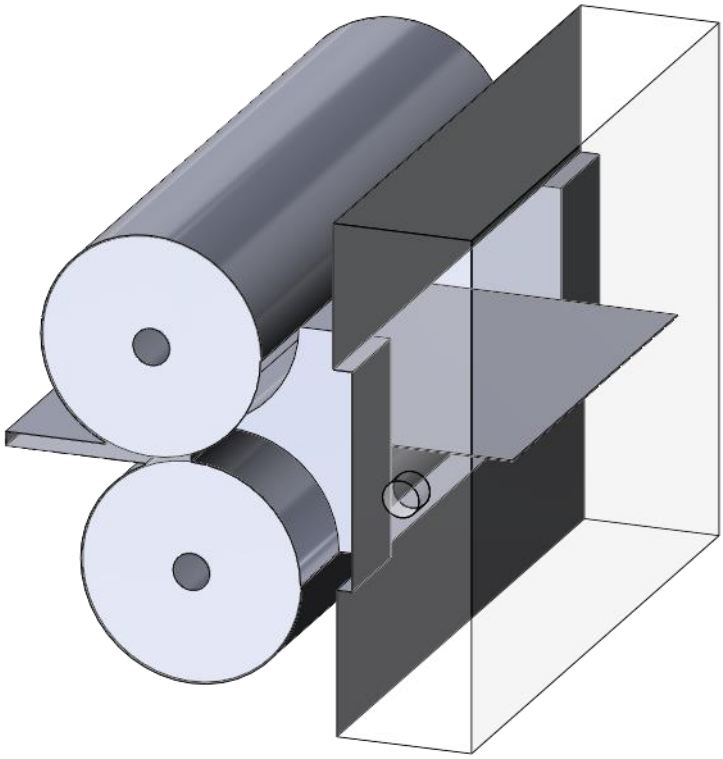

Figure 87: Vacuum lock design revision 6 air geometry

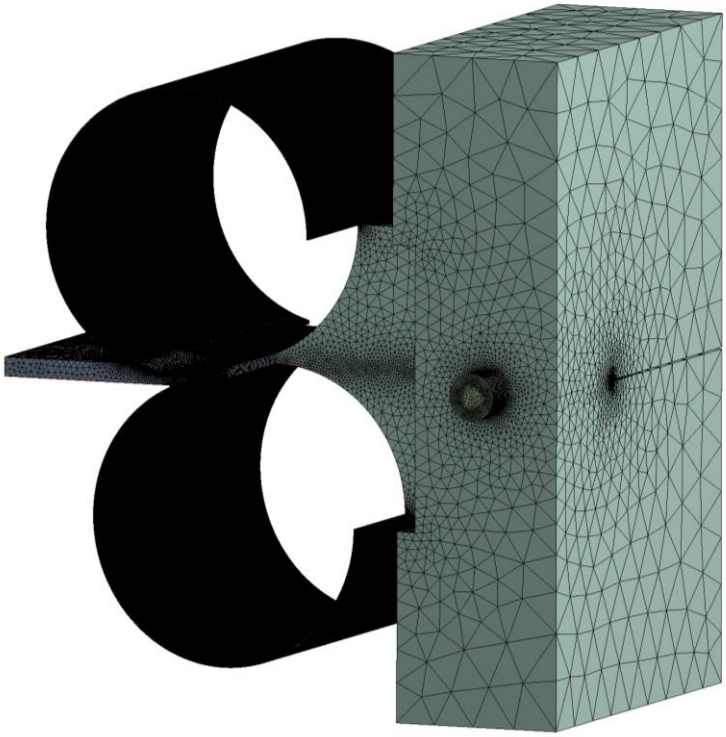

Figure 88: Vacuum lock design revision 6 air mesh

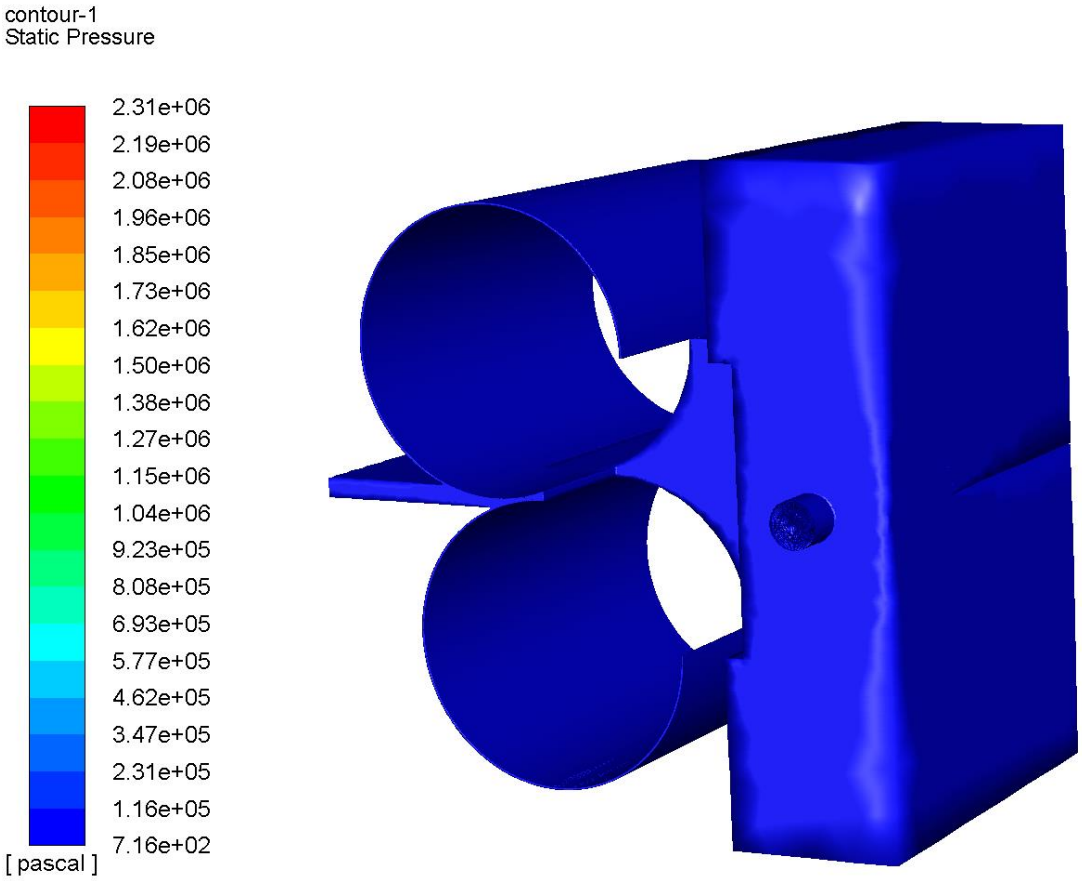

Figure 89: Static pressure contours after divergence occurs

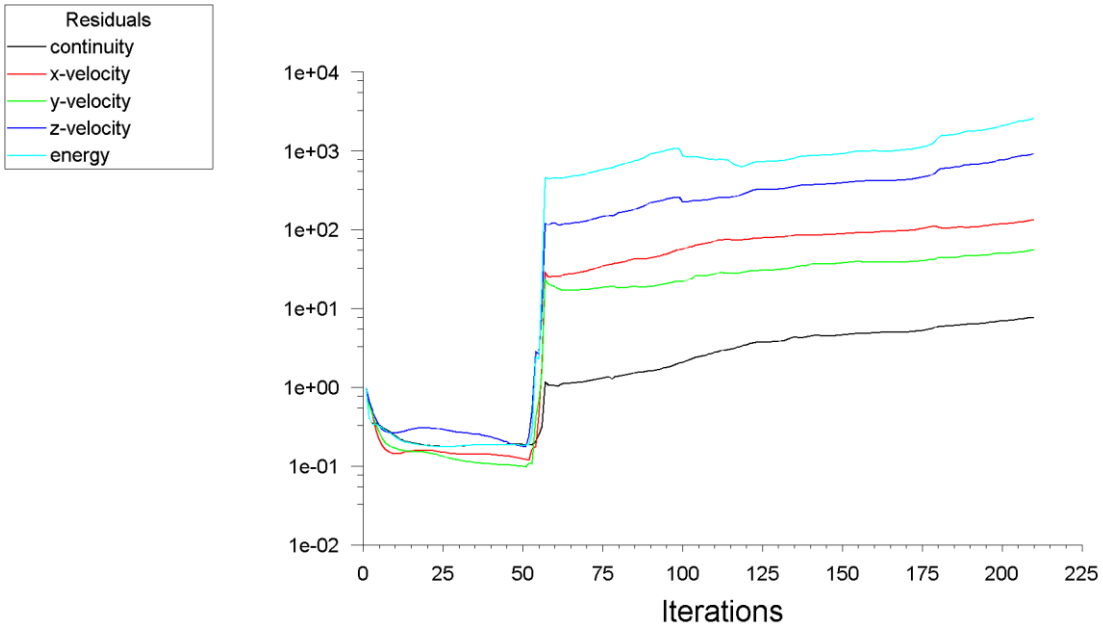

Figure 90: Residuals containing divergence

8.5.2 Pressure Inlet Mass Flow Outlet

In this set up an alternative to the benchmarking simulations was tested. The vacuum modelling literature indicated that the vacuum problems had been analysed for incompressible flow unsteady flow as Lai (2011) had used the PISO algorithm and Kale et al (2016) had used velocity at the inlet. As the velocity at the inlet was not possible to determine as it depends on the suction of the vacuum pump the alternative was to use the mass flow rate as this could be determined from the pumping speed of the pump. The pressure is known at the inlet because it is atmospheric so that was set to 101,325 Pa and a new boundary condition of mass flow rate was used at the outlet. The mass flow rate was set to 0.025 kg/s as it is a half model so this is 0.5 kg/s as the problem is symmetrical. A pressure based solver was used as this time there is a velocity term in the mass flow rate boundary condition. The SIMPLE algorithm was used as this is the least computationally expensive. The temperature was set at 300 Kelvin and the k-Epsilon viscous Model was used for turbulence.

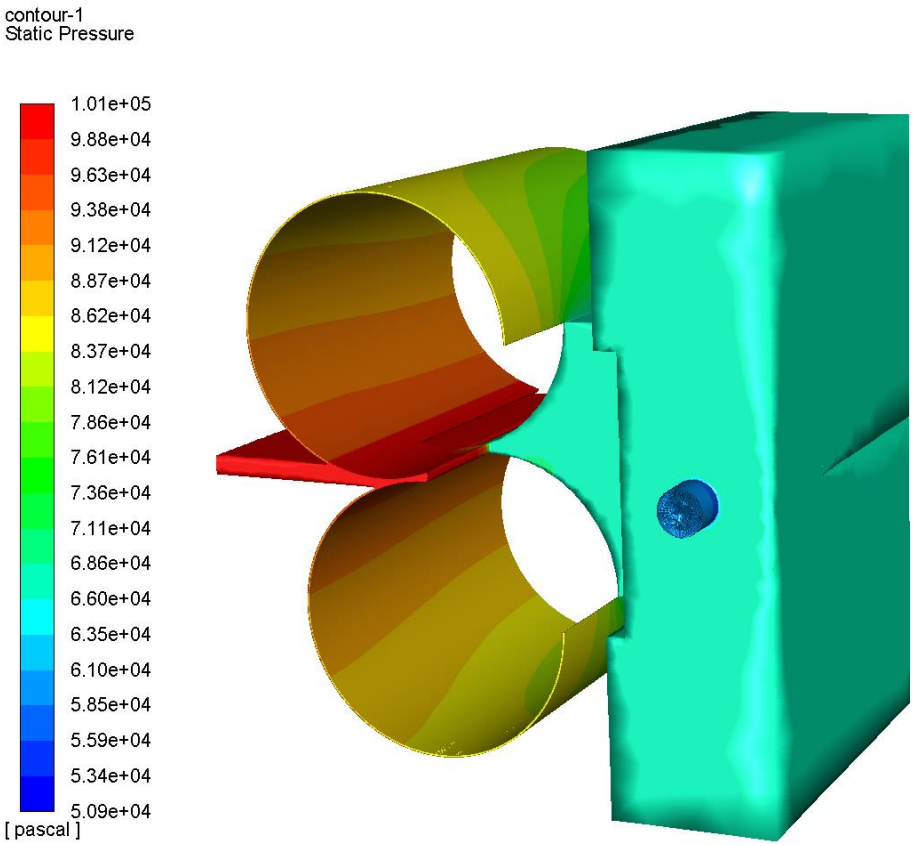

Figure 91: Contours of static pressure converging simulation

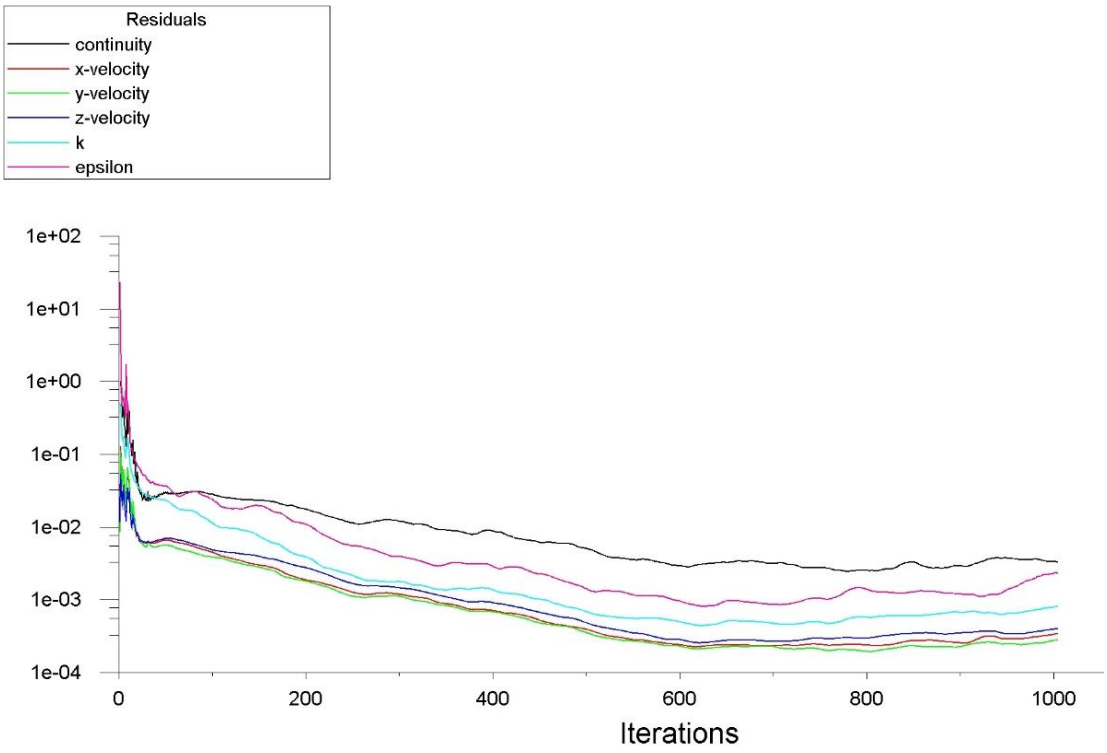

Figure 92: Converging residuals revision 6 mass flow rate outlet condition

Using a pressure inlet and mass outlet resulted in a more stable solution this time. The residuals did not converge however they were very close to converging and did not diverge or come up with any errors, figure 92 shows the more stable residuals. Figure 93 shows more reasonable velocity magnitude for the air. From chapter 4 where the likely velocities were calculated displayed in Figure 28 gave an outlet velocity of 20.79 m/s for a mass flow rate of 0.05 kg/s, here the highest value at the outlet taken from ANSYS is 79.6 m/s. However, the calculation performed using equation 4.45 used for the velocities in figure 28 is simplistic and does not consider the change of geometry between the inlet and outlet.

Velocity values in figure 93 are lower than the previous simulations and also have lower values around the outlet similar to the vacuum cleaner values, experimental measurements would validate the accuracy of these values but is difficult to measure as would have to get a flow meter into awkward geometries and they are usually attached or inserted into pipes. The worst case leakage area is highlighted again in

figure 81 where they are around 250 m/s at the inlet/outlet of the lock, this again confirms that this is a problematic area for restricting leakage into the system.

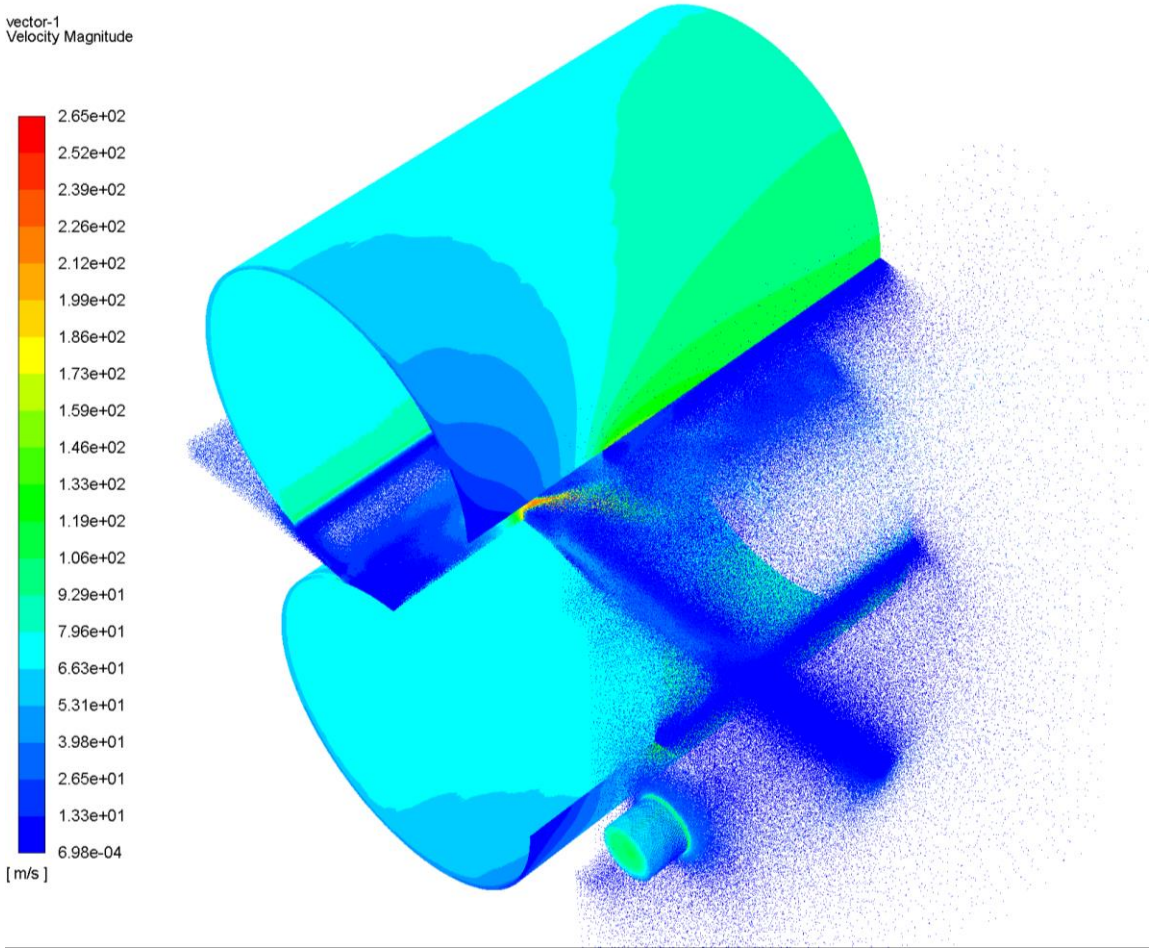

Figure 93: Velocity vector magnitude vacuum lock revision 6

Velocity is a very important consideration as it determines the type of flow (subsonic, critical and supersonic). However, the most important physical property for the coating system is the pressure as the achievable vacuum depends on the pressure in the system. In the final prototype the focus is solely on the pressure results. Figure 94 shows the leakage through the gap between the roller and the Teflon block. This is a significant area of leakage and although the Teflon block reduces the physical space there is still a gap here. The purpose of the air bearing mechanism is to reduce the air travelling through this gap and therefore resulting in the lock being more effective and requiring less pumping to achieve low pressure conditions.

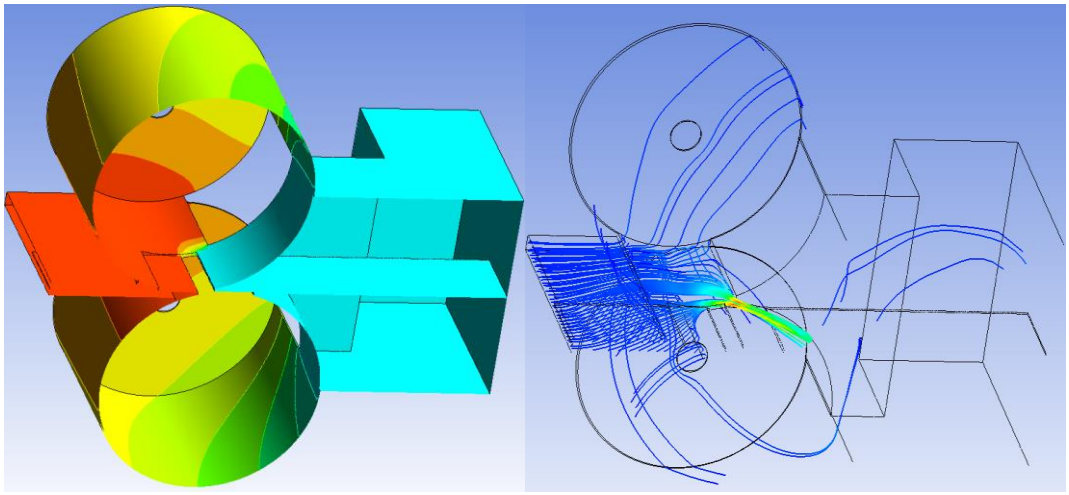

Figure 94: Streamline plot showing major leak in revision 6 design

8.6 Air Bars 2D Simulation

Two preliminary simulations were performed to check the effect the air bars will have on the vacuum lock. The first simulation is without the air bars at the inlet, the 2D geometry is the space between the upper and lower air restriction mounts shown in figure 95.

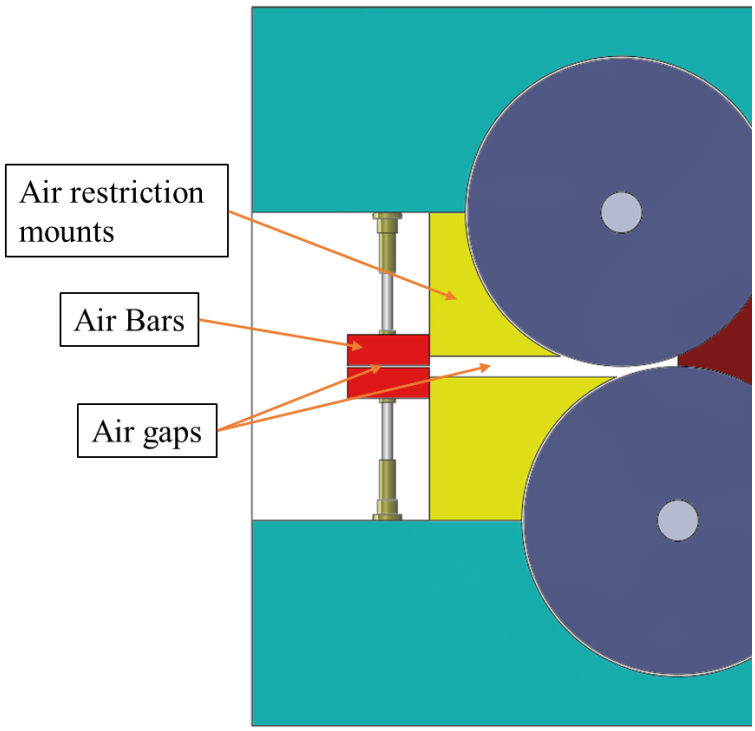

Figure 95: Air gap between the air restriction mounts and air bars

The second simulation includes the restriction of space with the air bars at the inlet again shown in figure 95. The second simulation is a half model of the air gap which is why the thin line that represents the gap between the air bars is not in the middle of the larger gap representing the space between the air restriction mounts (figure 97). For the simulation the pressure at the inlet is 101,325 Pa (atmospheric pressure) and for the simulation with the air bar the pressure at the smaller inlet where the air bars have reduced the gap to 0.1 mm is 145000 Pa, which is higher due to the compressed air from the air bars. The outlet was set at a mass flow rate of 67.37×10^{-3} kg/s this is converted from the pumping speed of the rotary pump which is 198 m^3/h.


```
   115  1.1905e-04  1.7186e-04  1.7399e-05  1.0105e-03  7.8017e-04  0:00:00  385
!  116 solution is converged
   116  1.1576e-04  1.7032e-04  1.7079e-05  9.9600e-04  7.6741e-04  0:00:00  384
Writing data to D:\Documents\EngD\Air Bars Inlet\Air Bars BC_files\dp0\FFF-2\Fluent\FFF-2.2.ip
    x-coord
    y-coord
    pressure
    x-velocity
    y-velocity
    k
    epsilon
    hyb_init-0
    hyb_init-1
Done.

Calculation complete.

                  Mass Flow Rate               (kg/s)
------------------------------ --------------------
                          inlet           0.06737718
                         outlet            -0.067375
               --------------- --------------------
                            Net        2.1795679e-06
```

Figure 96: 2D Flow simulation without air bearing boundary condition

With the air bars restricting the flow with a very small clearance at the inlet, this means less air getting into the lock for the Teflon block to restrict and removing the Teflon blocks is now a possibility. The results showed that without the air bars the pressure does not reduce from atmospheric pressure (figure 96). The addition of the air bars reduces the gap at entry into the lock. The additional pressure at the inlet starts higher than atmospheric pressure at 145 kPa but then reduces to negative gauge pressures. Even with the simulation converging there is an error as the negative pressures added to the operating pressure are still negative and it is not possible to have negative absolute pressure. No further work was completed on the 2D simulations as they failed to give conclusive results on effect of including air bars due to the negative pressure results.

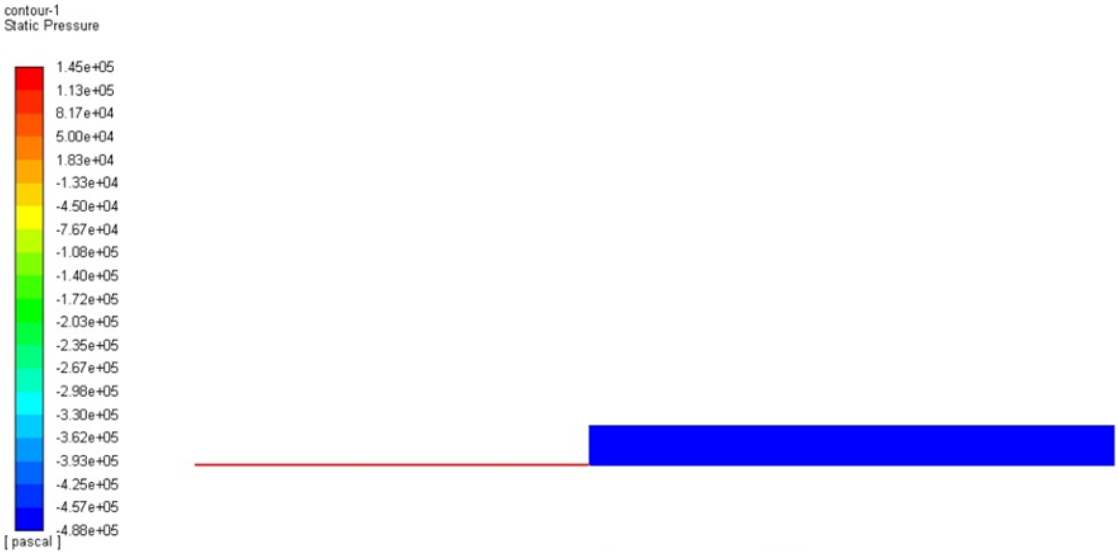


```
!  761 solution is converged
   761  7.4764e-06  8.4066e-04  3.8045e-04  7.5361e-04  9.9814e-04  0:00:16  239
Writing data to D:\Documents\EngD\Air Bars Inlet\Air Bars BC_files\dp0\FFF\Fluent\FFF.ip ...
     x-coord
     y-coord
     pressure
     x-velocity
     y-velocity
     k
     epsilon
     hyb_init-0
     hyb_init-1
Done.

Calculation complete.

                  Mass Flow Rate               (kg/s)
------------------------------ --------------------
                           inlet          0.068754632
                          outlet         -0.068749975
               --------------- --------------------
                             Net        4.6570511e-06
```

Figure 97: 2D Flow simulation with air bearing boundary condition

It is not just the pressure that is important here, it is also the amount of flow of air that will enter the lock, which should be less due to the smaller gap even if the pressure is higher from the air bars. The mass flow at the inlet of the air bearing inlet is very similar for both scenarios. The experimental validation will clarify if the air bars will provide improvement to reducing the pressure.

8.7 Vacuum Lock Revision 7 Simulation Results

In the final simulation the Teflon blocks are removed and the same for the experimental validation as the air bar system is considered sufficient to restrict the air into the lock without them explained earlier in section 7.2. A parametric simulation is performed in ANSYS Fluent using a pressure inlet at atmospheric pressure and a mass flow rate outlet. This allows a pumping curve to be produced for the lock by keeping the inlet at 101,325 Pa and changing the mass flow rate outlet through a range of mass outlet flows to determine what can be achieved with a rotary pump.

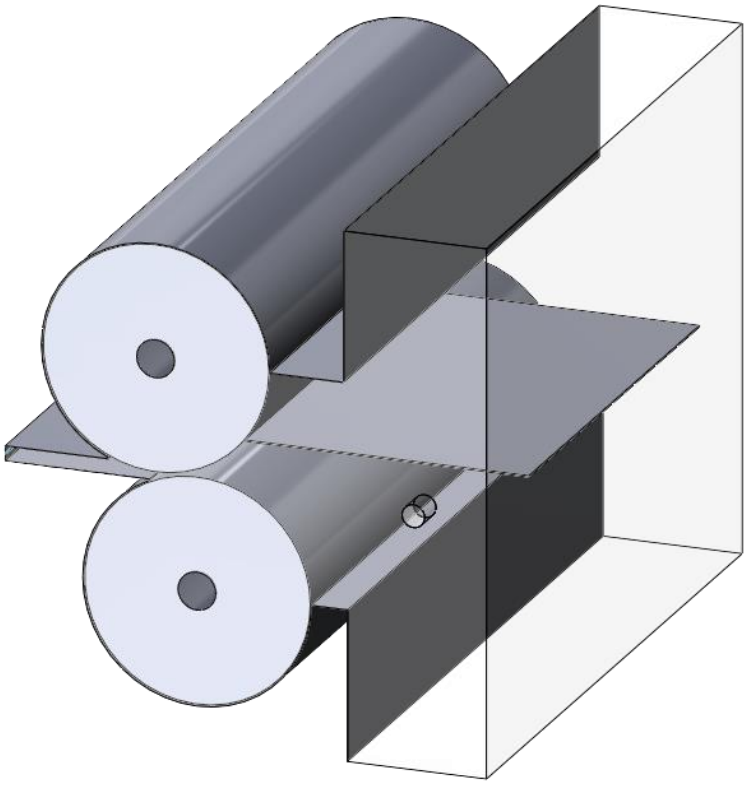

Figure 98: Vacuum lock design revision 7 air geometry

For revision 7 the same simulation set up for the pressure inlet and mass flow outlet was used as revision 6. The other algorithms SIMPLEC and PISO was also be tried as well as the other viscous models for turbulence terms K-epsilon, K-omega and SST mentioned in Son et al (2018) to see if convergence and more accurate results could be achieved. The PISO algorithm did give convergence for 0.05 kg/s but performed worse for other mass flow rates and K-Epsilon was the most stable for converging residuals therefore the parametric study was performed using the conditions used for 6. Figure 98 shows revision 7 air model and figure 99 is the mesh model. The mesh varies from coarse elements in the larger space and very fine mesh in the tight clearances this is to ensure there is a minimum of three elements across those boundaries.

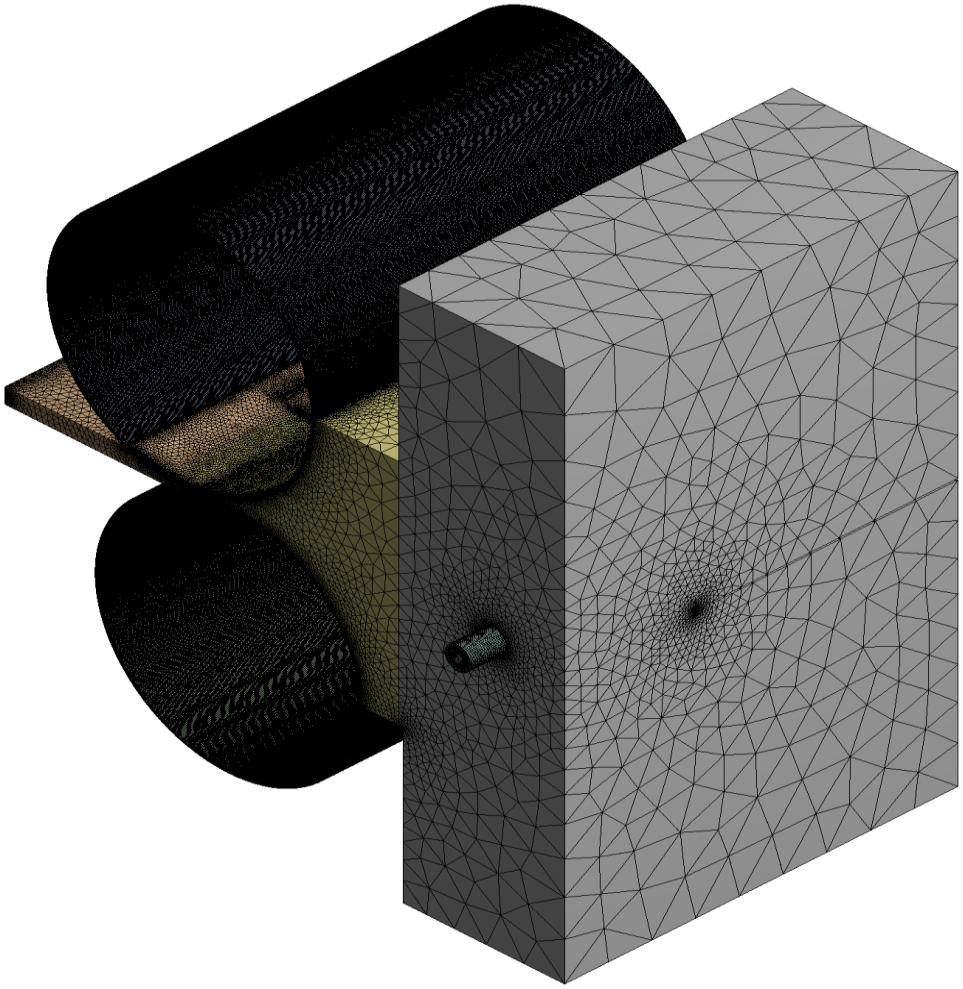

Figure 99: Vacuum lock design revision 7 air mesh

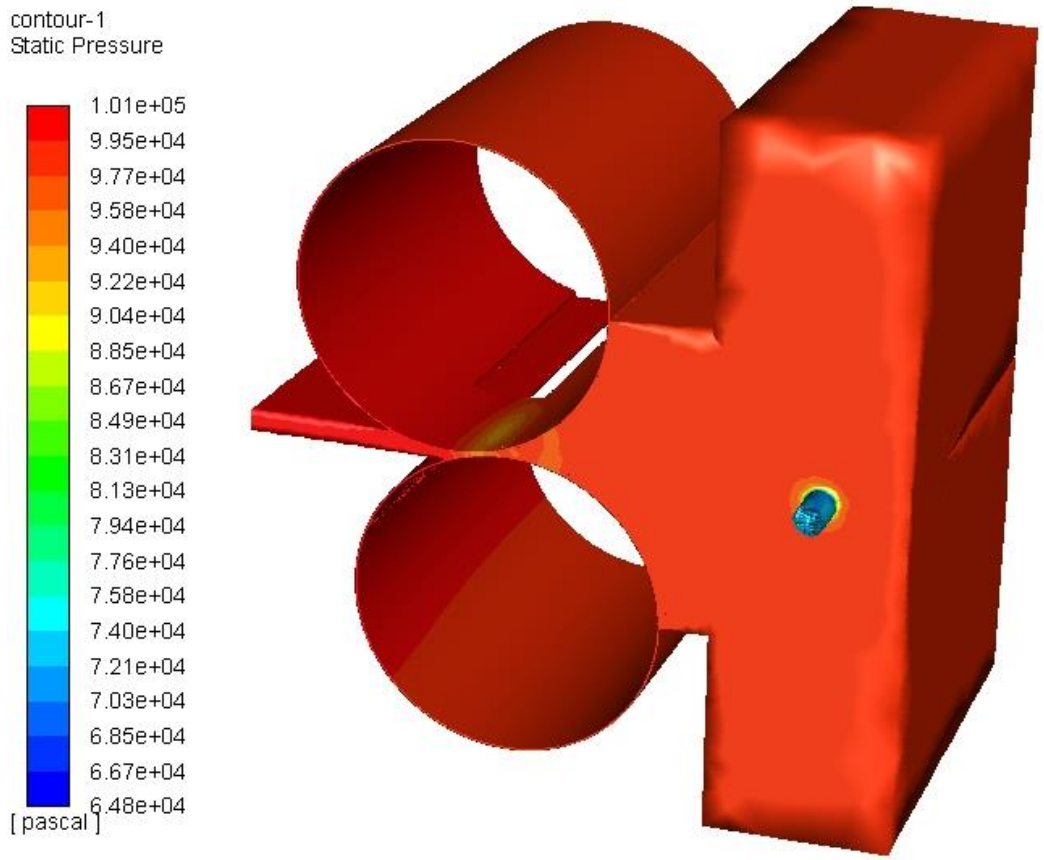

Figure 100: Contours of static pressure without the air bars in ANSYS Fluent

The results in figure 101 are from a parametric study performed in ANSYS Fluent. The exit wall pressures are the highest-pressure results on the right side panel of the lock, obtained from simulating the pumping down of the lock using a mass flow rate outlet. As the flow rate increases at the outlet, more air is drawn into the inlet, therefore air is leaking into the lock and air pressure within the lock is not reducing significantly. The actual simulation was conducted with a half model that means the outlet is on both sides due to symmetry, therefore the mass flow rate at the outlet is halved in the simulation but not in the graph (figure 101).

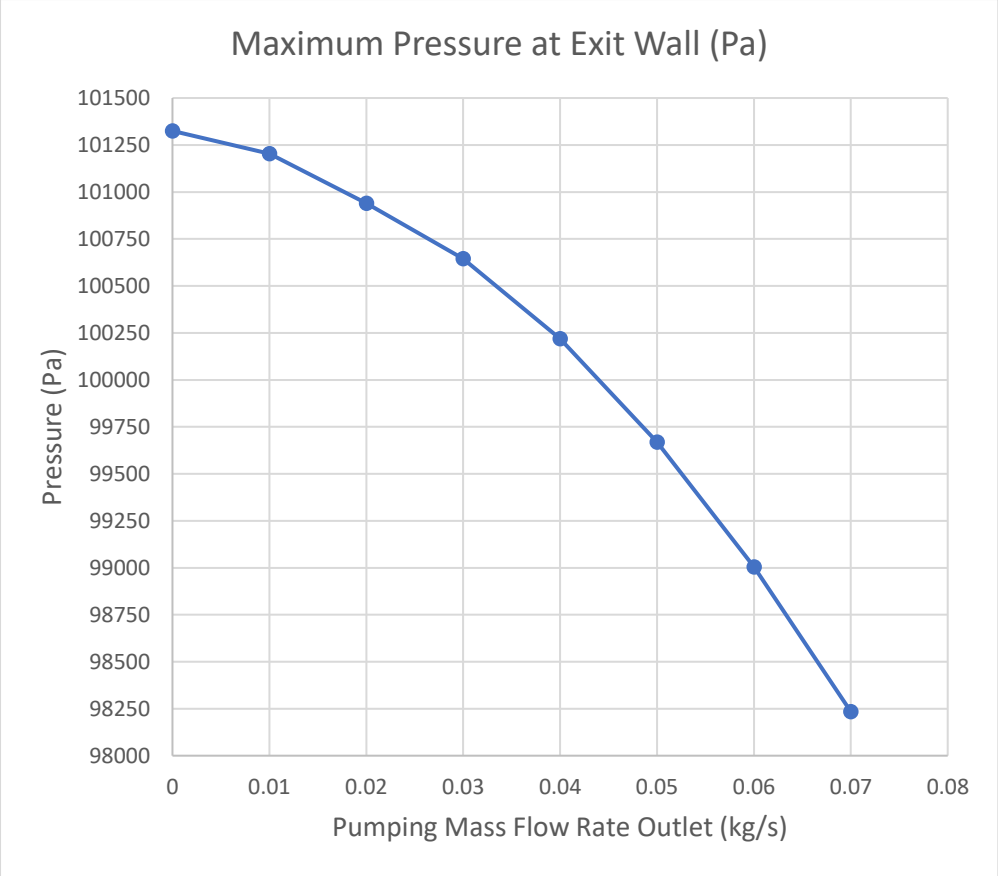

Figure 101: Maximum pressure at the exit wall with increasing mass flow rate

The operating pressure was set to zero for these simulations, therefore the pressure results are added to zero to get the gauge pressure. Although some simulations converged it tended to be the simulations with the lower mass flow rate and was temperamental. The simulations with the higher mass flow rate showed signs of residuals converging but did not converge although stayed around the 10^{-3} mark. Without the air bars and using a rotary pump at full capacity 198 m^3/h, the vacuum lock can only reduce by approximately 3 kPa. The inlet without the air bars is 450 mm by 10 mm with a 1 mm x 300 mm steel strip in the middle. The gap the air bars allows is 0.1 mm around the steel strip and then 1.2 mm at the edge of the steel strip to the side of the chamber, the slider is also 1 mm so that closes that gap as close as 5 mm to the strip edge. This much smaller gap was cut into the face of the 3D model and used as an inlet, the clearance is shown in red in figure 102.

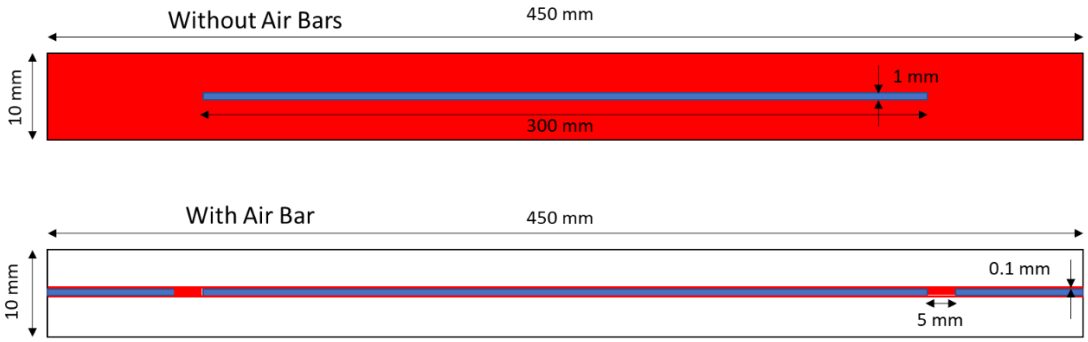

Figure 102: Clearance at the inlet of the vacuum lock with and without air bars

The geometry, now being very small in comparison to the rest of the lock included some very small mesh elements and the simulation did not converge, however the simulation did run, and results were obtained. Vacuum pressure is the atmospheric pressure plus the gauge pressure (negative) this was shown in figure 31. The results showed negative pressures, this would be reasonable if the pressure was negative gauge pressure and the operating pressure was set at atmospheric pressure, however operating pressure was set as zero in ANSYS, so these results are rejected as absolute pressure must not be less than zero. The simulation was re-run using atmospheric operating pressure and 145 kPa of additional pressure at the inlet due to the compressed air from the air bars. The mass flow rate at the outlet at 0.0336875 kg/s (half the real values due to symmetry) provided by the rotary vacuum pump. If a reading could be taken of the leak into the lock at the inlet from the Air Bars, this could be used as a mass flow inlet condition instead.

The pressures are shown to be higher with the air bars at the inlet initially but as the pressure increases the pressure reduces lower than before without the air bar inlet condition. The model did not converge but there was no floating point exception or any other errors, however the final pressure reducing to lower than zero would suggest there is not an accurate solution here. The predicted pressure of 56741 Pa is lower however and the air bars should in theory reduce the volume of leaked air into the lock. If ANSYS is giving accurate pressures as negative gauge pressures, then this model could be reasonable if also converge is achieved and experimental data backs up the obtained results.

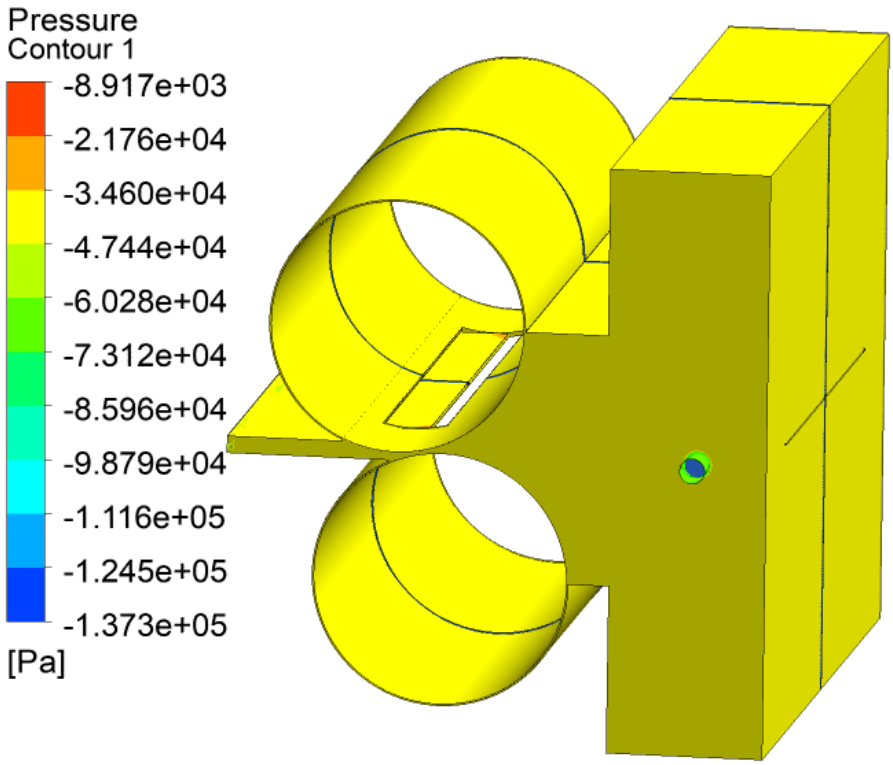

Figure 103: Simulation including air bars condition

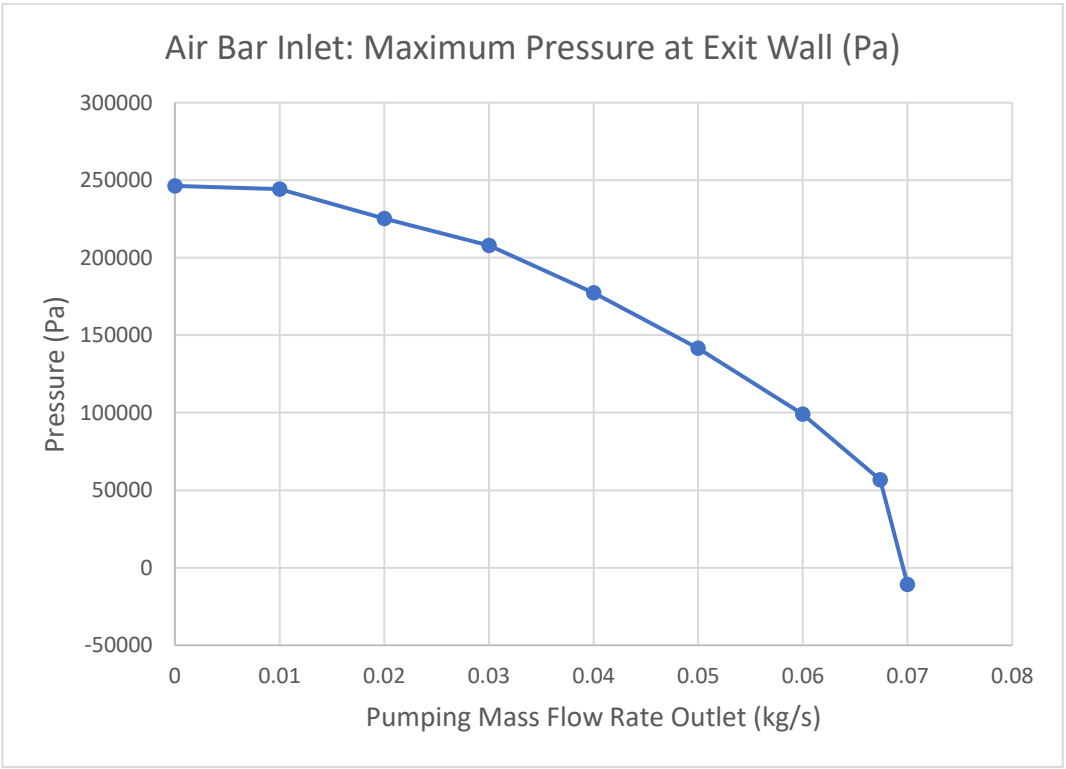

Figure 104: Air bar inlet: maximum pressure at the exit wall with increasing mass flow rate

The vacuum lock gained better simulation results using the pressure inlet and mass flow outlet boundary conditions however this is steady state incompressible flow so does not consider compressible flow which is likely to occur due to the air being chocked through tight gaps. The simulation is only solving for the continuum flow regime and this set up could only be used for the first vacuum lock where the pressure is not decreasing less than 1000 Pa. The error of negative pressure could be that flow is starting to change regime into slip or transitional flow and therefore the equations being solved for continuum is not suitable here. It is clear that experimental testing is required to get a much more reliable prediction of the flow and verification of whether the addition of air bars will benefit the pressure reduction of the lock as there is the consequence of added compressed air from them.

9. Experimental Validation of Prototype

To determine the accuracy of computational modelling results, a verification method is required. The verification can be numerical or experimental. It can get very difficult to verify a simulation mathematically depending on what has been simulated. Experimental validation gives real results and if the experiment has been conducted accurately these are very useful in determining the accuracy of a computational model. An experimental prototype was produced using the CAD drawings for revision 7 adding clamps, handles and fixings as well as fittings to connect a vacuum pumps and sensors. The author sourced the materials for the prototype as well as producing technical drawings in Appendix A and oversaw the assembly in the University Workshop. Pressure sensors were purchased to measure the pressures in the vacuum lock whilst the air was being removed with a rotary vacuum pump. The pressure sensors had not been used before therefore were not calibrated. An experiment was conducted with an off the shelf vacuum chamber to ensure that the pressure readings obtained from the pressure sensors could be trusted and act as an initial set up procedure before testing the protype vacuum lock.

9.1 Vacuum Chamber Experiment

A controlled leak was set into a sealed vacuum chamber measured with a Siargo MF5700 thermal mass flow meter connected to the drain valve. The flow of the leak through the drain valve can be measured and the pressure of the vacuum chamber to determine the effect the leaks have on the pressure in the chamber. The chamber has an internal geometry of 300mm cubed and 27 litres of space. The pressure was measured with a Keyence AP-40 pressure sensor connected to the air admittance valve, shown in the diagram (figure 105). The vacuum chamber already has an analogue vacuum gauge fitted. The readings on the analogue are not as accurate to read as the digital output of the Keyence sensor but can be used to check any deviation from the Keyence sensor readings.

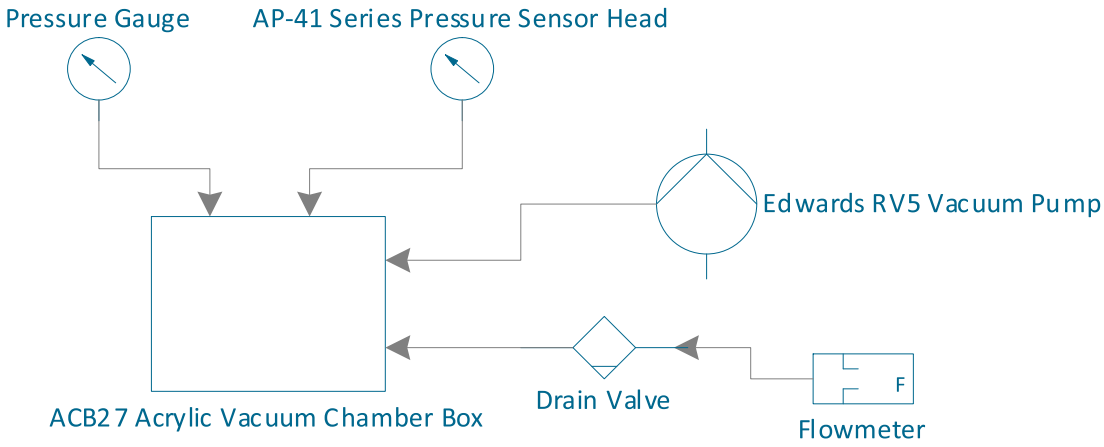

Figure 105: Diagram of vacuum chamber, controlled leak experiment

The leak was produced by first evacuating the chamber and then opening the drain valve taking a reading from the flow meter until the desired leak was achieved. Then the system was drained, the vacuum pump was turned back on and the pressures were recorded by video as the chamber was pumped down to the lowest pressure it could achieve at that leak rate. The leak was also checked to make sure it had not changed since it was first set.

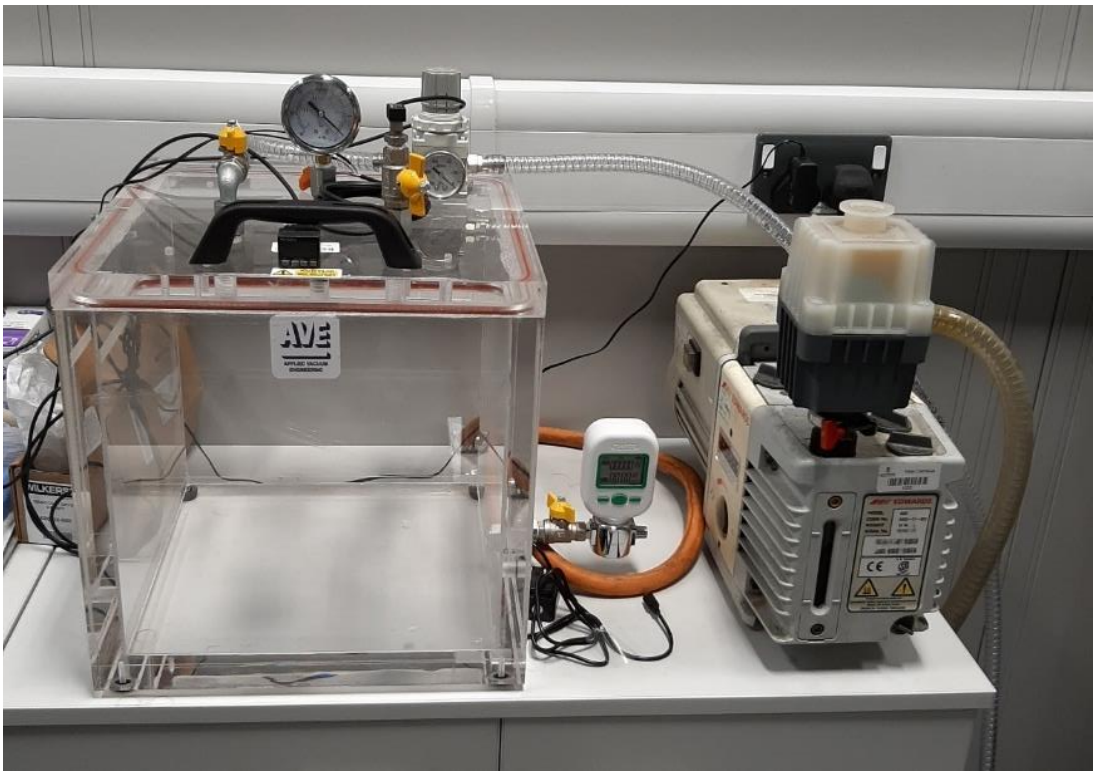

Figure 106: Vacuum chamber experiment

The video editing software hitfilm express was used to ensure the readings were taken at the exact time for each experiment, by checking the number of frames and the time reading. The readings on the analogue pressure gauge was also checked to be showing the same pressure which they were. Figure 106 is a photo of the set up. The flow rate meter is not certified for use in a vacuum but is connected externally reading the flow through the atmospheric pressured air into the chamber. The meter is supposed to read up to 20 standard litre of air per minute (SLPM) but the maximum leak that could be read was 11 SLPM. Standard refers to ambient temperature and pressure.

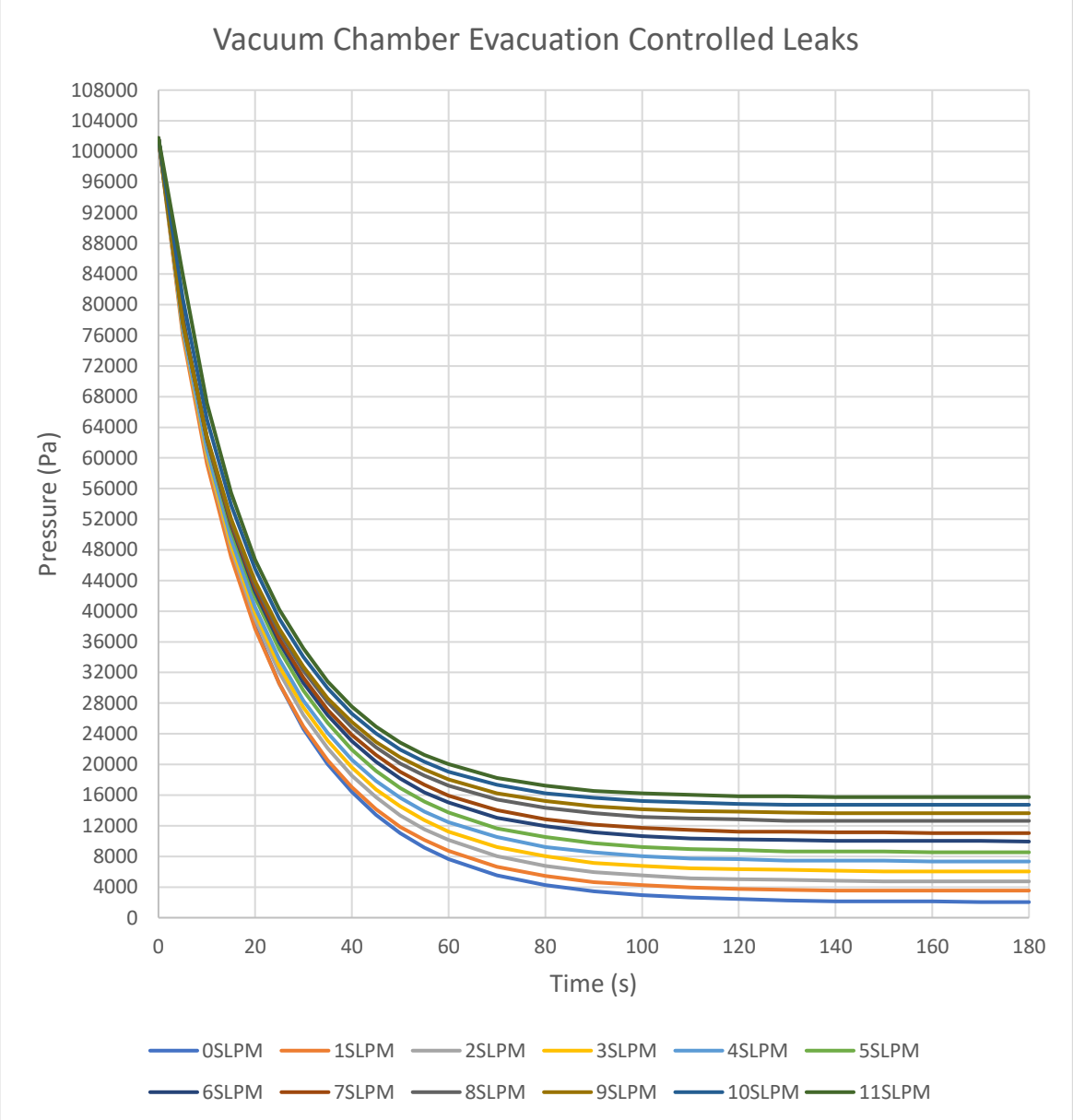

Figure 107: Vacuum chamber experiment – controlled leaks pressure results

The pressure and corresponding time readings from the video were input in excel and plotted for each leak shown in Figure 108. An obvious observation is that the larger the leak is in the chamber the higher the pressure is when fully pumped down. This is linked to the pump a more powerful pump might overcome these leaks and require a larger leak to impact the performance more. At the higher pressure the leak has less effect on the pressure and the curves are closer together. As the pressure decreases the deviation between the curves increases and the pressure differences are greater. This area has more significance as the vacuum coating pressure depends on the pressure in this region 120 seconds onwards where the achievable vacuum pressure stabilises.

9.2 Laboratory Chamber Results

The vacuum chamber experiment was conducted to obtain confidence in the pressure sensors. In addition to proving the pressure sensor readings can be trusted the results were deemed useful for predicting a pressure that can be achieved at a certain leak flow rate. It was decided to add a simulation of the process and compare results to see if an alternative method could be used to simulate the achievable pressure in a vacuum chamber with a known pumping capacity. As ANSYS had been used for the existing vacuum lock simulations, a simulation was performed in ANSYS Fluent. Slightly different boundary conditions were used as this time a leak rate into the inlet is used instead of a pressure inlet like before.

The initial operating pressure was set to atmospheric pressure as before the pump is switched on the air pressure is the same as the room. The other boundary flowed the set up in ANSYS for floating operating pressure as this is used when pumping gas into a closed system so was the closest model that could be found for pumping gas and a closed system. The other boundary conditions were ideal gas air density for a compressible flow, transient as it is a time dependent simulation and a mass flux outlet of 0.01 m^2 kg/m^2-s to match the performance of the Edwards rotary pump. Flow was considered laminar. The volume of gas in the chamber is 0.027 m^3 or 27 litres (internal dimensions 0.3m x 0.3m x 0.3m cube)

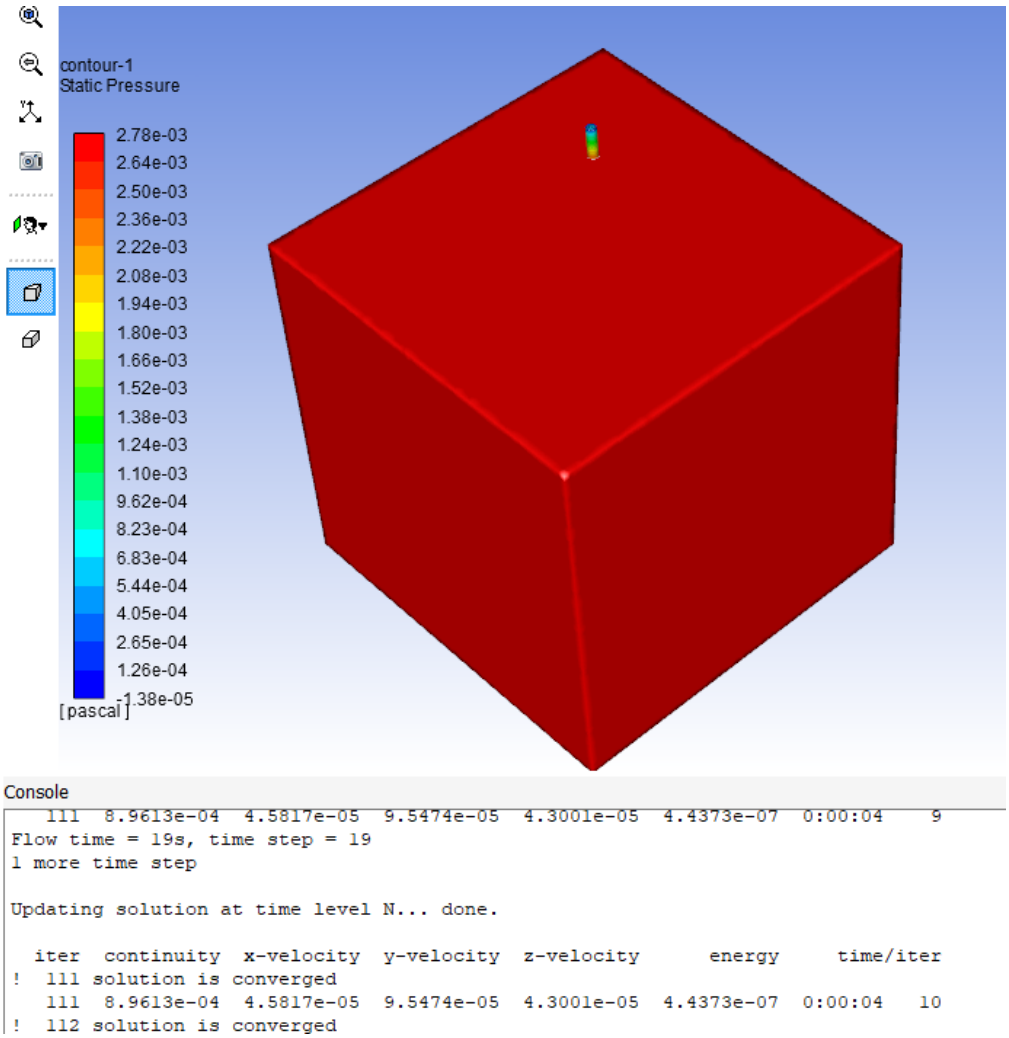

Figure 108: Vacuum chamber ANSYS simulation

Although the solution converged the pressures did not match the experiment and more computational investigation was required to gain a computational model that would match the experimental results. The author checked through the manuals of the engineering software and found that similar simulations to this had been performed in COMSOL. Access to the COMSOL software was not freely available for student or research purposes therefore a trial version of the commercial version was obtained to investigate whether the software could solve the problem.

Using a trial version of the engineering software COMSOL a solution was achieved that matched closely to the experimental results. The known values were the pressure

inside the vacuum chamber before air is evacuated is Atmospheric. The pumping speed of from the Edwards R5 vacuum pump is 5.1 m^3/hr and the leak rate from the drain valve is zero initially and then is increased by 1 litre/min up to 10 litres/min. A further reading of 11 litres/min was taken afterwards to see if the computational model could predict the next leak. To start with in COMSOL, a free molecular flow module was used, with an inlet set as a flow inlet having units of litre/min. The outlet was set as a vacuum pump boundary condition with a mass flow rate of the equivalent of 5.1 m^3/hr. Errors occurred and this condition did not solve, therefore COMSOL support was contacted for guidance to aid setting up the model with the boundary conditions with known values [116].

It was considered that the model would be simulating flow from atmospheric pressure to vacuum conditions, which could span over all four flow regimes (viscous, slip flow, transitional flow and molecular flow) and more than one model would be required to simulate the problem. However, after performing calculations in excel for the mean free path for the flow in the chamber at the experimental pressures recorded and corresponding Knudsen numbers, it was determined that the simulation only required the viscous flow regime as only a rough vacuum was achieved. With this information provided to COMSOL support suggested changing the model to a laminar flow interface with an ideal gas pressure dependency, however the models still did not match using the vacuum pump boundary condition, so this was changed to an outlet condition using a fully developed flow outlet type and a specified volumetric flow rate, instead of mass flow rate, which was used in ANSYS Fluent [116].

To match the time steps recorded in the experiment, a transient solution was used from the start. The step function in COMSOL starts at zero and runs a varied number of time steps, starting with fractions of the time step at the start of the simulation, this increased to the normal time step once the solution starts to compute [117]. COMSOL explains the reason for this is to avoid error occurring due to inconsistent boundary conditions, which is said to "occur most often when running transient fluid flow studies" [117]. This method is computationally expensive due to the very small time steps at the start of the simulation [117].

COMSOL uses a backward Euler method to take a small timestep that is a fraction of the initial timestep in order to attempt to resolve the inconsistent initial values [117]. “By default, the initial timestep is automatically determined based upon the total simulation timespan, but it is possible to manually set the initial timestep and also to change the fraction of that initial step used by the Backward Euler method for the consistent initialization” [117]. This final set up achieved similar results to the experimental results. However, the no leak resulted in negative pressures at 180 seconds, if the leak results were staggered by adding 3 litres per minute, then the values are very closely aligned. It is also a sensible to consider that there is outgassing and possibly some slight leak through the chamber lid into the system that would increase the overall leak into the chamber slightly and overpredicting the leak in the simulation is not unreasonable. The following figures show how well the COMSOL model matches the experimental results if 3 LPM is added to each COMSOL leak therefore the experimental matches up to COMSOL as follows.

Table 4: Leak Adjustment COMSOL and Experiment

Leak Experimental (SLPM)	Leak COMSOL (LPM)
0	3
1	4
2	5
3	6
4	7
5	8
6	9
7	10
8	11
9	12
10	13
11	14

The results from COMSOL showed a very similar profile to the experiemental results achieved shown in figure 109.

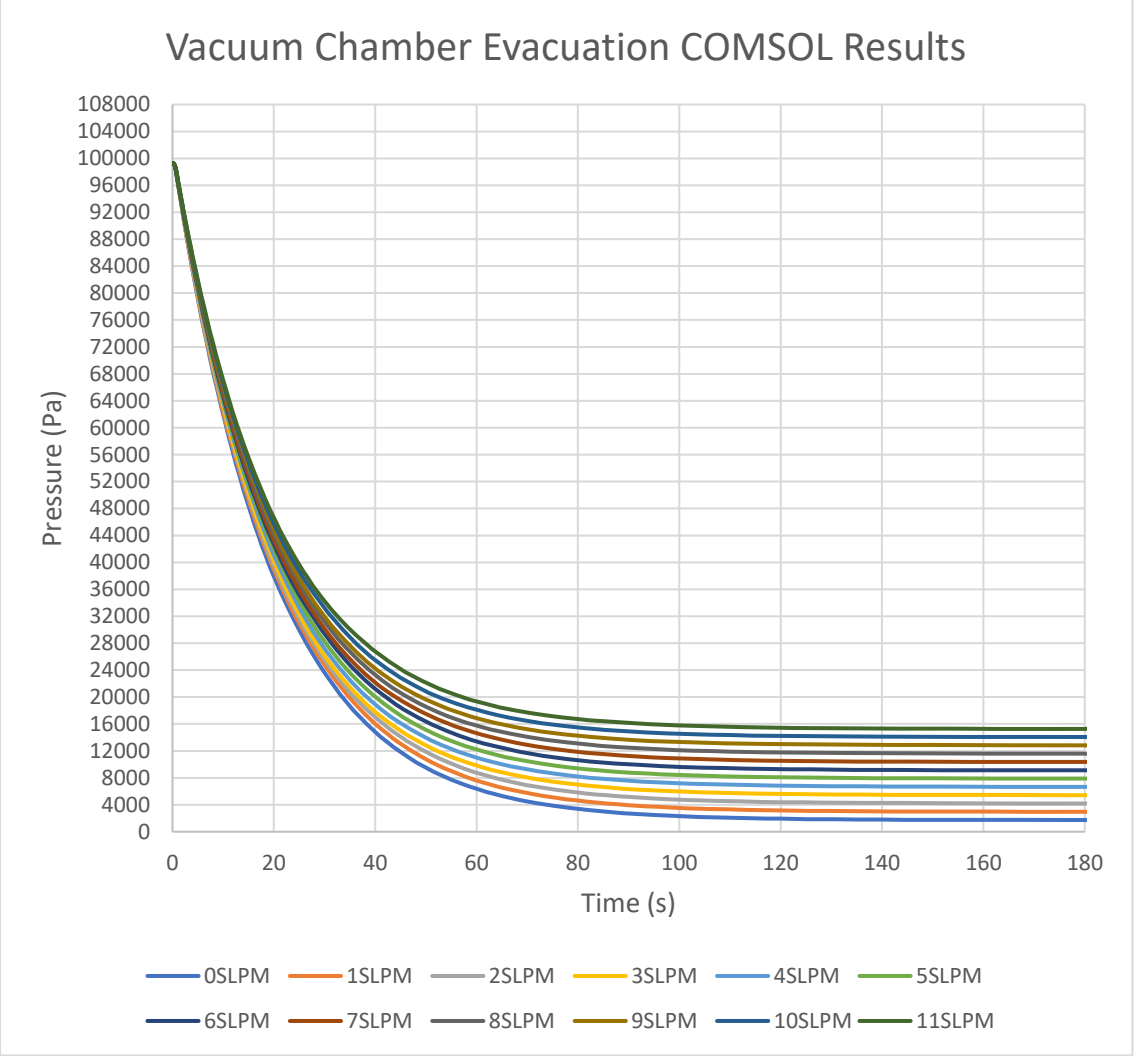

Figure 109: Vacuum chamber COMSOL – controlled leaks pressure results

It would be beneficial to run COMSOL for more leaks with 3 added so 15 to 23 LPM and then compare with experimental results 12 to 20 SLPM and see if the results continue to match. A new mass flow meter would be required, and results tested against existing readings to ensure accuracy. The important range of interest in the results is when the flow tends towards a steady state approximately around 120 seconds to 180 seconds depending on the leak. Figures 110 to 121 show the focused region with error bars added for the 2 percent accuracy the Keyence sensor reads to.

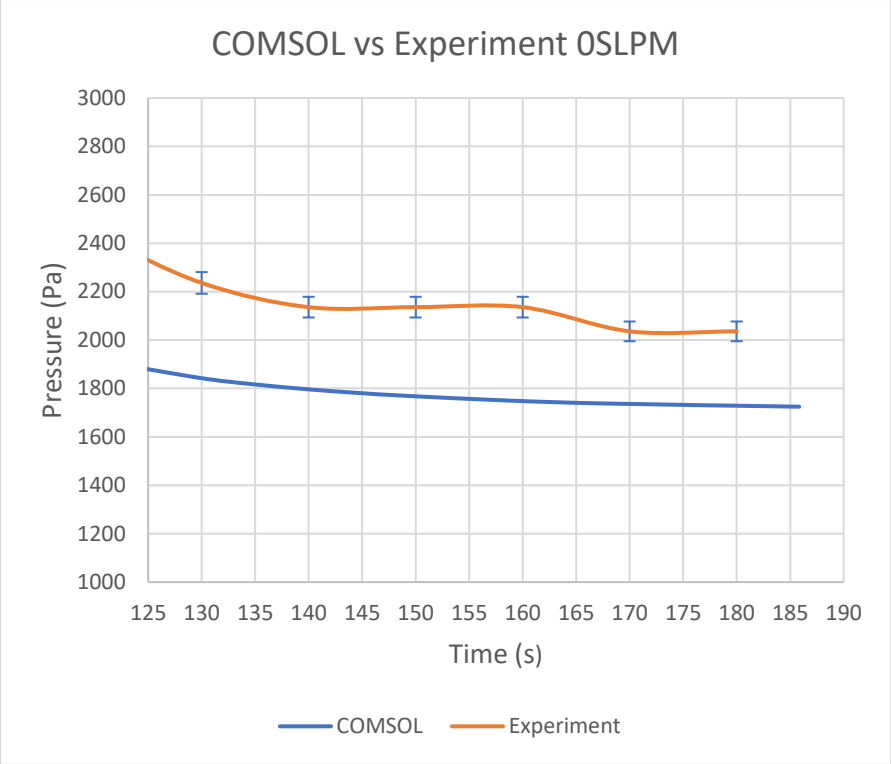

Figure 110: Controlled leak experiment result comparison 0 SLPM

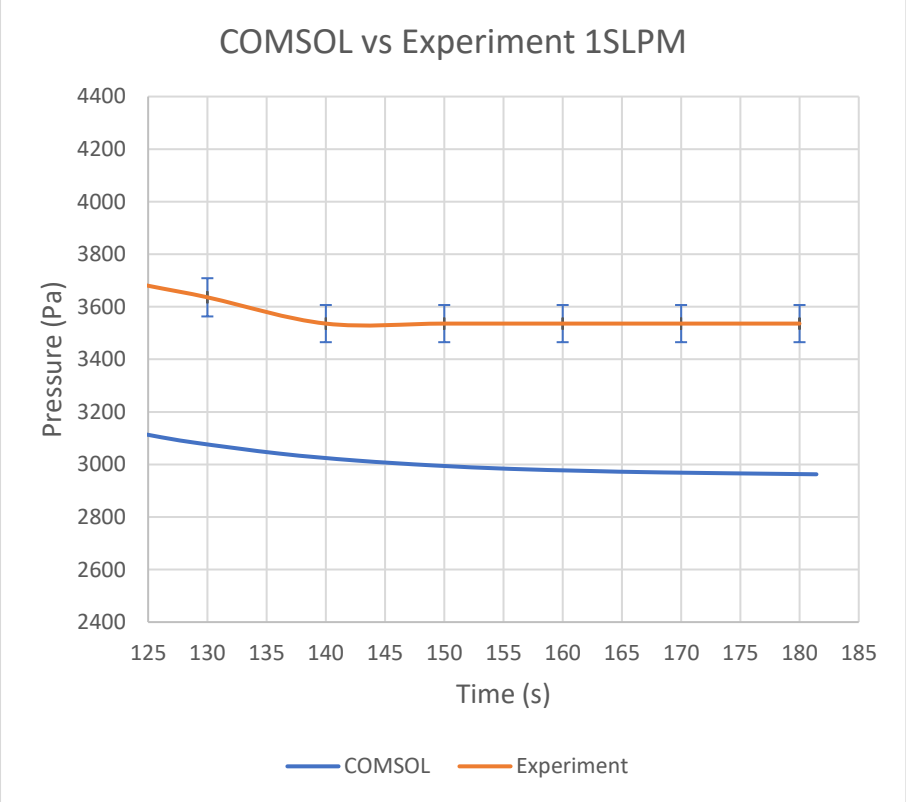

Figure 111: Controlled leak experiment result comparison 1 SLPM

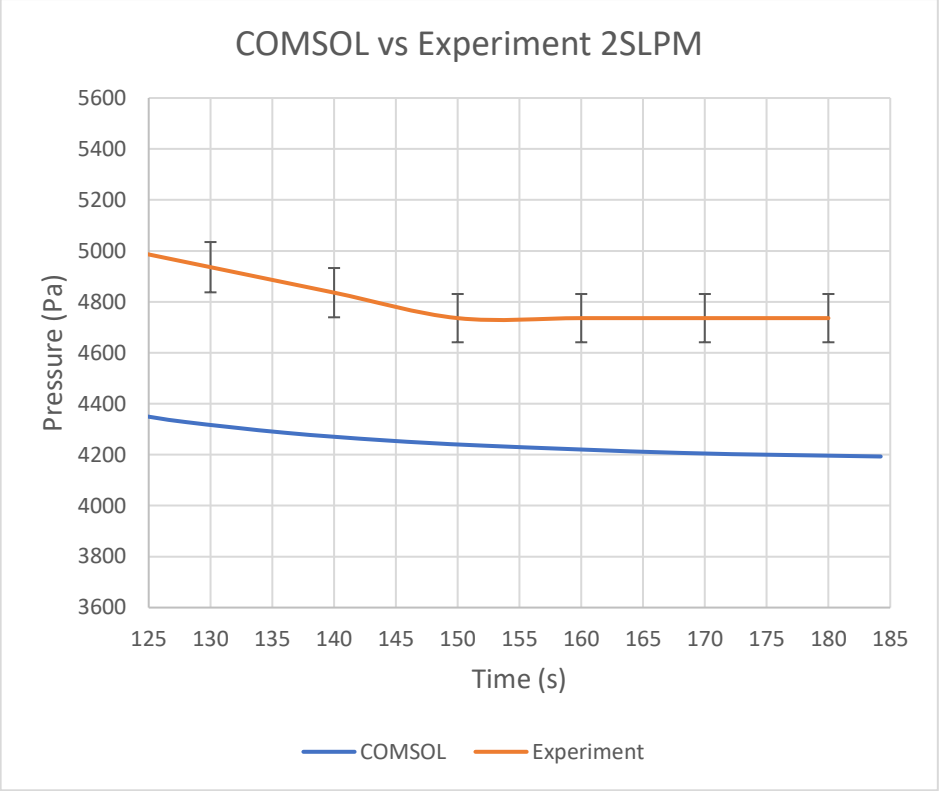

Figure 112: Controlled leak experiment result comparison 2 SLPM

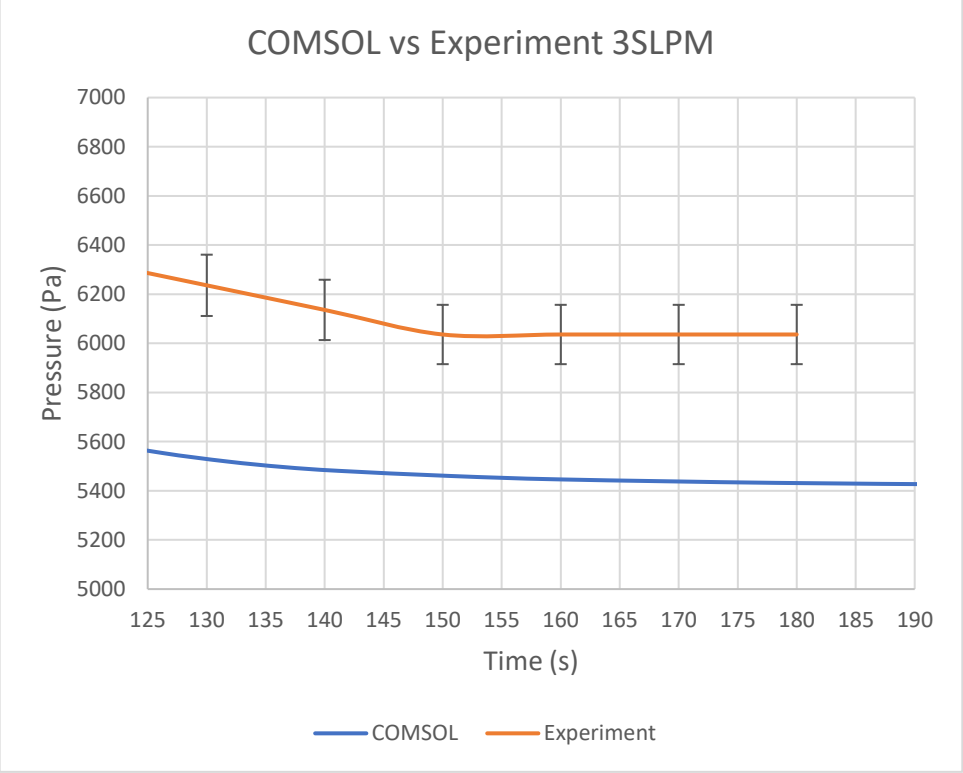

Figure 113: Controlled leak experiment result comparison 3 SLPM

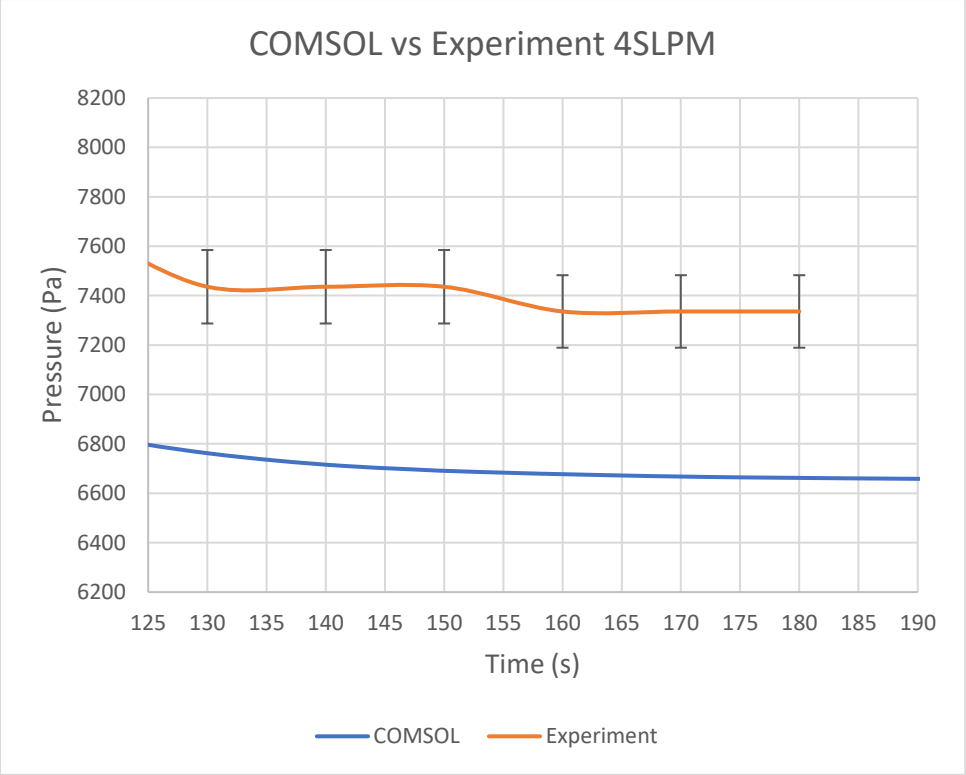

Figure 114: Controlled leak experiment result comparison 4 SLPM

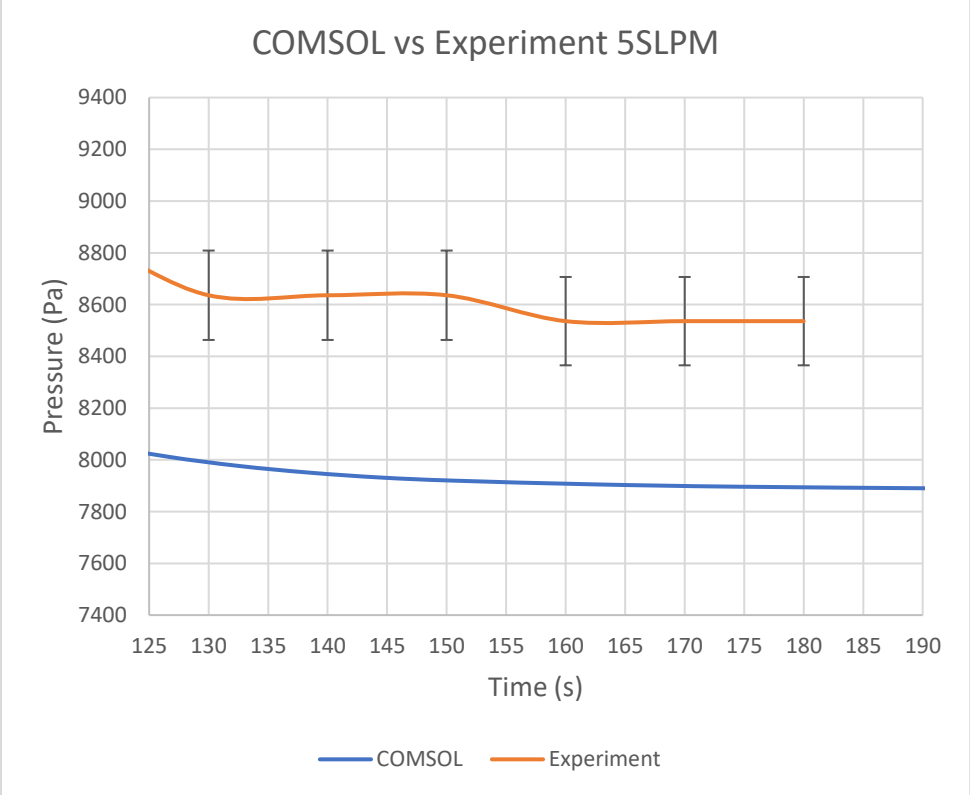

Figure 115: Controlled leak experiment result comparison 5 SLPM

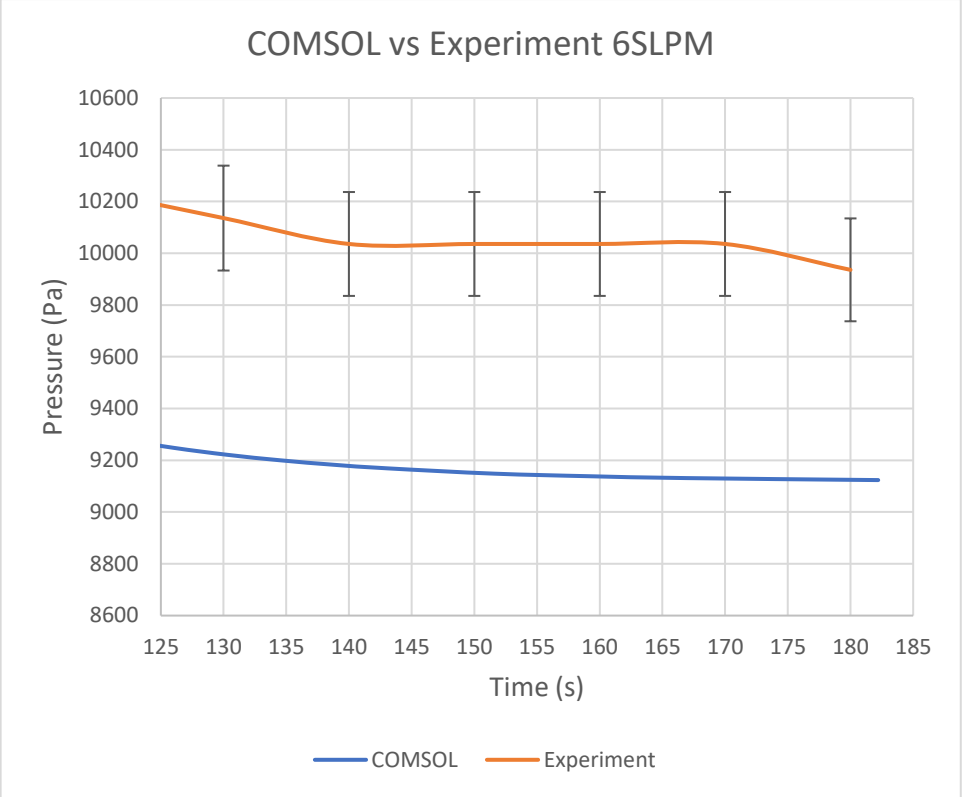

Figure 116: Controlled leak experiment result comparison 6 SLPM

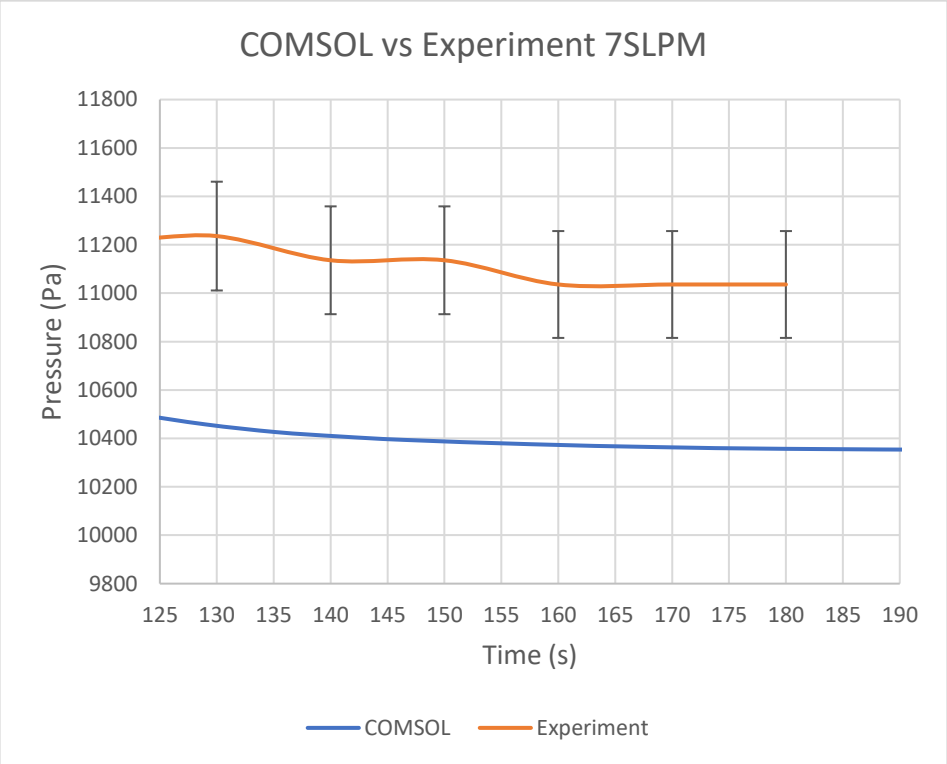

Figure 117: Controlled leak experiment result comparison 7 SLPM

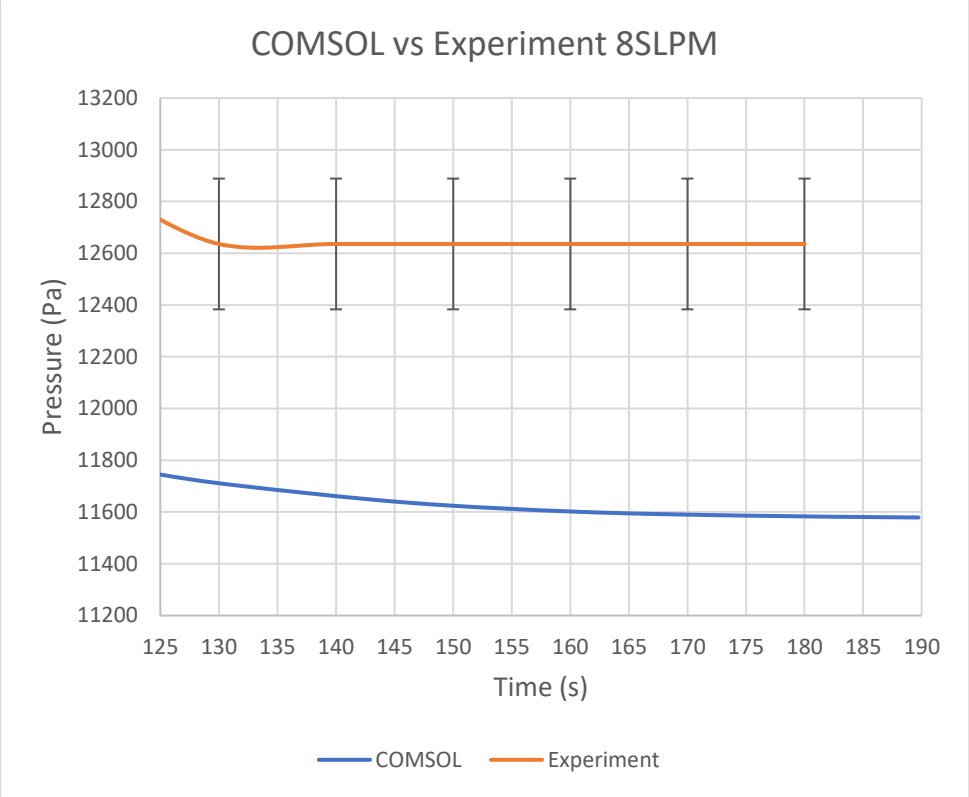

Figure 118: Controlled leak experiment result comparison 8 SLPM

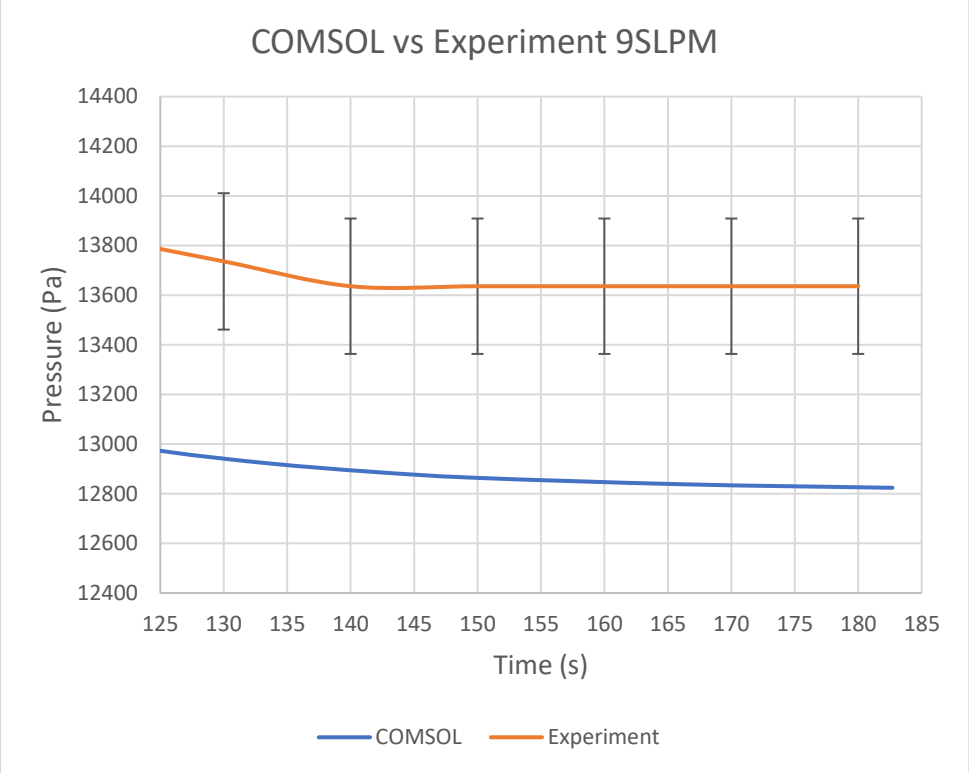

Figure 119: Controlled leak experiment result comparison 9 SLPM

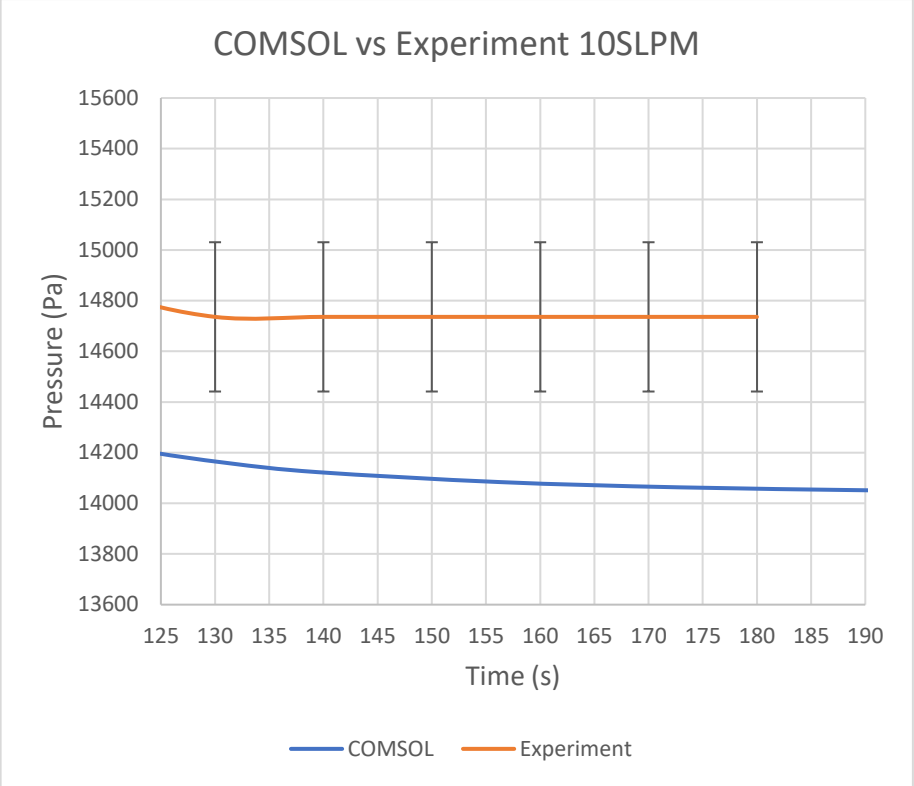

Figure 120: Controlled leak experiment result comparison 10 SLPM

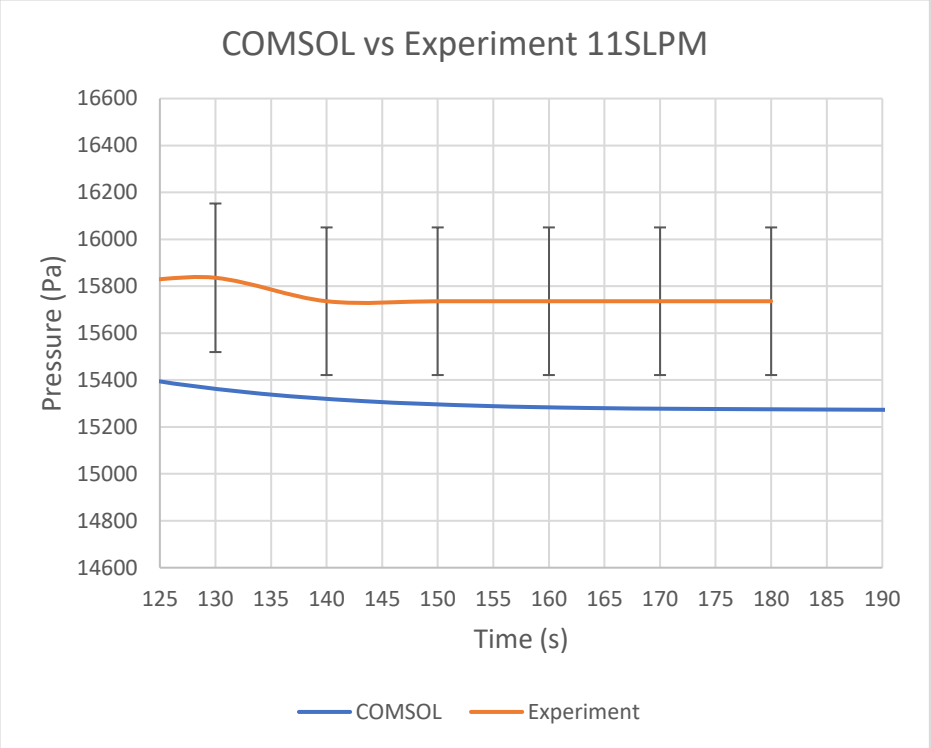

Figure 121: Controlled leak experiment result comparison 11 SLPM

Figures 110 to 121 show that the results are not as close together as they visually look in figure 107 and 109. This is because the scale is reduced from 100,000 Pa down to a focussed range of a few thousand pascals in the operating range. It is the pressure in the steady range that the vacuum lock will be operating at so these values are of more interest. There pressure sensor reads to an accuracy of plus or minus 2 percent. The error bars increase at the higher pressure this indicates the data varies more and there is higher precision at lower pressures. The differences between the simulation results and experimental results are not uniform they vary from a few hundred pascals in figure 110 and approximately a thousand pascals in figure 118. If the simulation and experiment final pump down pressure is taken from the largest variation out of the results which is figure 118. Then changed to a percentage of reduction from the original atmospheric pressure, the difference between the results is around one percent shown in equation 9.1 and 9.2. This gives more context to the results.

$$Figure\ 118\ Experiment\ \frac{101325\ Pa - 12636\ Pa}{101325\ Pa} \times 100\ = 87.5\% \qquad (9.1)$$

$$Figure\ 118\ COMSOL\ \frac{101325\ Pa - 11579\ Pa}{101325\ Pa} \times 100\ = 88.6\% \qquad (9.2)$$

9.3 FEA of Prototype Chamber

The vacuum lock chamber that is used in the experiment needs to be rigid enough to withstand the imploding force caused by pressure being lower inside the chamber than the atmospheric pressure on the outside of the chamber. A structural analysis was performed using the pressure difference of absolute vacuum from atmospheric pressure gives a uniform force of 101,325 Pa acting on the inner surfaces pulling the chamber walls inwards. The chosen thickness was 25mm as this is unlikely to deform or break under the low-pressure conditions. It is also a thickness used by manufacturers of acrylic vacuum chambers. For ease of construction and to use a transparent material for experimental observation Acrylic was used for the construction of the vacuum lock. A pressure test was performed in ANSYS Mechanical APDL to ensure the chamber walls were thick enough to withstand the

low pressure created within the chamber. The geometry is simplified from the revision 7 vacuum lock prototype design shown in figure 122.

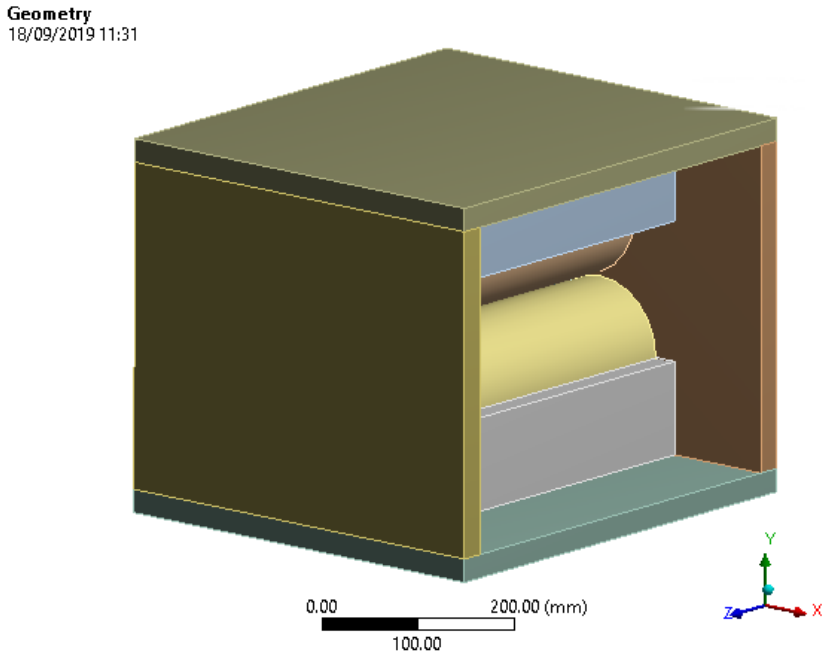

Figure 122: Internal view of vacuum lock chamber revision 7

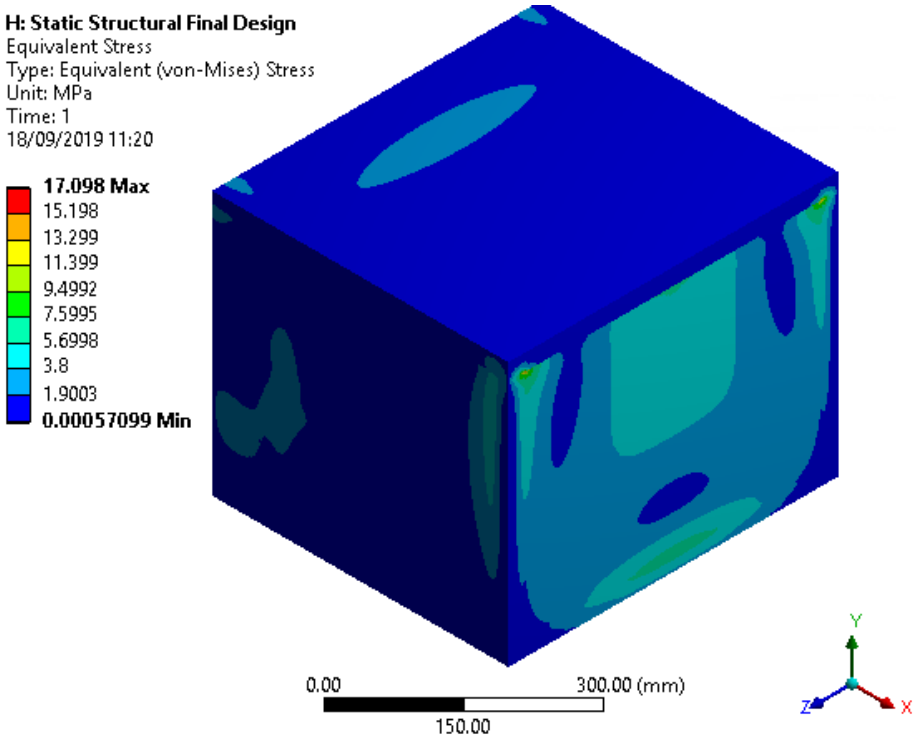

Figure 123: Revision 7 pressure vessel analysis – Equivalent (von-mises) Stress

A bonded type boundary condition was used for contacts that are bonded with Tensol 70, this is the default option and treats the surfaces as though they are glued together meaning there is no sliding or separation that can occur [118]. The bonded contact option was fine for the parts of the lock that are sealed together however the lid condition where it is not clamped against the right wall was less obvious and was considered as able to open and could potentially slide very slightly. The frictional boundary condition was used as the contact between the end panel on the right side, which shows the contours and the highest deflection at the top, as the lid is clamped on top, there is no structural support in this contact, and it is a weak area of the air lock. The frictional contact used the friction coefficient (Mu) value of 0.63 which is greasy rubber and Acrylic found in a material contact properties table from Slovak University [119]. This was to represent the friction between the Acrylic with Neoprene gasket and vacuum grease contact.

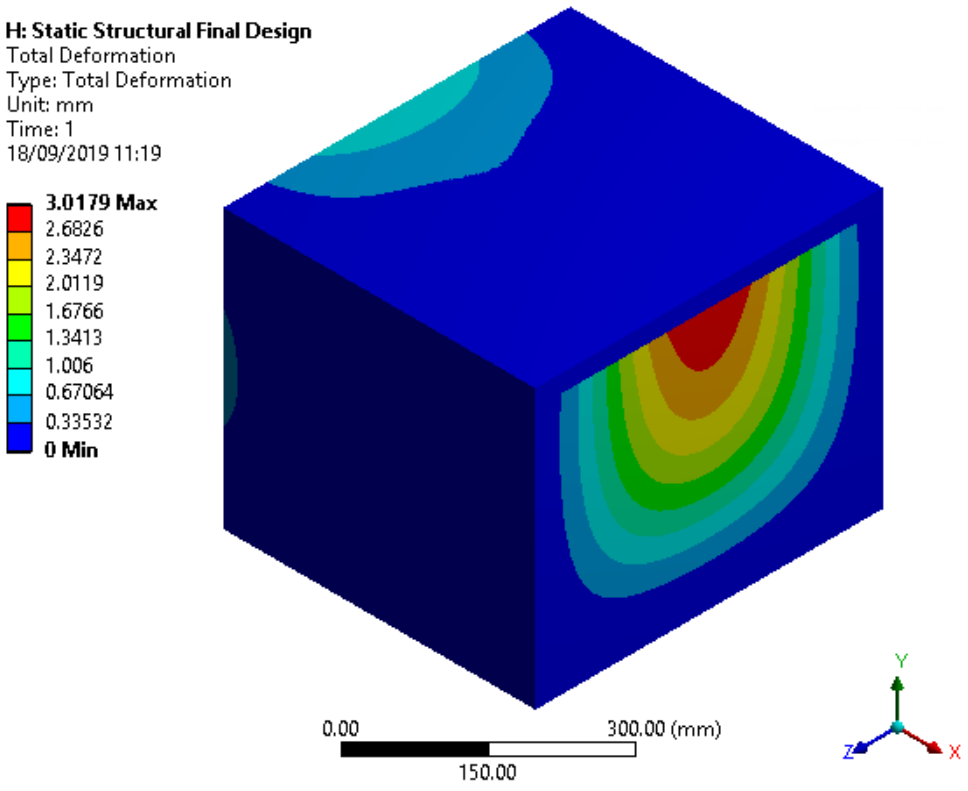

Figure 124: Revision 7 pressure vessel analysis – Total deformation

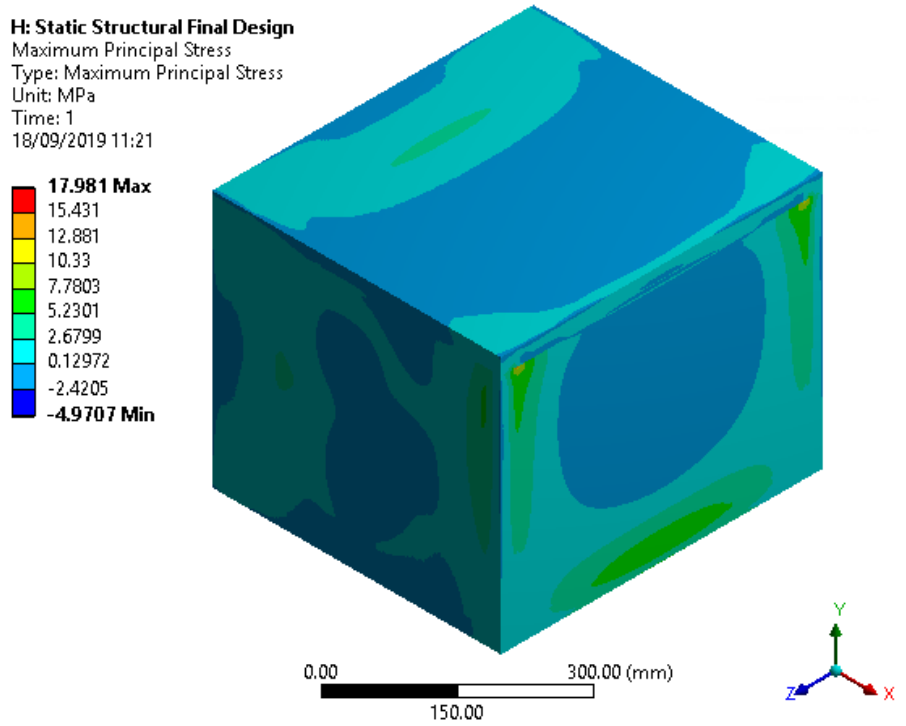

Figure 125: Revision 7 pressure vessel analysis – Maximum principal Stress

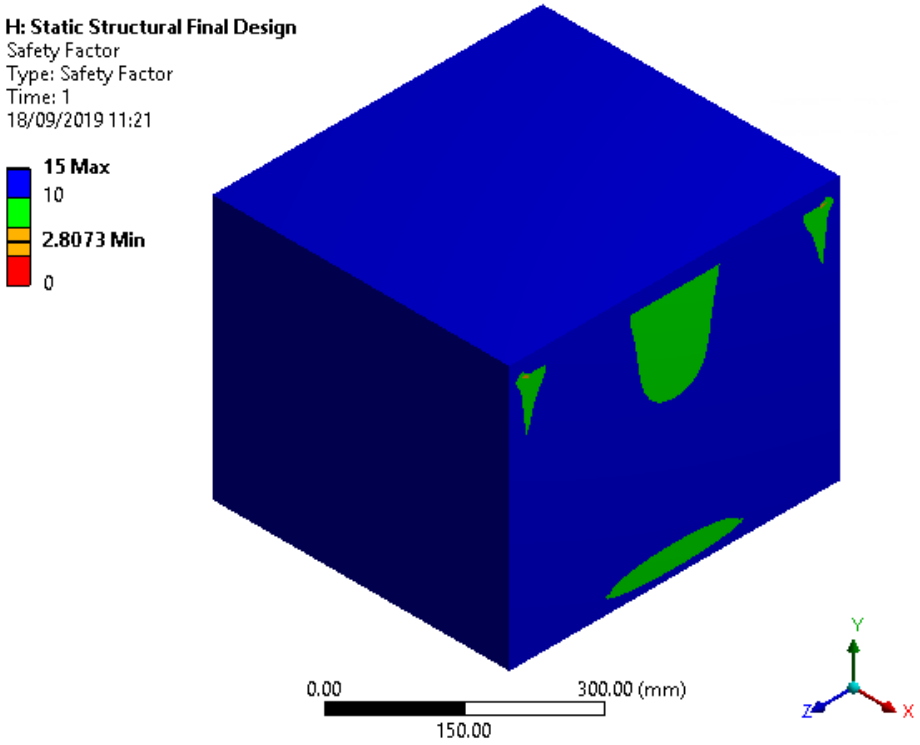

Figure 126: Revision 7 pressure vessel analysis – Safety factor

Figures 124,125 and 126 are the pressure test results from ANSYS mechanical APDL. The minimum factor of safety is 2.8 times the equivalent stress this is in the area that the lid sits on top without any bonding, furthest away from support of internal components and in the closed section behind the rollers and air bars where the vacuum pump is connected. The left of figure 127 shows this area location. The maximum deflection is 3mm but considering it is a thick brittle hard material to much deflection with cause the acrylic to shatter.

9.4 Vacuum Lock Prototype Experiment

Everything is now brought together to produce a prototype of the entry vacuum lock. To ensure meaningful and accurate results are obtained from the simulation work, an experimental apparatus was produced for validation. For validation of the vacuum lock design verification of the modelling work is required, this would be extremely difficult to do numerically due to the geometry and uncertain boundary conditions, therefore an experimental rig was deemed to be the most suitable method. Figure 127 is a CAD assembly of the prototype vacuum lock. The handles and the toggle clamps were off the shelf components and the steel strip was supplied by Tata. The CAD models for the screws, toggle clamps and handles were open source models found online from GrabCAD and or from the manufacturers of the parts.

Drawings from the CAD model were produced to manufacture the parts for the vacuum lock. The upper and lower air restriction mount were 3D printed on an Objet 1000 3D printer out of Vero White resin. The walls of the chamber are 25mm thick acrylic sheet, the rollers are acrylic tubes with discs bonded at each end and the sealing blocks were cast and machined by Northern Cast Acrylics. Once the final design drawings were complete and parts constructed. The vacuum lock was constructed by Swansea University workshop using the design parts and off the shelf components. The final construction is shown in Figure 128.

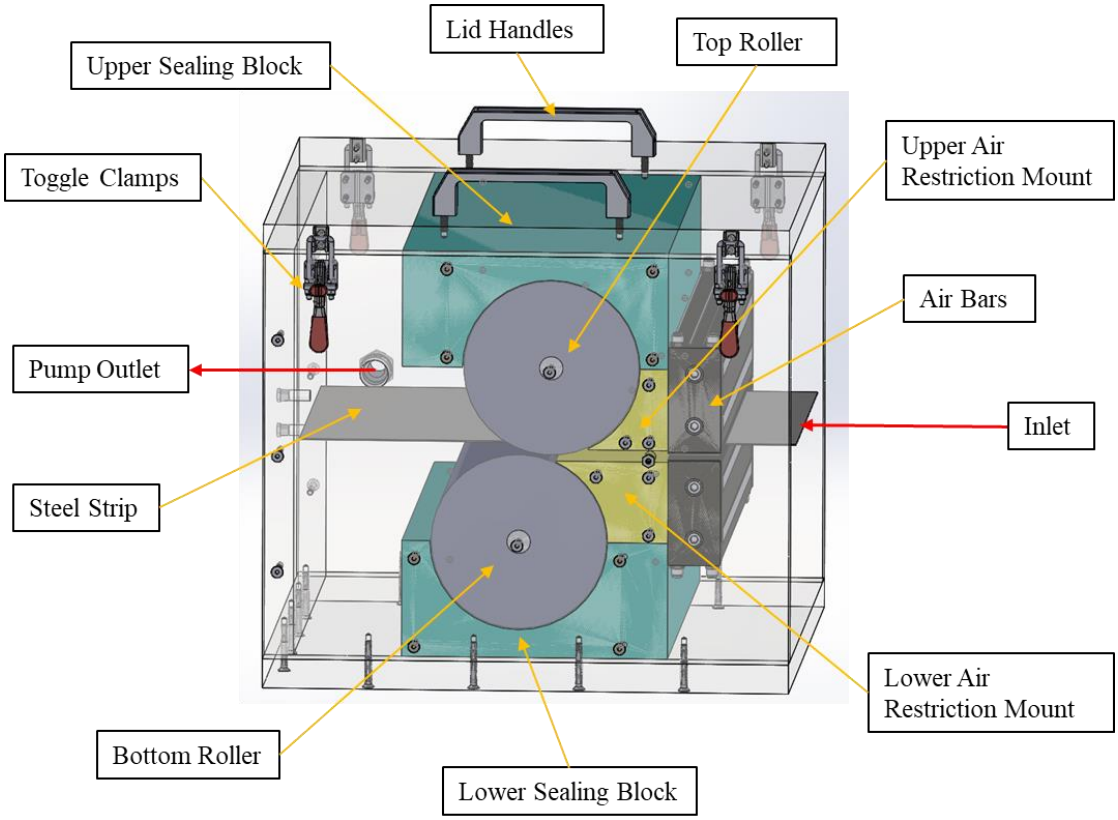

Figure 127: CAD image of vacuum lock experiment prototype

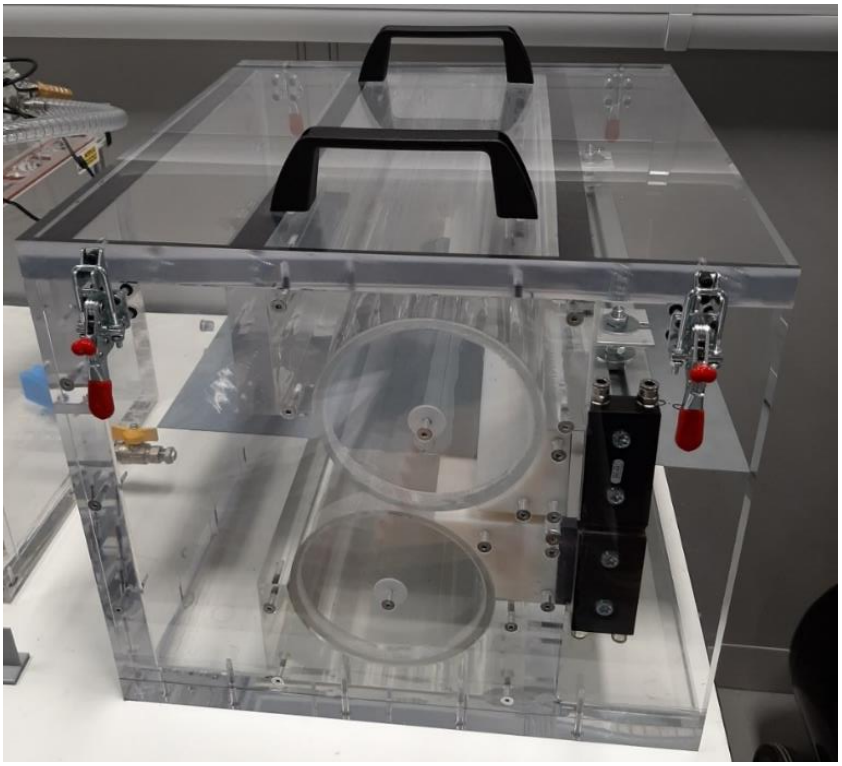

Figure 128: Vacuum lock experiment prototype

9.5 Experimental Procedure

The vacuum air lock was connected to an air compressor attached to the air bars by compressor hose, two Keyence pressure sensors and a rotary vacuum pump shown in the diagram in figure 129. Figure 130 and 131, show the placement of pneumatic straight threaded adapters that the Keyence gauges screwed into. The positions were chosen to measure the pressure near the air bars at the inlet and the pressure on the far wall as this will be the inlet pressure to the next lock.

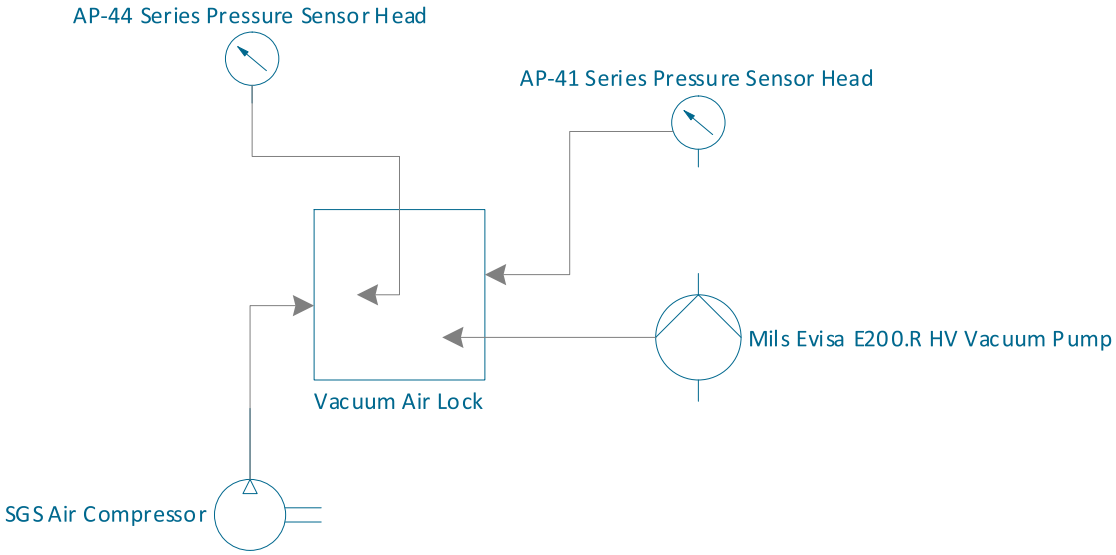

Figure 129: Diagram of vacuum air lock equipment set up

The experiment procedure was conducted as follows:

- Connect vacuum pump to barb connector with reinforced vacuum hose
- Connect Keyence pressure gauges AP-41 and AP-44 to the vacuum lock
- Connect air compressor to air bars using air hose and pneumatic push adapters
- Check for any cracks or damages of the lock
- Turn on vacuum pump
- Record pressure from pressure gauges
- Turn air bars on record new pressure readings

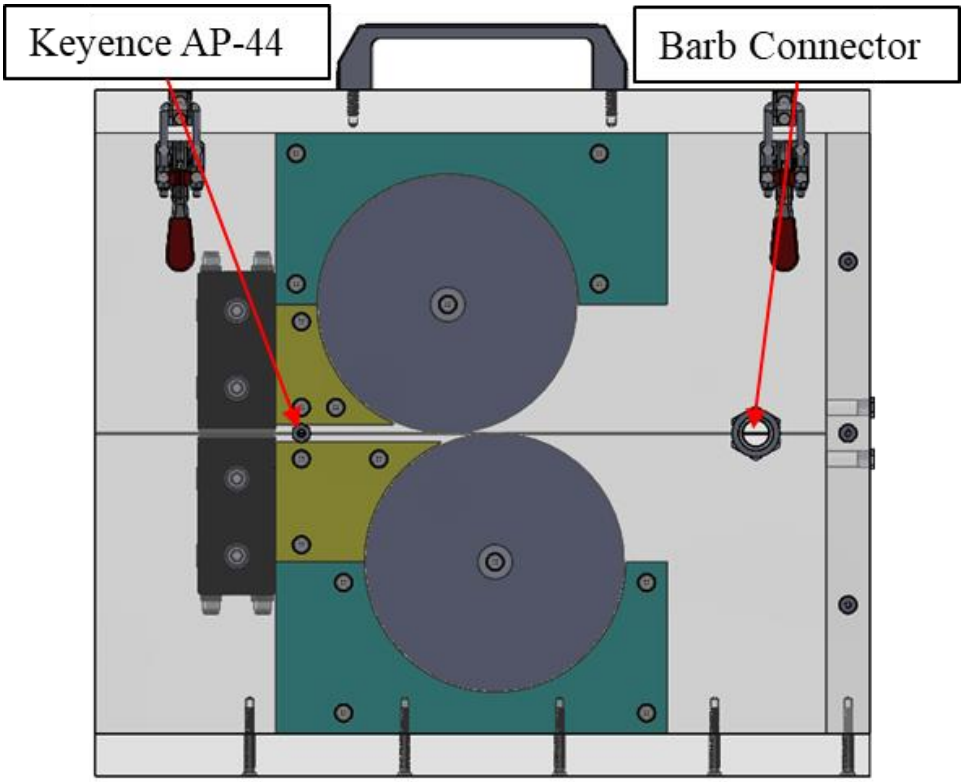

Figure 130: Keyence AP-44 pressure gauge location

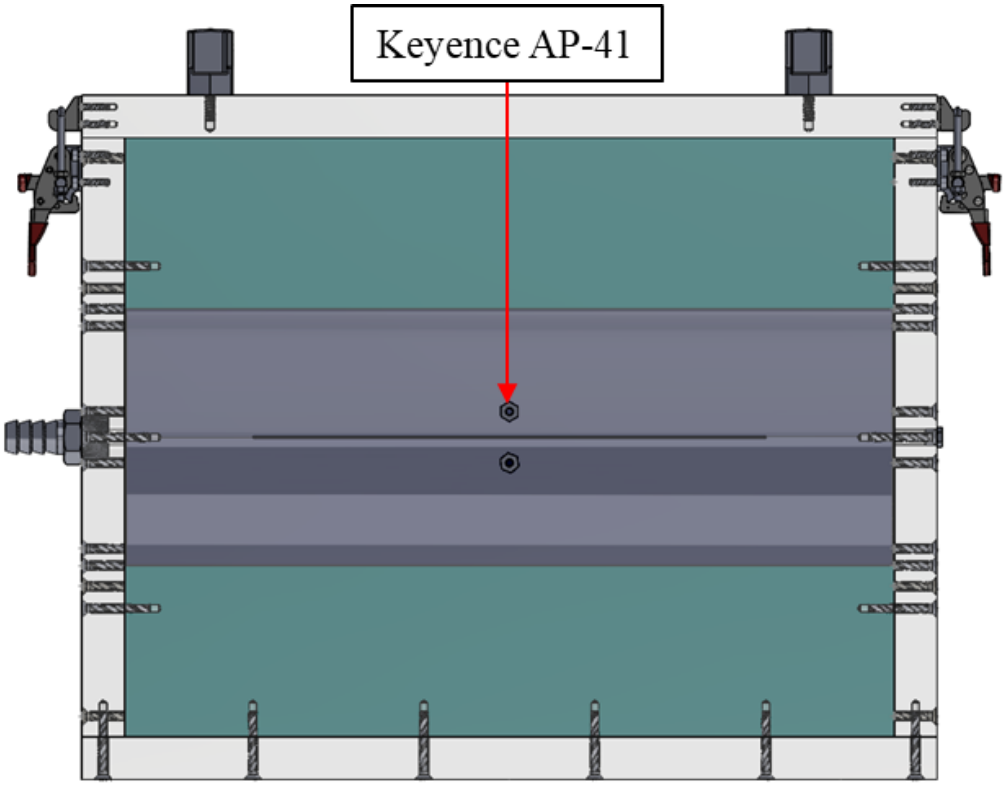

Figure 131: Keyence AP-41 pressure gauge location

Figure 132: Vacuum lock experiment with vacuum pump and compressor

The simple design did not include a hinge or section to connect the air bars to the block that is airtight, this is possible but for the purpose of the experiment the air bars were sealed using silicon sealant to only allow air to pass between the air bars and the strip and at the sides of the strip where the sliders fill the gap as the design intended. To start with there was a leak behind the bottom air bar and the lock only pumped down a few kPa due to the air getting in behind the air bar. Without the air bars the inlet size is 10mm by 450mm with a 300mm by 1mm steel strip running through. The Mil's Evisa E200.R HV rotary vacuum pumps pumping speed is 198 m^3/h or $67.37 \times 10^{-3} kg/s$ and the expected pressure without the air bars is approximately this can be found as 98453.45 Pa found from the using the 67.37×10^{-3} kg/s as the x value and using the equation of the trendline from the graph in figure 101. This is 2871.55 Pa less than atmospheric and the reading in figure 133 is -3.1 kPa with the leak around the air bars, so the values are similar.

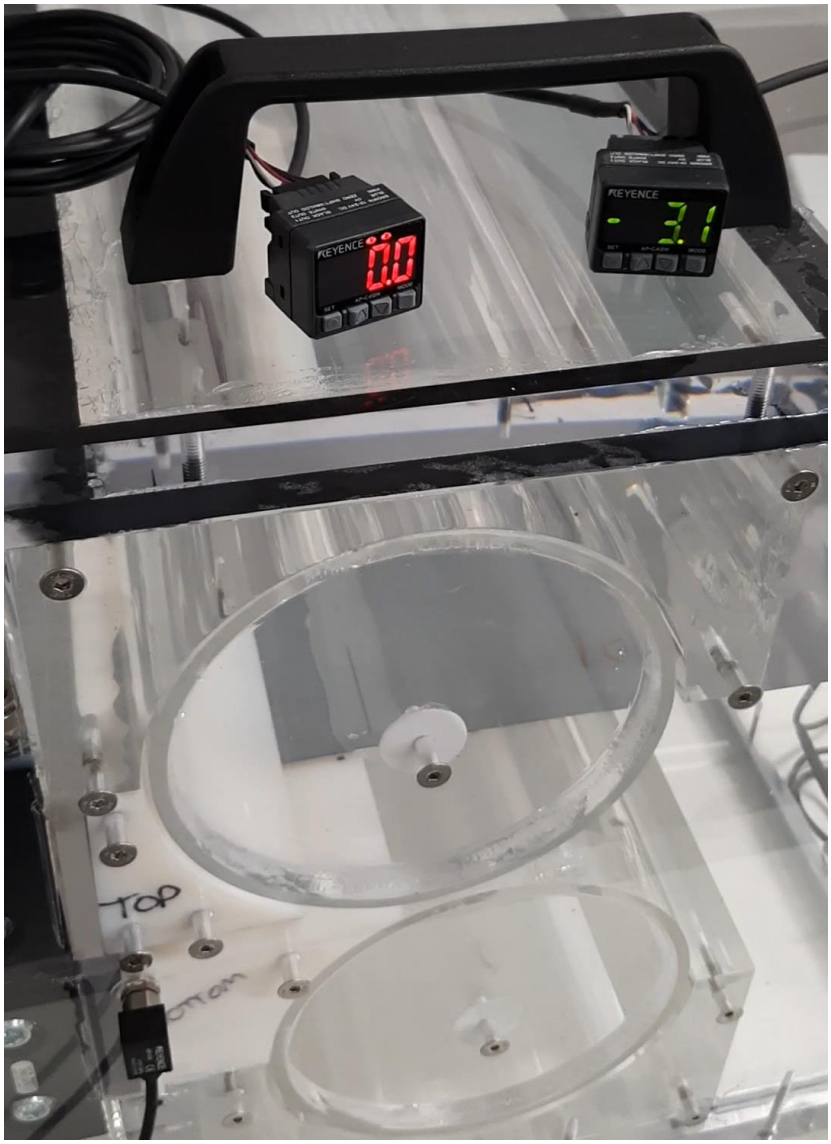

Figure 133: Vacuum lock pressure with leak behind the lower air bar, air bars switched off

Figure 133 shows the readings on the Keyence pressure gauges. The AP-44 is a compound pressure gauge shown on the left of figure 133 can measure plus or minus 101,325 Pa, therefore that gauge was placed near to the air bar where the pressure is expected to increase above atmospheric pressure due to the compressed air flowing out of the micro porous carbon block of the air bar. The Keyence pressure gauge AP-41 on the right of Figure 133, only measures negative pressure, this gauge is on the right chamber wall, the exit lock wall, Figure 130 shows the position. When compressor is turned on the pressure reduces both in the gauge near the air bar and the gauge on the exit wall, shown in Figure 134.

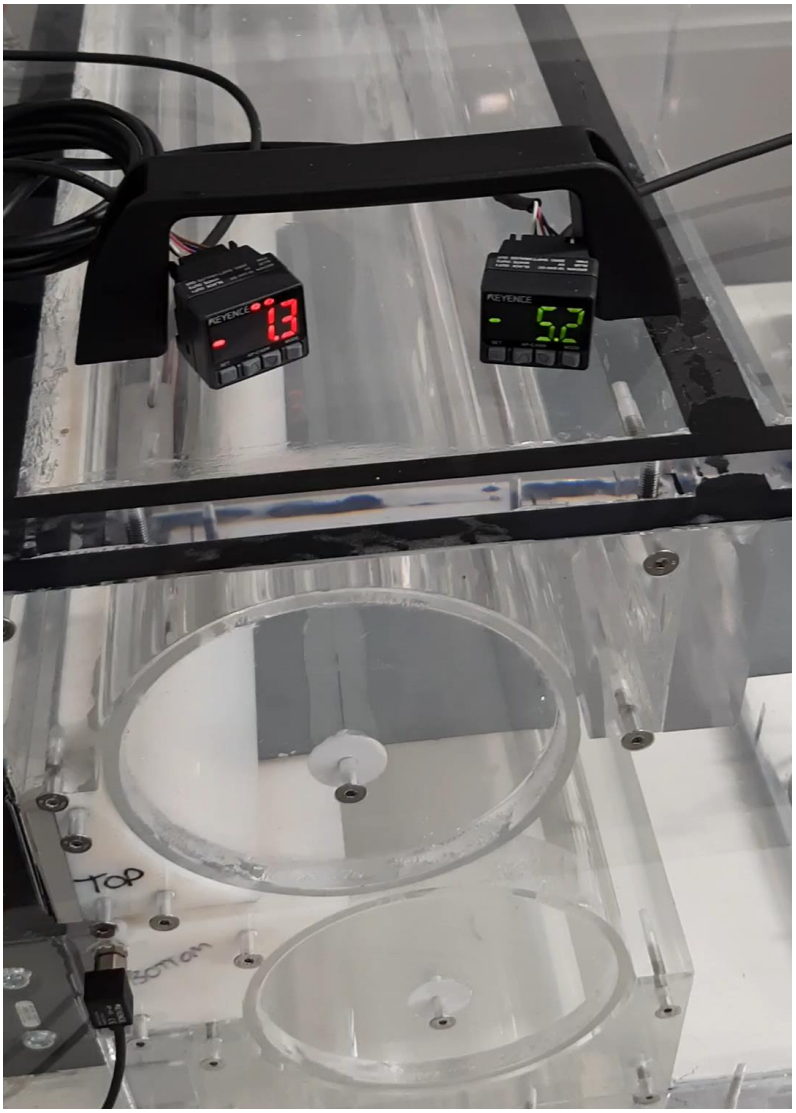

Figure 134: Vacuum lock pressure with leak behind the lower air bar, air bars switched on

9.6 Structural Failure of Prototype Vacuum Lock

The leak was stopped with more silicon sealant and the Vacuum Lock was sealed. The next time the experiment was conducted the lock performance so vastly improved that the pressure gauges showed rapid evacuation and lower pressures. The pressure in the lock was reduced to negative 51.3 kPa reading from the pressure sensor near the air bars and negative 79.3kPa at the exit wall therefore the lowest pressure in the lock was 22,025 Pa. The lock was holding at this pressure, however just before a photograph could be taken and the experiment re set for video, a structural failure occurred, and the exit wall imploded.

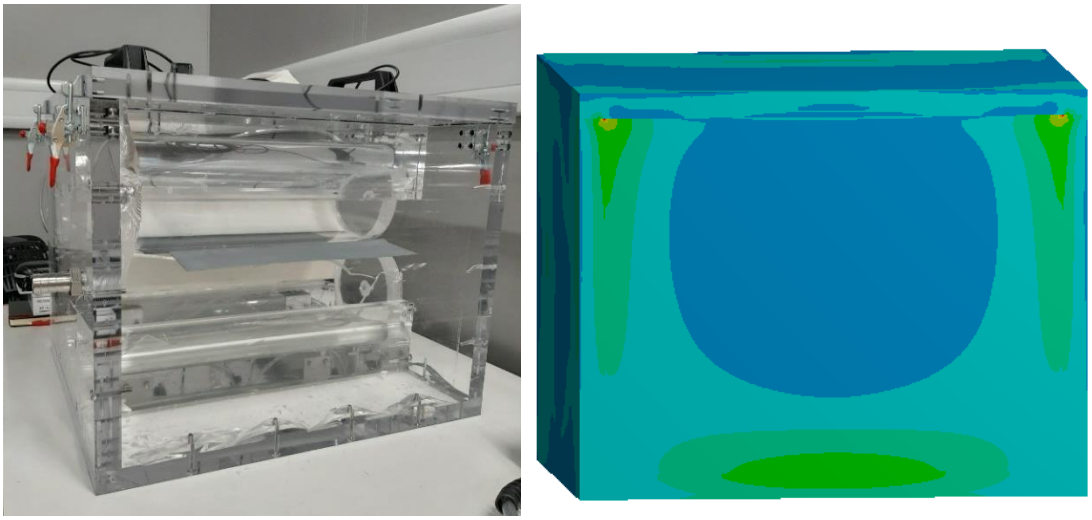

Figure 135: Structural failure of the experiment prototype and simulation of maximum principal stress

It can be seen in figure 135 that the lock failed in the areas of high stress indicated by the FEA analysis. The experiment should not have failed however the FEA analysis was performed for bonded surfaces, the vacuum lock was supposed to be bonded with Tensol 70 acrylic weld, however due to the fine adjustments required to be made for tight tolerances the workshop requested it to be screwed. The joints should have still been welded but the local stresses cause by the screws would still cause weak areas and cracking. The structural failures due to local stresses can be clearly seen in around the screws in figure 136.

Although the prototype failed to sustain the low pressure created within the lock, the end goal is to produce a significant pressure reduction for the vacuum coating chamber. The lock proved that a pressure reduction could be achieved and outperformed the prediction from the simulation. A pressure of 22,025 Pa was achieved which out performs the 26,700 Pa produced by the entry lock for the Nisshin Mitsubishi line [31] and the U.S. Patent 6334751 B1 with a pressure change of 50,000 Pa [40].

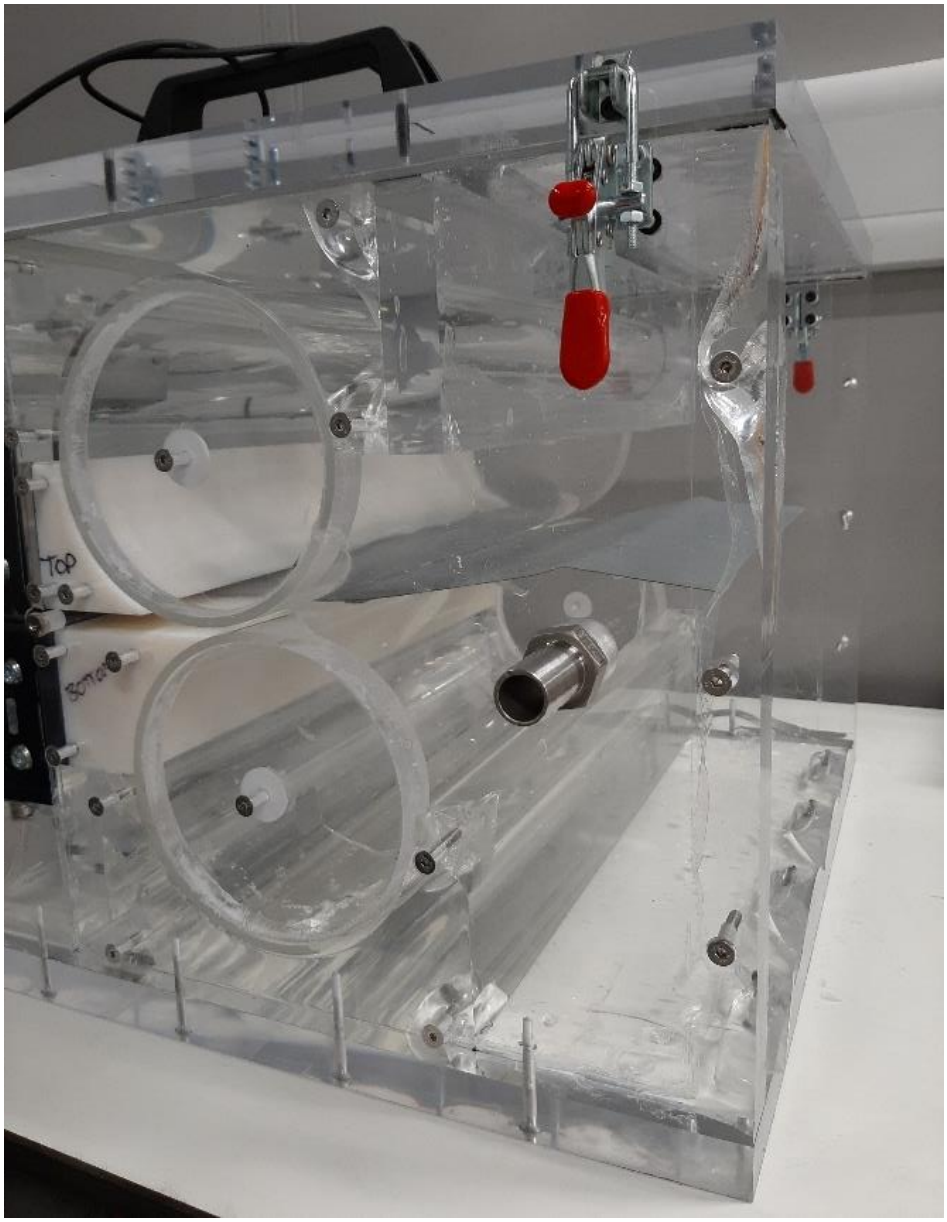

Figure 136: Vacuum lock structural failures

If the lock had not failed, then more experiments could have been conducted varying the pumping speed of the vacuum pump and recorded the pressures that could be achieved at the varied pumping capacity. This could be achieved by rebuilding the lock without the screws or by changing the material to a stronger material such as steel which would be the material the industrial line locks will be built of. Further development is required to add consecutive locks and complete the lock system in order to achieve the pressure required for the coating chamber.

10. Discussion

The research conducted in this thesis was to work towards producing a state of the art vacuum lock for a novel PVD galvanising process. The novel EML-PVD coating process developed by Tata Steel requires a system of vacuum locks that provide an overall pressure drop down to 0.01 Pa. The objectives were to produce a vacuum lock for continuous strip transport of varying widths and thicknesses into and out of a coating chamber whilst maintaining a steady vacuum. Vacuum locks are a niche technology and therefore it was difficult to obtain information. A review of patented vacuum lock inventions was completed to evaluate what already existed in the field and an iterative design process was conducted leading to a prototype. Computational modelling was performed as a part of the vacuum lock prototype design and an experimental rig was produced to verify simulation results. The prototype developed was the initial or entry vacuum lock and lowered the pressure down to 22,025 Pa before a structural failure occurred stopping the experiment. The pressure drop indicated that a rough/low vacuum had been achieved.

The pressure of 22,025 Pa measured in the prototype is lower than what was currently found in the literature. Figure 9 reveals a pressure of 26,700 Pa for the first lock from Maeda et al (1985) [30], which is 5675 Pa higher than the pressure obtained by the prototype produced in this thesis. Achieving a lower pressure than a batch system which closes the lock is an advancement as the prototype lock entry remains open. The limitation of the experimental rig is that there is no opening to the next vacuum lock in the system. The right side of the lock is closed which stops it being a fully open lock as it is only open at the entry side. This was done because the further locks would normally be attached to provide a restricted air path and as a consecutive lock was not connected this was the only practical option.

The Maeda et al (1985) lock system produced a coating chamber pressure of 1.33 × 10-3 Pa which is lower than the requirement for the EML-PVD process, but it is a batch process and not a continuous open system. Pressures lower than 5 × 10-3 Pa was also achieved by the continuous coating line in Kim et al (2013) [2]. There was no mention of the individual lock pressure stages therefore no comparison can be made

as to how well the prototype lock performs in comparison to this air to air PVD line. The literature search on the existing patented technologies returned little information on achievable pressures. None of the patents claimed to achieve pressures of 0.01 Pa or lower in the coating chamber therefore they could be deemed unsuitable for the EML-PVD process. The closest suitable pressure stated was 5 Pa in the lock that precedes the vacuum chamber in Erbkamm et al (1994) [38]. The existing vacuum locks found in literature have multiple locks to produce the step down in pressure required for the coating chamber. Only one lock was produced for the prototype therefore to compare directly to the multiple lock systems is not conclusive.

A deliverable was to make a comparison of the existing conventional vacuum lock technology and new air bearing technology. Very little information on air bearing lock technology was found and the information that was found contained New Way® air bearings. The air bearing lock by Devitt (2007) [42] achieved 530 Pa which is not low enough for the EML-PVD process. Limited comparisons were made between the two technologies due to the lack of dimensions, poor quality images, missing elements to the explanation of the inventions and missing values for pressures. This is typical as patent information is purposely vague to avoid revealing in depth information about the product but providing enough to cover intellectual property. The comparison found that air bearings can achieve very tight clearances reducing leakage into the vacuum lock, but additional compressed air is a consequence and they are generally used for more delicate substrates.

Another deliverable of the research was to identify how the air bearing technology can be applied in a steel line configuration with varying steel strip width and gauges. The air bearing technology could be applied to the strip to reduce the gaps between the strip and housing entering the lock. This is because air bearings developed by New Way® have a minimum clearance of 0.1 mm. This minimal gap could not be obtained without the frictionless surface. The air bar system (excluding the air bars) was a new design that had not been used before and was developed as a part of this research. The air bars are currently for flexible strip therefore rollers are still required due to the rigidity of the steel otherwise interference could cause wear.

The frictionless surface of the air bars provided an option to fill the space between the edge of the strip and the rollers by incorporating a new design of sliding spacers. This accommodated the varying width constraint and also the air bars could move out and in using automation which would also allow for the varying thickness. The mechanical system of the air bars was not completed in the prototype, so this is currently a concept that requires development into a working operation.

The other important aspect of varying widths and thicknesses was evident in existing technology. Lee et al (2015), [7] claimed that varying widths and thickness was achieved with pressures in the free molecular flow range but did not give a pressure value. The air to air PVD line can coat widths up to 1550 mm so varying widths may be possible but varying thicknesses was not mentioned Kim et al (2013) [2]. It is not possible to compare the air bar system directly with this existing technology as there is not enough information for widths, thicknesses and achievable pressures.

The design revision 7 prototype provided a concept that can accommodate varying widths and thicknesses. The prototype was built for verification of the attainable pressures was a static model that did not include finished working mechanisms. The concept design incorporates all widths and thickness for the total width of standard steel strip due to filling the gaps with the sliders and also all thicknesses of standard steel strip as the air bars can be moved apart. This is a further advancement than some of the existing patents that claim some thicknesses and widths but not all. Until the air bearing mechanism is produced and verified the concept cannot be claimed as a full working system at this time.

The research conducted used computational modelling to aid the design of the vacuum lock. There was no evidence found in the literature of computational modelling being used in the design process of the existing technology. The patents revealed claims of mechanical systems and design constraints but did not provide any engineering standards, design guides or vacuum physics calculations that the inventions had followed. The fundamentals of vacuum technology were explained in Umrath 2007 [32]. This gave a guide to calculating important aspects of vacuum systems but considered closed systems not open systems and for simple geometries. The advancement added by using the simulation tools is the ability to predict the

performance of the lock for more complex geometries than basic calculations could achieve.

The approach of simulation provides an advancement to the field as a new method. A pressure inlet and mass flow rate outlet used together as boundary conditions was not found in literature or manuals. Simulations of the revision 6 vacuum lock using these boundary conditions gave solutions that were close to converging with reasonable results that were within a few hundred pascals of the experimental value. The simulations only covered one of the flow regimes and to simulate the behaviour across the lock system, more development of the models is required.

Currently only the entry lock has been designed and initial experimental validation results attained. This does not provide the desired pressure required for the EML-PVD process. There is potential to meet the needs with further development of the vacuum lock system incorporating additional locks. The pressure measured by the prototype entry lock indicated a good first pressure drop. The lower the pressure in the lock preceding the next lock, the lower the starting point to be pumped down, therefore it is feasible that the system could achieve the desired pressure with less stages than the lock system developed by Maeda et al (1985) [30]. Using less locks than the existing designs could not be concluded as the work stopped at the initial lock.

The air bearing lock prototype model provided simulations resulting in predicted pressures that could be achieved from a range of pumping speeds modelled as a mass flow rate. The ANSYS Fluent computational models for the vacuum lock without the air bars was comparable to the vacuum lock experiment with the reading on the Keyence pressure gauge different by only 228.45 Pa. The pressure drop was only minimal and for a small pressure difference the simulation results are reasonable, as the values are within a few hundred pascals. This combined with the fact that the residuals were converging indicates that without the air bearings and at the higher pressures, this method could be used. More research would need to be conducted trying different pressures and mass flow rates in this pressure region to give confidence for this simulation approach to aid the further development of the locks.

When the computational modelling was performed with the air bar boundary conditions the simulation was less stable and results were less conclusive. The predicted value of 56741 Pa was far off the 22,025 Pa that was achieved by the prototype jig built at Swansea University. The computational model does not perform accurately in this case and results obtained from using the simulation to predict pressures could not be trusted. The current simulation method could not be used for lower pressures due to not being suitable for outside the continuum range. Therefore, the computational modelling conducted in this thesis could not predict the pressure for the complete vacuum lock system.

ANSYS Fluent does not have the required Multiphysics solvers required for the lower pressures and corresponding gas regimes. There is still a considerable amount of work required if computational modelling is used for the analysis of the complete vacuum lock system. The simulation needs to consider the addition of more locks and the change in pressures. OpenFOAM could be used for the lowest pressure and free molecular flow conditions using the DSMC solver. A combination of the DSMC solver and a continuum solver such as icoFoam could be combined in a hybrid method to analyse areas where transition between continuum and free molecular flow occurs. This would need to be written in C++ as it does not currently exist in the OpenFOAM library. In areas of slip flow additional terms would be required to be added that are not covered by the continuum solver alone or DSMC. COMSOL has Multiphysics solvers that cover all of the four gas regimes and the problem could be run for each one using a divided geometry for each region. This would be less computationally expensive than running an OpenFOAM hybrid code across the whole geometry but would require some trial and error to get the correct regions to apply the right physics solver.

The results were not as accurate in the lower pressure region in the ANSYS model for simulating revision 7 as the COMSOL model simulating the controlled leaks. The computational modelling in COMSOL gave a prediction of approximately one percent between the simulated operating pressure and measured experimental pressure. If the leak into a vacuum lock is measured, then the COMSOL model could be used to determine what pump is required to produce a certain pressure. The problem with the

COMSOL model is that the leak rate was increased for the model to predict the pressures more accurately. Also, only one type of pump was used with the COMSOL model, if the pump is more powerful then there is the possibility that the simulation may not provide accurate results. The leak into the vacuum lock is likely not to change and therefore the COMSOL model would be more useful if the leak is set and the volumetric flow rate is changed instead. This could be verified by varying the pumping or using different pumps. This would be more aligned with the ANSYS models and then the two could be compared to experimental results to determine the most accurate method of the two.

The results obtained from the simulations could not be compared with previous work as simulation results for vacuum locks are not available. It would have been useful to have other simulation models and results to compare or more experimental information from existing vacuum lock designs. The existing literature did not have information on the volume inside the vacuum lock or the power of the pump connected therefore it is not possible to compare this. The research is limited to the continuum regime and more investigation is required to simulate the entire vacuum lock system along with experimental verification. In comparison to existing literature the vacuum locks systems have been completely developed whereas in this research the lock system design stops at the first lock.

Some of the deliverables were not completed. It was intended for the vacuum lock to be patented to protect the intellectual property in the same way the existing technology has been protected. The vacuum lock patent was not finalised during the project and is still ongoing. The patent would not include the air bars as these are intellectual property of New Way® air bearings. It would be beneficial to protect the vacuum lock configuration and air bar system as it is a new development. Many products include third party parts and are still patented but it must be clear what is being patented and no infringement on existing patents occur.

Due to the structural failure in the vacuum lock verification experiment no further work was conducted, therefore the proposed optimisation of the most efficient operation of air bar pressure against pumping from the vacuum pump was not investigated. The design of the consecutive vacuum locks including simulation and

verification was not completed. It was not possible to complete the objectives by producing a fully operational vacuum lock system. The vacuum lock is incomplete and requires further design and experimental verification until it provides the required pressure of 0.01 Pa. This does not rule out that the required pressure could be achieved by increasing the chamber length and incorporating more locks and additional pumps. The air bar mechanism requires automation and a control system to be operational. Eventually the lock would then be connected to a chamber and set up as a pilot line for testing.

The experimental rig had internal parts that a conventional acrylic vacuum chamber does not. To improve the experimental rig, it would be advisable to build a new version out of Steel. The components could then be joined together without causing excessive local stresses. This would allow the mechanical assemblies to be added as the prototype is developed further into a fully operational system. The computational modelling was time consuming and more difficult to apply than conventional well established simulation problems like those in the benchmarking exercises. There is little that can be done to the design of the lock to remove the air leaks due to the clearance required for the strip. The clearances in the vacuum lock are highly dependent on the mechanical system which dictates the geometry. It would be less time consuming to remove the computational modelling all together and design from a logical approach. This could be achieved by setting up a test rig and trying varying mechanical configurations whilst recording results on the obtained pressure.

Engineering software has been used that is designed for finite element or finite volume method. Software based upon numerical methods have not been covered in this study. Lattice Boltzmann (LBM) method is another approach that could have been used for the simulation across the pressure range and varying gas regimes. The drawback compared to the continuum method is LBM is not as accurate for steady state problems and the efficiency of the method is limited by a small time step. LBM is however more efficient than the continuum method for unsteady problems when the time step of LBM and continuum methods are the same or the geometry is complex.

11. Conclusion

Objective I - Steel strip is to be continuously transported in and out of the vacuum coating chamber

Tata Steel is developing a prototype electromagnetic levitation (EML) physical vapour deposition (PVD) coating process to galvanise steel strip with a zinc-magnesium vapour. This EML-PVD process is a sealed batch process and requires a consistent pressure of 0.01 Pa in the coating chamber for optimised vapour diffusion. To scale-up the system for coating a continuous strip of steel it will be necessary to use vacuum locks leading to the vapour deposition location. The design of a suitable vacuum lock for continuous strip coating by PVD was the primary objective of this work.

A comprehensive background search was conducted of existing technology in the form of existing design patents, publications, and pilot PVD coating lines. The patents did not contain rigorous data, nor detailed drawings and there were differences in the claimed pressures each lock section could achieve. However, the design patents gave preliminary indications of how vacuum locks could be used, and growing confidence that the required pressure would be achievable.

Objective II - A specified pressure difference is to be maintained between the vacuum chamber and the outside atmosphere.

For this objective, a pressure of 0.01 Pa was set as the final target pressure within the coating chamber. To achieve this target a sequence of locks was envisaged, and much of the work has gone into the development of the first entry vacuum lock design, for which a preliminary drop to 10,000 Pa was deemed sufficient. The first lock is the most crucial as it has the highest pressure to start reduction from as it is exposed directly to the atmosphere. The design evolved based on roller arrangements and air restriction data in previous patents together with computational models developed with the objective of determining the performance efficiency. There was insufficient time to extend the design to the multiple locks required to pump down to the final lowest pressure.

Objective III - The vacuum lock system must deal with a varying strip width and thickness.

The inclusion of air bearings external to the vacuum chamber combined with sliders in the vacuum lock design is a new, possibly patentable, technique. The slider system fills the clearance between the rollers at the edge of the strip and ensures that variable strip widths can pass through without damage or danger of entanglement.

Deliverable I - Model an air bearing lock and to determine the required pumping capacity to achieve a certain pressure

At the start of the modelling investigation conventional style vacuum lock designs were simulated. It was not possible to have one model to fit all pressure drop requirements of all possible designs. Even for an initial first vacuum lock pressure drop to achieve an outlet pressure of 10,000 Pa, the continuum solution provided by ANSYS Fluent became increasingly less believable, including results with unrealistically high velocities were exasperated by the choice of pressure inlet and outlet boundary conditions.

The combination of mass flow rate at the outlet and inlet pressure boundary conditions allowed for a more realistic pumping rate to be determined and influence the design. To this extent it was possible to predict the attainable pressures for a set pumping capacity of 67.37×10^{-3} kg/s which is the actual value for a high-power rotary vacuum pump, thus meeting the objective to determine the required pumping capacity to achieve a certain pressure. Adding the air bars to the conventional lock design the ANSYS Fluent simulation resulted in higher inaccuracy than the previous ANSYS simulation, with convergence issues and unrealistic values of pressure and velocity.

There was more success found with the COMSOL simulation for a chamber experiment in the rough vacuum regime. To determine the required pumping capacity for the lower pressure of 0.01 Pa where the gas regime changes from continuum down to free molecular flow, the multiphysics solvers that cover transitional and free molecular flow such as the Molecular Flow Module in COMSOL or DSMC in OpenFOAM are required. The Knudsen numbers in the first lock were not high enough

to suggest regime outside continuum flow therefore the DSMC method or other COMSOL solvers were not incorporated.

Deliverable II - Comparison with conventional vacuum lock technologies

A comparison of the current air bearing/slider technology has been made against alternative conventional vacuum lock technologies available. Advantages are fewer mechanical parts to maintain, no physical air restriction such as bands or plates which wear, the slider system and air bars are external to the lock chamber therefore easier to access and the air is restricted into the lock with tighter clearances at entry. The disadvantages are the addition of pressurised air into the system, control system required to operate the sliders and ensuring only filtered air is supplied to the air bars.

Deliverable III - Identify how the air bearing technology can be applied in a steel line configuration with varying steel strip width and gauges.

The air bar technology from New Way® provides a uniform film of air through the microporous carbon block. This means the surface is frictionless and will not damage the steel strip and a tight clearance could be achieved that is not possible without an air bearing surface as it would otherwise be abrasive. The inclusion of the air bar in the air bar-slider system aided the reduction of clearances due to the technology providing a very small frictionless gap. A frictionless surface makes it possible for the slider blocks to fill the clearance without any wear or force applied to the steel. If the sliders come into contact, they will be repelled with minimal force.

The introduction of sliders to fill the space between the edge of the strip and rollers provides a solution to the objective of providing a lock that can accommodate varying strip widths. The concept of air bar system using automated movement enables the accommodation of varying strip thicknesses. The air bar slider system satisfies the first objective to transport steel strip in a continuous way into and out of the vacuum coating chamber. The full development of the air bar system is crucial for fulfilling this objective as without restriction of the ingress of air it will not be possible to transport the strip in and out of the coating chamber whilst maintaining 0.01 Pa of pressure.

Deliverable IV - Verification of the modelling work.

A vacuum chamber experiment was performed as an initial set up procedure to gain trust of the equipment that would be used for the vacuum lock experiment verification. A standard vacuum chamber with vacuum pump and drain valve was used. This experiment also used an alternative simulation technique using COMSOL to compare with ANSYS. The COMSOL simulation using the free molecular flow model predicted values close to the actual pressure readings from the experiment. The largest difference between the COMSOL simulation results and test readings was approximately 1 percent therefore provided a good approximation for the verification. An additional leak of 3 litres per minute (LPM) was added to the COMSOL model to account for any other leakage in the lock and match the experimental results more closely. This does manipulate the model to gain a closer match rather than just inputting the known boundary condition values.

Following this modelling study, a prototype was built based on the vacuum lock design to conduct experimental tests and compare with the ANSYS simulation results. ANSYS simulations were performed for the prototype in which one analysis excluded the air bar system and one included it. First the ANSYS Fluent simulation results for the prototype without the air bars were compared to the experimental test. When the mass flow rate was set to match the pumping capacity of the rotary pump at 67.37×10^{-3} kg/s the simulation predicted 2871 Pa below atmospheric pressure and the experimental result was 3100 Pa below atmospheric pressure. These figures are of close approximation.

The prototype was completed with the air bars fixed in place and switched on with the sliders placed between them next to the sides of the steel strip. Before the verification test was conducted another ANSYS Fluent simulation was run to replicate this giving a predicted pressure of 56,741 Pa with the mass flow rate set again at 67.37×10^{-3} kg/s to match the rotary pump. This predicated pressure is 34,716 Pa higher than the reading of 22,025 Pa taken from the vacuum lock prototype experiment. This is a significantly large mismatch of values and therefore it was concluded that using the additional pressure at the inlet to replicate the air bar in this model was inaccurate.

The pressure of 22,025 Pa achieved in the first lock prototype is not the target pressure of 0.01 Pa required for the EML-PVD process however it is a strong starting point towards achieving the required pressure as in comparison it is 5675 Pa lower than the lowest claimed pressure for a first lock found in the literature which was 26,700 Pa from the Nisshin Mitsubishi Zinc Vapour PVD Line. This subsequent attempt to get lower pressure led to the collapse of the prototype chamber wall preventing further testing.

Future Work

There is not enough modelling validation data available for vacuum lock design and the simulations and simple experiments performed in this research could be useful for future research in this field. The most crucial further development is to complete deliverable VII - Simulation of consecutive locks (daisy chained) showing pumping down to the adequate coating chamber pressure. This could be achieved through simulation, completing the experimental rig or a combination of both.

To complete the experimental rig the air bar system needs to be developed into an operational process including automation of the air bars to move away and towards the strip to account for the varying thickness and the sliders to be fed in from the side. Once the required pressure of 0.01 Pa has been achieved then optimisation of the process should proceed by investigating deliverable VI - Optimisation of air bar pressure and pumping to provide the most efficient operation and optimised energy consumption.

Once all work is completed the invention should be protected by a patent. Deliverable V was to patent the vacuum lock design. A patent process is pending to protect the intellectual property of this first vacuum lock. Swansea University granted Tata Steel permission to patent the prototype vacuum lock and Tata Steel stated the author will be lead inventor on the patent.

12. Bibliography

[1] Y. Chen *et al.*, “High Performance and Enhanced Durability of Thermochromic Films Using VO2@ZnO Core-Shell Nanoparticles,” *ACS Appl. Mater. Interfaces*, vol. 9, no. 33, pp. 27784–27791, 2017.

[2] T. Kim *et al.*, “Installation of a Wide PVD Pilot Plant in POSCO,” *new Technol. Recycl.*, pp. 521–526, 2013.

[3] ArcelorMittel, “ArcelorMittal, the Walloon government and Sogepa celebrate world-first for steel industry, developed in Liège.” [Online]. Available: https://corporate.arcelormittal.com/news-and-media/news/2017/feb/03-02-2017. [Accessed: 02-Feb-2018].

[4] W. S. Jung, C. W. Lee, T. Y. Kim, and B. C. De Cooman, “Mg Content Dependence of EML-PVD Zn-Mg Coating Adhesion on Steel Strip,” *Metall. Mater. Trans. A Phys. Metall. Mater. Sci.*, vol. 47, no. 9, pp. 4594–4605, 2016.

[5] V. Kuklík and J. Kudláĉek, *Hot-Dip galvanizing of steel structures*, 1st ed. Oxford: Butterworth-Heinemann, 2016.

[6] I. Daigo, S. Osako, Y. Adachi, and Y. Matsuno, “Time-series analysis of global zinc demand associated with steel,” *Resour. Conserv. Recycl.*, vol. 82, pp. 35–40, 2014.

[7] D. Lee *et al.*, “Strip passing apparatus for treating surface of strip with the same, and method for treating surface of strip,” U.S. Patent 8,926,756 B2, 2015.

[8] G. Bird, *The DSMC Method*. Sydney: CreateSpace Independent Publishing Platform, 2013.

[9] ANSYS FLUENT 13, “Ansys Fluent Theory Guide,” *ANSYS Inc., USA*. 2013.

[10] R. W. Pryor, *Multiphysics Modeling Using Comsol 4: A first Principles Approach*. Dulles: Mercury Learning and Information, 2012.

[11] C. J. Greenshields, *OpenFOAM User Guide v3*, no. 3.0.1. Creative Commons Attribution, 2015.

[12] K. Hencken, "Investigation of Metallic Vapor Condensation in a Vacuum Interrupter using dsmcFOAM DSMC," *9th OpenFOAM® Work. Croat.*, no. June, pp. 6–7, 2014.

[13] E. McCafferty, *Introduction to corrosion science*, 1st ed. New York: Springer-Verlag, 2010.

[14] V. John, "Oxidation, Corrosion and Other Effects," in *Introduction to Engineering Materials*, 3rd ed., London: Palgrave Macmillan, 2003.

[15] V. John, "Oxidation, Corrosion and Other Effects BT - Introduction to Engineering Materials," V. John, Ed. London: Palgrave Macmillan UK, 1992.

[16] J. H. La, M. G. Song, H. K. Kim, S. Y. Lee, and W. S. Jung, "Effect of deposition temperature on microstructure, corrosion behavior and adhesion strength of Zn-Mg coatings on mild steel," *J. Alloys Compd.*, vol. 739, pp. 1097–1103, 2017.

[17] Y. Sabooni, Soheil; Galinmoghaddam, Emad; Westerwaal, R. J.; Zoestbergen, Edzo; Pei and T., "Effect of Mg concentration & layer thickness on the adhesion of ZnMg-Zn bi-layered PVD coatings," in *Materials Characterization*, 2019.

[18] G. Krauss and D. K. Matlock, *Zinc-based steel coating systems : metallurgy and performance*. Warrendale: Minerals, Metals & Materials Society, 1990.

[19] P. Peißker and P. Maaß, Eds., *Handbook of Hot-Dip Galvanization*, 3rd ed. Weinheim: WILEY-VCH Verlag GmbH & Co. KGaA, 2011.

[20] S. Vemuri, "Galvanised to deliver," 2012. [Online]. Available:

http://www.tata.com/article/inside/3tFCAPRaeRg=/TLYVr3YPkMU. [Accessed: 24-May-2016].

[21] B. Jones, “Tata Steel completes upgrade of UK automotive coating line,” *Corporate News*, 2013. [Online]. Available: http://www.tatasteeleurope.com/en/news/news/2013/2013_uk_automotive_coating_line_corp. [Accessed: 24-May-2016].

[22] B. Navinšek, P. Panjan, and I. Milošev, “PVD coatings as an environmentally clean alternative to electroplating and electroless processes,” *Surf. Coatings Technol.*, vol. 116–119, no. September 1999, pp. 476–487, 1999.

[23] L. Baptiste *et al.*, “Electromagnetic levitation: A new technology for high rate physical vapour deposition of coatings onto metallic strip,” *Surf. Coatings Technol.*, vol. 202, no. 4–7, pp. 1189–1193, 2007.

[24] S. I. Shah, G. H. Jaffari, E. Yassitepe, and B. Ali, “Evaporation: Processes, Bulk Microstructures, and Mechanical Properties,” in *Handbook of Deposition Technologies for Films and Coatings*, 2010, pp. 135–252.

[25] T. Y. Kim and M. Goodenough, “Simultaneous Co-deposition of Zn-Mg Alloy Layers on Steel Strip by PVD Process,” *Corros. Sci. Technol.*, vol. 10, no. 6, pp. 194–198, 2011.

[26] D. M. Mattox, *Handbook of Physical Vapor Deposition PVD Processing*, 2nd ed. Oxford: Elsevier, 2010.

[27] P. M. Martin, *Handbook of Deposition Technologies for Films and Coatings - Science, Applications and Technology*, 3rd ed. William Andrew Publishing, 2010.

[28] E. U. Reinhold, J. Richter, H. Waydbrink, and E. Zschieschang, “Reflection enhancement of aluminum strips by EB-PVD in highly productive industrial lines,” pp. 14–20, 2000.

[29] E. Zoestbergen, T. F. J. Maalman, J. can de Langkruis, and M. R.

Goodenough, “Substrate with a Double Layered Coating,” WO Patent 2013/091889 A1, 2013.

[30] E. Zoestbergen, J. Van de Langkruis, T. Maalman, E. Batyrev, S. Melzer, and M. Zuijderwijk, “Diffusion of Zinc and Magnesium in Physical Vapour Deposited Thin Films at 175°C,” *Galvatech*, vol. 31, no. 0, pp. 36–43, 2015.

[31] M. Maeda, H. Furukawa, and Y. Shimozato, “Development of a Zinc Physical Vapor Deposition Process,” *Tech. Rev. Mitsubishi Heavy Ind.*, vol. 22, no. 2, pp. 185–191, 1985.

[32] N. Marquardt, “Introduction to the principles of vacuum physics,” *Vacuum*, no. 1661, pp. 1–24, 1999.

[33] W. Umrath, “Fundamentals of Vacuum Technology,” 2007. [Online]. Available: https://www3.nd.edu/~nsl/Lectures/urls/LEYBOLD_FUNDAMENTALS.pdf. [Accessed: 01-Jun-2016].

[34] D. Hoffman and B. Singh, *Handbook of vacuum science and technology*. London: Academic Press, 1997.

[35] N. Yoshimura, *Vacuum Technology Practice for Scientific Instruments*. Tokyo: Springer, 2008.

[36] S. Coolen, S. Gesves, D. Marneffe, B. D’Hondt, and C. De Felice, “Sealing lock for a deposition line in vacuum on a flat product,” U.S. Patent 7,931,750 B2, 2011.

[37] S. Hein, “Lock valve in particular for a processing unit,” U.S. Patent 8,499,784 B2, 2013.

[38] W. Erbkamm, J. Guenter, G. Kuehn, J. Senf, and E. Zschieschang, “Apparatus for reducing pressure in feeding channels leading to treatment chamber - using vacuum pumps connected in series to gradually reduce the pressure from atmospheric to the optimal pressure required,” (in German), DE Patent 42 40

488 C1, 1992.

[39] W. Erbkamm, J. Guenter, G. Kuehn, J. Senf, and E. Zschieschang, “System for feeding strip into treatment chamber - has rollers operating valve system between different pressure stages,” (in German), DE Patent 42 40 489 C1, 1994.

[40] P. Vanden Brande, “Air lock,” U.S. Patent 6,334,751 B1, 2002.

[41] L. Gottsmann, G. Laimer, and J. Reinhard, “Method of a sealing chamber and sluice device for a vacuum chamber,” (in German), EP Patent 1 862 567 A2, 2007.

[42] L. Gottsmann, G. Laimer, and J. Reinhard, “Method and apparatus for the treatment of strip-shaped substrate in a vacuum coating system,” (in German), WO Patent 2008/104169 A1, 2008.

[43] A. J. Devitt, “A method and a device for depositing a film of material or otherwise processing or inspecting, a substrate as it passes through a vacuum environment guided by a plurality of opposing and balanced air bearing lands and sealed by differentially pumped grove,” WO Patent 2007/016688 A1, 2007.

[44] A. J. Devitt, “A method and apparatus for in-line processing and immediately sequential or simultaneous processing of flat and flexible substrates through viscous shear in thin cross section gaps for the manufacture of micro-electronic circuits for displays.,” U.S. Patent 8,123,868 B2, 2012.

[45] Z. X. Tong, Y. L. He, and W. Q. Tao, “A review of current progress in multiscale simulations for fluid flow and heat transfer problems: The frameworks, coupling techniques and future perspectives,” *Int. J. Heat Mass Transf.*, vol. 137, pp. 1263–1289, 2019.

[46] K. Bobzin *et al.*, “Continuum and kinetic simulations of the neutral gas flow in an industrial physical vapor deposition reactor,” *Surf. Coatings Technol.*, vol. 237, pp. 176–181, 2013.

[47] A. Moarrefzadeh, “Simulation and modeling of physical vapor deposition (PVD) process,” *WSEAS Trans. Appl. Theor. Mech.*, vol. 7, no. 2, pp. 106–111, 2012.

[48] D. Halwidl, *Development of an Effusive Molecular Beam Apparatus*. Vienna: Springer Spektrum, 2016.

[49] F. J. Alexander and A. L. Garcia, “The Direct Simulation Monte Carlo Method,” *Computers in Physics*, vol. 11, no. 6. pp. 588–593, 1997.

[50] F. Sharipov, “Rarefied gas dynamics and its applications to vacuum technology,” *CAS 2006 - Cern Accel. Sch. Vac. Accel. Proc.*, pp. 1–13, 2007.

[51] G. S. de F. Barbosa, K. Vissing, and B. Mayer, “Creation and Evaluation of Construction Guidelines Using CFD for Low Pressure Plasma Gas Feed-in Systems to Homogenize the Precursor Gas Flow,” *Open J. Fluid Dyn.*, vol. 06, no. 04, pp. 391–405, 2016.

[52] Y.-L. He and W.-Q. Tao, “Multiscale Simulations of Heat Transfer and Fluid Flow Problems,” *J. Heat Transfer*, vol. 134, no. 3, p. 031018, 2012.

[53] C. White *et al.*, “DsmcFoam+: An OpenFOAM based direct simulation Monte Carlo solver,” *Comput. Phys. Commun.*, vol. 224, pp. 22–43, 2017.

[54] G. Abbate, B. J. Thijsse, and C. R. Kleijn, “Hybrid Navier-Stokes/DSMC Simulations of Gas Flows with Rarefied-Continuum Transitions,” in *Advanced Computational Methods in Science and Engineering*, B. Koren and K. Vuik, Eds. Berlin, Heidelberg: Springer Berlin Heidelberg, 2010, pp. 403–435.

[55] T. Scanlon and C. White, “Open Source DSMC Modelling Using dsmcFoam+ Training Course,” 2017. [Online]. Available: https://www.cfd-online.com/Forum/news.cgi/read/102325. [Accessed: 01-Apr-2017].

[56] Z. Shang and S. Chen, “3D DSMC Simulation of Rarefied Gas Flows around a Space Crew Capsule Using OpenFOAM,” *Open J. Appl. Sci.*, vol. 03, no.

01, pp. 35–38, 2013.

[57] E. Rathakrishnan, *Applied gas dynamics*, Second. Chichester: John Wiley & Sons, 2019.

[58] J. Jeans, *An Introduction to the Kinetic Theory of Gases*. Cambridge: Cambridge University Press, 1982.

[59] H. K. Versteeg and W. Malaskekera, *An Introduction to Computational Fluid Dynamics*, 2nd ed., vol. M. Harlow: Pearson Education Limited, 2007.

[60] T. J. Chung, *Computational Fluid Dynamics*, 2nd ed. New York: Cambridge University Press, 2010.

[61] Y. A. Çengel and J. M. Cimbala, *Fluid Mechanics: Fundamentals and Applications*, 1st ed. New York: McGraw-Hill, 2006.

[62] M. Andersen, C. Panosetti, and K. Reuter, "A practical guide to surface kinetic Monte Carlo simulations," *Front. Chem.*, vol. 7, no. APR, pp. 1–24, 2019.

[63] J. G. Amar, "The Monte Carlo method in science and engineering," *Comput. Sci. Eng.*, vol. 8, no. 2, pp. 9–19, 2006.

[64] D. P. Landau and K. Binder, *A Guide to Monte Carlo Simulations in Statistical Physics*, 2nd ed. Cambridge: Cambridge University Press, 2005.

[65] A. F. Voter, "Introduction To the Kinetic Monte Carlo Method," in *Radiation Effects in Solids*, 2007, pp. 1–23.

[66] T. Weckman, M. Shirazi, S. D. Elliott, and K. Laasonen, "Kinetic Monte Carlo Study of the Atomic Layer Deposition of Zinc Oxide," *J. Phys. Chem. C*, vol. 122, no. 47, pp. 27044–27058, 2018.

[67] J. Cho, S. G. Terry, R. LeSar, and C. G. Levi, "A kinetic Monte Carlo simulation of film growth by physical vapor deposition on rotating substrates," *Mater. Sci. Eng. A*, vol. 391, no. 1–2, pp. 390–401, 2005.

[68] A. Venkattraman and A. A. Alexeenko, “Direct simulation Monte Carlo modeling of metal vapor flows in application to thin film deposition,” *Vacuum*, vol. 86, no. 11, pp. 1748–1758, 2012.

[69] T. M. Rodgers, H. Zhao, and H. N. G. Wadley, “Integrated development of vapor deposition for non-lineof-sight substrates,” *Collect. Tech. Pap. - AIAA/ASME/ASCE/AHS/ASC Struct. Struct. Dyn. Mater. Conf.*, no. April, pp. 1–13, 2012.

[70] W. Wagner, “A convergence proof for Bird’s direct simulation Monte Carlo method for the Boltzmann equation,” *J. Stat. Phys.*, vol. 66, no. 3–4, pp. 1011–1044, 1992.

[71] A. Venkattraman and A. A. Alexeenko, “Molecular models for DSMC simulations of metal vapor deposition,” in *AIP Conference Proceedings*, 2011, vol. 1333, no. PART 1, pp. 1057–1062.

[72] G. A. Bird, *Molecular Gas Dynamics and the Direct Simulation of Gas Flows*. New York: Oxford University Press Inc, 1994.

[73] J. Daintith, “Dictionary of Chemistry,” 2008. [Online]. Available: https://app.knovel.com/web/toc.v/cid:kpDCE00011/viewerType:toc/root_slug:dictionary-chemistry/url_slug:boltzmann-constant?b-q=boltzmann constant&b-subscription=true&b-group-by=true&b-sort-on=default&b-content-type=all_references&issue_id=kt008IFRN2. [Accessed: 19-Jan-2018].

[74] A. Bejan, *Convection Heat Transfer*, 4th ed. Hoboken: John Wiley & Sons, 2013.

[75] J. M. Cimbala, “The Ideal Gas,” *Penn State University*, 2014. [Online]. Available: http://www.mne.psu.edu/cimbala/learning/general/gas_constant.pdf. [Accessed: 01-Aug-2017].

[76] CFD Online, “Sutherland’s Law.” [Online]. Available: https://www.cfd-

online.com/Wiki/Sutherland%27s_law. [Accessed: 01-Sep-2018].

[77] R. Nave, “Refinement of mean free path.” [Online]. Available: http://hyperphysics.phy-astr.gsu.edu/hbase/Kinetic/menfre.html. [Accessed: 12-Jun-2017].

[78] N. Hall, “Mass Flow rate,” *2015*. [Online]. Available: https://www.grc.nasa.gov/www/k-12/airplane/mflow.html. [Accessed: 01-Sep-2018].

[79] SimWiki, “What is the Reynolds Number?” [Online]. Available: https://www.simscale.com/docs/content/simwiki/numerics/what-is-the-reynolds-number.html. [Accessed: 01-Sep-2018].

[80] Kurt. J. Lesker Company, “Basic Pumping Concepts.” [Online]. Available: https://www.lesker.com/newweb/technical_info/vacuumtech/pumps_00_basicconcept.cfm. [Accessed: 05-Mar-2018].

[81] A. Chambers, *Modern Vacuum Physics*. London: Chapman & hall, 2005.

[82] VAC AERO International, “The Fundamentals of Vacuum Technology,” 2018. [Online]. Available: https://vacaero.com/information-resources/vac-aero-training/170466-the-fundamentals-of-vacuum-theory.html. [Accessed: 01-Oct-2018].

[83] Pfeiffer Vacuum, “1.2.8 Conductance,” 2019. [Online]. Available: https://www.pfeiffer-vacuum.com/en/know-how/introduction-to-vacuum-technology/fundamentals/conductance/. [Accessed: 05-Mar-2019].

[84] P. Fan, J. Chu, and J. Shao, “Conduction calculation of long tubes with rectangular cross section and annular cross section in the full pressure range,” *Vacuum, Surf. Eng. Surf. Instrum. Vac. Technol.*, 2002.

[85] A. Sharma, *Introduction to Computational Fluid Dynamics Development, Application and Analysis*. Chichester: John Wiley & Sons, 2017.

[86] T. D. Canonsburg, “ANSYS Fluent Tutorial Guide,” vol. 15317, no. November, pp. 724–746, 2013.

[87] A. Bakker, “Applied Computational Fluid Dynamics,” 2002. [Online]. Available: http://www.bakker.org/dartmouth06/engs150/06-bound.pdf. [Accessed: 01-Sep-2017].

[88] B. Koren and K. Vuik, “Advanced Computational Methods in Science and Engineering,” *Lect. Notes Comput. Sci. Eng.*, vol. 73, pp. 403–435, 2010.

[89] ANSYS Inc, “Introduction to ANSYS Fluent,” 2010. [Online]. Available: http://imechanica.org/files/fluent_13.0_lecture04-boundary-conditions.pdf. [Accessed: 01-Sep-2017].

[90] ANSYS Inc, “Boundary Conditions Introductory FLUENT Training,” 2006. [Online]. Available: http://www.southampton.ac.uk/~nwb/lectures/GoodPracticeCFD/Articles/BCs_Fluent-v6.3.04.pdf. [Accessed: 01-Sep-2017].

[91] COMSOL, “Comsol Multiphysics User’s Guide: Version 4.3,” 2012. [Online]. Available: https://www.researchgate.net/profile/Rayudu_Nithin_Manohar/post/Can_any_one_please_give_me_a_link_that_would_help_me_to_understand_clearly_comsol_multiphysics/attachment/59d635aec49f478072ea380a/AS:273666233831428@1442258523089/download/COMSOLMultiphysics. [Accessed: 06-Jun-2018].

[92] ESI, *OpenFOAM Foundation Course: Version 1606+*. London: OpenCFD Ltd, 2016.

[93] T. J. Scanlon, E. Roohi, C. White, M. Darbandi, and J. M. Reese, “An open source, parallel DSMC code for rarefied gas flows in arbitrary geometries,” *Comput. Fluids*, vol. 39, no. 10, pp. 2078–2089, 2010.

[94] K. Gott, “A hybrid CFD-DSMC model designed to simulate rapidly rarefying flow fields and its application to physical vapor deposition,” Penn State

University, 2015.

[95] H. C. Kuhlmann and F. Roman, “The lid-driven cavity,” in *Computational Modelling of Bifurcations and Instabilities in Fluid Dynamics*, Cham: Springer, 2019, pp. 233–309.

[96] U. Ghia, K. N. Ghia, and C. T. Shin, “High-Re Solutions for Incompressible Using the Navier-Stokes Equations Multigrid Method,” *J. Comput. Phys.*, vol. 48, no. 3, pp. 387–411, 1982.

[97] P. N. Shankar and M. D. Deshpande, “Fluid Mechanics In The Driven Cavity,” in *Computational and Theoretical Fluid Dynamics Division, National Aerospace Laboratories*, 2000, pp. 93–136.

[98] C. Greenshields, “OpenFOAM v4 User Guide,” 2015. [Online]. Available: https://cfd.direct/openfoam/user-guide/v4-cavity/#x5-40002.1. [Accessed: 01-May-2016].

[99] Fluent Inc, “Tutorial 1. Flow in a Lid-Driven Cavity,” 2005. [Online]. Available: http://dl.mr-cfd.com/tutorials/ansys-fluent/lid-driven-cavity-simulation.pdf. [Accessed: 01-May-2016].

[100] A. Straccia, “How to Solve a Classic CFD Benchmark: The Lid-Driven Cavity Problem,” *COMSOL Blog*, 2018. [Online]. Available: https://uk.comsol.com/blogs/how-to-solve-a-classic-cfd-benchmark-the-lid-driven-cavity-problem/. [Accessed: 08-May-2018].

[101] Y. A. Çengel and M. A. Boles, *Thermodynamics: An Engineering Approach*. Boston: McGraw-Hill, 2004.

[102] C. Robinson, “Flow Through a de Laval Nozzle,” 2016. [Online]. Available: https://www.google.co.uk/url?sa=t&rct=j&q=&esrc=s&source=web&cd=12&cad=rja&uact=8&ved=2ahUKEwihur3EuKjkAhX1QUEAHW0jCwwQFjALegQIARAC&url=http%3A%2F%2Fwww.bu.edu%2Fufmal%2Ffiles%2F2016%2F12%2FRobinsonProject.pdf&usg=AOvVaw0wKR4G_ODVugzDknT6Zkq_. [Accessed: 27-Mar-2019].

[103] N. Hall, “Rocket Thrust Summary,” 2018. [Online]. Available: https://www.grc.nasa.gov/WWW/K-12/airplane/rktthsum.html. [Accessed: 01-May-2018].

[104] joshtheengineer.com, “Solving the area-mach number relation,” 2019. [Online]. Available: http://www.joshtheengineer.com/2016/11/16/solving-the-area-mach-number-relation/. [Accessed: 01-Mar-2018].

[105] J. Fan, D. Boyct, and C. Shelter, “Monte Carlo Modeling of YBCO Vapor Deposition Deposition,” in *AIP Conference Proceedings*, 2001, pp. 214–221.

[106] A. Venkattraman and A. A. Alexeenko, “Direct simulation Monte Carlo modeling of e-beam metal deposition,” *J. Vac. Sci. Technol. A Vacuum, Surfaces, Film.*, vol. 28, no. 4, p. 916, 2010.

[107] H. Fink, D. Gentsch, and M. Heimbach, “New vacuum interrupters for contactors and switches,” *ABB Review*, no. 3, pp. 32–36, 1999.

[108] F. B. M. Suah, W. S. W. Ngah, and C. S. Saidin, *Basic Analytical Chemistry*. Penerbit Universiti Sains Malaysia, 2018.

[109] P. J. Carlos, *Coversation with Samuel Minshell*. 2018.

[110] New Way Air Bearings, “Designing with air bearings,” 2006. [Online]. Available: https://www.newwayairbearings.com/technology/design-basics/designing-with-air-bearings/. [Accessed: 01-Mar-2018].

[111] New Way Air Bearings, “PA-Rail Series,” 2019. [Online]. Available: https://www.newwayairbearings.com/catalog/pa-rail-substrates-conveying/. [Accessed: 15-Jan-2019].

[112] Kale, P. Patil, M. B. Korade, DJagtap, and K. R, “Experimental and CFD Analysis of Vacuum Cleaner Exhaust Muffler,” *IOSR J. Mech. Civ. Eng.*, vol. 13, no. 1, pp. 21–27, 2016.

[113] J. Hesse, R. Andres, C. F. X. Berlin, and S. Gmbh, “Cfd Simulation of a Dry

Scroll Vacuum Pump Including Leakage Flows," *Int. Compress. Eng. Refrig. Air Cond. High Perform. Build. Conf.*, pp. 1–10, 2016.

[114] I. H. Son, Y. Noh, E. H. Choi, J. Y. Choi, Y. J. Ji, and K. Lim, "Optimization of the flow path efficiency in a vacuum cleaner fan," *J. Mech. Eng.*, vol. 64, no. 4, pp. 258–268, 2018.

[115] X. B. Lai, H. S. Wang, and H. S. Liu, "Research on duct flow field optimisation of a robot vacuum cleaner," *Int. J. Adv. Robot. Syst.*, vol. 8, no. 5, pp. 104–112, 2011.

[116] A. Young, *Email to Samuel Minshell*. 2019.

[117] COMSOL, "Solving time dependent models with inconsistent initial values," *COMSOL Knowledgebase*, 2019. [Online]. Available: https://www.comsol.com/support/knowledgebase/1172/. [Accessed: 16-Aug-2019].

[118] O. Sunar, "Contact Types and Behaviours in ANSYS," 2018. [Online]. Available: http://www.mechead.com/contact-types-and-behaviours-in-ansys/. [Accessed: 12-Dec-2018].

[119] Slovak University of Technology Faculty of Mechanical Engineering, "Material Contact Properties Table," 2008. [Online]. Available: http://atc.sjf.stuba.sk/files/mechanika_vms_ADAMS/Contact_Table.pdf. [Accessed: 12-Dec-2018].

13. Appendix A: Drawings

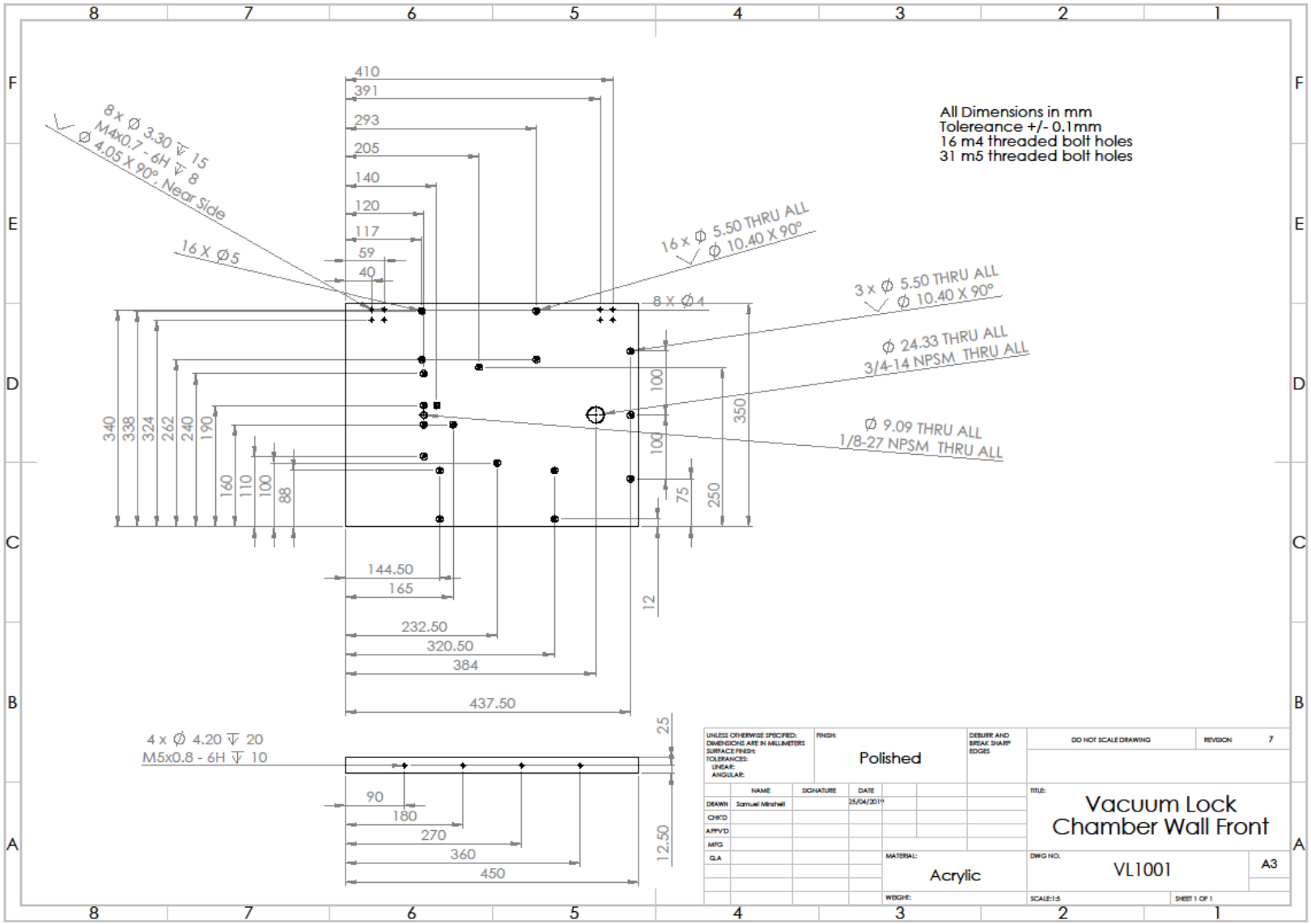
All Dimensions in mm
Tolereance +/- 0.1mm
16 m4 threaded bolt holes
31 m5 threaded bolt holes
8 x Ø 3.30 ↧ 15
M4x0.7 - 6H ↧ 8
Ø 4.05 X 90° : Near Side
16 X Ø5
16 x Ø 5.50 THRU ALL
Ø 10.40 X 90°
8 X Ø4
3 x Ø 5.50 THRU ALL
Ø 10.40 X 90°
Ø 24.33 THRU ALL
3/4-14 NPSM THRU ALL
Ø 9.09 THRU ALL
1/8-27 NPSM THRU ALL
4 x Ø 4.20 ↧ 20
M5x0.8 - 6H ↧ 10
410
391
293
205
140
120
117
59
40
340
338
324
262
240
190
160
110
100
88
100
100
350
75
250
144.50
165
232.50
320.50
384
437.50
12
25
12.50
90
180
270
360
450
Polished
Acrylic
Vacuum Lock
Chamber Wall Front
VL1001
A3
DO NOT SCALE DRAWING
REVISION 7
Samuel Minshall
25/04/2019

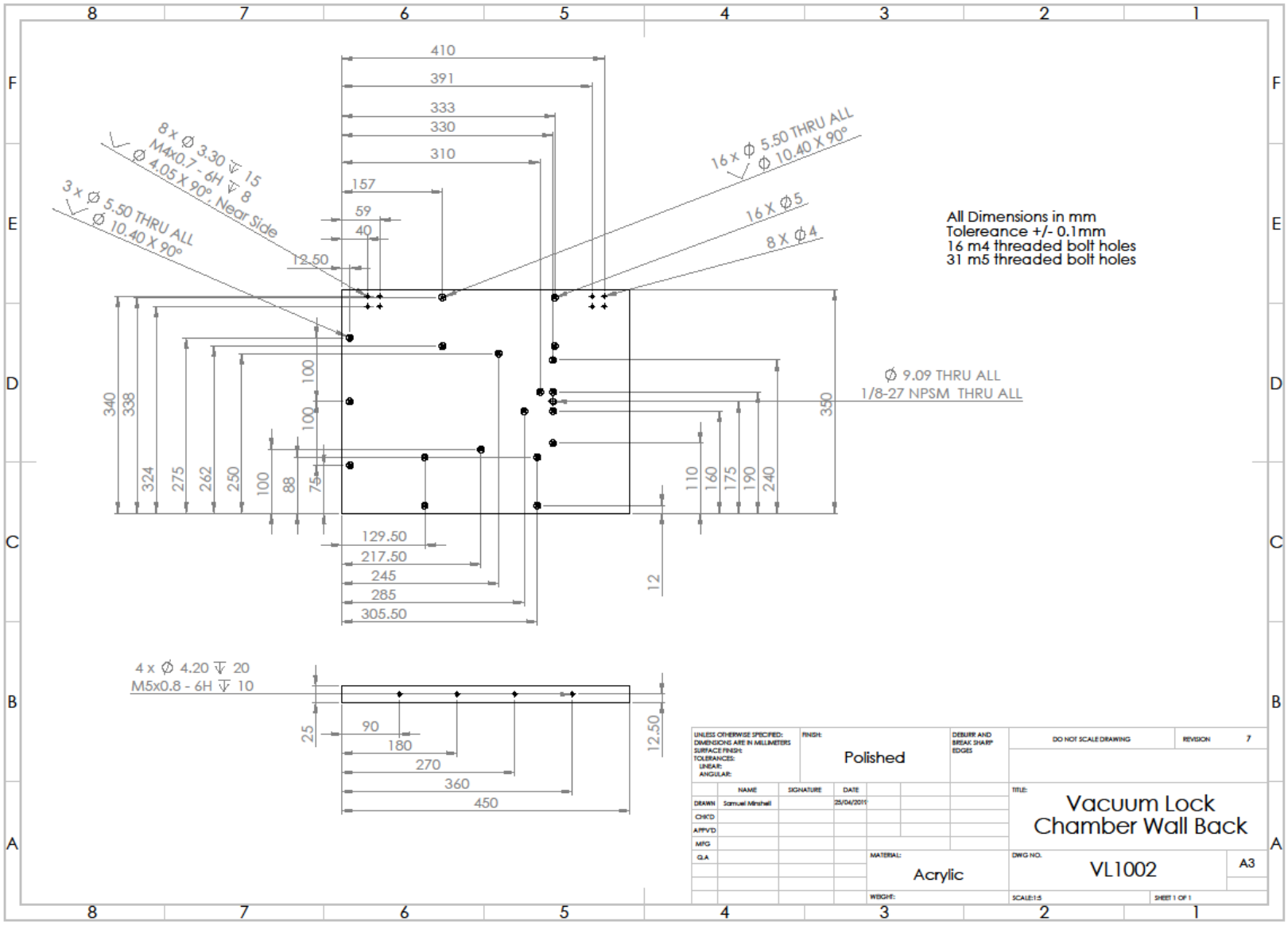
410
391
333
330
310
157
59
40
12.50
8 x ∅ 3.30 ↧ 15
M4x0.7 - 6H ↧ 8
∅ 4.05 X 90°, Near Side
3 x ∅ 5.50 THRU ALL
⌴ ∅ 10.40 X 90°
16 x ∅ 5.50 THRU ALL
⌴ ∅ 10.40 X 90°
16 X ∅5
8 X ∅4
All Dimensions in mm
Tolereance +/- 0.1mm
16 m4 threaded bolt holes
31 m5 threaded bolt holes
∅ 9.09 THRU ALL
1/8-27 NPSM THRU ALL
340
338
324
275
262
250
100
88
75
100
100
100
350
110
160
175
190
240
129.50
217.50
245
285
305.50
12
4 x ∅ 4.20 ↧ 20
M5x0.8 - 6H ↧ 10
25
90
180
270
360
450
12.50
UNLESS OTHERWISE SPECIFIED:
DIMENSIONS ARE IN MILLIMETERS
SURFACE FINISH:
TOLERANCES:
LINEAR:
ANGULAR:
FINISH:
Polished
DEBURR AND BREAK SHARP EDGES
DO NOT SCALE DRAWING
REVISION 7
NAME
SIGNATURE
DATE
DRAWN Samuel Minshall 25/04/2019
CHK'D
APPV'D
MFG
Q.A
MATERIAL:
Acrylic
WEIGHT:
TITLE:
Vacuum Lock
Chamber Wall Back
DWG NO.
VL1002
A3
SCALE:1:5
SHEET 1 OF 1

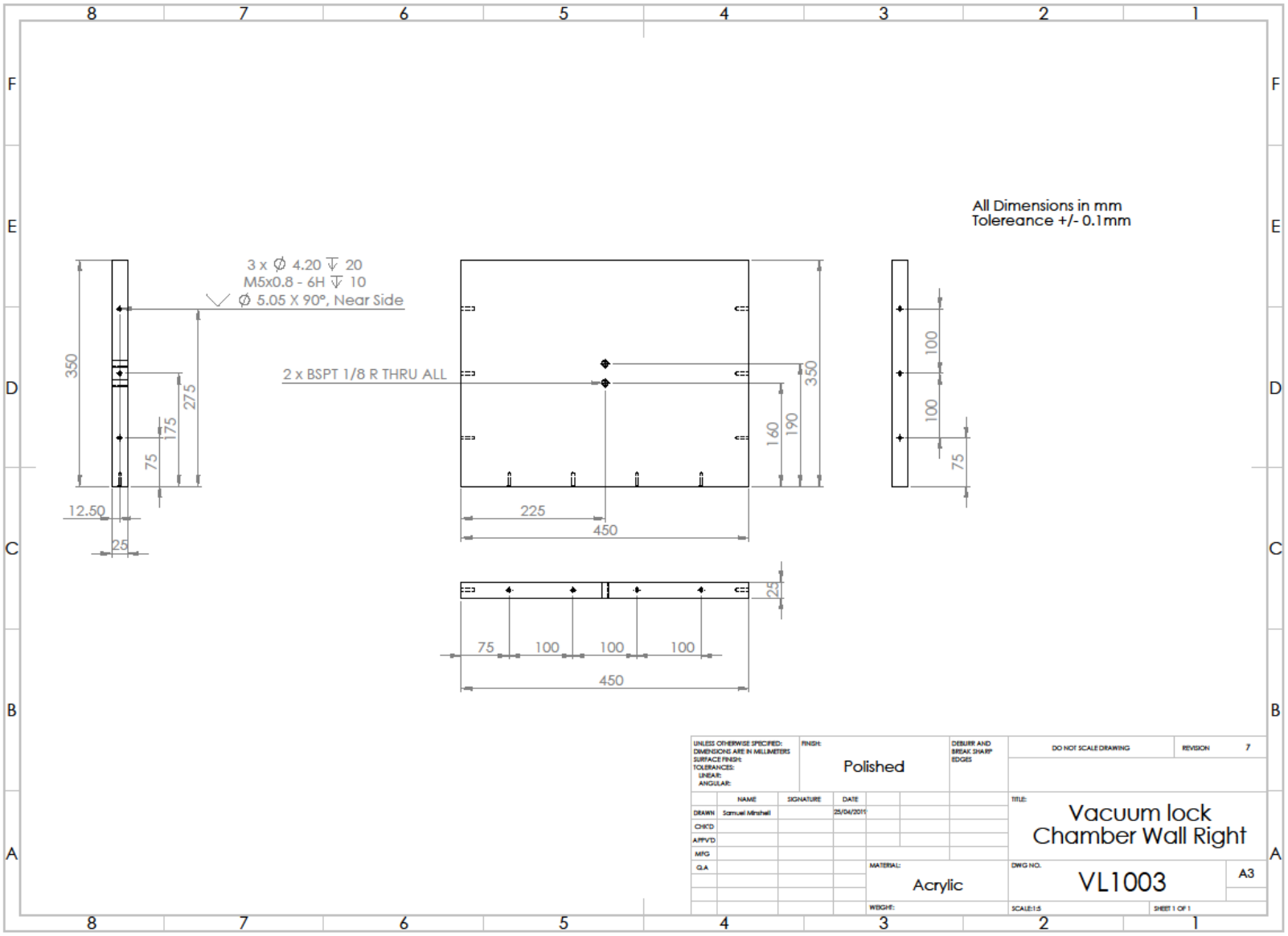
All Dimensions in mm
Tolereance +/- 0.1mm
3 x ⌀ 4.20 ↧ 20
M5x0.8 - 6H ↧ 10
⌀ 5.05 X 90°, Near Side
2 x BSPT 1/8 R THRU ALL
350
275
175
75
12.50
25
225
450
160
190
350
100
100
75
25
75
100
100
100
450
UNLESS OTHERWISE SPECIFIED:
DIMENSIONS ARE IN MILLIMETERS
SURFACE FINISH:
TOLERANCES:
LINEAR:
ANGULAR:
FINISH:
Polished
DEBURR AND BREAK SHARP EDGES
DO NOT SCALE DRAWING
REVISION 7
NAME
SIGNATURE
DATE
DRAWN Samuel Minshall 25/04/2011
CHK'D
APP'VD
MFG
Q.A
MATERIAL:
Acrylic
WEIGHT:
TITLE:
Vacuum lock
Chamber Wall Right
DWG NO.
VL1003
A3
SCALE:1:5
SHEET 1 OF 1

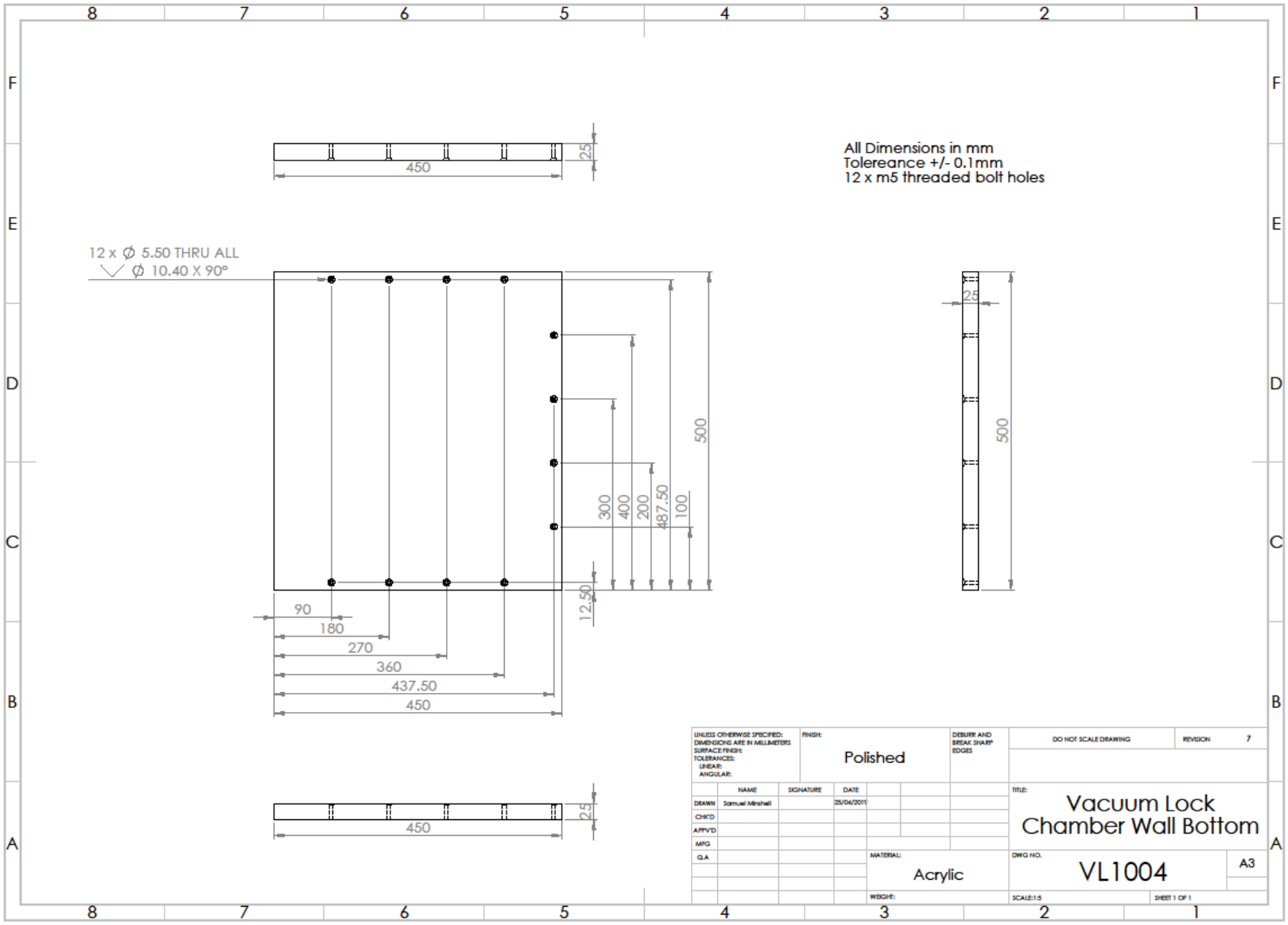
All Dimensions in mm
Tolereance +/- 0.1mm
12 x m5 threaded bolt holes
12 x ⌀ 5.50 THRU ALL
⌀ 10.40 X 90°
450
25
500
300
400
200
487.50
100
12.50
90
180
270
360
437.50
450
Polished
Vacuum Lock
Chamber Wall Bottom
VL1004
A3
Acrylic
Samuel Minshall
25/04/2019

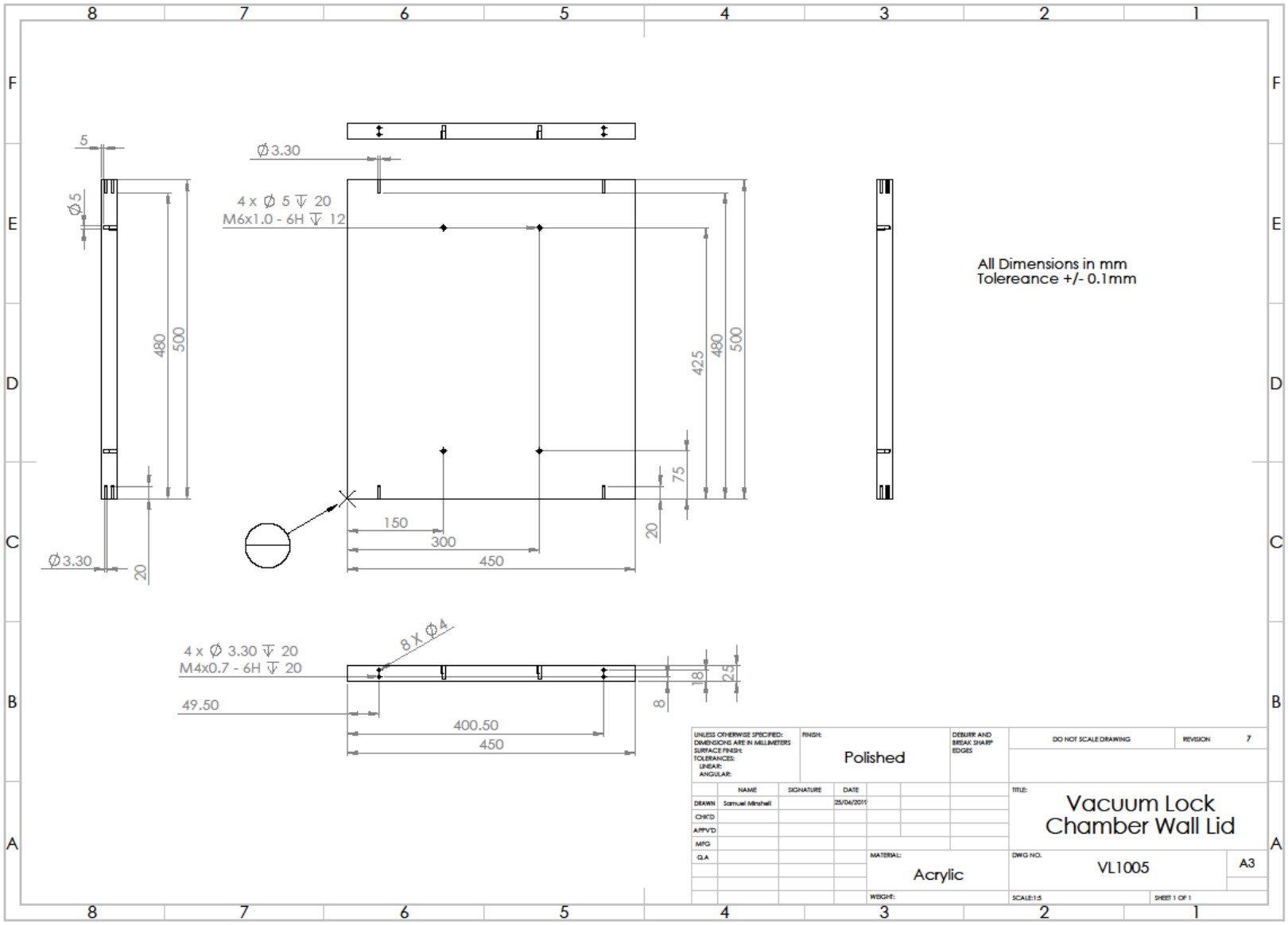
5
Ø5
480
500
Ø3.30
20
Ø3.30
4 x Ø 5 ↧ 20
M6x1.0 - 6H ↧ 12
425
480
500
75
20
150
300
450
All Dimensions in mm
Tolereance +/- 0.1mm
4 x Ø 3.30 ↧ 20
M4x0.7 - 6H ↧ 20
8 X ØA
49.50
400.50
450
8
18
25
UNLESS OTHERWISE SPECIFIED:
DIMENSIONS ARE IN MILLIMETERS
SURFACE FINISH:
TOLERANCES:
LINEAR:
ANGULAR:
FINISH:
Polished
DEBURR AND BREAK SHARP EDGES
DO NOT SCALE DRAWING
REVISION 7
NAME
SIGNATURE
DATE
DRAWN Samuel Minshall 25/04/2019
CHK'D
APPV'D
MFG
Q.A
MATERIAL:
Acrylic
WEIGHT:
TITLE:
Vacuum Lock
Chamber Wall Lid
DWG NO.
VL1005
A3
SCALE:1:5
SHEET 1 OF 1

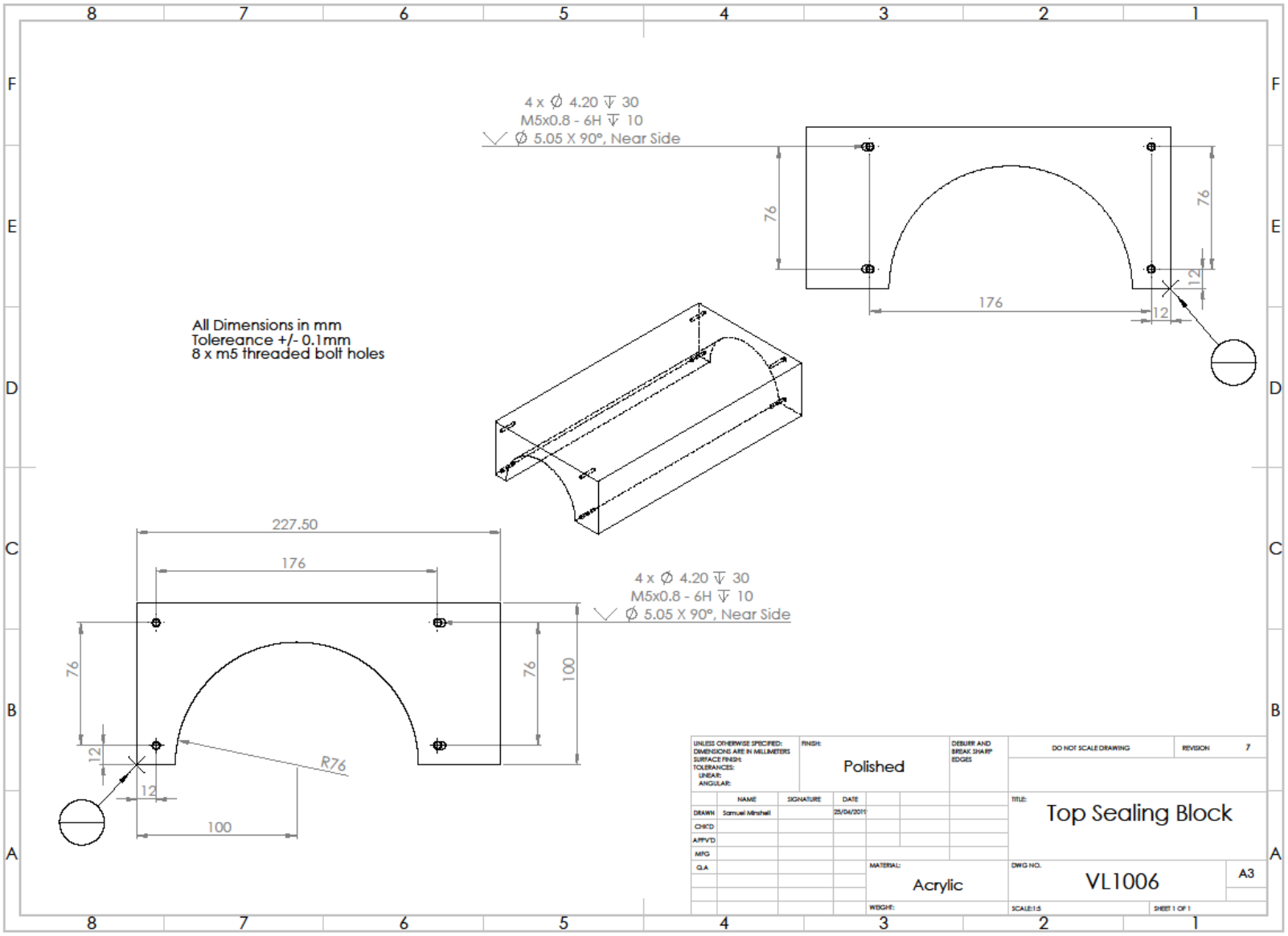
4 x ⌀ 4.20 ↧ 30
M5x0.8 - 6H ↧ 10
⌀ 5.05 X 90°, Near Side
All Dimensions in mm
Tolereance +/- 0.1mm
8 x m5 threaded bolt holes
227.50
176
76
100
12
R76
Polished
Acrylic
Top Sealing Block
VL1006
A3

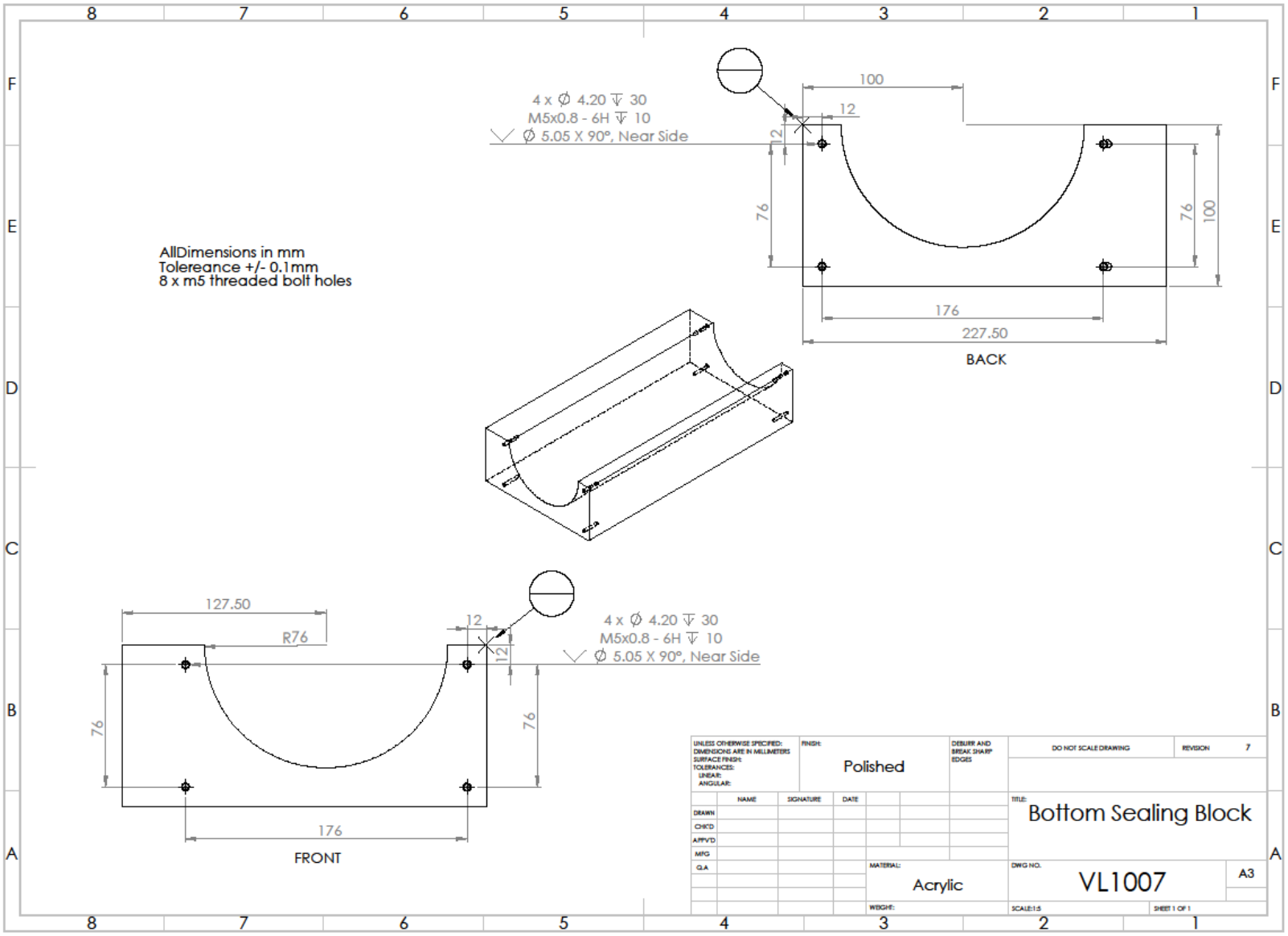
4 x ∅ 4.20 ↧ 30
M5x0.8 - 6H ↧ 10
∅ 5.05 X 90°, Near Side
100
12
12
76
76
100
176
227.50
BACK
AllDimensions in mm
Tolereance +/- 0.1mm
8 x m5 threaded bolt holes
127.50
R76
12
12
4 x ∅ 4.20 ↧ 30
M5x0.8 - 6H ↧ 10
∅ 5.05 X 90°, Near Side
76
76
176
FRONT
UNLESS OTHERWISE SPECIFIED:
DIMENSIONS ARE IN MILLIMETERS
SURFACE FINISH:
TOLERANCES:
LINEAR:
ANGULAR:
FINISH:
Polished
DEBURR AND BREAK SHARP EDGES
DO NOT SCALE DRAWING
REVISION 7
NAME
SIGNATURE
DATE
DRAWN
CHK'D
APPV'D
MFG
Q.A
TITLE:
Bottom Sealing Block
MATERIAL:
Acrylic
DWG NO.
VL1007
A3
WEIGHT:
SCALE:1:5
SHEET 1 OF 1

All Dimensions in mm
Tolereance +/- 0.1mm
6 x m5 threaded bolt holes

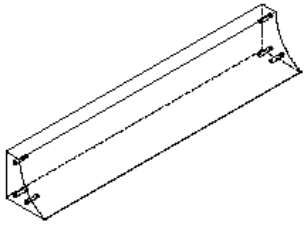

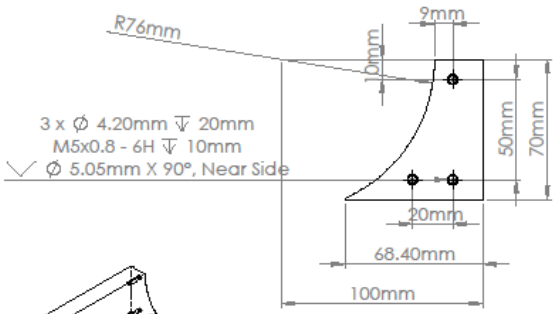

BACK
Scale 1:2

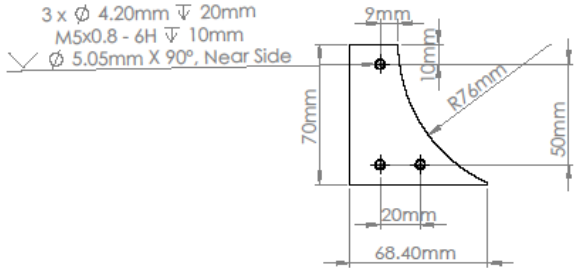

FRONT
Scale 1:2

UNLESS OTHERWISE SPECIFIED: DIMENSIONS ARE IN MILLIMETERS SURFACE FINISH: TOLERANCES: LINEAR: ANGULAR:	FINISH: Sanded		DEBURR AND BREAK SHARP EDGES	DO NOT SCALE DRAWING	REVISION 7	
	NAME	SIGNATURE	DATE	TITLE: Air Restriction Mount Upper		
DRAWN	Samuel Minshall		25/04/2019			
CHK'D						
APPV'D						
MFG						
Q.A				MATERIAL: VeroWhite Resin	DWG NO. VL1008	A3
				WEIGHT:	SCALE:1:5	SHEET 1 OF 1

All Dimensions in mm
Tolereance +/- 0.1mm
6 x m5 threaded bolt holes

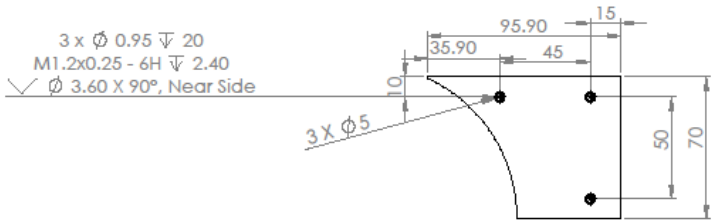

BACK
Scale 1:2

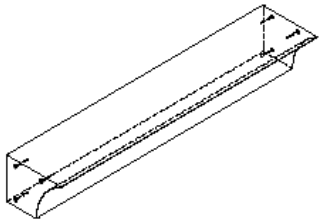

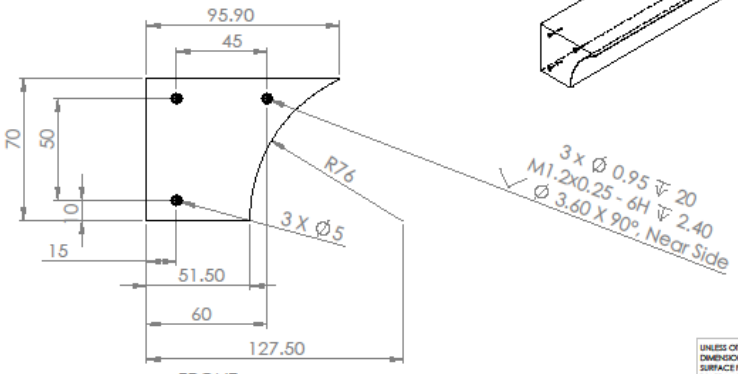

FRONT
Scale 1:2

UNLESS OTHERWISE SPECIFIED: DIMENSIONS ARE IN MILLIMETERS SURFACE FINISH: TOLERANCES: LINEAR: ANGULAR:	FINISH: Sanded		DEBURR AND BREAK SHARP EDGES	DO NOT SCALE DRAWING	REVISION 7
	NAME	SIGNATURE	DATE	TITLE: Air Restriction Mount Lower	
DRAWN	Samuel Minshall		25/04/2019		
CHK'D					
APP'D					
MFG					
Q.A					
				MATERIAL: VeroWhite Resin	DWG NO. VL1009 A3
				WEIGHT:	SCALE:1:5 SHEET 1 OF 1

All Dimensions in mm
Tolereance +/- 0.1mm
2 x m5 threaded bolt holes

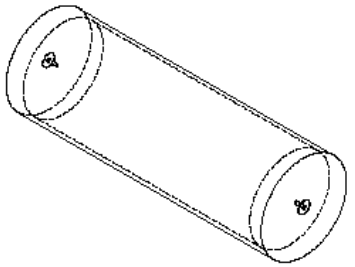

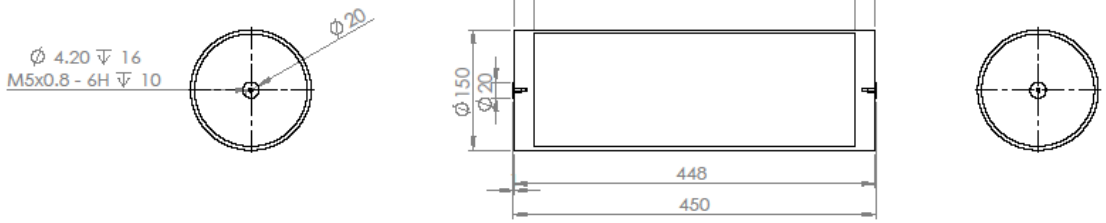

UNLESS OTHERWISE SPECIFIED: DIMENSIONS ARE IN MILLIMETERS SURFACE FINISH: TOLERANCES: LINEAR: ANGULAR:	FINISH: Polished		DEBURR AND BREAK SHARP EDGES	DO NOT SCALE DRAWING	REVISION 7	
	NAME	SIGNATURE	DATE	TITLE: Roller		
DRAWN	Samuel Minshall		25/04/2019			
CHK'D						
APP'VD						
MFG						
Q.A				MATERIAL: Acrylic	DWG NO. VL1010	A3
				WEIGHT:	SCALE:1:5	SHEET 1 OF 1

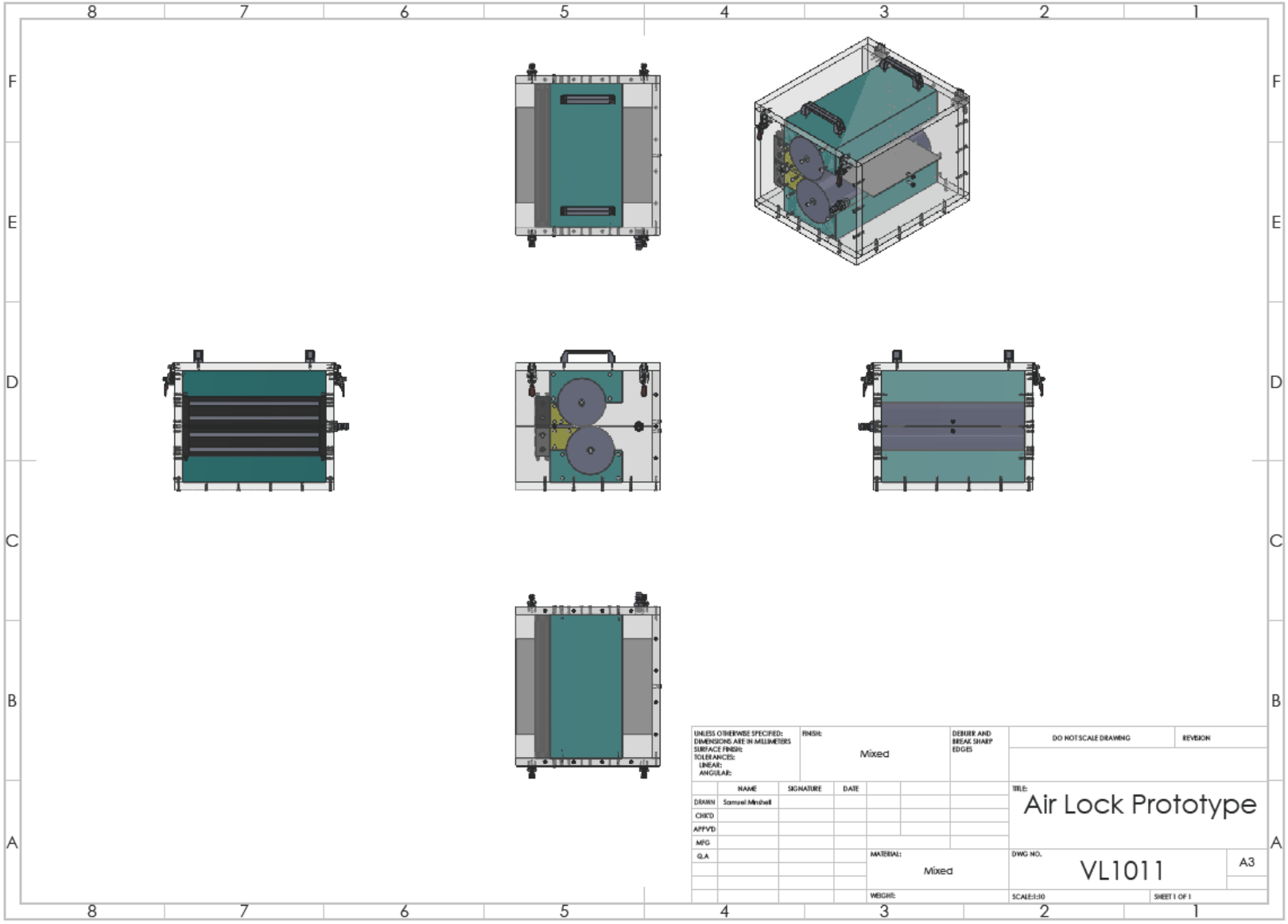
8 7 6 5 4 3 2 1
F E D C B A
UNLESS OTHERWISE SPECIFIED:
DIMENSIONS ARE IN MILLIMETERS
SURFACE FINISH:
TOLERANCES:
LINEAR:
ANGULAR:
FINISH:
Mixed
DEBURR AND BREAK SHARP EDGES
DO NOT SCALE DRAWING
REVISION
NAME
SIGNATURE
DATE
DRAWN
Samuel Minshall
CHK'D
APPV'D
MFG
Q.A
MATERIAL:
Mixed
WEIGHT:
TITLE:
Air Lock Prototype
DWG NO.
VL1011
A3
SCALE:1:10
SHEET 1 OF 1